SEISMIC PERFORMANCE OF CORRODED REINFORCED CONCRETE BRIDGE PIERS

By

KAVEH ANDISHEH

Department of Civil and Natural Resources Engineering

UNIVERSITY OF CANTERBURY

A thesis submitted in partial fulfilment of the requirements for the degree of Doctor of Philosophy in Structural Engineering

March 2017

b

d

ABSTRACT

The impact of general and pitting corrosion on the effective mechanical properties of reinforcing bars under monotonic tensile loading was explored experimentally. Reduction in the effective mechanical properties of steel reinforcement due to pitting corrosion was found. A novel methodology was used to develop corrosion-induced deterioration models for steel reinforcement embedded in concrete, based on comparing the configuration of mass loss in corroded bare reinforcement and reinforcement corroded while embedded in concrete. In this method an advanced 3D scanning measurement technique was employed to scan the surface of corroded bars. The impact of corrosion pattern was used to develop an analytical model to predict tensile behaviour of corroded steel reinforcement embedded in concrete. The corrosion process was simulated in a laboratory environment using an accelerated corrosion procedure. A deterioration model for cracked concrete cover due to reinforcement corrosion was developed, based on experimental compression tests on concrete core samples and statistical normal distribution. The concrete core samples were taken from noncorroded and corroded full-scale reinforced concrete columns. The effects of corrosion on the stress–strain response of confined concrete subjected to reinforcement corrosion were experimentally investigated. An analytical model based on the deterioration models developed in this study was used to predict the stress–strain response of confined concrete due to reinforcement corrosion. The analytical model was validated using the experimental results. The results of more than 100 corroded bare steel reinforcement columns, and 20 corroded full-scale reinforced concrete columns were analysed in order to develop the deterioration models in this research. The deterioration models developed for materials and the model developed for confined concrete subjected to reinforcement corrosion were then used to numerically investigate the impact of corrosion on the nonlinear pushover response of bridge piers subject to corrosion. Parametric studies were carried out to investigate the effects of important parameters on the moment–curvature or force–drift response of the corroded bridge piers. The quasistatic cyclic response of three large-scale precast bridge piers that emulate the behaviour of cast-in-place (ECIP) piers through the formation of plastic hinges in the piers were experimentally investigated. Development of advanced deterioration models due to corrosion, and implementing the models to evaluate the structural response of corroded bridges under seismic loading significantly improve the durability design approach. Moreover, they help to more accurately assess the condition of existing bridges subjected to both seismic loading and corrosive agents. The models can also improve the durability design methodology of RC structures. The results of this research will help bridge managers and owners to develop a rigorous maintenance strategy to evaluate and predict the performance of their bridge network and will also help engineers to optimise the life-cycle design of reinforced concrete bridges subjected to earthquakes and corrosion.

ACKNOWLEDGEMENT

The research undertaken and the work presented in this thesis were supervised by Senior Lecturer Allan Scott and Professor Alessandro Palermo to whom I am deeply grateful for giving me opportunity to study PhD at the University of Canterbury, for their support through all stages of this project, for sharing their profound knowledge and for providing guidance and many inspiring input to my research.

Completion of this research would have not been feasible without the financial support provided by Natural Hazard Research Platform (NHRP) New Zealand, Project "Advanced Bridge Construction and Design for New Zealand (ABCD, NZ); and the QuakeCoRE, New Zealand. The contributions of all organisations and colleagues are immensely acknowledged.

I would like to thank all of the supportive technicians in the structural laboratory who have helped to accomplish the experimental phases of this research by their valuable inputs and technical expertise. Special thanks go to John Maley and Tim Perigo who was directly involved throughout the experimental stage of this project. Without their diligent efforts accomplishment of such delicate tests would have not been possible. I am also grateful for the supports provided by David MacPherson, Peter Coursey, Gavin Keats, Stuart Toase, Mosese Fifita, and Russell McConchie.

I would also like to thank all the fellow postgraduate students at the Department of Civil Engineering at UC for creating a nice working environment, and for many valuable discussions.

Finally, I wish to express my deepest gratitude to my family, to my parents Abdolrahman and Hadigheh; my supportive wife Sara; My lovely son Karen; my sisters Nashmil; and my brother Kamran for all their love, understanding and encouragements during the past few years.

Deputy Vice-Chancellor's Office
Postgraduate Office

UNIVERSITY OF CANTERBURY
Te Whare Wānanga o Waitaha
CHRISTCHURCH NEW ZEALAND

Co-Authorship Form

This form is to accompany the submission of any thesis that contains research reported in co-authored work that has been published, accepted for publication, or submitted for publication. A copy of this form should be included for each co-authored work that is included in the thesis. Completed forms should be included at the front (after the thesis abstract) of each copy of the thesis submitted for examination and library deposit.

Please indicate the chapter/section/pages of this thesis that are extracted from co-authored work and provide details of the publication or submission from the extract comes:

Chapter 2:

ANDISHEH, K., SCOTT, A. & PALERMO, A. 2016b. Seismic Behavior of Corroded RC Bridges: Review and Research Gaps. *International Journal of Corrosion,* 2016.

Chapter 3:

ANDISHEH, K., SCOTT, A. & PALERMO, A. 2016a. Modeling the influence of pitting corrosion on the mechanical properties of steel reinforcement. *Materials and Corrosion,* 67**,** 1220-1234.

Chapter 6:

ANDISHEH, K., SCOTT, A. & PALERMO, A. 2016. Comparison seismic performance of high damage and low damage bridge piers subjected to corrosion via experimental cyclic tests. *Maintenance, Monitoring, Safety, Risk and Resilience of Bridges and Bridge Networks,* 9**,** 422.

Please detail the nature and extent (%) of contribution by the candidate:
The candidate was responsible for the developing the test plan, conducting the experiments, analysing the data and writing the papers.

Certification by Co-authors:

If there is more than one co-author then a single co-author can sign on behalf of all
The undersigned certifys that:

- The above statement correctly reflects the nature and extent of the PhD candidate's contribution to this co-authored work
- In cases where the candidate was the lead author of the co-authored work he or she wrote the text

Name: Allan Scott Signature: Date: *30 Mar 2017*

Table of Contents

List of Figures

List of Tables

1 INTRODUCTION AND SCOPE OF THE RESEARCH

1.1 BACKGROUND

Reinforced concrete is one of the most widely used materials used by construction industry. It is the most common material used for transport infrastructure such as bridges, tunnels, retaining walls, and harbour structures. The raw materials are relatively cost-effective and available all over the world. The built structures are, in general, high fire rated and durable if properly designed and executed. However, the ingress of corrosive ions such as chloride or sulphates will finally lead to deterioration. The main cause of degradation of reinforced concrete structures is the corrosion of embedded steel reinforcement, in particular when subjected to marine environment or de-icing salts. De-icing salts have been used rarely in New Zealand, but according to Statistics New Zealand, 65% of New Zealanders lived within five kilometres of the coast in 2006 compared to 61% in 1981 (Statistics New Zealand, 2013).

Once reinforcement corrosion starts, structural serviceability is affected by concrete cracking and spalling of concrete cover. Significantly developed corrosion, however, decreases load-carrying capacity and ductility of reinforced concrete members, which leads to negative impacts on structural safety. Not only are the functionality and reliability of bridges vital for a society and its economy, but also it is critical that bridges remain safe and open after seismic events. The construction of bridge structures has traditionally been cast-in-place (CIP). The seismic resistance of CIP bridges is achieved by properly designed piers for both strength and ductility (Mander 1983). It is very uneconomical to design a bridge pier to remain elastic under severe seismic events. Current design codes, therefore, accept designed-in-ductility for the piers. The ductile bridge piers dissipate the energy of earthquake events by the formation of plastic hinges (NZTA 2013). CIP has proven to be efficient at achieving life safety and structural collapse prevention, whereas it has been criticised due to its low construction speed and quality of fabrication. Emulative cast-in-place (ECIP) using precast concrete solutions achieved similar seismic performance to CIP, while not having the disadvantages of CIP (White 2014).

New Zealand is an earthquake-prone country that inevitably experiences medium to large

ground motions that can damage structures. The Kaikoura Earthquake on 14 November 2016, for example, badly affected a number of the bridges located in the northern part of the South Island. Many bridges in New Zealand have been located in coastal regions, so they are subjected to chloride-induced corrosion due to the marine environment. The bridges located in aggressive environments are more vulnerable to future seismic events than those located in noncorrosive areas.

Expensive maintenance and retrofits of corroded bridges increases the life-cycle cost of bridges. While in some countries using stainless steel materials for bridges is considered a solution to achieve an optimal life-cycle cost, Sarraf et al (2013) noted that there is a limitation to the fabrication capability of large stainless steel components in New Zealand. Durability design approaches aiming at establishing how the construction materials and bridge members behave over time under certain environmental conditions need to be used to design bridges located in aggressive environments in New Zealand. Although durability design has been addressed in the NZ Bridge Manual, uncertainties in estimation of key parameters affecting chloride-induced corrosion, the effective mechanical properties of corroded steel reinforcement and concrete materials limit achievement (NZTA 2013). In addition, some important data are still lacking and some aspects of seismic behaviour of corroded bridges are incompletely understood. Limitations and difficulties in numerical modelling worsen the situation to predict seismic behaviour of corroded bridges. Development of advanced deterioration models due to corrosion, and implementing the models to evaluate the structural response of corroded bridges under seismic loading significantly improve the durability design approach. Moreover, they help to more accurately assess the condition of existing bridges subjected to both seismic loading and corrosive agents.

There are two methods to show the effects of corrosion on residual capacity of steel reinforcement: (1) effective section, (2) effective mechanical properties. In this research the effective mechanical properties was used because it directly depends on residual capacity of corroded steel reinforcement.

1.2 RESEARCH OBJECTIVES

The purpose of this research is to investigate and improve prediction of the seismic performance of ECIP corroded reinforced concrete bridge piers, through materials and large-scale structural

testing and analytical modelling. The specific research objectives can be summarised as follows:

(1) Development of a corrosion-induced deterioration model for steel reinforcement and concrete materials.

The above objectives consist of three deterioration models as follows:

i. Deterioration model for pitting-corroded steel reinforcement.

ii. Deterioration model for corroded bare bar and corroded steel reinforcement embedded in concrete.

iii. Deterioration models for cracked concrete materials due to reinforcement corrosion.

The above deterioration models were developed in terms of reduction in the effective mechanical properties of steel reinforcement or concrete materials due to corrosion.

(2) Development of an experimentally validated analytical model to predict the compressive stress–strain response of confined concrete subjected to reinforcement corrosion.

This objective includes the following goals

i. Experimentally investigate the stress–strain relationship of confined concrete due to pitting-corroded transverse steel reinforcement.

ii. Experimentally investigate the stress–strain relationship of corroded and noncorroded confined concrete with different volumetric ratios subjected to general reinforcement corrosion.

iii. Development an analytical model to predict the stress–strain response of confined concrete with various degrees of corrosion.

(3) Determine the quasi-static cyclic response of large scale bridge pier

The objective (3) can be summarised as follows:

i. Provide high quality experimental evidence on the behaviour of corroded bridge piers.

ii. Use data obtained from these tests to develop and validate numerical models describing the force-deformation behaviour and residual capacity of corroded bridge piers.

iii. Implement the developed deterioration model to numerically investigate force-displacement and moment-curvature response of corroded bridge piers

iv. Parametric analysis to study the effects of corrosion on key parameters affecting moment-curvature or force-displacement response of bridge piers.

1.3 OUTLINE OF THE THESIS

The thesis consists of seven chapters. Figure 1-1 illustrates the structure of the thesis. Figure 1-1 shows the main objectives of this research, the key contribution of each chapter, excluding the introduction and conclusions, to achieve the research goals, and the relationships of the chapters.

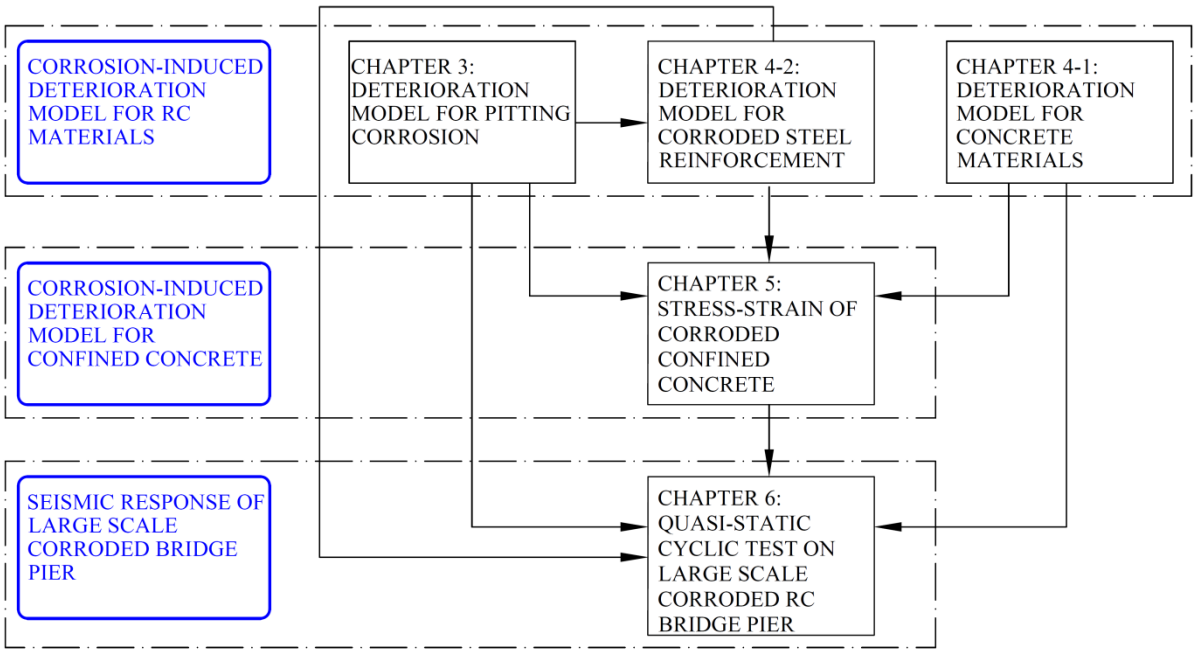

Figure 1-1 Thesis structure

Chapter 1 is an introduction intended to present the background of the research project as well as the objectives and limitations.

Chapter 2 summarizes the state of the current situation by presenting a brief description of chloride-induced corrosion, its main characteristics and influencing factors, a summary of experimental published data, and existing corrosion-induced deterioration models, together with the numerical and experimental methods used to evaluate corroded RC bridge piers. The main objective of Chapter 2 is to highlight research gaps and the critical need for further studies in this field.

Chapter 3 provides an estimate for pit depth based on a time-dependent corrosion rate model. The effects of pit depth on the cross-section parameters, tensile behaviour, and the mechanical properties of reinforcing steel subject to static tensile loading are determined for a range of pit depths and reinforcing bar diameters. Finally, the experimental results have been used to develop reduction factors and deterioration models for pit-corroded steel reinforcement. The results from

this work can be used to help evaluate the life-time seismic and structural performance of reinforced concrete structures subjected to pitting corrosion.

Chapter 4 has two parts. The first part of Chapter 4 will study the effects of corrosion of steel reinforcement on the axial compressive strength and the ultimate strain of concrete materials in RC columns. Then, reduction factors for the axial compressive strength and the ultimate strain of concrete materials in corroded RC columns will be suggested. The second part of Chapter 4 will study the effects of corrosion on corroded bare bars and corroded bars while embedded in concrete. A new methodology is developed to model corrosion-induced deterioration of steel reinforcement embedded in concrete. Based on the results observed from inspection of corroded steel reinforcement, an analytical model is developed to predict the tensile behaviour of corroded steel reinforcement while embedded in concrete. The deterioration models developed can be used for numerical simulation of corroded reinforced concrete structures, or to estimate the residual capacity of corroded RC members, or the design of structures subjected to corrosion over their life-time.

Chapter 5 presents an analytical model for the stress–strain behaviour of corroded confined concrete. The analytical model developed is based on a modification of Mander's model using corrosion-induced deterioration models for reinforcement steel and concrete materials presented in Chapter 3 and 4. The presented model is compared with the results of experimental programme of 12 full-scale RC columns with varying degrees of corrosion. The experimental programme consisted of 10 circular RC and 2 plain columns subjected to a monotonic compressive concentric load with a deformation rate of 0.1 mm per minute. The RC columns had identical size, the same longitudinal steel reinforcement, and spiral confinement type with different spiral pitches. The results of this chapter are very useful for estimation of the residual ductility of corroded reinforced concrete members.

In Chapter 6, the cyclic response of fixed pier to foundation connection of bridge piers with

varying degrees of corrosion were experimentally studied. Three ECIP large bridge piers with three foundations were constructed in accordance with Advanced Bridge Construction (ABC) technology. Two piers out of the three were corroded using an accelerated corrosion method – the impressed current. A 500 mm length of each pier from the top of the foundation was exposed to corrosion. Penetrating salt water into bridge piers extended the length of corrosion to about 800 mm. The two bridge piers were corroded in accordance with relatively low (less than 10% average mass loss in reinforcement) and high (more than 20% average mass loss in reinforcement) degrees of corrosion. The quasi-static cyclic tests were performed on all corroded and noncorroded bridge piers. A series of three cycles at increasing level of drift followed by a half single cycle was applied through a horizontal hydraulic actuator. Three large-scale quasi-static cyclic tests were carried out in total. The load-displacement responses of the noncorroded pier were compared with those of corroded piers. The results show that corrosion causes a reduction in seismic capacity of the corroded piers in terms of energy dissipated and displacement ductility. Finally, to numerically study the effects of different key parameters on the seismic response of corroded bridge piers a parametric study was carried out to investigate the effects of various parameters on the moment-curvature response of corroded bridge piers.

Chapter 7 presents the conclusions of this research project and give some suggestions for future work based on the experience gained during this period of study.

2 SEISMIC BEHAVIOR OF CORRODED RC BRIDGES: REVIEW AND RESEARCH GAPS

2.1 INTRODUCTION

In recent years, growing attention has been given to the effects of corrosion on the structural performance of reinforced concrete (RC) structures. According to National Association of Corrosion Engineers (NACE), the direct annual cost of corrosion of infrastructure was more than $22 billion in the US in 2002. American Society of Civil Engineers (ASCE) has reported that the US should invest $2.2 trillion over the next five years to repair and upgrade more than 300,000 bridges in the US that are approaching the end of their design life (Hansen, 2009). While RC structures in pristine condition can be expected to satisfy the code requirements of a given era, corrosion of reinforcing steel affects the seismic performance of the structure over time. Therefore, old corroded RC structures become vulnerable to probable future earthquakes. It should be noted that there are two well-known forms of corrosion: Carbonation-induced and Chloride-induced corrosion. Carbonation-induced corrosion is defined as chemical reaction between atmospheric carbon dioxide and the product of cement hydration, mainly calcium hydroxide (Hussain and Ishida, 2009) . Chloride-induced corrosion is defined as electrochemical reaction between chloride product (such as iron (II)-Chloride) and water. In this chapter, Chloride-induced corrosion has been studied. The vast majority of deterioration in RC structures is a result of corrosion of reinforcing steel due to ingress of chloride ions from either de-icing salts or marine environment. Corrosion changes effective characteristics and mechanical properties of materials leading to possible degraded seismic performance of corroded RC structures. This problem is very critical for bridges and more importantly for bridge piers since they dissipate earthquake energy through the formation of plastic hinges. Corrosion is a time-dependent process. Therefore life-time analysis is needed to evaluate seismic and structural performance of corroded structures. Long-term seismic performance of RC structures subject to corrosion includes three main parts that are shown in Figure 2-1: (1) Chloride-induced corrosion (2) Deterioration of RC structures or elements due to corrosion(3) life-time (time dependent) seismic analysis and performance of corroded RC bridge pier.

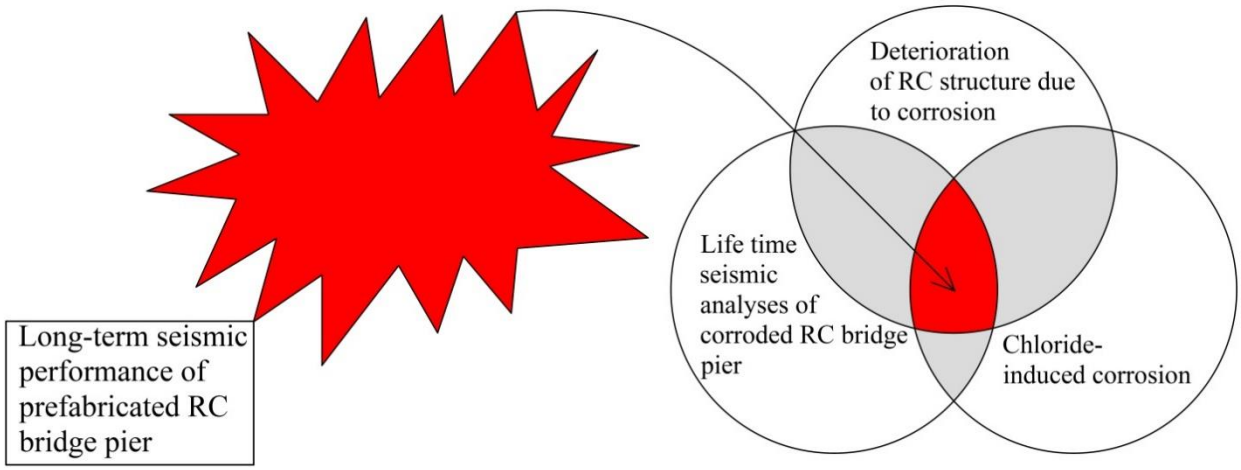

Figure 2-1 Outline of long-term seismic performance of corroded structures

Figure 2-2 shows an overview of the aforementioned three main parts. Two critical phenomena are the reduction in cross section area of reinforcing steel and the formation of corrosion by-product leading to cracking and spalling of concrete in RC structures. Hence, corrosion-induced deterioration of RC structures can be classified into four groups as follows:

1. Reduction in mechanical properties of steel reinforcements
2. Deterioration of bond between steel and concrete
3. Degradation of confinement (decreasing shear strength)
4. Damage to concrete material

Traditional seismic analysis cannot be used for RC structures subjected to corrosion hazard for following reasons. The first reason is that corrosion depends on time, so mechanical properties of structural elements are a function of time. The second reason is lack of robust analytical/numerical cyclic models to predict behavior of corroded RC structures subjected to earthquakes. Hence, Life-time analysis of corroded RC structures is needed taking into consideration the corresponding deterioration models for corroded RC structures, amount of corrosion, and important factors influencing corrosion process such as corrosion initiation time. Figure 2-3 illustrated force displacement response of a corroded bridge pier over time. The outcomes of life-time seismic analysis of corroded RC structures can be represented in terms of reduction in structural capacity or increase in probability of failure over time.

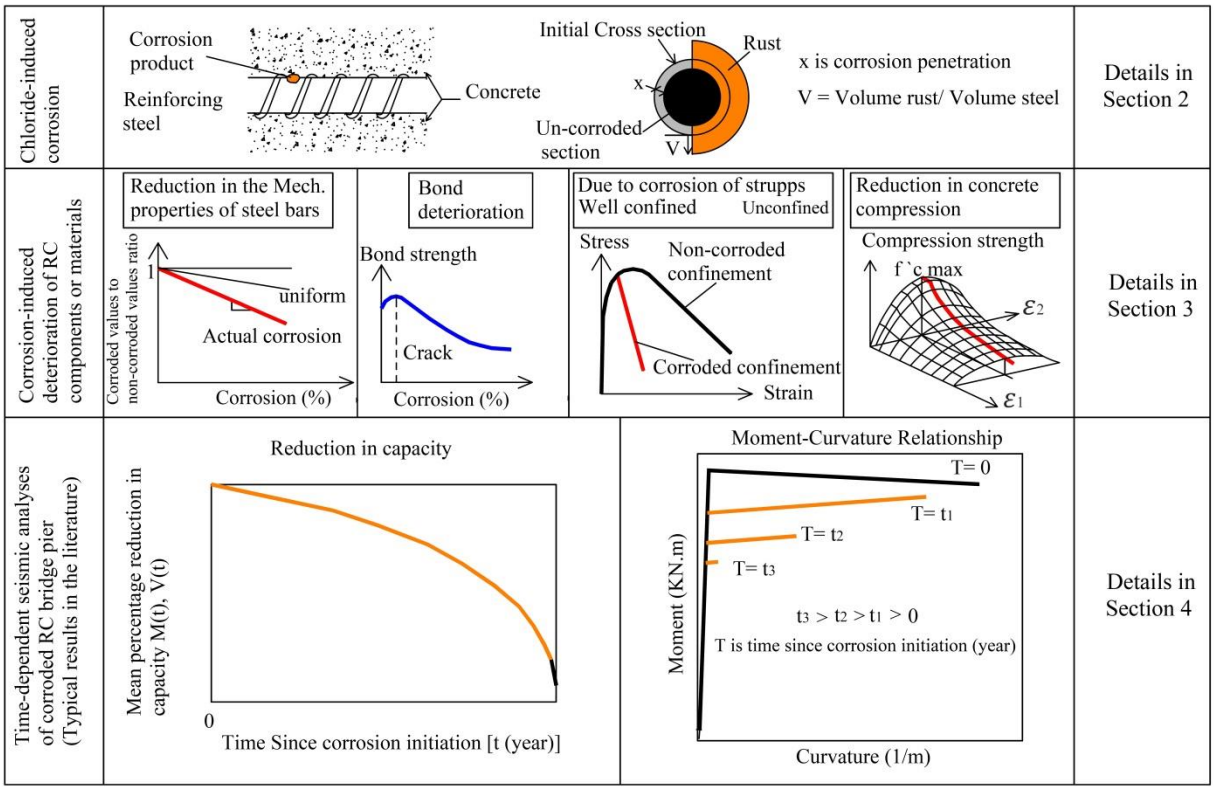

Figure 2-2 Overview of main parts of long-term seismic performance of corroded RC bridge pier

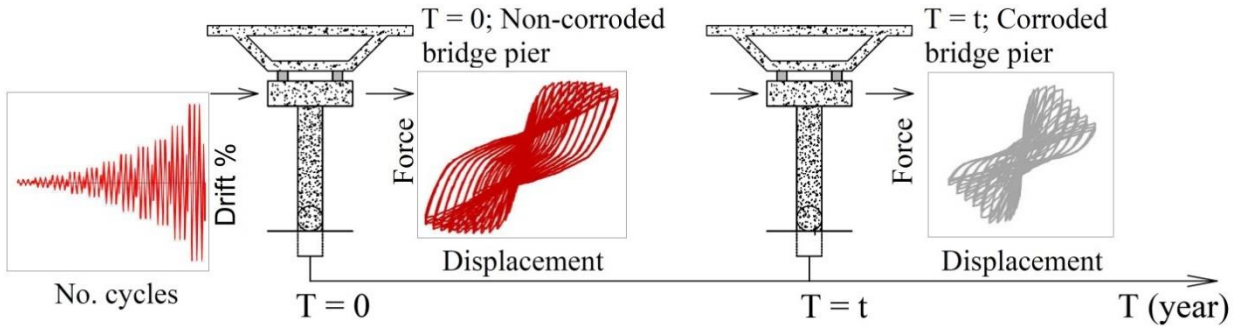

Figure 2-3 Force-displacement response of a corroded bridge pier over time

This chapter summarizes the state of art by presenting a brief description of chloride-induced corrosion, its main characteristics and influencing factors, a summary of experimental published data, and existing corrosion-induced deterioration models together with numerical and experimental methods used to evaluate corroded RC bridge pier. The main objective of this chapter is highlighting research gaps and critical need to further studies in this field.

2.2 CHLORIDE-INDUCED CORROSION

Corrosion of reinforcing steel embedded in concrete is an electrochemical process. The process is initiated as soon as aggressive ions such as chloride penetrate the concrete cover and reach the steel reinforcement. Once the corrosion process commences, not only does the cross sectional area of the corroding reinforcing steel decrease but also corrosion by-products such as rust are formed. The irregular loss of cross section leads to alterations in mechanical properties of reinforcing steels. The average volume of rust is approximately 2-4 times greater than that of the steel resulting in the development of tensile stresses in concrete, which ultimately lead to cracking and spalling of the cover concrete (Vu and Stewart, 2000, Coronelli and Gambarova, 2004). Moreover, bond between steel and concrete decreases. It should be noted that a low level of corrosion can result in a slight increase in bond strength, but increasing corrosion level lead to reduction in bond between concrete and steel reinforcement (Stanish et al., 1999, Auyeung et al., 2000, Lee et al., 2002, Fang et al., 2006b, Berto et al., 2008, Kivell, 2012).

2.2.1 CHLORIDE CONTENT IN REINFORCED CONCRETE STRUCTURES-INITIAL STAGE AND THRESHOLD VALUE

Chloride content is the amount of chloride ion at the surface of steel reinforcement. To initiate corrosion, it should reach a certain level called critical chloride content (C_{crit}). C_{crit} is a threshold value need to propagation of chloride ion. However, there is difference between the scientific and practical definitions of C_{crit}. In scientific definition, C_{crit} is the threshold required to propagate on the surface of the steel, while in practical definition it is associated with the acceptable deterioration of reinforcing steel.

Angst et al. (2009) have summarized the values of C_{crit} experimentally measured from steel embedded in cement based material in laboratory condition, from real structures and from steel directly immersed in solution, reported by 32 published articles. The maximum and minimum values of C_{crit} based on the review of aforementioned experimental results together with maximum allowable total Cl^- % cement weight proposed by various ACI documents is presented in Table 2-1.

Table 2-1 Maximum and minimum critical chloride content based of 32 experimental work reviewed by [18] compared with C_crit proposed by ACI codes

Maximum- Minimum	C_{crit} from steel embedded in cement based material		
	Total Cl^- % binder weight	Cl^-/OH^- ratio	Free Cl^- (mol/l) ; %bw
	0.04- 8.34	**0.09- 45**	**0.045- 4; 0.07-1.16**
	C_{crit} real structures	C_{crit} from the steel directly immersed in solution	
	Total Cl^- (%bw)	Cl^-/OH^- ratio	Free Cl^- (mol/l)
	0.1- 1.96	**0.01- 4.9**	**0.0056- 0.42**
C_{crit} Expressed as total chloride content relative to cement weight proposed by various ACI documents for pre-stressed RC structures in service			
ACI documents	ACI 357	ACI 222	ACI 201
C_{crit} expressed as Cl^- % binder weight	**0.06**	**0.08**	**Not stated**
	0.1	**0.2**	**0.1**

Moreover, Hussain and Al-Gahtani (1996) estimated critical chloride of steel embedded in cement based material, and showed that threshold of Free Cl^- , independent from C_3A content, varies from 0.22 to 0.29 %cw (cement weight), while threshold of total chloride, dependent on C_3A content, varies from 0.48 to 1.2 %cw for various amounts of C_3A content. The results agree with the associated range represented in Table 2-1. Ann and Song (2007) stated that measurement accuracy of C_{crit} in terms of free Cl^- and Cl^-/OH^- ratio is relatively low. Expressing C_{crit} in terms of total Cl^- (% cement weight) takes into consideration inhibiting effect of cement and the aggressive nature of chloride. Angst et al. (2009) also have reported important factors influencing C_{crit} based on reviewing 24 articles. The important factors influencing C_{crit} has been categorized into three groups: Steel type and condition, Concrete and binder properties and External factors. In addition to this, Alonso et al. (2000) concluded that the type of steel doesn't significantly affect the critical chloride value, but after de-passivation the average of rate of corrosion slightly higher in ribbed bar. Glass and Buenfeld (2000) showed that chloride binding reduced free chloride due to the removal of chloride ions from the pore solution of concrete. It also reduced total chloride content at depth. Maruya et al. (2003) concluded that because of condensation and ion absorption due to pore wall in wetting and drying cycles, increasing the cycle rises total chloride in RC structures. Polder (2009) stated that from a theoretical point of view, the effect of concrete resistivity on critical chloride value still remains unclear. Based on information above, the table presented by Angst et al. (2009) has been updated. The update also includes additional new factors marked as "*". Finally Table 2-2 presents important factors influencing critical chloride content in terms of total Cl^- , Cl^-/OH^- ratio and Free Cl^-.

Table 2-2 Important factors and their effects on critical chloride content

Factor	**Effect on critical chloride content**		
	Total Cl^- % cement weight	**Cl^-/OH^- ratio**	**Free Cl^-**
Steel type and condition			
Defect at steel-concrete interface	↓	↓	↓
Polishing, sandblasting	↑	↑	↑
Steel potential ($> -200\ mV\ SCE$)	O	O	O
Steel potential ($< -200\ mV\ SCE$)	↓	↓	↓
Steel type*	O	O	O
Concrete and binder properties			
W/b ratio	↓	↓	↓
Chloride binding*	↓ ↑	O	↓ O
pH	↑	↑	↑
Electrical resistivity*	↑ N.C	↑	↑
Silica fume	↓	↓	↓
Fly ash	↓ ↑ 0^b	↓ 0^b	↓ 0^b
GGBS (Ground granulated blast furnace slag)	↓ ↑ 0^b	O	O
SRPC (low $C_3A + C_4AF$ content)	↓	N.S	N.S
External factors			
Moisture in rather dry concrete	↓	↓	↓
Moisture in nearly saturated concrete	↑	↑	↑
Moisture variation	↓	↓	↓
Oxygen availability	↓	↓	↓
Temperature	↓	↓	↓
Condensation in wet and drying cycle*	↑	N.S	N.S

↓ ↑ Indicating decreasing and increasing critical value with an increase of concerning factor; N.S: result not stated; N.C: the effect of the concerning factor is unclear; O: the concerning factor has no effect, b: contradictor results reported in the literature. SRPC: Sulphate resistant Portland cement

It is worth noting that Angst et al. (2011b) have developed a probabilistic model to investigate the effect of specimen size on C_{crit} measured in laboratories. They have concluded that increasing sample's geometrical dimension decreases C_{crit}, but to apply this result to steel embedded in concrete it has to be verified through experimental studies.

A number of methods for determining the total chloride content and the free chloride content are applied in practical applications. For measuring the total chloride content, drilled cores from hardened concrete are analyzed. The total chloride content in concrete powder-nitric acid solution can be measured by a number of methods such as: titration, use of ion selective electrodes or spectrophotometric methods. However, a more expensive but very accurate method is to determine the total chloride content in concrete powder using X-ray fluorescence spectrometry (XRF). To determine the free chloride content, pore solution expression, leaching techniques and ion selective electrodes are used in the literature (Angst et al., 2009). Further

information can be found in (Angst et al., 2009) and its corresponding references.

2.2.2 PITTING CORROSION- LIMIT STEP TO START PITTING CORROSION

It has been shown that the formation of macro-cell, i.e. small anodic area in comparison with large cathodic area, is observed in pitting (localized) corrosion (Andrade et al., 1992, Raupach, 1996, Raupach, 2007, Warkus and Raupach, 2008, Warkus and Raupach, 2010). It has been confirmed that three transitions occur in pitting corrosion: the first, transition from initiation stage to propagation stage, called de-passivation (Tuutti, 1982); the second, transition from de-passivation to re-passivation (the re-passivation phase called metastable) and the third, transition from metastable to pit growth. As mentioned before, the first transition is related to existing critical chloride content. In metastable, nucleation occurs, also called re-passivation, depending on chemistry or metallurgy condition. Then in case of maintaining aggressive chemical composition in pit cavity, the transition from nucleation to stable pit growth occurs. This transition is due to the simultaneous ingress of H^+ and Cl^- and other anions into pit cavity (Pistorius and Burstein, 1992, Burstein et al., 1993, Laycock and Newman, 1997). Bertolini et al. (2004) stated that pitting corrosion for reinforcement steel in concrete is due to the acidification of pit cavity and ingress of Cl^- into the pit. Broomfield (2002) found that steel reinforcement corrosion start with the formation of a number of pits. Increasing the number of pits causes them to join up and form a general corrosion. Angst et al. (2011a) concluded that a transition from anodic to cathodic control occurs in pitting corrosion. However, it is not clear in which chloride content this transition takes place, so further investigation in this area should be carried out. It is clear that pitting corrosion occurs due to existence of high amount of chloride ion in a certain location. This means that corrosion potential is greater than pitting potential in that location(Angst et al., 2009). Since pitting corrosion causes significant cross-section loss in reinforcing steels, in structural analysis the amount of cross-section loss due to pitting corrosion is a very important parameter. Therefore, researchers estimated a factor called “pitting factor” that is used to calculate pit depth and related loss of steel cross-section. Pitting factor is the ratio of maximum pit depth on average corrosion penetration. Pitting factors reported in the literature have been collected from 8 experimental investigations, and are/have been summarized in Table 2-3.

Table 2-3 Pitting factors obtained from literature

Authors and date	$D_{(mm)}$	$L_{(mm)}$	**Time (day)**	**No. of samples**	$i_{corr}(\mu A/cm^2)$	**Pitting factor: (R)** Mean ; COV
Gonzalez et al. (1995)	8	500	6 years	N.S	0.1 - 7.0	4.4-5.9 ; N.S
	16	400	30		10 - 100	5.9-16.1 ; N.S
Rodriguez et al. (1996)	6	650	100- 200	18	100	4-11.7 ; 0.05-0.22
Rodriguez et al. (1997)	12	2300	100- 200	16	100	4.0 ; 0.15
Torres-Acosta (Torres-Acosta and Mart ı´ nez-Madrid, 2003)	13	310	700	35	N.S	5.5 ; 0.59
Stewart (2004)	8	800	50 years		1	7.00 ; 0.18
	16					7.68 ; 0.16
	24					8.08 ; 0.16
	28					8.23 ; 0.15
	32					8.36 ; 0.15
	36					8.48 ; 0.15
	10	100				1.65 ; 0.22
Cairns et al. (2005a)	16	N.S	100- 400	25	10 - 50	23.8 ; 0.56
Torres-Acosta et al. (2007)	10	1500	40, 80, 200	8	80	11.7 ; N.S
Stewart and Al-Harthy (2008)	16	100	78	32	160 - 185	6.20 ; 0.18
	27				125 - 150	7.10 ; 0.17

Figure 2-4 shows the relationship between diameter size of reinforcing steel and pitting factor regressed from the results represented in the Table 2-5. According to this figure, pitting factor increases with the growth of diameter sizes of reinforcing steels.

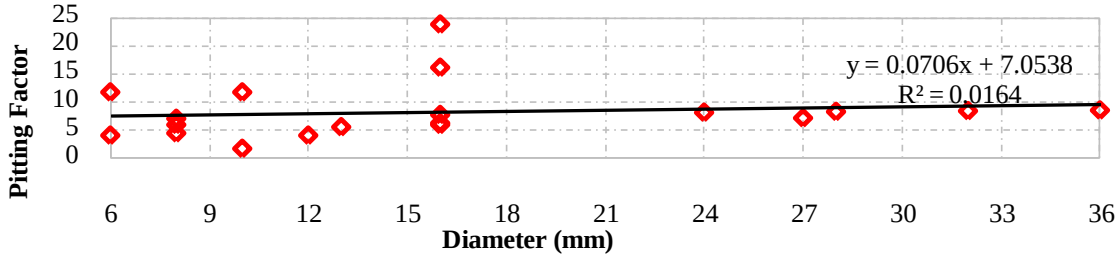

Figure 2-4 : Pitting factor for different diameter sizes of bars regresses from results represented in Table 2-5

Average corrosion penetration can be calculated based on mass loss due to corrosion and estimation of associated equivalent diameter of corroded bar (Torres-Acosta and Mart ı´ nez-Madrid, 2003). It has been stated that pitting factor rises with increase of reinforcing steel bars diameter (Stewart, 2009).

Using Faraday's law, assuming hemispherical form for pits, the maximum pit depth is as follows (Val and Melchers, 1997):

$$p(t) = 0.0116 \times R \times i_{corr}(l) \times t \qquad 2\text{-}1$$

Where, $p(t)$ is the maximum pit depth (mm), R is pitting factor, $i_{corr}(l)$ is corrosion current density ($\mu A/cm^2$), and t is time (year).

2.2.3 PREDICTING THE RATE OF CORROSION

Rate of corrosion and time of the commencement of corrosion are very important factors influencing the deterioration of RC structures as they are related to residual capacity of corroded structures. Many factors affect the corrosion rate which is classified in three groups: named steel condition, concrete and binder properties and external factors. Based on the empirical and mathematical models developed by past studies, Table 2-4 shows important factors affecting corrosion rate and initiation time of corrosion (Alonso et al., 1988, Lopez and Gonzalez, 1993, Yalcyn and Ergun, 1996, Katwan et al., 1996, Balabanić et al., 1996, Balabanic et al., 1996, Kranc and Sagüés, 1997, Liu and Weyers, 1998a, Alonso et al., 1998b, Alonso et al., 1998a, Raupach and Gulikers, 1999, Isgor and Razaqpur, Takewaka et al., 2003, Gulikers, 2005, Scott and Alexander, 2007, Huet et al., 2007, Martínez and Andrade, 2009, Otieno et al., 2011, Otieno et al., 2012). Among all factors, one may notice that increasing total chloride raises corrosion rate. This means that all factors affecting total chloride (see Table 2-2) influence corrosion rate. Increasing saturation degree of pore in empirical model causes both reduction and rising of corrosion rate. On the other hand, the mathematical model showed that increasing the degree of saturation pore from 30% to 50% causes increasing corrosion rate, while further increase from 60% to 100% causes reduction in corrosion rate (Lopez and Gonzalez, 1993).

Table 2-4 Important factors and their effects on corrosion rate and start time of corrosion

Factor	Empirical corrosion rate (r_{corr}) model	Mathematical corrosion rate	
		Start time	r_{corr}
Steel condition			
Temperature at steel level	↑		
Galvanic coupling	↑		
Corroding area to exposure area			↓
Anodic and cathodic resistivity			↑
Concrete and binder properties			
W/b ratio	↑		↑
Total Cl^- %	↑		
pH	↓		
Electrical resistivity	↓		↓
permeability	↑		
Cracks		↓	N.C
Size distribution of aggregates		↓	
Initiation crack width		↓	
Degree saturation of pore	↓ ↑		(60%-100); ↓ (30%-50%) ↑
External factors			
Slag concentration	↓		
Chloride conductivity			
RH	↑		
time	↓		
Oxygen availability	↑		
Aging of oxides in dry concrete	↓		
Aging of oxides in wet concrete	O		
Cover	↓		↓

↓ ↑ Indicating decreasing and increasing corrosion rate value with an increase of concerning factor; N.C: the effect of the concerning factor is unclear; N.S: not stated; O: the concerning factor has no effect, b: contractor results reported in the literature.

While measuring corrosion accurately is difficult, there are some simple methods based on corrosion potential and corrosion rate that can be used by researchers and practical engineers to estimate active corrosion in RC structures. For example, according to ASTM C-876-91, if corrosion potential, V, is less than -0.35, probability of active corrosion is more that 95% (Standard). Elsener et al. (2003) have stated that corrosion potential ranging from -0.4 to -0.6 means that steel is corroding. Liang et al. (2002) have reported that using corrosion current density to corrosion duration ratio the grade of corrosion can be evaluated according to Table 2-5.

Table 2-5 Simple method to evaluate grade of corrosion

Corrosion grade	Non-	Slight	Moderate	Severe
Corrosion current density [μA/cm^2] / Corrosion duration [year]	< 0.0066	0.0066 - 0.05	0.05 – 2.5	> 2.5
Corrosion duration [year]	> 15	10 to 15	2 to 10	< 2

2.2.4 CORROSION BY-PRODUCTS AND CORROSION-INDUCED CRACKING

As discussed earlier, when corrosion initiates, corrosion by-products are formed. The volume of corrosion by-products is greater than that of steel. Therefore, volumetric expansion causes tensile stress leading to propagation of cracks into concrete cover. Zhao [172] have suggested the expansion coefficient of 2.64, 2.85 and 3.02 for samples corroded in NaCl solution, near or on the coast and in splash zone respectively. Table 2-6 presents the volume expansion of different components of corrosion by-product found by past studies.

Table 2-6 Volume expansion of corrosion by-product components

References	Volume expansion coefficient of different components of corrosion by-product										
	FeO	Fe_3O_4	Fe_2O_3	αFeOH	γFeOH	$Fe_2O_3.H_2O$	βFeOH	$Fe(OH)_2$	$Fe(OH)_3$	$Fe(OH)_3 3H_2O$	$Fe_2O_3.3H_2O$
(Liu, 1996)	1.82	2.08	2.17	-	-	-	-	3.76	4.24	6.46	-
(Marcotte, 2001)	1.74	2.1	2.11, 2.26	2.9	3.12	-	3.5	3.7	4		6.24
(Bhargava et al., 2005)	1.8	2	2.2	-	-	-	-	3.75	4.2	6.4	-
(Caré et al., 2008)	-	2.08	2.12	2.91	3.03	-	3.48	-	-	-	-
(Raupach et al., 2010)	1.77	2.1	2.14	2.92	3.06	3.12	-	3.71	4.82	-	6.5
(Zhao et al., 2011)	-	2.1	-	2.95	3.07	-	3.53	-	-	-	-

Predicting the expansion volume of rusts is very important to improve the knowledge of service life of reinforced concrete structures. The variation in expansion coefficient reported by past studies clearly indicates need for further studies on rust compositions are demanded.

With respect to mechanical properties and characteristics of corrosion by products, Care et al [46] have stated that Young's modulus of rust layers depends on the diameter of un-corroded steel bar and thickness of the rust layers. Zhao [172] has shown that environmental parameters such as amount of humidity and oxygen availability vary the volume expansion coefficient. Increasing the amount of humidity and oxygen raises the expansion coefficient.

Past studies investigated corrosion-induced cracking and shared the influencing factors and

measured crack width based on experimental data. A summary of 18 reviewed works has been presented in Table 2-7 showing crack width measured in addition to some details such as amount, current density and/or type of corrosion and time of exposure. Table 2-7 can give an overall view on corrosion-induced cracking. It is worth noting that the maximum crack width reported in the literature so far has been 6mm (Torres-Acosta and Mart ı´ nez-Madrid, 2003). Few models have been developed for predicting width of crack in the literature. Andrade et al. (1993), for example, presented a simple formula to predict average width of crack in elements exposed to natural corrosion (Andrade et al.):

$$w = k\left[\frac{P_x}{C/\phi}\right] \qquad 2\text{-}2$$

Where, w is the crack width (mm), k is a non-dimensional factor, C/ϕ is concrete cover/ diameter of the bar ratio, P_x is penetration of the corrosion in time t (year) and equal to:

$$P_x = 0.0115\, r_{corr} t \qquad 2\text{-}3$$

Where, r_{corr} $(\frac{mm}{year})$, is the corrosion rate.

Andrade et al. () validated his formula with 15-year-old RC specimens. They proposed k=9.5 for their formula. Du et al. (2005) showed that both decrease of w/c ratio and increase of cover are important factors to resist cracking due to ingress of chloride. It's clear that rate of corrosion always is an important factor affecting crack-induced corrosion.

The relationship between corrosion current density, icorr (mA/m2), and corrosion rate, rcorr (μm/year) can be expressed in the following equation [177]:

$$r_{corr} = \frac{0.327(Mi_{corr})}{n\rho} \qquad 2\text{-}4$$

Where, M (g/mol) is the atomic weight, n is the ion valence and ρ is the density (g/cm3).

Table 2-7 Relationship between crack widths with corrosion obtained from literature

References	Type of Specimen	Time (day)	$i_{corr}(\mu A/cm^2)$	A_{corr} (%)	Crack width (mm)
(Al-Sulaimani et al 1990)	beam	N.S	2000	< 4.5	1.3
(Tachibana et ai 1990)	beam	3 - 15	0.5	2.5 - 12	0.1 - 0.75
	Bond-pull		500	N.S	N.S
(Andrade et al 1993)	prism	1 - 100	10, 100	0.5 – 2.5	0.05 – 0.5
(Cabrera 1996)	beam	28		0.8 – 9.2	N.S
	Bond-pull	1 - 28		3.6 – 19.2	0.06 – 0.46
(Rudrigues et al 1996)	column	106-204	100	9.1 – 17.8	0.8 – 4.0
(Rudrigues et al 1997)	beam	100- 200	100	10.1 – 26.3	0.2 – 0.6
(Almusallam et al 1997)	slabs	1 – 2.5	3	1 - 75	N.S
(Huang and Yang 1997)	beam	126 hour	5×10^8	< 1	N.S
(Alonso et al 1998)	prism	68 - 221	10, 100	N.S	0.06 – 1
(Amleh and Mirza, 1999)	prism	N.S	5 V current	0, 12	0.35, 0.8
Mangat and Elgarf (1999)	Beam	15 - 18	1 - 4	2.5 - 10	N.S
Mangat and Elgarf (1999)	beam	16-64 h	3	1.25 - 5	N.S
Torres-Acosta and Mart ı´ nez-Madrid (2003)	prism	700		Up to 51	0 - 6
El Maaddawy and Soudki (2003)	prism	815, 766, 380, 306	100, 200, 350, 500	4.38, 7.3, 6.5, 7.26	0.25 - 1
Vidal, Castel et al. (2004)	beam	17 years	Saline Environment	26	1.6
	beam	14 years		12	1.8
Vu, Stewart et al. (2005)	Slab	2-9 month	100	N.S	0.05 – 1.5
Andrade, Muñoz et al. ()	T-beam	2-15 year	Average: 0.128	N.S	0.31 – 3.94
	column	2-15 year		N.S	0.2 – 0.51
Zhang, Castel et al. (2012)	Wall spec.	20-56 weeks	$R_p = \pm 20$ mV	Up to 6.5%	0.01- 1

Predicting time of corrosion cracking is another important factor in corrosion-induced cracking topic and is used for predicting the service life of corroded RC structures. Predicting the time of corrosion cracking has been addressed by a number of researchers including (Liang et al., 2002). In this regard, a few mathematical models have been developed by (Liu, 1996, Liu and Weyers, 1998b, Pantazopoulou and Papoulia, 2001, Bhargava et al., 2005, Bhargava et al., 2006, El Maaddawy and Soudki, 2007).

Figure 2-5 shows the relationship between percentage of cross section loss in steel bars and crack width (mm) based on the results represented in the Table 2-7.

Figure 2-5 shows increasing percentage loss of cross section due to corrosion raises crack width.

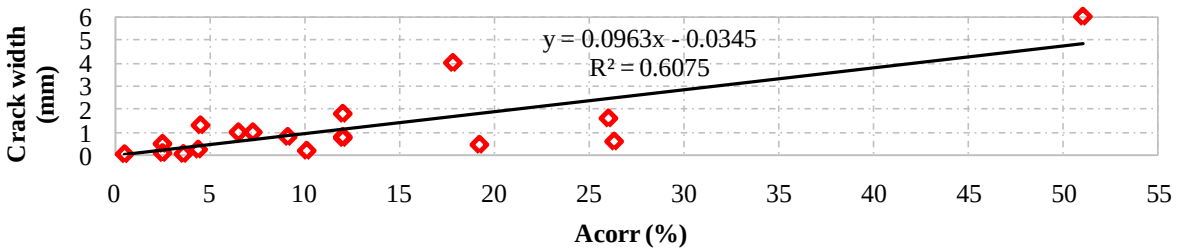

Figure 2-5 Crack width vs percentage loss of cross section regresses from results represented in Table 2-7

The reason for rising crack width with corrosion percentage is that more corrosion by-product in higher level of corrosion leads to increase of crack width.

2.2.5 RESEARCH GAPS

The main research gaps in chloride induced corrosion can be summarizes as follows:

- More accurate value of critical content of chloride concentration for real RC structures
- Factors and their effects on the critical content of chloride
- Robust pitting factors for real corroded structures
- Factors and their effects on corrosion rate and time of initiation
- Robust corrosion rate and time of initiation prediction
- More accurate values volume expansion for corrosion by-product and rust components specially for real corroded RC structures

Research studies at aiming to fill the above research gaps will lead to decrease of uncertainties in estimation of chloride-induced corrosion.

2.3 CORROSION-INDUCED DETERIORATION OF RC STRUCTURES

As discussed earlier, the two main outcomes of corrosion are decreasing cross-section area of steel reinforcement and volumetric expansion caused by corrosion by-products. As a result, mechanical properties of steel reinforcement such as modules of elasticity, force, stress and strain at yield and ultimate points alter with corrosion. Regarding cyclic behavior of steel reinforcement, in particular, corrosion changes energy dissipating characteristic and number of cycles needed for failure. Bond between concrete and steel varies in corroded reinforced concrete members. The stress-strain model of confined concrete in compression region is affected by corrosion and maximum compression stress of concrete decreases because of cracks propagated into concrete cover due to corrosion. Up to date, there is no experimentally study showing the effects of corrosion on stress-strain relationship on RC columns. It is worth to note that the similar experimental study is in progress by authors. Therefore, materials characteristics of corroded reinforced concrete members have to be applied for analyses and simulations of corroded structures.

2.3.1 EFFECT OF CORROSION ON MECHANICAL PROPERTIES OF STEEL REINFORCING

Irregular decreases in cross-sectional area of steel reinforcing causes changes in mechanical properties of reinforcements. A number of monotonic tensile tests on bare bars and RC elements and bending tests on RC beams and slabs have been carried out to estimate the reduction factors corresponding to the mechanical properties. Reduction factors indicate that the percentage of reductions in mechanical properties that will happen for 1% reduction in cross-section, and they have been estimated from experimental results and reported by past studies. In this chapter a survey on 18 experimental works has been done and the results and references have been presented in Table 2-8. The following investigated mechanical properties were included: yield and ultimate (stress or force) strength, elongation, and module of elasticity. Equations 2-5- 2-10 are typical models regressed from experimental data used by past studies that can be used to calculate mechanical properties of corroded steel reinforcements:

$$\sigma_y^c = [100 - \alpha_y \times A_{corr}\%]\sigma_y \quad 2\text{-}5$$

$$\sigma_u^c = [100 - \alpha_u \times A_{corr}\%]\sigma_u \quad 2\text{-}6$$

$$E_s^c = [100 - \alpha_E \times A_{corr}\%]E_s \quad 2\text{-}7$$

$$\delta_s^c = [100 - \alpha_{\varepsilon u} \times A_{corr}\%]\delta_s \quad 2\text{-}8$$

$$F_y^c = [100 - \alpha_y^* \times A_{corr}\%]F_y \quad 2\text{-}9$$

$$F_u^c = [100 - \alpha_u^{**} \times A_{corr}\%]F_u \quad 2\text{-}10$$

Where: σ_y^c, σ_u^c, E_s^c, δ_s^c, F_y^c, F_u^c are yield stress, ultimate stress, module of elasticity, elongation, yield force and ultimate force of corroded bars respectively, α_y, α_u, α_E, $\alpha_{\varepsilon u}$, α_y^*, α_u^{**} are their associated reduction factors, $A_{corr}\%$ is the percentage loss of cross section, and σ_y, σ_u, E_s, δ_s, F_y, F_u are yield stress, ultimate stress, module of elasticity, elongation, yield force and ultimate force of non-corroded bars.

Table 2-8 Corrosion-induced reduction factors of mechanical properties of steel reinforcing

References	Sample(D); test	Corrosion Method and condition	A_{corr}%	α_y	α_u	α_E	$\alpha_{\varepsilon u}$
(Maslehuddin et al., 1990b)	Ribbed (8-32); T	Open air (Environment);	0- 0.5	0.0	0.0		
	Plain (8-32); T						
(Andrade et al 1991)	Ribbed (12); T	Acc. 0.5- 2.0 mA/cm^2	0-11	0.45	0.33		
(Allam et al., 1994)	Bare; T	Open air (Environment); Arabian coast	0-1	0.0	0.0		
(Saifullah 1994)	Ribbed (8);Tensile	Acc. 0.5 mA/cm^2	0- 28	0.16	0.44		
	Plain (8);Tensile			0.28	0.68		
(Zhang et al 1995)	RC- Ribbed (10-25); T	Open air (Environment); Carbonation	0- 67	0.04	0.05		
	RC- Plain (8-14); T						
(Morinaga, 1996)	RC	Open air (Environment); Chloride	0- 25	0.6	0.63		
(Lee et al., 1996a)	Ribbed (10), Tensile	Acc. 13.0 mA/cm^2	0- 25	0.21	N.S		
(Castel et al 2000)	RC beam (6, 12); B	Chlorides; Saline environment	0- 20*	N.S	N.S		3.5
Du 2001	Rib- RC (8,16, 32);T	Acc. 0.5- 2.0 mA/cm^2; 3.5% Na-Cl; Tensile	0- 25	0.12	0.15		
	Plain- RC (8,16); T		0- 25	0.49	0.65		
(Almusallam, 2001)	6mm	Acc. 2.0 mA/cm^2	0- 75		1.98**	N.S	4.6
	12mm		0- 80		0.74**	N.S	N.S
(Palsson and Mirza 2002)	N.S	Open air (Environment); Chloride	0->30	0.00	0.00		
(Du et al 2005)	Ribbed (8,16, 32) and RC; Tensile	Acc.0.5-2.0 mA/cm^2; 3.5% Na-Cl; yield force	0- 25	1.14- 1.28*			
		Acc.0.5-2.0mA/cm^2; 3.5% Na-Cl; ultimate force	0- 25	1.22- 1.39**			
		Acc.0.5-2.0mA/cm^2;3.5%Na-Cl; yield Strength	0- 25	0.16- 0.36			
		Acc.0.5-2.0mA/cm^2; 3.5%Na-Cl; ulti. Strength	0- 25	0.26- 0.48			
	Plain (8,16) and RC; Tensile	Acc.0.5-2.0 mA/cm^2; 3.5% Na-Cl; yield force	0- 25	1.60, 1.48*			
		Acc.0.5-2.0mA/cm^2; 3.5% Na-Cl; ultimate force	0- 25	1.71, 1.26**			
		Acc.0.5-2.0mA/cm^2;3.5%Na-Cl; yield Strength	0- 25	0.79, 0.58			
		Acc.0.5-2.0mA/cm^2; 3.5%Na-Cl; ulti. Strength	0- 25	0.94, 0.44			
(Carins et al 2005)	RC cube; Tensile	Acc. 0.01- 0.05 mA/cm^2; cyclic wet-dry	0- 3	1.2	1.1	N.S	3
	RC cylinders; T	Acc. (Electric); 5% Na-Cl					
(Apostolopoulos and Papadopoulos, 2007)	S400, 10mm	Salt spray corrosion	1.5-8.5	1.47	1.31	N.S	6.97
(Lee and Cho 2009)	RC Ribbed (10, 13);T	Accelerated Uniform (Electric); 3% Na-Cl	0- 35	1.24	1.07	1.75	1.95
	RC Ribbed (10, 13);T	Acc. Pitting (Chloride induced); cyclic wet-dry	0- 35	1.98	1.57	1.15	2.95
(Oyando et al 2011)	RC beam; Bending	Open air (Environment); 1- 12 years	0- 50	N.S	1.97*	N.S	N.S
	RC beam; Bending	Accelerated (Electric); 3% Na-Cl	0- 50	N.S	1.59*	N.S	N.S
	Ribbed; Tensile	Open air (Environment); 1- 12 years	0- 50	N.S	1.41	N.S	N.S
	Ribbed; Tensile	Accelerated (Electric); 3% Na-Cl	0- 50	N.S	1.34	N.S	N.S
(Hawileh et al., 2011)	BS B500B; 10mm; T	N.S	9.5-19.6	1.21	1.38	N.S	1.91
(Zhang et al., 2012b)	RC plain (6.5mm);T	Naturally carbonation-induced corroded	14- 38	1.12	1.36	N.S	N.S
	RC Ribbed (12);T	Acc. 0.1 mA/cm^2; 5% Na-Cl	4- 28	1.1	1.22	N.S	N.S

While the results presented in the literature have a wide variation, some conclusions reported by the above reviewed references are as follows:

- Very low corrosion may not affect the mechanical properties of the steel reinforcing
- Usually reduction factors for environment corrosion and plain steel reinforcement are higher than accelerated corrosion and deformed steel reinforcement.
- The greatest reduction factor is related to elongation. This is very important for seismic behavior of RC structures.
- Usually pitting corrosion and irregularities in corrosion increase the reduction factors. On the other hand, reduction factors for pitting corrosion is greater than those for general corrosion (Lee and Cho, 2009).
- The reduction factors for corroded bare steel reinforcement and those corroded while embedded in concrete are similar (Du et al., 2005).
- The effects of type (plain or deformed type) and diameter of reinforcing steels on reduction factors can be neglected (Du et al., 2005).

To illustrate the variation of the published reduction factors, the minimum and maximum reduction factors of four mechanical properties of steel reinforcement based on the data represented in Table 2-8 is shown in Figure 2-6. The mechanical properties include elongation, modulus of elasticity (E), yield stress and ultimate stress. Since linear regression has been employed by all past studies to estimate reduction factors, the minimum and maximum reduction factors shown in Figure 2-6 is represented based on linear regression.

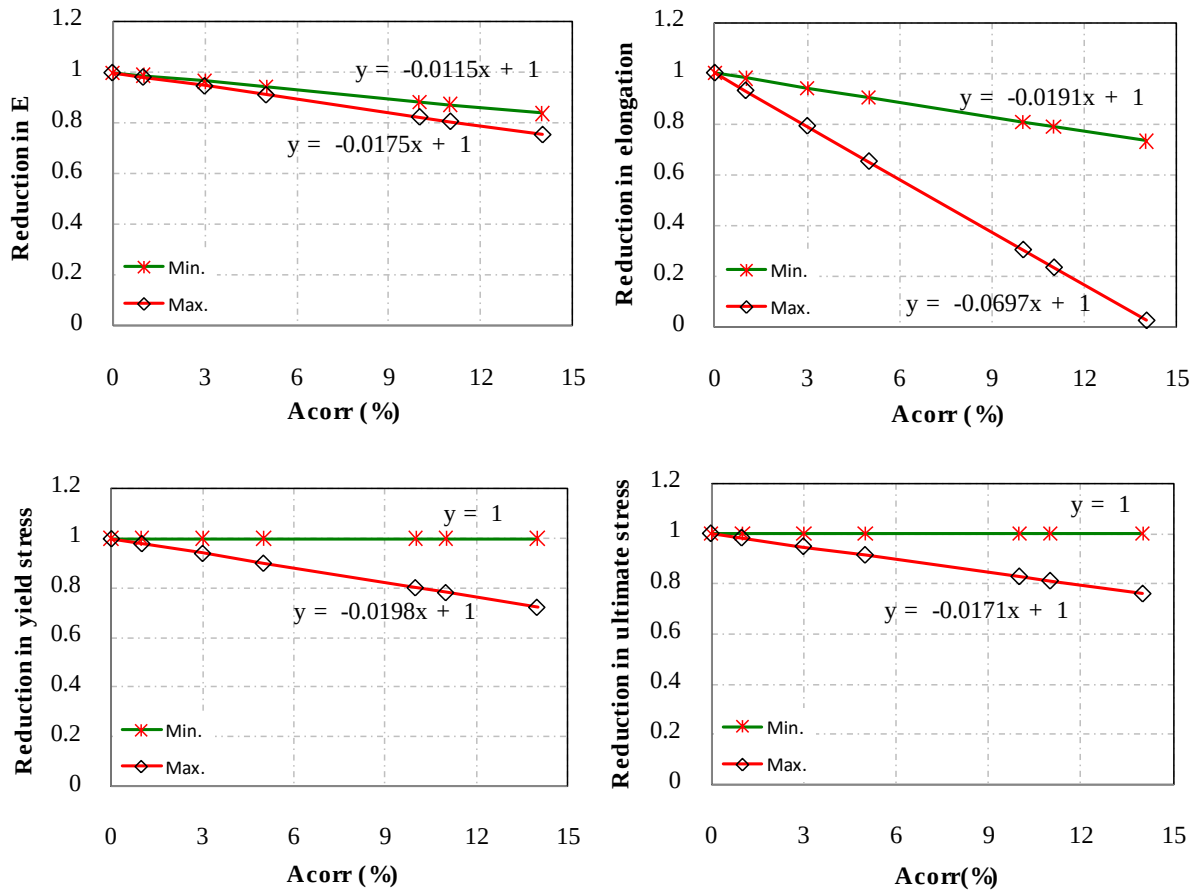

Figure 2-6 Mmaximum and minimum reduction factors for elongation, modulus of elasticity, yield stress and ultimate stress

Figure 2-6 shows that corrosion deteriorates the mechanical properties of reinforcing steel. However, there are big variations in results published in the literature based on monotonic tests. The results also show the maximum reduction factors and the greatest difference between minimum and maximum reduction factors have been reported for elongation.

A few number of studies identified cyclic behavior of corroded steel reinforcements. Apostolopoulos and Papadopoulos (2007) have shown that a mass loss less than 2% and 3% cause 22% and 47% reduction to the number of maximum cycles required for rupture respectively. Apostolopoulos and Pasialis (2010) have studied the low cycle fatigue behavior of smooth and ribbed steel reinforcement for different degrees of corrosion. They have reported that smooth bars showed a better cyclic behavior than that of ribbed bars for low strain amplitude and up to 8% loss of mass due to corrosion. On the other hand, smooth bars can dissipate more energy and need higher number of cycles to fail in low strain magnitude ($\pm$1%) than those of ribbed bars. These advantages disappear as strain amplitude increases. Hawileh et al. (2011) studied the effect of corrosion on cyclic behavior of BS B500B bars. They have

demonstrated that corrosion decreases low cycle fatigue life of the bars. They have pointed out that lower strain amplitude (±4%) causes more reduction in dissipating energy and more cycles are needed for failure than those of higher strain amplitude (±6%). Zhang et al. (2012b) have found that increasing the degree of corrosion causes reduction in fatigue life of corroded bars. They also have claimed that the impact of corrosion on fatigue behavior and naturally corroded is more than that of monotonic behavior and artificially corroded respectively.

2.3.2 THE EFFECTS OF CORROSION ON BOND-STRENGTH BETWEEN STEEL AND CONCRETE

Table 2-9 shows the effect of the percentage of corrosion on bond strength based on 16 experimental works reviewed by the authors. As an overall trend low corrosion percentage increases the bond strength, while high percentage of corrosion always decreases the bond strength. Type of steel bars and confinement are the important factors that influence the change of bond strength due to corrosion. In spite of the above general trends the variation is very high indicating the significance of further investigation in this area. Since chloride-induced corrosion is a function of concrete cover, and always stirrups have less cover than longitudinal bars, further research should be performed to consider this problem that to the best of the authors' knowledge there is no report on, in the literature. Moreover, high level of corrosion causes a critical reduction in bond under cyclic loading, while corrosion under 5% increases bond capacity (Fang et al., 2006a). It has been reported that confinement efficiently decreases bond degradation under cyclic loading (Fang et al., 2006a).

Table 2-9 Effect of corrosion on bond strength between concrete and steel reinforcement

Authors and date	Sample(D); test	Corrosion Method	Time exposure	A_{corr}%	bond strength; % of change
(Al-Sulaimani et al., 1990)	14mm bending	2000 $\mu A/cm^2$	N.S	0.55	↑ ; 40
	10mm pullout			0.55	↑ ; 42
	10mm pullout			3.5- 7.4	↓ ; 0- 66
	14mm pullout			0.65	↑ ; 28
	14mm pullout			2.6- 5.7	↓ ; 0- 65
	20mm pullout			0.43	↑ ; 25
	20mm pullout			1.6- 4	↓ ; 0- 47
(Almusallam et al., 1996)	12mm, pull out	0.4 A Current electric	N.S	< 4	↑ ; 17
				5-7	↓ ; 30-69
				8-12	↓ ; 70-78
				12-80	↓ ; 78-86
(Cabrera, 1996)	12mm, pull out	2-64 A current electric	< 28 days	0.7	↑ ; 18
				2.42, 12	↓ ; 5, 60
(Fu and Chung, 1997)	19mm, pullout	Saturated in $Ca(OH)_2$	< 5 *weeks*	N.S	↑ ; N.S
			> 5 *weeks*	N.S	↓ ; N.S
(Stanish et al., 1999)	10mm, bending	0.1 A Current electric	21-63 days	20	↓ ; 74
(Auyeung et al., 2000)	19mm, pullout	12 A current electric	> 3 *days*	0-5.2	↓ ; 78
(Lee et al., 2002)	13mm, pullout	1 A Current electric	N.S	3	↓ ; 35
			N.S	16.8	↓ ; 77
			N.S	13*	↓ ; 13
			N.S	24*	↓ ; 38
(Soudki and Sherwood, 2003)	10mm, pullout, 15mm cover specimen	140 $\mu A/cm^2$	N.S	5	↑ ; ≅15
				10	↓↑ ; ≅35
(Chung et al., 2004)	10mm, bending	12 A current electric	N.S	2	; 30
				2.8, 15	↓ ; 0, 77
(Fang et al., 2004)	Deformed pullout	0- 2 A Current electric	10-12 days	4, 9	↓ ; 45, 68
	Deformed pullout			3.8*, 6*	↓ ; 4, 12
	Smooth, pullout			3.3	↑ ; 21
(Fang et al., 2006b)	20mm, pullout	0- 2 A Current electric	N.S	4	↓ ; 45
				3.8*	↓ ; 5
(Ouglova et al., 2008)	20mm, pullout	500 $\mu A/cm^2$	8- 48 h	0.2, 0.36	↑ ; 50, 20
			56- 96 h	0.4, 0.76	↓ ; 20, 84
Berto et al. (2008)	10mm, pullout	N.S	N.S	4.27	↓ ; 12
				7.8	↓ ; 75
Chung et al. (2008)	13mm, pullout	12 A Current electric	> 3 *days*	< 3	↑ ; 40
				3- 7	↓ ; 27
Kivell (2012)	Deformed, 20mm Pullout	0.1A Current electric	10- 50 days	0.6*, 11*	↓ ; 6, 50
				20*	↓ ; 76
	Def. 20mm Cyclic			18.6*	↓ ; 59

↓↑ Indicating decreasing and increasing bond strength of corroded bar in comparison with sound bar; * Indicating confined reinforced concrete; ** Indicating reduction in bond strength of corroded bar in comparison with sound bar after 10 cycles. It should be noted that increasing cycles also cause a reduction in bond strength.

The information collected in Table 2-9, has been graphically presented in Figure 2-7. Figure 2-7, therefore, shows bond strength of corroded to non-corroded steel reinforcement ratio over corrosion percentage based on past published experimental studies. The data have been classified into two groups including confined and unconfined RC samples.

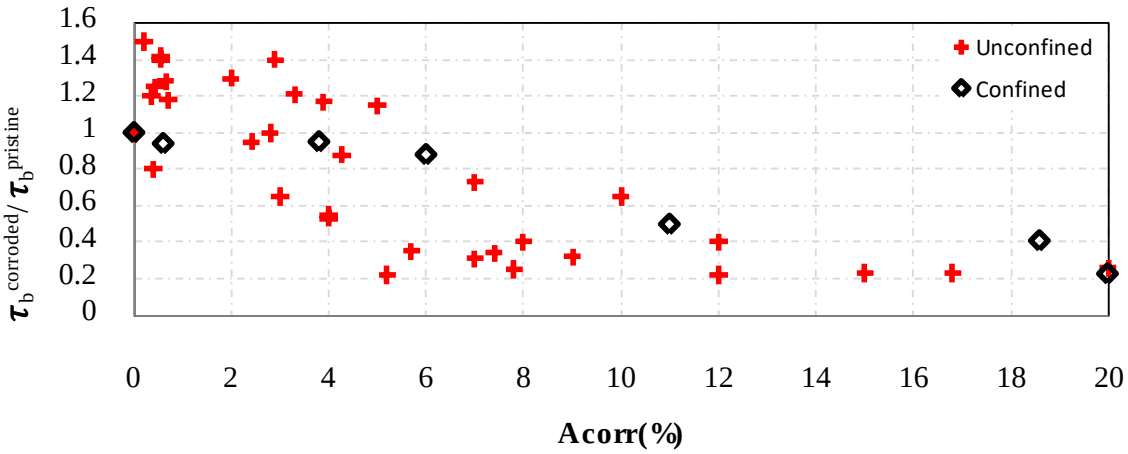

Figure 2-7 The relationship between bond strength of corroded to non-corroded reinforcing steels and corrosion for confined and unconfined RC samples based on collected experimental results

2.3.3 THE EFFECTS OF CORROSION ON STRESS STRAIN MODEL OF CONFINED CONCRETE

As far as confinement is concerned, corrosion of lateral steel bars alters confinement properties of reinforced concrete members. However, there is no evidence indicating how the stress-strain model of a confined concrete changes due to corrosion. Mander et al. (1988b) stated: "Confinement is defined as sufficient lateral reinforcement in the form of the circular or rectangular arrangement of steel." They also stated "the aim is to confine reinforced concrete members under compression to avoid the buckling of longitudinal bars, and to prevent shear failure." Confinement is a critical factor in plastic hinge region, because it ensures the ductility capacity demanded in seismic events. Transversal steel reinforcements are the closest steel bars to the surface of RC members. Therefore they are corroded more severely than longitudinal bars. The effect of corrosion on confinement is very rare and only one report (Ou et al., 2013a) was found on this subject in the literature. (Ou et al., 2013a) analytically calculated confining strength ratio based of corroded steel reinforcing and ultimate strain of confined concrete based on reduction in mechanical properties of reinforcing steels. It is clear further investigation is needed in this area.

2.3.4 THE EFFECTS OF CORROSION ON CONCRETE STRENGTH OF REINFORCED CONCRETE STRUCTURES

As discussed earlier, corrosion causes propagating cracks into concrete core influencing compression and tensile strength of concrete material. A few studies have identified the effects of cracks on tensile and compression strength of concrete materials. Vecchio and Collins (1986), for example, presented the following equation that addresses the effect of cracks on the compressive strength of concrete:

$$f_c^* = \frac{f_c}{0.8 - 0.34\varepsilon_1/\varepsilon_c} \qquad 2\text{-}11$$

Where, f_c^*: compression stress of cracked concrete, f_c: maximum compression stress of non-cracked concrete $\varepsilon_1/\varepsilon_c$: the ratio of principle tensile strain to maximum strain corresponding to maximum compression stress (f_c). It is clear that $\varepsilon_1/\varepsilon_c$ is negative.

The above equation has been improved by following research studies (Vecchio and Collins, 1993, Capé, 1999).

Further investigation is critically needed to identify the effects of corrosion on concrete cracks and consequent concrete strength.

2.3.5 TIME DEPENDENT DETERIORATION MODELS FOR REINFORCED CONCRETE MEMBERS

Corrosion and consequent degradation are time dependent. Therefore, deterioration models are time variant mathematical equations showing relationships between the deteriorated mechanical properties and time. For example, with replacement of A_{corr} with an equation showing relationship between A_{corr} and time, equations 2-4 to 2-9 will be time dependent deterioration models for mechanical properties of reinforcing steels.

There are two different types of deterioration models for RC structures called macro model and micro model. The macro deterioration model has been developed based on growing micro cracks. Growing micro cracks lead to macro cracks and also to accelerated ingress of aggressive ions (Mehta, 1994, Basheer et al., 1996).

The micro deterioration model frequently used in the literature, has been developed based on three models including transport model of aggressive ions, electrochemical model of corrosion and structural model. The structural model can be developed corresponding to decrease of

dimension, reduction in strength or increase of cracks (Basheer et al., 1996). Fick's second law of diffusion is used for ion transport model (Tuutti, 1982). There are a few studies that have been developed on the degradation of reinforced concrete structures due to corrosion (Thoft-Christensen et al., 1996, Vu and Stewart, 2000, Choe et al., 2008, Val et al., 1998).

2.3.6 MAIN RESEARCH GAPS

The main research gaps in corrosion-induced deterioration of RC structures can be summarizes as follows:

- Robust deterioration model for corroded steel reinforcement considering cyclic behavior of steel reinforcement in seismic events
- Robust deterioration model to predict bond between steel and concrete in corroded RC structures
- Corrosion-induced stress-strain model of confined concrete
- Corrosion influence compression strength of concrete

2.4 EVALUATION OF SEISMIC PERFORMANCE OF CORRODED REINFORCED CONCRETE BRIDGE PIERS

According to what has been discussed so far, corrosion degrades mechanical and structural characteristics leading to negative impact on seismic performance of RC structures. Bridge piers are earthquake-resistance elements of bridges. Therefore assessing seismic performance of bridge piers exposed to corrosion is very important. Numerical simulation of corroded bridge piers is very complicated, and a number of uncertainties have limited utilizing the numerical simulation. On the other hand, both numerical and experimental investigations are needed for a comprehensive study called long-term seismic performance of corroded bridge piers. A number of studies have developed methods and formulations to predict initiation and propagation time of corrosion, corrosion cracking time, time of breaking of bond between steel and concrete, minimum load carry capacity, maximum deformation, maximum permeability or failure probability (Bazant, 1979b, Bazant, 1979a, Ng and Moses, 1996, De Brito and Branco, 1996, Enright and Frangopol, 1998, Liang et al., 2002, Biondini and Frangopol, 2008). Then, developing methodologies for performance-based earthquake engineering and developing seismic fragility of bridges made a basis to evaluate seismic performance of RC bridges and other structures using fragility curves based on probability of failure (Moehle and Deierlein,

2004, Moehle et al., 1999, Mander and Basöz, 1999, Gardoni et al., 2002, Shinozuka et al., 2000, Porter, 2003, Matsuki et al., 2006). The seismic performance assessment using fragility function can be applied for either a member or the whole bridge structure. Recently, Akiyama and Frangopol (2013) have presented a procedure to estimate life-cycle seismic reliability of corroded bridge piers based on integration of probabilistic assessment of seismic and airborne chloride hazard. Ou et al. (2013a) have developed a simple seismic evaluation of corroded RC bridges based on nonlinear static pushover analysis. They have presented seismic capacity and demand of the RC bridges in terms of peak ground acceleration (PGA). Actually, the number of years that the seismic demand (collapse PGA) becomes greater than the seismic capacity (design PGA) has been calculated for real RC bridges.

However, as mentioned earlier, difficulties and uncertainties in numerical simulation of RC bridge piers subjected to corrosion and seismic hazards indicating critical needs for further investigation, and advanced numerical methods are needed in this content. The next generations of numerical methods to evaluate seismic performance of corroded RC bridge piers are possibly as follows:

- Developing a new formulation of finite element methods based on fiber element or fiber beam method (Dietz et al., 2012).
- Real-time signal processing and finite element model updating of existing bridges based on vibration and corrosion potential measurements.
- Artificial intelligence methods such as genetic algorithm (Less and Adeli, 2010).

2.4.1 NUMERICAL METHODS TO SIMULATE DEGRADATION OF REINFORCED CONCRETE BRIDGE PIERS EXPOSED TO CORROSION

Numerical methods to simulate seismic behavior of RC bridge piers exposed to corrosion can be classified into three groups including cross-section, member, and system level analysis. This classification is similar to the one applied for non-corroded RC bridge piers. The integration of non-linear analysis and finite element method is a popular numerical method that has been used for corroded and non-corroded RC bridge piers (Less and Adeli, 2010, Lv et al., 2011, Palermo and Pampanin, 2008, Biondini et al., 2013). According to the literature, remarkable results obtained from numerical simulations of seismic behavior of bridges with corroded RC piers can be summarized as follows:

- Corrosion alters mechanism of collapse (Biondini et al., 2013).
- Corrosion decreases load carrying capacity due to increasing seismic demand and decreasing seismic capacity leading to increase of probability of failure (Choe et al., 2009, Ghosh and Padgett, 2010, Simon et al., 2010).
- Corrosion increases uncertainty in probabilistic model-based analysis models (Gardoni and Rosowsky, 2011)

Cross-section level analysis is probably the oldest numerical method among the three methods used to simulate deterioration of RC bridge piers. Corrosion causes damage to concrete material and bond between steel and concrete leading to loss in section ductility. The loss of section ductility can be calculated using moment-curvature analysis (Dagher and Kulendran, 1992, Capozucca, 1995). There are some studies where degradation of RC bridge piers caused by corrosion has been investigated using moment-curvature analysis of cross-section. Seismic capacity of corroded cross-section can be also achieved using the cross-section level analysis (Biondini et al., 2004, Biondini et al., 2006, Biondini et al., 2013, Ghosh and Padgett, 2010).

Member level analysis is a numerical method providing an opportunity to evaluate the seismic performance of whole corroded bridge piers. Finite element formulation is used to simulate seismic behavior of a corroded bridge pier. To this aim, a relationship, for example, between lateral force and displacement is developed (Akiyama et al., 2011). The simulation should take into consideration deterioration models to simulate degradation due to corrosion. Failure modes and seismic response of corroded RC bridge piers can be obtained from the member-level analysis.

System level analysis is aiming to assess dynamic response of a corroded bridge exposed to ground motions. There are a number of studies in the literature where the system level analysis of corroded bridges has been done using fragility estimation (Choe et al., 2008, Choe et al., 2009, Ghosh and Padgett, 2010, Simon et al., 2010, Kumar and Gardoni, 2011). However, Lv et al. (2011), for example, have evaluated the effects of corrosion on seismic performance of curved beam with height piers using time-history analysis of the bridge finite element model. They found that corrosion deteriorates the seismic performance of the bridge, and two main factors including pier-height and pier-corrosion are responsible for increasing plastic strain.

2.4.2 LARGE SCALE EXPERIMENTAL TESTS TO EVALUATE SEISMIC PERFORMANCE OF CORRODED BRIDGE PIERS

As mentioned earlier, numerical simulations of corroded bridge piers are very complicated and they probably cannot capture all the effects of corrosion on seismic performance of bridge piers. Therefore, large scale experimental tests need to assess seismic performance of corroded bridge piers. Some studies have been reported on the effects of corrosion on cyclic behavior of RC columns (Ma et al., 2012, Meda et al., 2014). However, according to the best knowledge of the authors large scale seismic experimental test on corroded bridge piers is rare and only one case (Dietz et al., 2012) was found in the literature. Dietz et al. (2012) designed a reinforced concrete bridge pier to EC2. They corroded the bridge piers using accelerated corrosion technique by ponding a part of the pier in NaCl solution for 6 months and applying current electricity, and loaded lateral cyclic up to 50kN using hydraulic actuator. They measured deflection at the top, rotation at the base, strains in the concrete and steel bars and width of cracks. From a structural point of view, the bridge pier rigidly connected to the foundation is high damage system because formation of plastic hinge at the end(s) of the pier is the mechanism of dissipating energy in seismic events. The high damage system is the traditional seismic resistant system that has been criticized by past studies because of high repair time and cost and problems arising from traffic interruption (Palermo and Mashal, 2012).

2.5 SEISMIC, STRUCTURAL AND DURABILITY BEHAVIOR OF REPAIRED BRIDGE PIERS EXPOSED TO CORROSION-INDUCED DAMAGES

The need for retrofit of corroded bridge piers has been addressed by past studies. There is a traditional method to rehabilitate corroded bridge pier including two stages: first, all critically corroded areas should be removed then an overlay of materials with low-permeability have been used (Weyers et al., 1993, Vaysburd and Emmons, 2000). Gergely et al. (1998) rehabilitated corroded bridge pier samples using fiber-reinforced plastic composites. They compared seismic performance of the piers through numerical and large-scale experimental tests and found that shear capacity and ductility have been improved significantly. However to simulate the effect of corrosion on steel reinforcement, they cut three stirrup loops of column and three stirrup loops of each side of the cap-beam near the joint. They noted that an advantage of using FRP composite

is that it doesn't increase weight of column. Toutanji (1999) has found that the confinement provided by FRP warps improves compression strength and ductility of RC columns. However, durability is affected by the type of epoxy used. Demers and Neale (1999) have showed that type of FRP influences ductility and strength of RC columns. Pantazopoulou et al. (2001) compared alternative methods to assess seismic performance of repaired corroded bridge piers using external fiber-reinforced polymer (FRP) wraps. They stated that the best repair strategy in terms of post repair corrosion, strength recovery and ductility was cleaning the damaged surface (without removal of materials) then jacketing using layers of FRP. However, further experiments are needed to confirm the efficiency of the proposed strategy in practice. Baiyasi and Harichandran (2001) have concluded that a greater amount of glass fiber than carbon fiber was needed to achieve the equivalent structural performance of post-corrosion repair. Teng et al. (2003) have reported while FRP increases durability characteristics of RC columns, it possibly has some negative impacts on mechanical properties of the RC columns. A number of studies have revealed that FRP doesn't fully stop chloride-induced corrosion, but decreases the rate of corrosion (Berver et al., 2001, Debaiky et al., 2002, Pantazopoulou et al., 2001, Mullins et al., 2001, Wootton et al., 2003, Sen, 2003, Baiyasi and Harichandran, 2001, Green et al., 2006, Gadve et al., 2009, Lee et al., 2000, El Maaddawy et al., 2006). To answer an important question of what the best strategy is to repair corroded bridge pier using FRP? Sen (2003) stated that the best strategy to protect concrete columns against chloride-induced corrosion is applying FRP jackets and filling gaps between the column and jackets using epoxy so that following conditions satisfy:

- Applying FRP jacket over the full length when no visible corrosion-induced sign can be found.
- Utilizing appropriate epoxy as a surface corrosion barrier and to fill gap between the column and jacket.
- Utilizing at least two layers of FRP

Sen (2003) has argued that confined concrete by FRP warps changes corrosion diffusion. He also has recommended to not using FRP warps before visible corrosion sign to minimize repair cost. Wootton et al. (2003) have concluded that FRP warps protect the RC columns better than that of epoxy alone. It has been shown that low amount of corrosion (up to 4.2%) does not influence eccentric load carrying capacity of RC columns, and the strength of damaged columns fully warped with carbon FRP was higher than undamaged columns. The performance of full

length covered by CFRP was better than that of partially covered by CFRP (Maaddawy, 2008). Li et al. (2009) have analyzed seismic performance of corroded RC columns confined by FRP and steel jacket. They showed that FRP and steel jacket enhance the seismic performance of RC columns, and applying both jackets improves seismic performance better than applying one alone. A recent survey carried out on corroded RC bridges in New York state, emphasized the demand for retrofitting corroded RC bridge columns, in particular, corroded lap-splice, to decrease possible damages in future seismic events (Aboutaha et al., 2013).

2.5.1 DEVELOPMENT IN TIME-DEPENDENT SEISMIC EVALUATION OF CORRODED RC BRIDGE PIERS REPORTED IN THE LITERATURE

Traditional structural analysis is not able to analyze systems and structures under multiple time-invariant hazards. A time-dependent analysis during lifetime, therefore, is needed to take into consideration all hazards. In case of RC structures (in particular RC bridge pier) subjected to corrosion and earthquake, two hazards are corrosion-induced deterioration and seismic events. There are some studies in the literature, mainly published in recent years, showing that corrosion influences the seismic performance of bridge piers over time. However, different criteria have been used by past studies. Biondini et al. (2006), for example, have presented time dependent bending moment resistance of a bridge pier exposed to corrosion. They have shown that the bending moment resistance of the corroded bridge pier decreased over time. Time-dependent deformation capacity, drift ratio demand, shear capacity and demand of a corroded bridge pier have been studied (Choe et al., 2008, Choe et al., 2009, Zhong et al., 2012). Time-dependent probability of failure (time-dependent fragility analysis) of corroded bridge piers have been developed by past studies that can be directly used for seismic analysis purposes (Choe et al., 2008, Choe et al., 2009, Ghosh and Padgett, 2010, Alipour et al., 2010, Zhong et al., 2012, Choe et al., 2010). Moreover, a fragility increment function has been developed that is a function of time and given deformation or shear demand, and can be used to predict fragility of corroded bridge piers in life-cycle analysis and risk assessment (Choe et al., 2010, Gardoni and Rosowsky, 2011).

2.6 RESEARCH GAPS

The main research gaps in Evaluation of seismic performance of corroded reinforced concrete bridge piers can be summarizes as follows:

- Robust numerical modeling of corroded bridge piers.
- Large scale experimental tests on seismic behavior of corroded bridge piers and bridge structures (half scale and full scale tests).
- Experimental tests on efficiency of repair methods used for corroded bridge piers.
- Robust numerical model to evaluate time dependent seismic performance of RC bridges exposed to corrosion.

In this chapter chloride-induced corrosion, the effects of corrosion on structural and mechanical properties of RC structures or elements and seismic performance of corroded RC bridge pier have been reviewed. To meet this aim, a large number of published papers with all their experimental and numerical details have been collected and reviewed. From the present literature review, the following main conclusions are drawn:

(1) The results of published papers represented in this chapter have been obtained from samples or structures mainly utilizing ordinary Portland cement material, and the behavior of upcoming and more recent cement materials need further investigations.

(2) Damage prediction of RC structures due to chloride-induced corrosion significantly depends on estimation of important input parameters such as: corrosion rate, critical content, limit step to start pitting corrosion and corrosion-induced cracking. However, results reported by past studies exhibit critical problems including contradictory results, uncertainty in experimental techniques and reported results. Moreover, the obtained results cannot be transferred to real structures. Therefore, further investigations are needed in these areas.

(3) More reliable deterioration models are highly demanded for seismic evaluation and analysis of corroded RC structures. On the other side, the deterioration models have been mainly developed for artificial corroded samples, while the relationship between natural and artificial corrosion in many aspects is unknown. Hence this area is an important direction of research.

(4) Seismic analysis of corroded RC structures (in particular bridge piers) is very complicated, and many uncertainties limit utilizing of numerical methods. Hence developing more recent numerical methods and large scale experimental tests are needed for the analysis of RC structures under multiple hazards (corrosion and earthquake).

(5) While few researchers based on their modelling have already started to build fragility

functions to be integrated in a lifetime seismic performance framework, however still many gaps need to be covered in testing and modelling.

(6) Long-term seismic performance of RC bridge pier exposed to chloride incorporates the three main sub-areas reviewed in sections 2 to 4 in this chapter aiming at development of the following steps that are in common with LCA of corroded RC bridge piers:

- Time-dependent deterioration models
- Time dependent seismic performance of corroded structure

3 MODELLING THE INFLUENCE OF PITTING CORROSION ON THE MECHANICAL PROPERTIES OF STEEL REINFORCEMENT

3.1 INTRODUCTION

Chloride induced corrosion of reinforcing steel in concrete is one of the major causes of premature deterioration in infrastructure, resulting in considerable maintenance costs and vulnerability against seismic events. Chloride induced corrosion often leads to the development of localized pits in the reinforcing steel. This localized corrosion can cause significant reduction in cross section area of steel bars affecting the safety and performance of reinforced concrete (RC) structures [1].

Faraday's law provides a relationship between corrosion current density and mass loss. Assuming uniform corrosion, a corrosion current density, $i_{corr} = 1\,\mu A/cm^2$, will result in 11.6 $\mu m/yr$ loss of cross section [2]. There are three time-dependent models available to calculate the corrosion related reduction in the cross sectional area of steel bars. The first and third models have been developed for general and pitting corrosion respectively using a constant value of corrosion rate. However, the second model has been developed for general corrosion using a time dependent corrosion rate. The first model presented in the literature estimates a constant value of corrosion rate based on the average deterioration of reinforcement in concrete [3]. The time-dependent diameter of reinforcement bars the first model is as follows [3]:

$$D(t) = D_0 - C_{corr} \times t \times i_{corr} \qquad 3\text{-}1$$

Where $D(t)$ (mm) is the diameter of the corroded bar at time t; D_0 (mm) is the diameter of non-corroded bar; C_{corr} is a corrosion coefficient; t (years) is time after corrosion starts; i_{corr} ($\mu A/cm^2$) is the corrosion rate.

The second model is based on a time-varying corrosion rate which employed the time-dependent corrosion rate developed by researchers [4-5]. It was showed that the corrosion rate is not constant, and they suggested a time-dependent corrosion rate (see Equation 3-3) [5].

The third model has developed for pitting corrosion build up on the constant value of corrosion rate based on the average deterioration of reinforcement in concrete (see Equation 3-2) [6]. However, past studies indicate that the rate of corrosion decreases over time due to the formation

of corrosion products around the bar causing impedance of the diffusion of iron ions [4-5].

Corrosion alters the effective mechanical properties of the reinforcing bar. To quantify the reduction in mechanical properties due to corrosion, reduction factors have been proposed by researchers. A number of monotonic tensile tests on corroded steel bare bars (corroded by exposure to the environment or using accelerated corrosion) have been carried out to estimate the reduction factors corresponding to the effective mechanical properties [7-16]. Beam bending tests have also been carried out in past studies to estimate the reduction factors [11, 16]. To produce the corrosion of reinforcing bars in the previously mentioned tests, three different methods have been employed. The first method for producing corrosion is to let the samples naturally corrode in open air [7, 8, 10, 12, 16, 17]. The second method is to use accelerated corrosion, which has the benefit of reduced corrosion time, [9, 13, 14, 15, 16, 17, 18, 19, 20]. Finally the third method of producing pitting corrosion is to simulate pit cavities by direct mechanical removal of material [13].

Despite the number of studies on the effects of corrosion on the effective mechanical properties of steel, there is a large variation in the results of the studies for the same amount of corrosion, and very few studies have been carried out on pitting corrosion. This indicates that there is a need to investigate the effects of pitting corrosion on the effective mechanical properties of reinforcing steel.

A number of studies have numerically investigated the effects of pitting corrosion on the reliability of concrete structures, where pitting damage has been modeled as hemispherical cavities [1, 6, 21]. However, only one study has experimentally simulated pit corrosion as a mechanically produced cavity [13]. It should be noted that Cairns et al [13] produced hemispherical groves in the bars where the pit depth was less than the milling radius. Most numerical studies however assume the center of the pit is located on the circumference of the bar as was done in the current investigation.

In this chapter, the expermental and analytical work was carried out to extend the existing data base and advance underastanding the effects of pitting corrosion on tensile behaviour and the effective mechanical properties of steel reinforcement. The analytical model was developed to study the effects of pitting corrosion on the overal tensilr behavior of corroded steel reinforcement, whseas the experimental tests were designed to valdate the analytical model and to underastand the effects of key parameters of pitting corrosion on the effective mechanical properties of corroded reinforcing steel.

The current work provides an estimate for pit depth based on a time-dependent corrosion rate model. The effects of pit depth on the cross section parameters, tensile behavior, and mechanical properties of reinforcing steel subject to static tensile loading is determined for a range of pit depths and reinforcing bar diameters. Finally, the experimental results have been used to develop reduction factors and deterioration models for pit corroded steel reinforcement. The results from this work can be used to help evaluate the life-time seismic and structural performance of reinforced concrete structures subjected to pitting corrosion.

The experimental results of this study were used in chapter 5 to estimate the effective mechanical properties (Eq. 5-9 and 5-13) of transverse reinforcement of pitting corroded RC column subjected to axial compression.

3.2 TIME-DEPENDENT PIT DEPTH BUILD UP ON DURABILITY PARAMETERS

Assuming hemispherical pits, the maximum pit depth can be related to the corrosion current density as follows [6]:

$$p(t) = 0.0116 \times R \times i_{corr} \times t \qquad 3\text{-}2$$

Where, $p(t)$ is the maximum pit depth (mm), R is pitting factor, i_{corr} is corrosion current density ($\mu A/cm^2$), and t is time after corrosion initiation (years). The pitting factor is the ratio of maximum pit depth to average corrosion penetration. The average corrosion penetration can be calculated based on knowing the mass loss due to corrosion and estimating the equivalent diameter of the corroded bar [22].

To account for the variation in corrosion rate over time, the time-dependent corrosion density $i_{corr}(t)$ can be represented as follows [5]:

$$i_{corr}(t) = i_{corr}(1) \times 0.85 \times t^{-0.29} \qquad 3\text{-}3$$

Where the corrosion current density, $i_{corr}(1)$ ($\mu A/cm^2$), is the predicted corrosion at the start of corrosion initiation, which can be represented as [5]:

$$i_{corr}(1) = \frac{37.8 \times (1 - {}^{w}/_{c})^{-1.64}}{d} \qquad 3\text{-}4$$

Where ${}^{w}/_{c}$ and d (mm) are the durability parameters of water to cement ratio and concrete cover.

The estimated corrosion rate for reinforcing steel in concrete provided in Equation 3-4 is given for purely illustrative purposes. It is well known that there are a number of additional factors which influence the rate of corrosion including binder type and resistivity [23]. Actual in service corrosion rates will vary considerably not only between structures but also for any given structure over the course of a year due to temperature and moisture effects.

Assuming a time-dependent corrosion rate and having a pit in each investigated cross section, Equations 3-5 and 3-6 show differential pit depth and maximum pit depth respectively.

$$dp(t) = 0.0116 \times R \times i_{corr}(t) \times dt \qquad 3\text{-}5$$

$$p(t) = \int_0^t 0.0116 \times R \times i_{corr}(t) \times dt \qquad 3\text{-}6$$

By considering Equations 3-3 and 3-4, Equation 3-6 can be expressed as:

$$p(t) = \frac{0.0116 \times R \times 37.8 \times (1 - {}^{w}/_{c})^{-1.64} \times 0.85}{d} \int_0^t t^{-0.29}\, dt \qquad 3\text{-}7$$

Finally, the time-dependent pit depth can mathematically be represented as:

$$p(t) = \frac{0.525 \times R \times (1 - {}^{w}/_{c})^{-1.64}}{d} \times (t)^{0.71} \qquad 3\text{-}8$$

The pitting factor R typically varies from 4 to 8 for natural corroding steel and from 5 to 13 for steel subjected to accelerated corrosion technics [24]. If the pitting factor of 7 is assumed for a 25 mm diameter reinforcing steel, and 10 years have passed after corrosion initiation ($t = 10$ years), Equation 3-8 can be graphically represented in Figure 3-1 clearly shows that the pit depth increases with an increase of water to cement ratio and increases with a reduction in concrete cover.

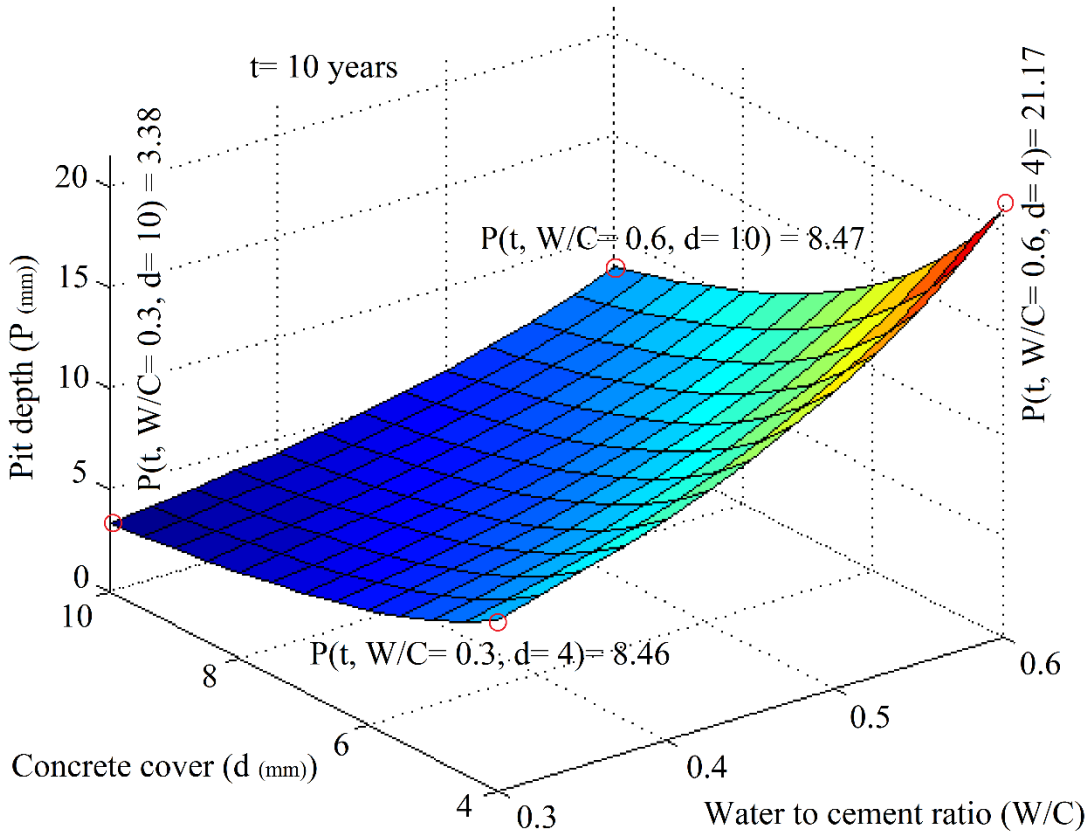

Figure 3-1 The effects of concrete cover and water to cement ratio on pit depth

3.2.1 THE EFFECTS OF PIT CAVITIES ON CROSS SECTION PARAMETERS AND TENSILE BEHAVIOR OF STEEL BARS

The cross sectional area, centroid location, and moment of inertia of the corroded section are the main geometrical characteristics of the cross section of steel reinforcement which are affected by the pitting of steel reinforcement. To evaluate the effects of pit damage on the cross section parameters, Equation 3-8 has been employed. The values of 10 mm and 0.5 were assigned to concrete cover and w/c respectively. As previously noted the pitting factor is not constant and varies from approximately 4 to 13 depending on the corrosion conditions [24]. Past studies found that the pitting factor rises with an increase in steel bar diameter [1]. In this chapter, pitting factors estimated by past studies have been utilized [1]. Therefore, a pitting factor of 5.65, 6.2 and 7 has been employed for D10 mm, D16 mm and D25 mm reinforcing steel respectively. Hence, the only variable in right hand side of Equation 3-8 is time. Based on the assigned values, Equation 3-8 is graphically represented in Figure 3-2 and compares pit depth over time for 10 mm, 16 mm and 25 mm reinforcing steel. The graph shows that the pit depth increases over time, and that the pit depth increases with increasing bar diameter.

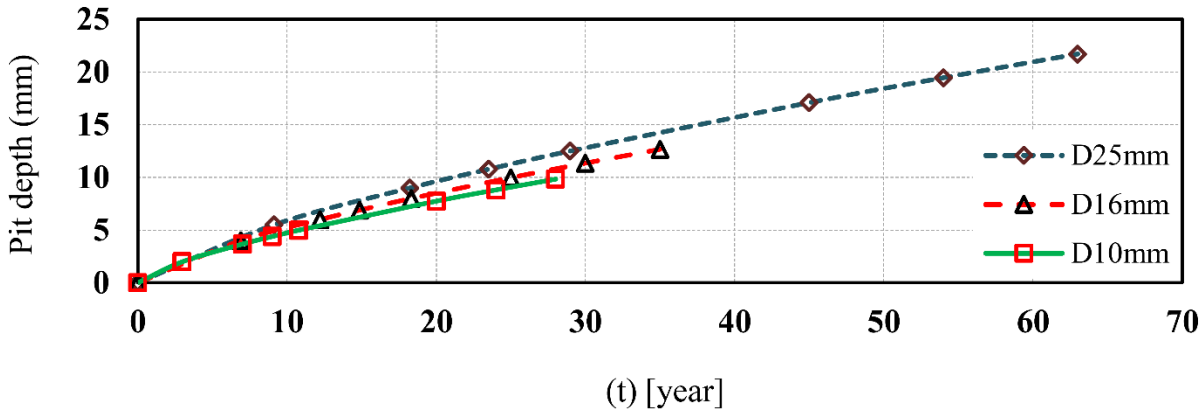

Figure 3-2 Growing pit depth over time after corrosion initiation

The assumption that the pits are of hemispherical form is common in the analytical modeling of pitting corrosion [1,6]. For this type of pit the relationship between pit width, $b(t)$ (in mm), and pit depth, $p(t)$ (in mm) is as follows:

$$b(t) = 2p(t)\sqrt{1 - \left(\frac{p(t)}{D_0}\right)^2} \qquad 3\text{-}9$$

Where D_0 = non corroded diameter of steel reinforcement (mm).

Figure 3-3 and Figure 3-4 compare the change of pit width and depth over time respectively for 10 mm, 16 mm and 25 mm reinforcing steel. As expected, the pit width increases with growth of pit depth reaching a maximum value that is equal to the non-corroded diameter of the steel bar. If corrosion of the reinforcing steel continues beyond this point the apparent pit width begins to decrease despite the increase in the depth of the pit. At this point very little cross sectional area is left of reinforcing steel.

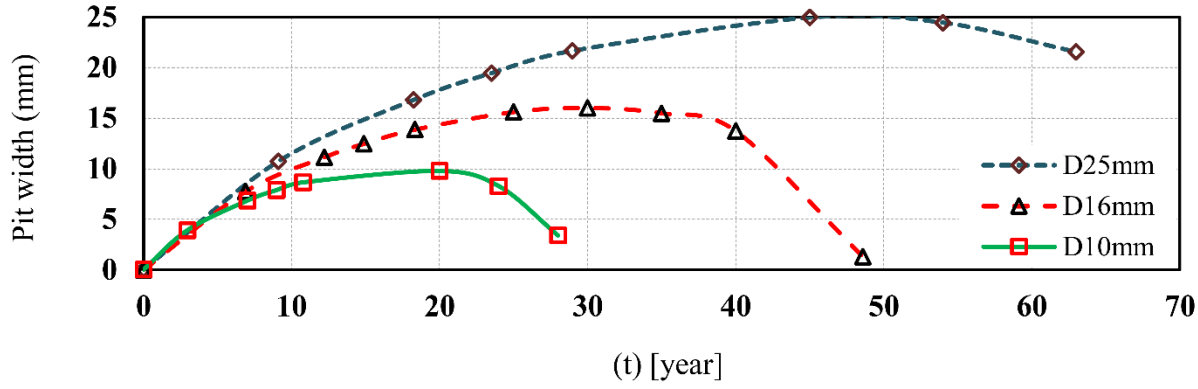

Figure 3-3 Changing pit width over time after corrosion initiation

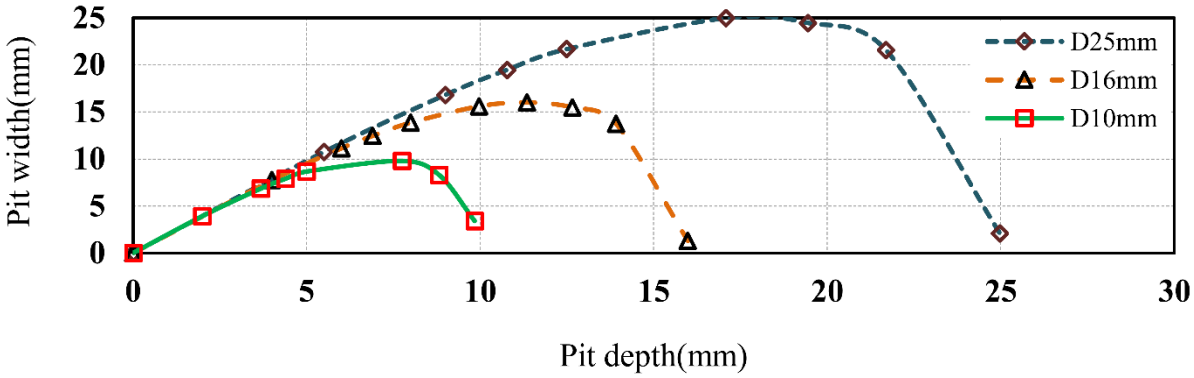

Figure 3-4 Pit depth- pit width relationship for 10mm, 16mm and 25mm steel reinforcement

As mentioned earlier, the hemispherical form of the pits have been assumed such that the center of the pit is located on the surface of the steel bar. Therefore, the time-dependent corroded area, $A_{pit}(t)$ (mm^2), due to pitting corrosion is mathematically expressed as:

$$A_{pit}(t) = \begin{cases} \frac{R^2}{2}(\theta_1 - \sin\theta_1) + \frac{(p(t))^2}{2}(\theta_2 - \sin\theta_2) & p(t) < \sqrt{2}R \\ \frac{R^2}{2}(2\pi - \theta_1) + p(t)\sqrt{1 - \left(\frac{p(t)}{2R}\right)^2} \times R \times \sin\left(\frac{\pi - \theta_1}{2}\right) + \frac{(p(t))^2}{2}(\theta_2 - \sin\theta_2) & \sqrt{2}R \le p(t) < 2R \\ \pi R^2 & p(t) \ge 2R \end{cases} \quad 3\text{-}10$$

Where:

$$\theta_1 = 2 \times \sin^{-1}\left(\frac{b(t)}{2R}\right) \quad 3\text{-}11$$

$$\theta_2 = 2 \times \sin^{-1}\left(\frac{b(t)}{2p(t)}\right) \quad 3\text{-}12$$

And $R = \frac{D_0}{2}$ is radius of non-corroded reinforcing steel.

Figure 3-5 shows the hemispherical pit geometry and all the variables of Equation 3-10. The area of pit cavity, A_{pit}, has been illustrated with light gray color.

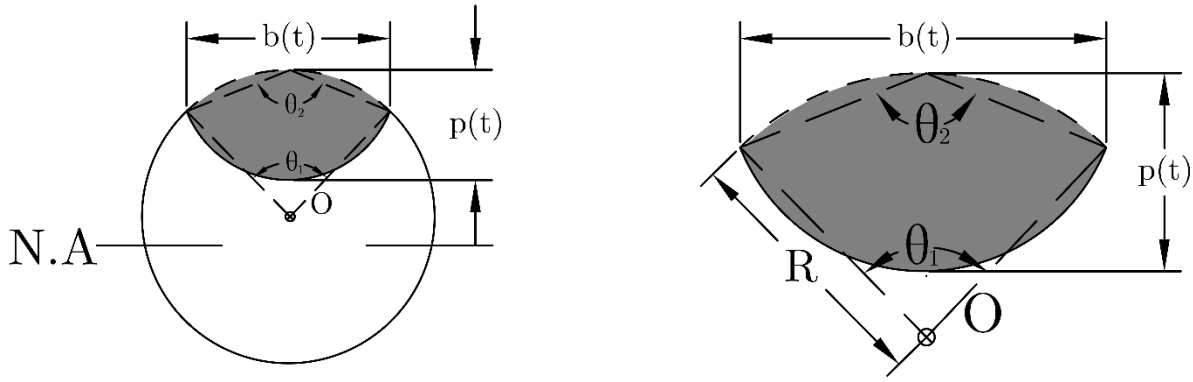

Figure 3-5 Configuration of pit and variables of pit cavities

Putting Equations 3-8 and 3-9 in Equation 3-10, the normalized decrease of cross section over time for 10 mm, 16 mm and 25 mm steel reinforcing has been compared in Figure 3-6. Increasing pit depth over time decreases the cross sectional area. As can be seen in the graph, more time is required to corrode the cross sectional area of a steel bar with greater diameter when compared to a bar of smaller diameter.

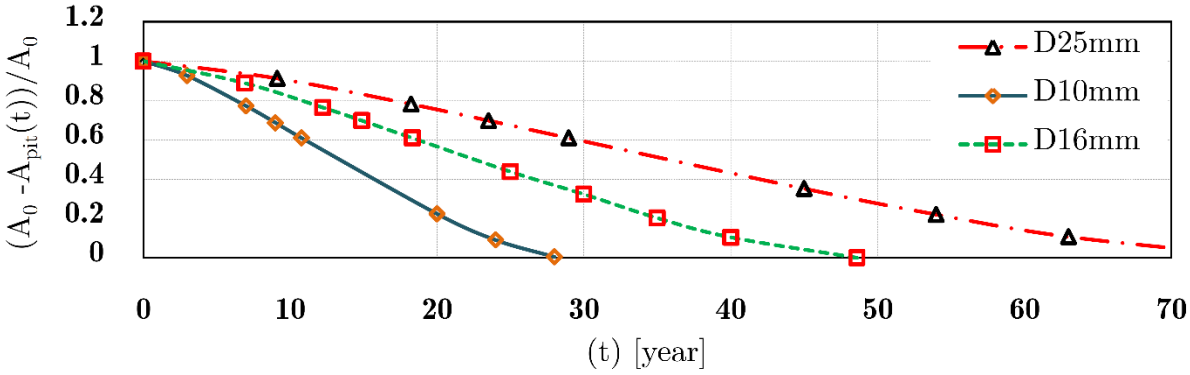

Figure 3-6 Normalized decrease of cross section for 25mm, 16mm and 10mm pitting corroded steel bar

The cross sectional centroid of a round bar is located in the center of the circle. When pitting corrosion occurs and grows the location of the centroid alters continuously leading to change of cross sectional moment inertia and the geometrical parameters of the corroded cross section. In fact, the centroid relocation is the distance between the neutral axis of the corroded section and center of non-corroded circle. Figure 3-7 shows the values of centroid relocation of corroded 16 mm steel reinforcing for 4 mm, 6 mm and 8 mm pit depth. It is clear that the centroid relocation, Δc, of the corroded steel bar increases with increasing pit depth. Center of the reinforcing bars before damage (O), and the neutral axis of damaged cross sections (N.A.) have been shown. Figure 3-7 also compares the values of h_{PB}, h_{PF} and the relationship between I_{pit} and $I_{pristine}$

for a pitting corroded D16 mm steel reinforcing bar. Where $I_{pristine}$ is the second moment of area of the non-corroded cross section about the axis crossing point O. Figure 3-7 clearly shows that as the pit depth increases both h_{PB} and h_{PF} decrease, and the ratio of h_{PF}/h_{PB} increases.

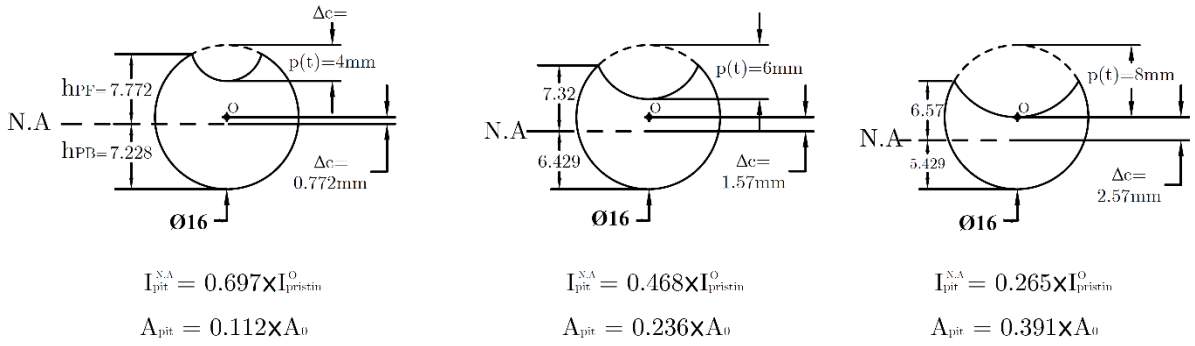

Figure 3-7 Cross section parameters and centroid relocation of pitting corroded steel bars for 4mm, 6mm and 8mm pit depth

Figure 3-8 has compared relocation of centroid, Δc (in mm), for pitting corroded 10 mm, 16 mm and 25 mm steel bars over time and over pit depth separately. The graphs show that the centroid relocation corresponding to specific pit depths or time, inversely, depends on the diameter of steel reinforcement.

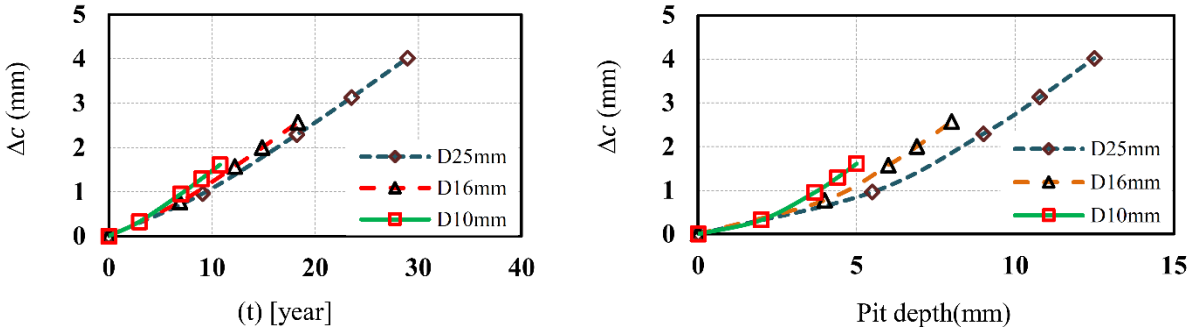

Figure 3-8 Centroid relocation of pitting corroded steel bars; (left): over time (right): over pit depth

Assume that a sample of steel reinforcement is subject to a tensile load (F) applied at point O. It is obvious that the sample has fix end boundary conditions. The magnitude of the bending moment is dependent on both the magnitude of the tensile force and the amount of centroid relocation. The relationship between the bending moment generated by pitting and the applied tensile force can be mathematically represented as follows:

$$M_{pit} = F \times \Delta c \qquad 3\text{-}13$$

Where, M_{pit}, is the bending moment in the corroded cross section, F is the tensile force, and Δc is the centroid relocation of the cavity formed by pitting.

Due to eccentricity of the axial force at the damaged section, tensile forces are generated on the side of the cross-section corresponding to pit damage, called the pit face side; and compression forces are generated in the back side of the pit damaged cross-section, called pit back side. Therefore, the maximum elastic strain in the pit back side and pit face side at the damaged cross section can be calculated as follows:

$$\varepsilon_{max}^{C} = \frac{F}{E(A_0 - A_{pit})} - \alpha \times \frac{F \times |\Delta c| \times |h_{PB}|}{EI_{Pit}} \quad 3\text{-}14$$

$$\varepsilon_{max}^{T} = \frac{F}{\mathrm{E}(A_0 - A_{pit})} + \alpha \times \frac{F \times |\Delta c| \times |h_{PF}|}{EI_{Pit}} \quad 3\text{-}15$$

Where: ε_{max}^{C} is the maximum elastic strain at the pit back side, ε_{max}^{T} is the maximum elastic tensile strain at the pit face side; $A_0 - A_{pit}$ is the remaining area of the corroded cross section; A_0 is the cross sectional area of non-corroded reinforcing steel; E is module of elasticity; α is a cofficient depending on end conditions the sample, geometrical parameters of the sample and pit relocation; I_{Pit} is the second moment of area of the corroded cross section about the neutral axis (N.A); h_{PB} is the distance between the neutral axis, and the farthest point on the pit back side; h_{PF} is the distance between the neutral axis, and the farthest point on the pit face side. It is important to note that other than the parameter F, all other parameters in Equations 3-14 and 3-15 are dependent on pit depth. Therefore, theses Equations are time-dependent due to pit depth being time-dependent after corrosion initiation. It should also be noted that the maximum elastic strain in non-corroded reinforcing steel is mathematically represented as follows:

$$\varepsilon_0 = \frac{F}{EA_0} \quad 3\text{-}16$$

Where ε_0 is the maximum elastic strain in non-corroded reinforcing steel.

Figure 3-9 is a schematic, showing, the relationship between centroid relocation due to pitting corrosion of a bar under axial tensile force and its effect on the induced bending moment depending on different boundary conditions. Figure 3-9a shows the bending moment diagram of the corroded bar when the sample has free rotation end conditions, whereas 9b shows the bending moment diagram for the same bar but with fixed rotation end conditions. Both cases have M_{pit} in common that depends on centroid relocation and pit depth. However, the values of bending moment at the pit location and non-damaged parts are different. The boundary condition corresponding to reinforcing steel samples in tensile tests, and bare bars in real structures (such as, dissipaters in rocking systems or un-bonded post-tensioned steel bars) are fixed rotation end conditions. Therefore their schematic bending moment diagram is similar to 9b.

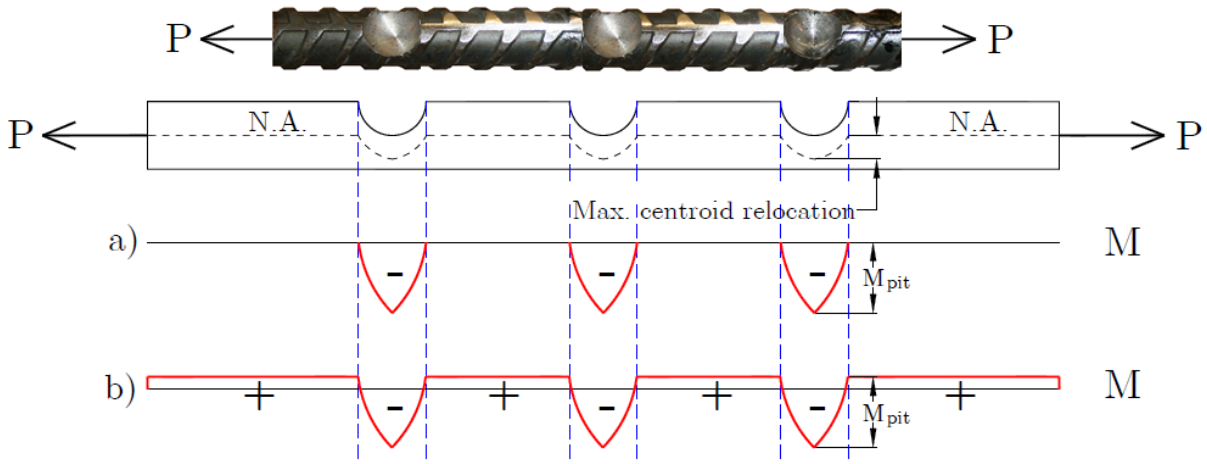

Figure 3-9 Photo of pit damaged bar and the model of centroid relocation in pit locations and pit induced bending moment depending on boundary conditions; a) free rotating ends b) fix rotating ends

Figure 3-10 compares two parameters as a function of pit depth for different diameters of reinforcing steel. The first parameter is the ratio of the second moment of area of the corroded cross section about the N.A axis to the second moment of area of the non-corroded cross section about the horizontal axis crossing point O. The second parameter is the ratio of the maximum distance between the neutral axis and farthest point on the pit face side to the maximum distance between the neutral axis and farthest point on the pit back side. While the graphs show that pit depth growth causes a decrease in $I_{pit}^{N.A}/I_{pristine}^{O}$ and an increase of h_{PF}/h_{PB} ratio, both changes are more significant for smaller diameter when compared with greater diameter bars for a specific time or pit depth. Figure 3-11 compares the two aforementioned parameters as a function of pit depth normalized by reinforcing bar diameter for different sizes of reinforcing steels. Comparing the graphs presented in Figure 3-10 with corresponding graphs shown in Figure 3-11, reveals that the overall trends are similar, but the graphs presented in Figure 3-11 are independent of steel bar diameter. A given pit depth results in different loss of cross section percentage for different diameter sizes of bars. However when pit depth is normalized to the non-corroded bar diameter, certain $p(t)/D_0$ ratio for different diameter sizes of bars is associated to the same loss of cross section percentage. The two parameters presented in Figure 3-11 and Figure 3-12 are dependent on loss of cross section percentage not on diameter size of steel bars.

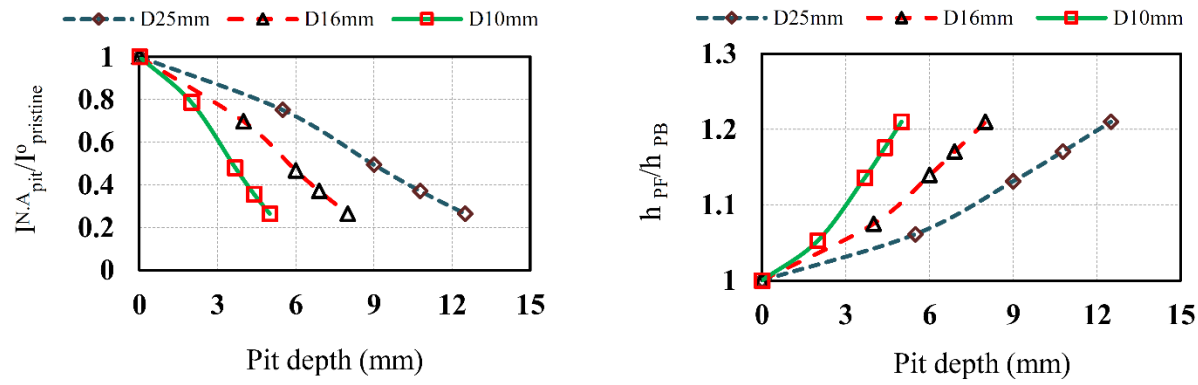

Figure 3-10 (left): $I_{pit}^{N.A}/I_{pristine}^{O}$ over $p(t)$, (right): h_{PF}/h_{PB} over $p(t)$

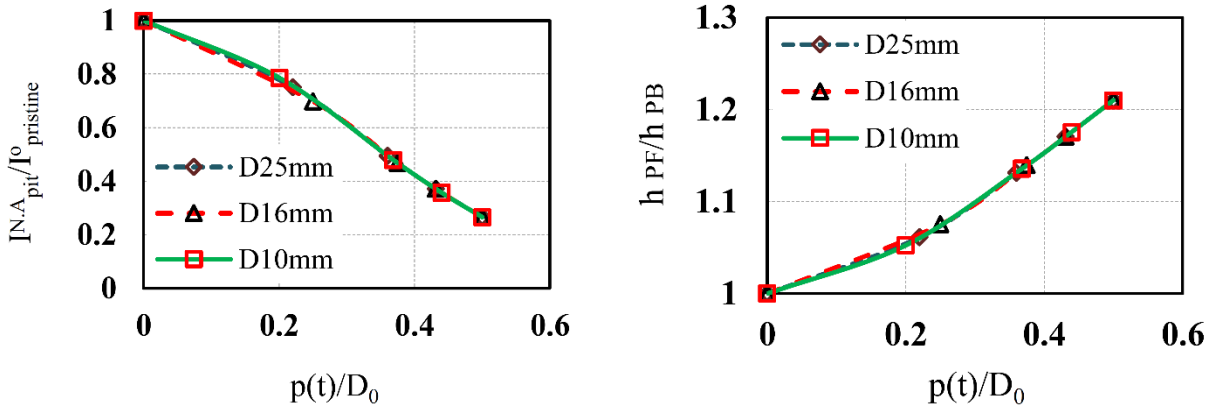

Figure 3-11 (left): $I_{pit}^{N.A}/I_{pristine}^{O}$ over $p(t)/D_0$, (right): h_{PF}/h_{PB} over $p(t)/D_0$

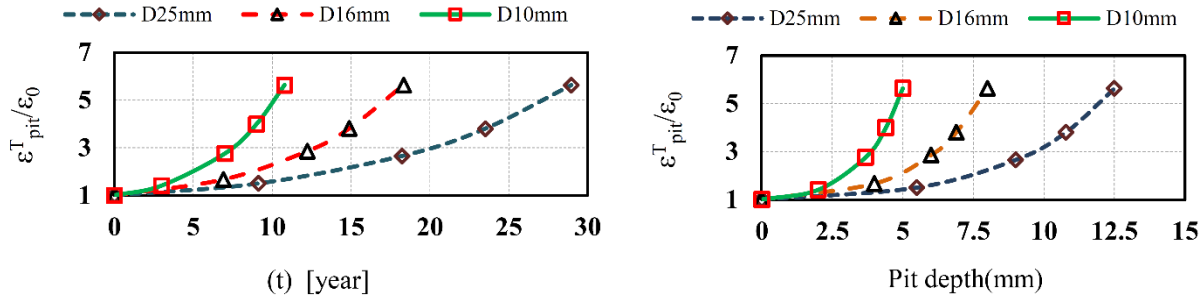

Figure 3-12 Normalized change of maximum elastic strain in pit location on pit face side over; (left): time (right): pit depth

The effects of pitting damage on the change of maximum elastic strain at the pit location for non-corroded and corroded bars have been analytically investigated. However, it should be noted that only the free rotation end condition has been taken into consideration in the analytical model. Figure 3-12 and Figure 3-13 compare the ratio of the change of maximum elastic strain

of corroded to non-corroded bars as a function of time and pit depth for different sizes of reinforcing steels for the pit face and the pit back side respectively. The maximum elastic straines have been calculated using Equations 3-14 to 3-16. As expected, the graphs show an increase of normalized maximum elastic strain at the pit face side and a decrease of normalized maximum elastic strain at the pit back side. This is because the eccentric tensile force causes a bending moment which leads to tensile strain at the pit face side and compression strain at the pit back side at the section of pit damage.

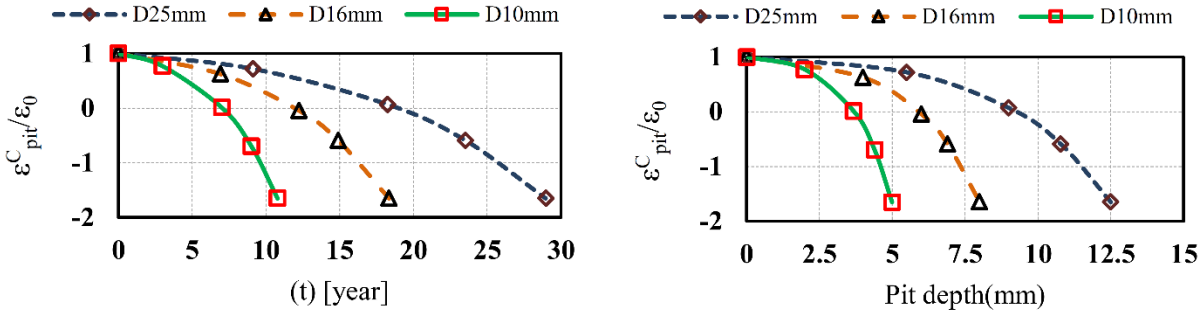

Figure 3-13 Normalized change of maximum elastic strain in pit location on pit back side over; (left): time (right): pit depth

The results show when the pit depth approximately reaches 3.7 mm, 6 mm and 9.1 mm for 10 mm, 16 mm and 25 mm steel bars respectively, the maximum elastic strain at the pit back side is zero ($\varepsilon^C_{max} = 0$). On the other hand, with a further increase of pit cavity depth the elastic strain at the pit back side becomes negative.

3.3 EXPERIMENTAL PROGRAM

The experimental program consisted of two phases: simulation of pit cavities, and monotonic tensile testing. Pit damage was artificially induced by machining hemispherical cavities in the steel. Three different pit depths were selected for each diameter size of steel reinforcement. Deformed 10 mm, 16 mm and 25 mm grade 300 steel reinforcement was studied in this research. In reality pitting corrosion is distributed on the steel reinforcement surface, so the effects of spatial variability on the behavior of reinforcing steel needed to be considered. A procedure has been presented to consider the effects of spatial variability of pitting damage on structural fragility and reliability [25]. In this chapter, the same procedure has been employed to take into consideration the effects of spatial pitting corrosion on the behavior of corroded steel bars subject to tensile load. To meet this aim, the gauge length of the samples has been divided to 100

mm lengths. One pit was modeled in the middle of each 100 mm length, because past studies have suggested that the length of each element containing a pit defect should be greater than two bar diameters but no more than 100 mm [21]. All pits simulated on a sample have identical geometry to investigate the effects of pit depth on the mechanical properties of steel reinforcement. Therefore, three pits with the same pit depth on each 300 mm length gauge bar were fabricated. The three pits were located on the same face of the bar to simulate natural corrosion of reinforcing steel in concrete [26]. Having six samples for each pit size on each diameter size of steel reinforcement, 54 samples in total were prepared. The three pit sizes were selected corresponding to low, medium and high corrosion levels. Figure 3-14 shows a typical 3D pit configuration; its cross section; pit width and depth. Table 3-1 compares the geometries of the pits including depth, width, and the percentage loss in cross-sectional area modelled for 10 mm, 16 mm and 25 mm deformed reinforcing steels corresponding to different pitting corrosion levels.

The pit depth corresponds to the size of the cutter used to simulate pitting corrosion, and the pit width was calculated based on the Equation 3-9.

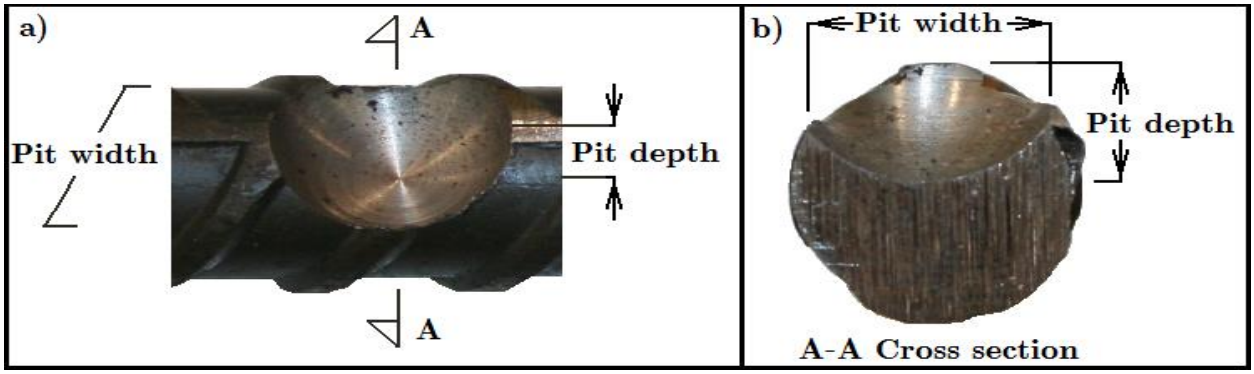

Figure 3-14 (a) A typical 3D of pit configuration and (b) its cross section with pit depth and width

Table 3-1 Pit depth and width for different levels of corrosion for 10mm, 16mm and 25mm deformed steel reinforcement

Diameter (mm)	corrosion level	Notation (number of samples)	Pit depth (mm)	Pit width (mm)	Cross section loss in pit location (%)
10	Non corroded	D10 (3)	0	0	0
	Low	D10-PL1 (6)	2	3.9	7.3
	Medium	D10-PL2 (6)	4	7.3	26.5
	High	D10-PL3 (6)	5	8.7	39.1
16	Non corroded	D16 (3)	0	0	0
	Low	D16-PL1 (6)	4	7.7	11.2
	Medium	D16-PL2 (6)	6	11.1	23.6
	High	D16-PL3 (6)	8	13.9	39.1
25	Non corroded	D25 (3)	0	0	0
	Low	D25-PL1 (6)	5.5	10.7	8.8
	Medium	D25-PL2 (6)	9	16.8	21.9
	High	D25-PL3 (6)	12.5	21.7	39.1

Fifty four machine simulated pit damaged samples and 9 sound (noncorroded) samples, each 600 mm in total length with 300 mm gauge length, were tested under static tensile tests. The tensile tests were run with a loading rate of 1 mm of deformation per minute in the elastic region and 2 mm per minute in the plastic region. All tests were continued until rupture of the samples. Four mechanical properties of the steel reinforcement (yield stress, ultimate stress, elongation and modulus of elasticity) have been recorded to develop the deterioration models for pitting corroded steel reinforcement. Strain at the middle of the non-damaged part of the samples and strain at the locations of pit damage were measured during tensile. To meet these goals, two synchronized strain gauging consisting of a contact extensometer and a remote vision based strain measurement device were employed for each sample. The contact 25 mm-length extensometer was installed in the middle of the clear distance between two pits either on the pit face or pit back side. The non-contact vision based strain device was utilized to measure strain between two points located on the sides of a pit. The pits and regions within their vicinity were painted black, and then two white pointers were attached on the sides of the pits to make a grey pattern required by the vision system. The strain between the two white points was measured by the remote vision system. At the points where the contact sensor was installed, the surface was slightly smoothed by sand blasting. Figure 3-15 shows a sample prepared for tensile testing employing both remote sensing using a vision system and contact extensometer. The distance between the camera and the measuring point was 1 m, and 14 images per second were captured.

Figure 3-15 Whole length of a sample; (b) Gauge length of the sample prepared for tensile test

Digital Image Correlation was used for processing the images taken and output the real time strain of pit damage [27]. The efficiency of the remote vision sensing system was evaluated using both a remote vision system and contact strain sensors for non-corroded steel bars. Figure 3-16 compares stress-strain relationship of a non-corroded sample measured by contact extensometer and the vision based sensor. After the tensile tests, changes in the pit width and length were measured along with deformation of different parts of samples.

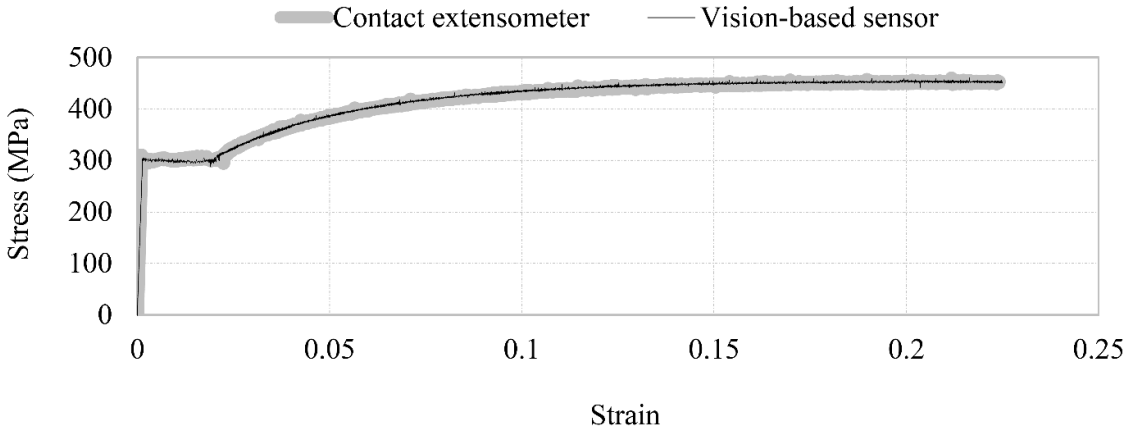

Figure 3-16 Comparison between stress-strain measured by contact extensometer and vision-based sensor

The nature of pitting for a length of longitudinal reinforcement taken from a 500 mm diameter RC column is shown in Figure 3-17. If the actual corroded bar from Figure 17 is compared to the machined bar shown in Figure 3-15 it is evident there are a number of similarities. The back side of the real corroded bar showed very little if any pitting while extensive pitting was observed on the front of the bar which was facing the concrete cover. While it is not possible to capture every detail, the machined pit illustration given in Figure 3-9, provide a reasonable approximation of the pitting which occurs in corroding reinforcement while embedded in concrete.

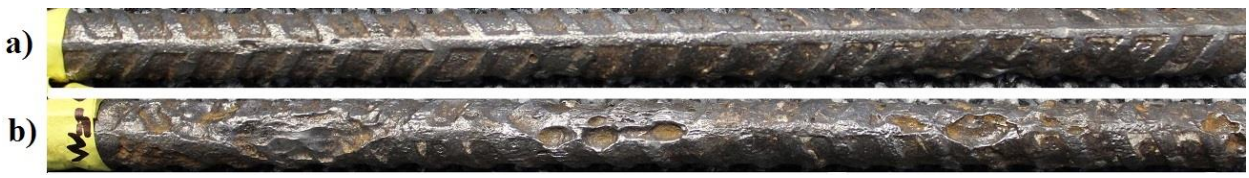

Figure 3-17 A real pitting corroded steel reinforcement in concrete; (a) back side; (b) face side

The behavior of steel surrounded by concrete is obviously different from that of a bare bar subject to uniaxial forces. Once the corrosion of steel reaches a critical level cracking, spalling and de-bonding will occur. The response of a portion of severely corroded reinforcing steel in concrete subject to tensile forces therefore is likely to be similar to that of bare bars. The testing of bare bars with different levels of corrosion provides useful information on the behavior at one end of the possible level of corrosion evident in structures. Further investigation is need to evaluate the behavior of pitted reinforcing steel subject to axial forces where the concrete cover is partially intact.

Figure 3-18 shows photos of the two different test setups (contact extensometer installed on the pit face side and pit back side respectively) and also compares the stresses and strains measured by both strain measurement systems for the sample D25-PL2. Graph marked (a) corresponds to measurements made by the remote vision system, graph marked (b) corresponds to data from the contact extensometer installed in pit face, and graph marked (c) corresponds to data from contact extensometer installed in pit back side.

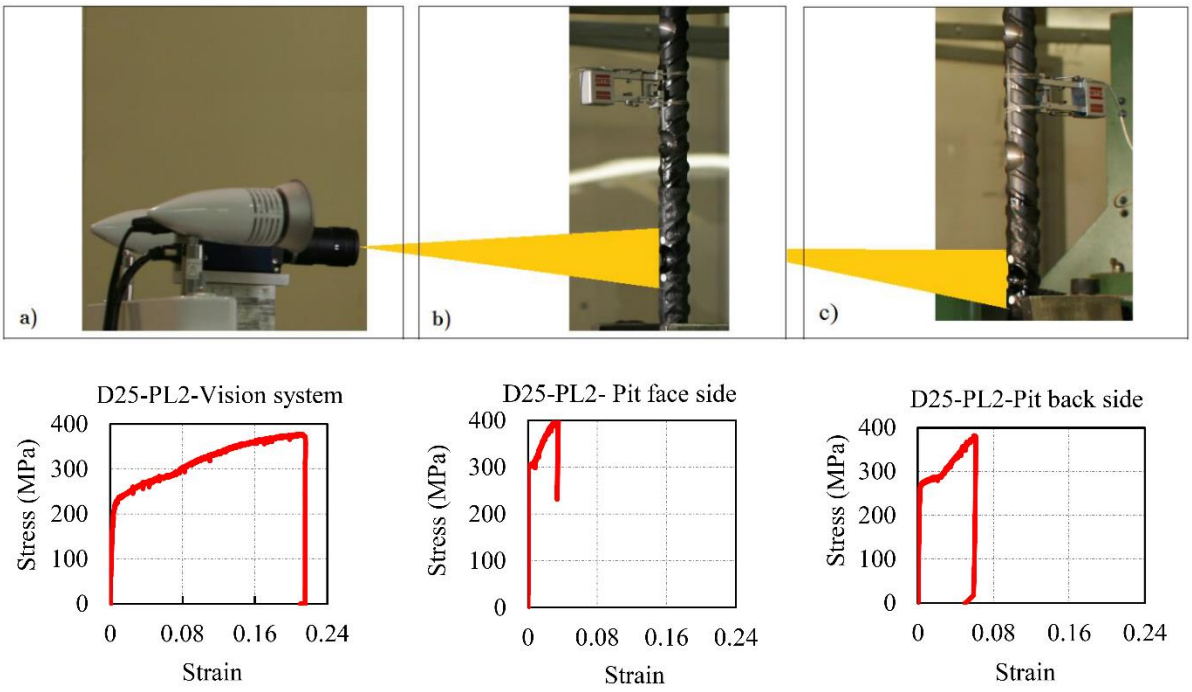

Figure 3-18 Photos of tensile test setup measurement with stress-strain measured by a) remote vision installed on pit face b) contact extensometer installed on pit face and c) contact extensometer installed on pit back side for D25-PL2

3.4 RESULTS AND DISCUSSIONS

As shown in Figure 3-18 synchronized strain measurements by the remote sensor and contact sensor were made on the samples subject to axial tensile force. The stress-strain relationship of the pit cavities was measured by remote system and stress-strain relationship of points located between two sequential pits was measured by the contact sensor.

Examining the samples after testing, the section of steel reinforcement located between two pits was found to be bent. Figure 3-19 compares the steel reinforcement before and after tensile testing. Based on experimental results, two bending deformation parameters, called A, and B, have been proposed and are shown in Figure 3-19. Table 3-2 contains the values of A and B measured for all tested samples. The experimental results show that the following Equation is in very good agreement with the measured A and B values:

$$B = 2 \times A \qquad 3\text{-}17$$

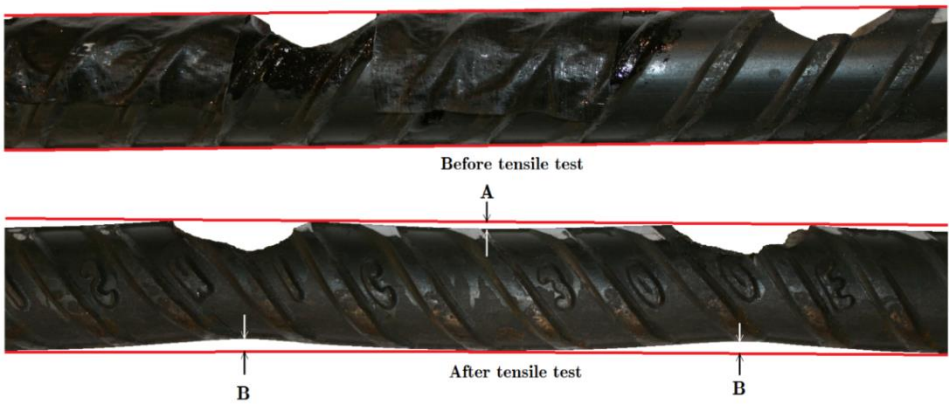

Figure 3-19 Pitting corroded steel bar before and after tensile test

Table 3-2 The deformation parameters of pitting corroded steel reinforcement

Diameter of bar (mm)	Sample notation	After tensile	
		A (mm)	**B (mm)**
10	D10-PL1	0.3	0.6
	D10-PL2	0.7	1.6
	D10-PL3	1	1.9
16	D16-PL1	0.5	1
	D16-PL2	1.1	2.2
	D16-PL3	1.3	2.4
25	D25-PL1	0.8	1.6
	D25-PL2	1.2	2.5
	D25PL3	1.8	3.5

Deformed samples after tensile testing indicate that the strain in the pit back side and pit face side is different due to bending deformation caused by the pitting cavities. The stress-strain relationships measured by the contact extensometers for all pitting corrosion levels and sizes of steel bars have been compared in Table 3-3. The main results achieved from all tests are summarized as follows:

Elongation of the pit back side is greater than that of the pit face side. The difference between elongation of the pit back and the pit face side increases with increasing corrosion level. Contraction elongation at the pit face side has been observed for all samples with PL3 level of corrosion with increasing bending deformation, and the contraction elongation increasing with the diameter of reinforcing steel. With exception of PL1, the stress-strain relationships show that the modulus of elasticity for the pit face side is greater than that of the non-corroded sample. Pitting corrosion degraded the effective mechanical properties of steel reinforcement including yield stress, ultimate stress, elongation, and modulus of elasticity on the pit back side. The stress-strain relationships measured by the contact extensometers for all pitting corrosion levels and sizes of steel bars have been shown in Appendix A.

Table 3-3 Comparing the effective mechanical properties of reinforcing steel measured from pit back and face side

Sample name	Yield stress (MPa)		Ultimate stress (MPa)		Elongation		Modulus of Elasticity (GPa)	
	Back side	Pit side	Back side	Pit side	Back side	Pit side	Back side	Pit side
D 10 mm- PL1	271	269	410	401	0.12	0.11	186	185
D 10 mm- PL2	233	237	338	342	0.021	0.017	156	229
D 10 mm- PL3	194	185	286	281	0.007	0.0003	119	300
D 16 mm- PL1	276	290	434	420	0.097	0.096	168	188
D 16 mm- PL2	252	242	380	368	0.05	0.028	154	231
D 16 mm- PL3	197	190	294	287	0.012	0.008	117	311
D 25 mm- PL1	284	295	434	442	0.112	0.091	157	189
D 25 mm- PL2	270	283	386	398	0.065	0.033	137	234
D 25 mm- PL3	204	193	308	289	0.018	-0.0035	100	321

Some geometry factors of the pits including, pit length and width; and distance between two pits before and after tensile tests were measured. Figure 3-20 shows a sample with the parameters before and after tensile testing. Table 3-4 shows the measured aforementioned parameters. The pit widths measured in Table 3-4 and pit widths calculated in Table 3-1 using Equation 3-9 are up to 8 % different in value. The reason for this is that the calculation of the pit depths using Equation 3-9 was performed assuming a circular cross section, while, deformed bars are not completely circular in cross section.

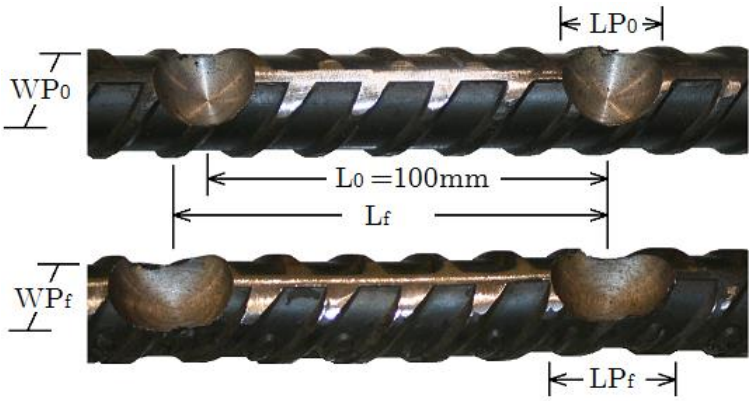

Figure 3-20 Pit geometry parameters before and after tensile test

Table 3-4 Geometry parameters of pits before and after tensile tests

Diameter of bar (mm)	Sample notation	Before tensile			After tensile		
		L_0 (mm)	LP_0 (mm)	WP_0 (mm)	L_f (mm)	LP_f (mm)	WP_f (mm)
10	D10-PL1	100	3.9	3.7	111.7	5.3	2.8
	D10-PL2	100	7.8	6.9	103.5	9.7	5.4
	D10-PL3	100	9.8	8.2	102	11.7	6.7- 6.9
16	D16-PL1	100	7.9	7.4	111.4	11.1	5.9
	D16-PL2	100	11.7	10.3	106.7	16.2	8
	D16PL3	100	15.8	13	103.3	18.7	11.1
25	D25-PL1	100	11.8	10.2	112.5	16.5	9
	D25-PL2	100	17.5	16.4	108	22.7	12.8
	D25-PL3	100	24.8	20.2	104	28.5	17.5

The total strain undergone by a specimen under tensile loading is the sum of the elastic strain plus plastic strain:

$$\varepsilon_{Tot} = \varepsilon_{El} + \varepsilon_P \qquad 3\text{-}18$$

Where: ε_{Tot} is total strain, ε_{El} is elastic strain and ε_P is plastic strain.

The change in pit length after testing is given by $LP_f - LP_0$, and it is the plastic deformation of pit cavities. If the plastic deformation is divided by the pit length measured before tensile testing, the plastic strain is calculated as follows:

$$\varepsilon_P = \frac{LP_f - LP_0}{LP_0} \qquad 3\text{-}19$$

The stress-strain relationships of two points on the sides of the pit were measured using a non-

contact vision based sensor. Table 3-5 shows the effective mechanical properties of steel reinforcement corresponding to all levels of pit damage (PL1, PL2 and PL3) and bar sizes.

The elongations measured by the vision sensor are the elastic strain plus the plastic strain. The plastic strains of the pits measured by the remote vision sensor and directly by measurements before and after tensile tests agree well with each other indicating the high accuracy of the vision sensor measurements. The strain measured by the vision sensor is the strain between the centers of the two white points. The points are 7 mm apart and drawn by white marker on both sides of a pit. Therefore, the strains shown in Table 3-5 include the strain of the pit and the strain of a 7 mm length of the non-damaged part of the samples.

Table 3-5 Experimental results of the effective mechanical properties of reinforcing steel measured by vision sensor

Sample name	Yield stress (MPa)	Ultimate stress (MPa)	Elongation	Modulus of Elasticity (GPa)
D 10 mm- PL1	289	444	0.33	167
D 10 mm- PL2	260	377	0.216	64
D 10 mm- PL3	190	283	0.147	38
D 16 mm- PL1	275	436	0.25	176
D 16 mm- PL2	258	377	0.187	132
D 16 mm- PL3	200	279	0.18	31
D 25 mm- PL1	270	395	0.192	111
D 25 mm- PL2	223	336	0.153	94
D 25 mm- PL3	188	275	0.124	53

3.5 REDUCTION FACTORS FOR THE EFFECTIVE MECHANICAL PROPERTIES OF STEEL REINFORCEMENT DUE TO PITTING DAMAGE

Pitting corrosion degrades the effective mechanical properties of steel reinforcement. The degradation caused by corrosion is not uniform. It means that a 1 % loss of cross section causes more or less a 1 % reduction in the effective mechanical properties of reinforcing steel (yield stress, ultimate stress, elongation and modulus of elasticity). Past studies have modelled the reduction in the effective mechanical properties of steel reinforcement using linear regression [15,16]. However, the test results of this study confirm that linear regression is not appropriate for pitting corrosion.

The effective mechanical properties of steel reinforcement measured by the contact

extensometer for corroded and non-corroded reinforcing steels have been employed for modelling pitting corrosion induced reduction in the effective mechanical properties of steel. The investigated mechanical properties include yield, ultimate stress, elongation, and modulus of elasticity. The normalized deterioration for the effective mechanical properties of corroded steel bars, for both pit back and pit face sides are presented in Figure 3-21. In this Figure, symbol of mechanical properties with and without "c" correspond the mechanical properties of corroded and non-corroded steel bars respectively. The results confirm that non-linear regression is more suitable in the case of pitting corrosion. The normalized reduction in elongation, for example, clearly shows that degradation cannot be modeled using linear regression.

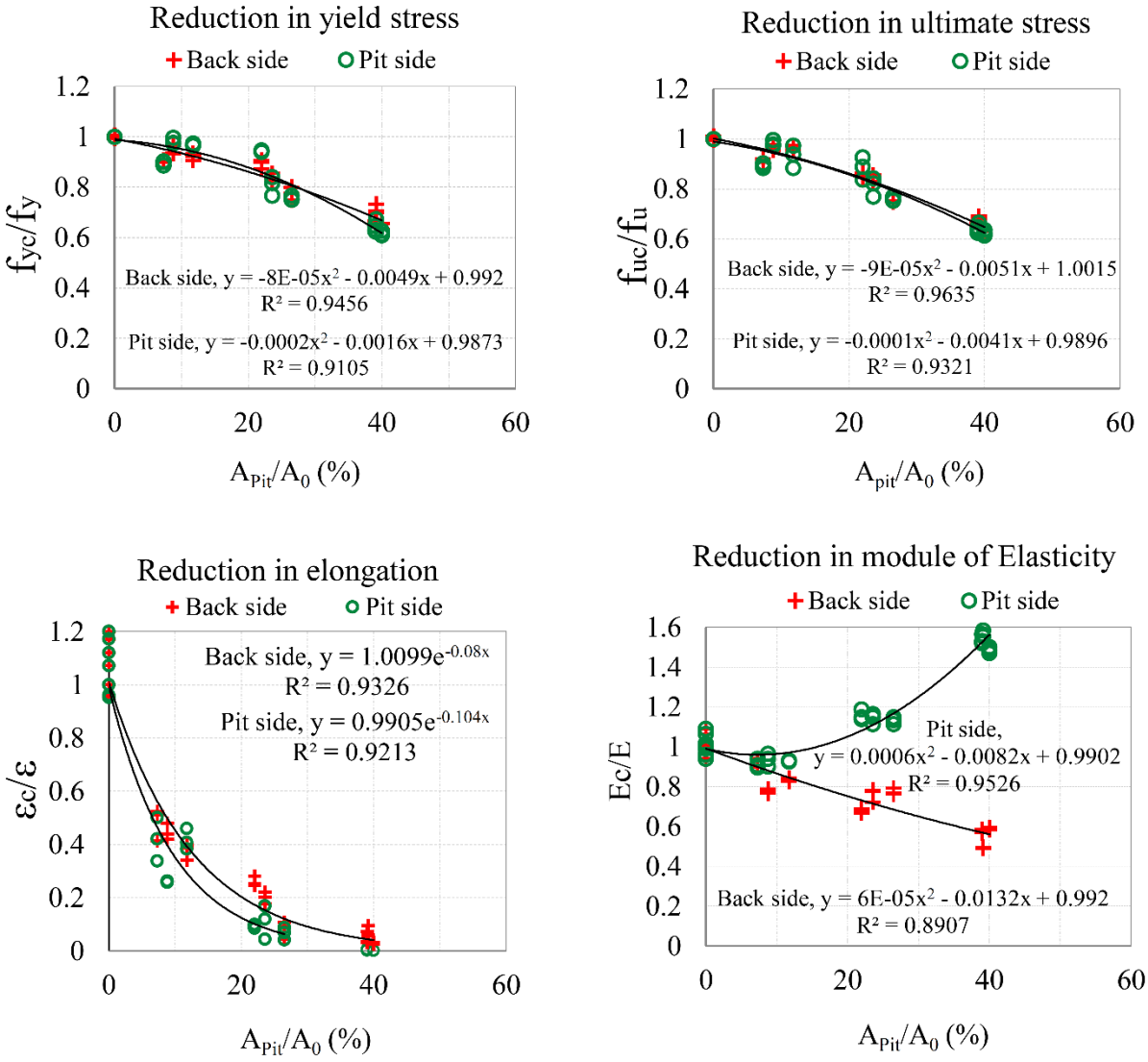

Figure 3-21 Normalized reduction in the effective mechanical properties of reinforcing steel

The results show that relative reduction in elongation for both pit back and pit face sides for the pit level 1 (PL1) are much higher than that for PL2 and PL3. The modulus of elasticity for the

pit back side degrades due to pitting corrosion, but the trend for the pit face side is very different. At the pit face side, the normalized modulus of elasticity almost remains the same with very small pits (PL1), however it increases when the level of pit damage rises. Therefore, the effective modulus of elasticity of PL2 and PL3 corroded steel reinforcement samples is greater than that of the non-corroded samples. The main reason is that the samples subjected to central tensile tests have fixed rotation ends conditions, meaning that the bending moment diagram is similar to that presented in Figure 3-9b. Hence, the non-damaged parts of samples between two sequential pits are subjected to a bending moment leading to bending deformation. When compared with non-corroded bars, the same force causes more deformation in pit back side and less deformation in pit face side. Therefore, pitting corrosion causes a reduction in apparent modulus of elasticity in the pit back side and an increase of apparent modulus of elasticity in pit face side. Figure 3-22 illustrate the aforementioned statement for rising modulus of elasticity in the pit face side. Where: D_F is the deformation of the non-damaged part of the sample with length L due to tensile force, D_M^T is the maximum bending-induced deformation at the pit back side, D_M^C is the maximum bending-induced deformation at the pit face side, E_0 is modulus of elasticity of non-corroded steel bar, E_T is apparent modulus of elasticity in the pit back and E_C is apparent modulus of elasticity in pit face side. The above parameters can be mathematically represented as follows:

$$D_F = \frac{F \times L}{E_0 \times A} \qquad 3\text{-}20$$

$$D_M^T = D_M^C \propto \frac{F \times \Delta c \times D_0 \times L}{2 \times E_0 \times I_{pristine}} \qquad 3\text{-}21$$

To validate the above statement, E_C/E_T ratio calculated using Equations 3-20 and 3-21 and Figure 3-22 was compared to the experimental results presented in Table 3-3 for D16-PL2 sample. In accordance with Table 3-3, E_C/E_T ratio has a value of 1.5. Alternatively, E_C/E_T ratio can be calculated under fixed end rotation condition from bending moment-induced deformation as follows:

$$D_M^T = D_M^C \cong 0.19 \frac{F \times \Delta c \times D_0 \times L}{2 \times E_0 \times I_{pristine}} = 6.66\, D_F \qquad 3\text{-}22$$

Using Equation 3-22 and Figure 3-22, E_C/E_T has a value of 1.35. The difference of 10 % from experimental results confirms that the above formula gives good agreement with the experimental results.

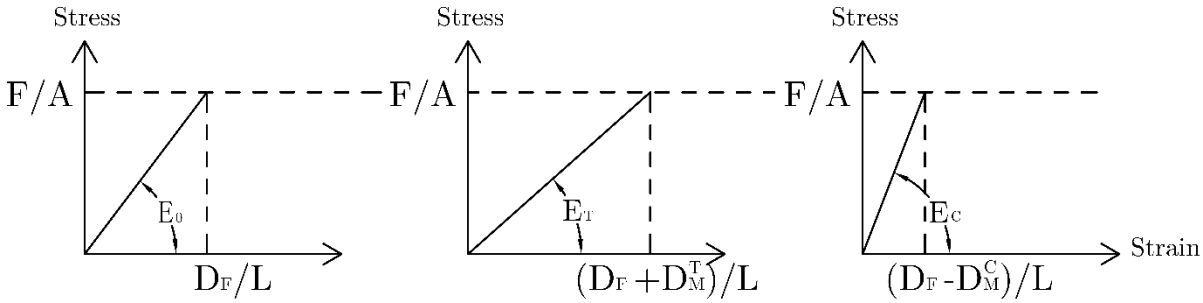

Figure 3-22 . Stress-strain relationship (left): sound sample, (middle): corroded sample, measured at pit back side, (right): corroded sample, measured at pit side

To validate elastic strain at damaged section, $\varepsilon^{T}_{max-D16-PL2}/\varepsilon_0$ ratio (the maximum strain of D16-PL2 to D16 (non-corroded) at the pit face side) measured by the vision sensor was compared with that calculated using Equations 3-15 and 3-16. Figure 3-23 compares the measured strains for non-corroded with those for D16-PL2. Considering fixed end rotation condition, the maximum elastic strain at pit face side of D16-PL2 using Equation 3-15 is as follows:

$$\varepsilon^{T}_{max} = \frac{F}{0.764\,EA_0} + 0.81 \times \frac{F \times 0.00157 \times 0.00732}{0.468 \times 0.25 \times (0.08)^2 \times EA_0} = 2.55\frac{F}{EA_0} \qquad 3\text{-}23$$

The calculated elastic stress ratio ($\varepsilon^{T}_{max-D16-PL2}/\varepsilon_0$) has a value of 2.55. As shown in Figure 3-23, when elastic stress is 200 MPa, the measured $\varepsilon^{T}_{max-D16-PL2}/\varepsilon_0$ has a value of 2.8. The difference of 9% confirms that the analytical formula gives good agreement with the experimental results.

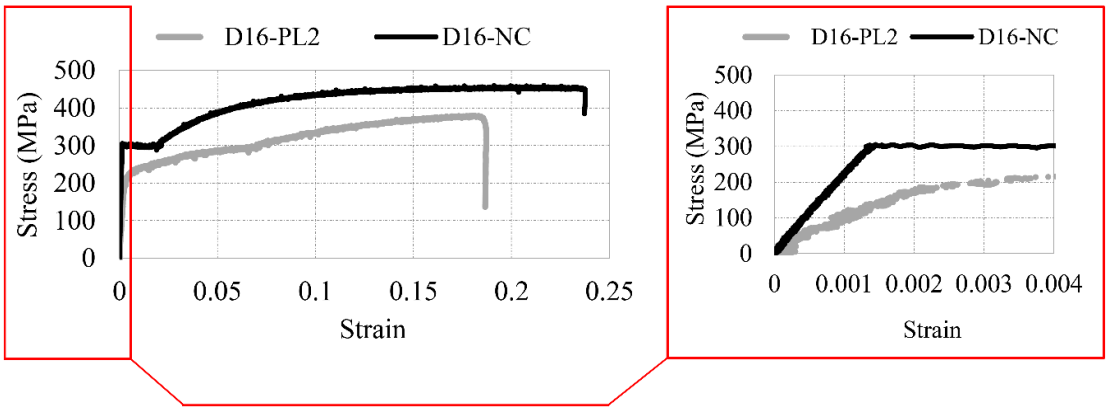

Figure 3-23 Comparing elastic strain for non-corroded and PL2, 16 mm samples measured by the vision sensor at pit face side of damaged section

To simplify the estimate of reduction factors for the effective mechanical properties of reinforcing steels, the non-linear trends have been replaced by piecewise linear trends consisting

of three segments. The segment boundaries have been selected considering pitting corrosion levels and the intersection of two sequential segment lines. This simplification provides the possibility to compare the results of this article with results in literature. Since past studies employed linear trends to develop the reduction factors, proposing different reduction factors for different corrosion intervals should lead to less variety in reduction factors reporting in future experiments. Assuming a linear trend, the ratio of the effective mechanical properties of corroded to non-corroded reinforcing steels can be generally expressed as:

$$\frac{P_c}{P} = \left[100 - \gamma\left(\frac{A_{pit}}{A_0} \times 100\right)\right] \qquad 3\text{-}24$$

Where: P_c and P are the effective mechanical properties of corroded and non-corroded reinforcing steel respectively and γ is the reduction factor that was regressed from the test results.

Table 3-6 compares reduction factors for the mechanical properties of reinforcing steels for both pit face (pit) and pit back (back) sides. The upper boundaries of the three segments are 9 %, 24 % and 40 %. The boundaries are very close to the pit levels. It is expected that the reduction factors estimated for yield and ultimate stress on the pit face and back sides are similar. Hence, the reduction factors of the two sides of the corroded bar for each mechanical property (yield stress, ultimate stress and elongation), and given segment have been replaced by the average of the two values obtained from different test setups and are represented in Table 3-7.

Table 3-6 Reduction factors γ regressed from experimental results

Loss of cross section in pit location (%) $[(A_{Pit}/A_0) \times 100]$	**Reduction factors (γ) in:**							
	Yield stress f_{yc}/f_{y0}		Ultimate stress f_{uc}/f_{u0}		Elongation $\varepsilon_c/\varepsilon_0$		Modulus of Elasticity E_c/E_0	
	Back side	Pit side	Back side	Pit side	Back side	Pit side	Back side	Pit side
$0 < [(A_{Pit}/A_0) \times 100] \leq 9$	0.75	0.29	0.48	0.53	6.34	6.81	1.73	0.79
$9 < [(A_{Pit}/A_0) \times 100] \leq 24$	0.63	0.8	0.87	O.81	1.82	1.76	0.67	-1.38
$24 < [(A_{Pit}/A_0) \times 100] \leq 40$	1.1	1.41	1.08	1.24	0.95	0.6	1.09	-2.45
Correlation coefficient, R^2	0.95	0.91	0.96	0.93	0.93	0.92	0.89	0.95

Table 3-7 Reduction factors γ averaged from regressed experimental results of back and face pit sides

Loss of cross section in pit location $[A_{Pit}/A_0]$ (%)	**Reduction factors in:**				
	Yield stress f_{yc}/f_{y0}	Ultimate stress f_{uc}/f_{u0}	Elongation $\varepsilon_c/\varepsilon_0$	Modulus of Elasticity E_c/E_0	
	Average	Average	Average	Back side	Pit side
$0 < A_{Pit}/A_0 \leq 9$	0.52	0.51	6.57	1.73	0.79
$9 < A_{Pit}/A_0 \leq 24$	0.72	0.84	1.79	0.67	-1.38
$24 < A_{Pit}/A_0 \leq 40$	1.25	1.18	0.78	1.09	-2.45

The mechanical properties of corroded bars can be easily estimated using Equation 3-24 and information presented in Table 3-4 or Table 3-5 as a function of the mechanical properties of the non-corroded bars. Consider the ratio of elongation of pitted corroded to non-corroded steel bar with $\frac{A_{Pit}}{A_0} \times 100$ ratio of 35% on the pit back side, using Table 3-6 and Equation 3-24 can be calculated as follows:

$$\left(\frac{\varepsilon_c}{\varepsilon}\right) \% = 100 \% - [(9 \times 6.34) + (15 \times 1.82) + (11 \times 0.95)] \% = 5.19 \%$$

The calculation has been carried out based on selecting the appropriate reduction factors proposed for each segment. The sample has 35 % loss of cross section. Hence, for the first 9 % loss of cross section, γ is 6.34, for the second more 16 % loss of cross section γ is 1.82 and for the last 11 % loss of cross section γ is 0.95.

The experimental results of this study were used in chapter 5 to estimate the effective mechanical properties (Eq. 5-9 and 5-13) of transverse reinforcement of pitting corroded RC column subjected to axial compression.

3.6 LIMITATIONS

The results presented in this chapter were obtained assuming the same pit sizes on samples. Pit damage was artificially induced by machining hemispherical cavities. In real corrosion, pit cavities have different depths and have random distributed on reinforcement surface.

3.7 CONCLUSIONS

The presented time-dependent pit depth model for localized corrosion based on time-dependent corrosion rate can be employed in life time analysis of RC corroded structures to calculate time-dependent loss of cross section area of reinforcing steel due to pitting corrosion.

The results indicated that Pitting corrosion not only alters the overall effective mechanical properties of steel reinforcement but also causes specific changes to the pit back compared to the pit face side.

In this regard, the results show that relative reduction in elongation for pit face side is greater than that for pit back side for a given level of corrosion. Moreover, moderate to severe pit damage (for example PL2 and PL3) leads to a normalized apparent modulus of elasticity (E_C/E) greater than 1 on the pit face side which is a caused by local bending moment at the location of

contact extensometer. Locally, the pit face is under compression while the pit back is in tension.

While past studies employed linear regression to model corrosion-induced degradation in the effective mechanical properties of steel reinforcement, this study has shown that non-linear regression should be applied for pitting corrosion. To simplify the model for the degradation of the effective mechanical properties due to pitting corrosion, a piecewise linear trend consisting of three linear lines was employed for 0 to 9 %, 9 % to 24 % and 24 % to 40 % loss of cross section at pit locations.

The displacements readings obtained by remote visual sensing were in good agreement with those obtained from the contact sensor on the un-corroded sections of steel. The agreement in the values obtain from the two displacement monitoring devices provided confidence in the use of remote visual sensing for the pit face where use of the contact sensor was not possible.

The analytical modelling reveals pit cavities had significant impact on cross section parameters affecting tensile behavior of pitting corroded steel bars. The analytical formulas were validated using the experimental results.

4 CORROSION INDUCED- DETERIORATION IN CONCRETE MATERIALS AND STEEL REINFORCEMENT

Corrosion of reinforcing steel embedded in concrete is an electrochemical process. When aggressive ions such as chloride penetrate the concrete cover and reach the steel reinforcement, the process of active corrosion is initiated. Once the corrosion process commences, not only does cross sectional area of the corroding reinforcing steel irregularly decrease but also corrosion by-products such as rust are formed. Irregular loss of cross section leads to alter the effective mechanical properties of reinforcing steels. Moreover, the average volume of rust is 2-4 times greater than that of the steel. Therefore, the corrosion by-product causes volume expansion developing tensile stresses in concrete, which ultimately results in propagating of cracks and spalling of the cover concrete and softening of the concrete core (Vu and Stewart, 2000, Coronelli and Gambarova, 2004).

The chapter 4 will present development of deterioration models for concrete materials and steel reinforcement due to chloride-induced corrosion, and it contains two sections. The section 4-1 presents the results of an experimental investigation into the residual capacity of cracked cover concrete due to reinforcement corrosion. In addition, the effects of reduction in the mechanical properties of concrete materials on moment-curvature response of a corroded bridge pier were numerically studied. The section 4-2 is aimed at development of reduction factors for the effective mechanical properties of corroded steel reinforcement. Moreover, the difference between corroded steel bare bar and corroded bars while embedded in concrete is presented that is currently not well addressed

4.1 EXPERIMENTAL EVALUATION OF THE RESIDUAL COMPRESSION STRENGTH AND ULTIMATE STRAIN OF CORROSION INDUCED DAMAGED CONCRETE

4.1.1 INTRODUCTION

In recent years, growing attention has been given to the effects of corrosion on the structural performance of reinforced concrete (RC) structures. Corrosion of reinforcing steel embedded in concrete is an electrochemical process commenced when aggressive ions such as chloride penetrate the concrete cover and reach the steel reinforcement. Once the corrosion process commences corrosion by-products such as rust are formed. The average volume of rust is approximately 2-4 times greater than that of the steel resulting in the development of tensile stresses in concrete, which ultimately lead to cracking and spalling of the cover concrete. Cracking of the concrete due to corrosion causes a reduction in ductility capacity of RC columns (Akiyama and Frangopol, 2014). Akiyama et al. (2011) presented an analytical model to predict curvature at the onset of buckling of longitudinal reinforcement of corroded RC column considering cracked concrete cover due to corrosion. Tapan and Abutaha found "cover to longitudinal bar diameter ratio has a critical effect on load carry capacity of deteriorated RC columns. They also found steel corrosion and loss of concrete cover critically decrease load carry capacity of RC columns (Tapan and Aboutaha, 2011). Past studies showed cracking in the concrete cover plays important role in inelastic buckling behaviour of longitudinal steel reinforcement of RC columns (Bayrak and Sheikh, 2001, Monti and Nuti, 1992, Mau and El-Mabsout, 1989).

To model the effects of corrosion on the compression strength and the ultimate strain of the deteriorated concrete materials due to corrosion, some analytical methods were followed by researchers. The two analytical methods were presented as follows:

Coronelli and Gambarova (2004) used a model proposed by Vecchio and Collins (1986) and improved by Capé (1999) to predict reduction in the compressive strength of cover concrete due to reinforcement corrosion.

In accordance with the modified model, the following equation was used to estimate the effect of cracks on the compressive strength of concrete (Coronelli and Gambarova, 2004):

$$f_c^* = \frac{f_c}{1-0.1\varepsilon_1/\varepsilon_{co}} \quad 4\text{-}1$$

Where, f_c^*: compression stress of cracked concrete, f_c: maximum compression stress of non-cracked concrete, ε_{co} strain at the peak compressive stress. ε_1 is average (smeared) tensile strain in the cracked concrete at right angles to the direction of the applied compression. ε_1, can be approximated using expansion of section width due to corrosion induced cracking.

Biondini et al. (2014) used the model proposed by Coronelli and Gambarova (2004) to predict residual compression strength of corrosion induced damaged concrete cover.

Ou et al. (2013b) used a model presented by Hsu (1992) to predict stress-strain curve of cracked concrete due to reinforcement corrosion. It was assumed that corrosion can develop transverse tensile strain in cover concrete. The transverse tensile strain was calculated using the following equation (Hsu, 1992):

$$\varepsilon_r = \frac{\sum w_{cr}}{b_0} \quad 4\text{-}2$$

Where, ε_r is transverse tensile strain, $\sum w_{cr}$ is total crack width and b_0 is circumference of a concrete section.

The softening coefficient of concrete cover due to reinforcement corrosion was calculated using the following equation (Hsu, 1992):

$$\zeta = \frac{0.9}{\sqrt{1+600\varepsilon_r}} \quad 4\text{-}3$$

Where, ζ, is the softening coefficient of concrete cover.

Finally the softening coefficient of concrete cover was used to calculate stress-strain curve of cracked concrete cover (Hsu, 1992).

It is evident that modelling corrosion-induced reduction in mechanical properties of concrete materials in RC structure is important. However, there are no known experimental study specifically investigating the effects of corrosion on the residual compression strength and the ultimate strain of concrete materials in corroded RC structures (Andisheh et al., 2016b).

In chapter 4, section 4-1, an experimental program was designed to create data base showing the relationship between axial compressive strength and ultimate strain of concrete material and degrees of reinforcement corrosion of RC columns. Full-scale RC columns were corroded using an accelerated corrosion method and core samples were taken from corroded and noncorroded

RC columns. The samples were subjected compressive loading, and during the test axial stress and strain of concrete materials were recorded. The developed deterioration model in this research will improve numerical models used for analysis of corroded RC structures and assessment of residual capacity of existing RC structure subjected to corrosion.

The first objective of chapter 4-1 is to study the effects of corrosion of steel reinforcement on the axial compressive strength and the ultimate strain of concrete materials in RC columns. The second objective is suggesting deterioration factors for the axial compressive strength and the ultimate strain of concrete materials in corroded RC columns. Akiyama and Frangopol (2014) highlighted the needs for such deterioration models to establish a numerical method for analysing corroded RC structures.

4.1.2 EXPERIMENTAL PROGRAM

The experimental component of this part of the investigation included a total of three circular reinforced concrete columns, with two of the columns being corroded using an impressed current technique. The non-corroded column and the corroded columns were placed horizontally and cut at the middle to provide six specimens with identical height. The specimens were vertically erected and concrete core samples with different sizes were taken. In addition to the core samples taken from columns with varying degrees of corrosion, five 100 mm diameter concrete cylindrical samples poured at the time of fabricating of the RC columns. All core cylindrical samples were prepared for compressive testing.

4.1.2.1 CONSTRUCTION

Reinforcing caging were prefabricated with a construction tolerance of 2 mm. Prefabricated modular plastic moulds with 500 mm diameter and 300 mm and 600 mm height allowed for varying range of total height. Three cylindrical column moulds were vertically erected on a horizontal plywood sheet. 50 mm concrete spacer blocks were used to attach the reinforcing cages to the moulds to cast RC column with 50 mm concrete cover. Pre-mixed concrete was poured in three layers, and each layer was mechanically vibrated prior to pouring the next layer. The fabricated columns were cured at 20^{o}c and their top surfaces were covered by wet hessian and polythene to keep moisture. After seven days curing, the columns were stripped and kept in the laboratory until testing or corroding. Figure 4-1 shows details of construction of the three columns.

Figure 4-1 Details and process of construction of RC columns

The reinforcing bars for all specimens and their components, were specified as Grade 300 according to AS/NZS 4671. The concrete material with designed compression strength of 40 MPa, water to cement ratio of 0.6 and aggregate size of 19 mm used to prefabricate all columns.

4.1.2.2 CORROSION TESTING SETUP

Two RC columns with various volumetric ratios of confining steel were corroded. In order to corrode the RC columns within a reasonable time period, an accelerated corrosion method, called the impressed current method, was used in this study. An accelerated corrosion rate of 600 to 900 $\mu A/cm^2$ was achieved by applying a constant electrical current to the steel reinforcement by a power supply. The RC columns were submerged in a 3.5% NaCl solution. The steel reinforcement of the RC columns, acting as the anode, was directly connected to the positive terminal. Some stainless steel plates, submerged in the NaCl solution, acting as the cathode, were directly connected to the negative terminal. The current flowed from the steel reinforcing to the stainless steel plates through the 3.5% NaCl solution, acting as electrolyte. Figure 4-2 shows details and a photo of the corrosion test set up of the columns. The 600 mm length of columns from bottom and all connections were covered by a thick rubber material to limit corrosion in this area. Therefore, the central 450 mm length of each column was corroded. Figure 4-3 shows prepared columns for corrosion and a corroded column. Figure 4-3b confirmed that vertical cracks were propagated on concrete cover of corroded columns. The corrosion tests were conducted at two predetermined time to obtain two different degrees of corrosion.

Faraday's law provides a relationship between corrosion current density, mass loss and time. According to Faraday's law, for steel reinforcement a uniform corrosion current density of $i_{corr} = 1\,\mu A/cm^2$, will result in 11.6 $\mu m/yr$ loss of cross section. Faraday's law was used to theoretically predict degrees of corrosion corresponding to corrosion exposure time. To meet this aim the electricity current of each column was monitored hourly and the average was recorded daily. The goal was achieving two levels of corrosion corresponding relatively low and high degrees of corrosion. In this study, for relatively low degree of corrosion (LC) the average corrosion of less than 5% and 12 % were achieved for longitudinal and transverse reinforcement respectively. For relatively high degree of corrosion (HC) the average corrosion of 13% and 33 % were achieved for longitudinal and transverse reinforcement respectively. The corrosion percentage of transverse and longitudinal reinforcement for each column was experimentally measured using the mass loss approach. The results show that average corrosion of transverse reinforcement is much greater than that of longitudinal reinforcement because transverse reinforcement is closer to surface of column subjected to corrosion. Details comparing average corrosion of longitudinal and transverse corrosion can be found in Chapter 6, section 6-3-1-1.

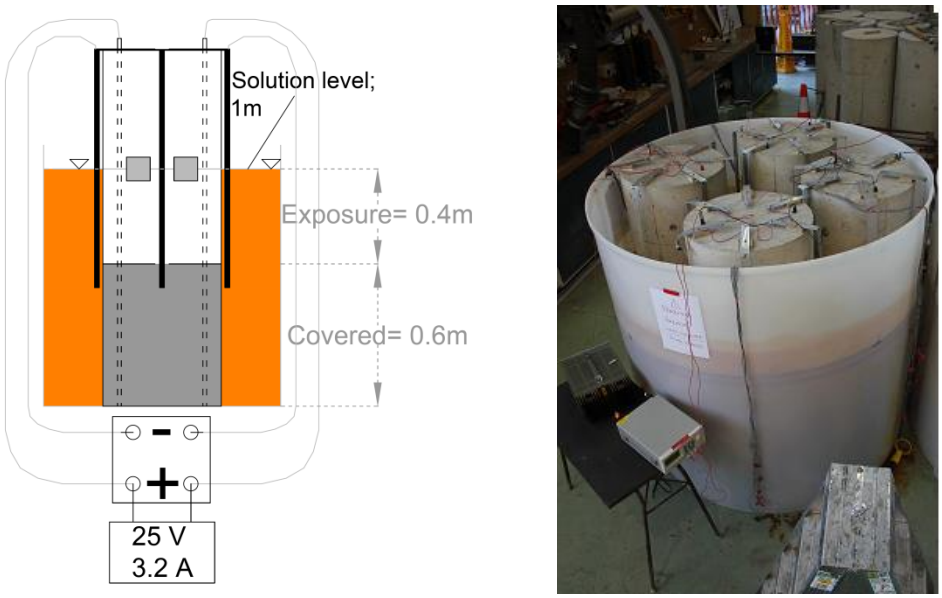

Figure 4-2 Details and a photo of corrosion test setup of RC columns

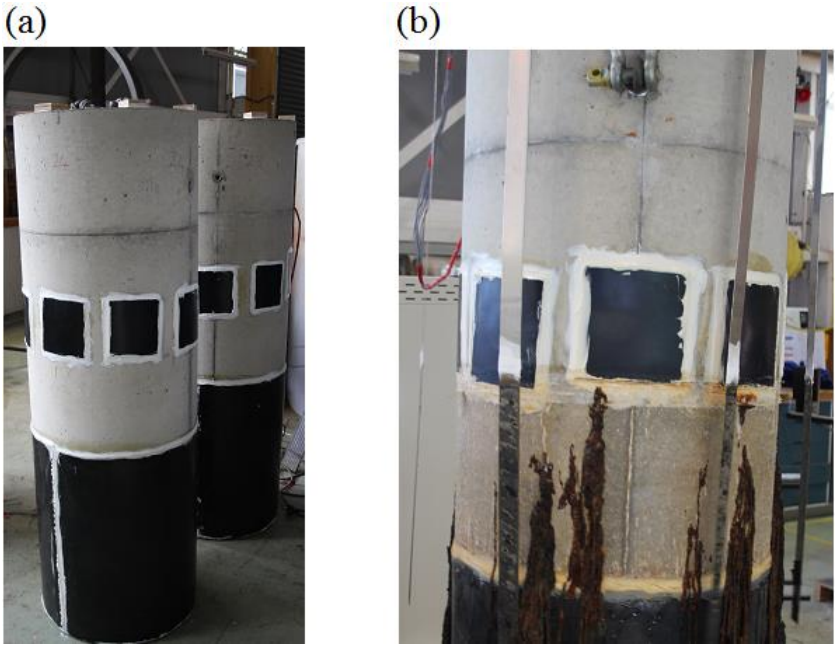

Figure 4-3 The RC columns: (a) prepared columns for corrosion; (b) corroded RC column

Regarding reinforcement corrosion induced concrete cracking, six vertical cracks with maximum crack width of 0.7 mm and eleven vertical cracks with maximum crack width of 1.3 mm were observed for LC and HC columns respectively.

4.1.2.3 CUTTING COLUMNS AND TAKING CONCRETE CORES

The details of cutting the columns are illustrated in Figure 4-4. The columns consisted of one non-corroded and two corroded RC columns with varying degrees of corrosion. To cut columns, the columns were horizontally placed and the middle of the columns was marked. A 300 mm diameter concrete cutter was used to cut the columns. Figure 4-5 shows cut columns and the cross section of the specimens with varying degrees of corrosion. Cracks propagated in concrete cover were observed in cross section of specimens of corroded columns.

Figure 4-4 Details of cutting RC columns

The cut concrete columns were vertically erected with cut surface facing up. The locations of cores were marked on the cross section of the specimens. 35 mm dimeter cores were taken from concrete cover and central part of the specimens. 93 mm diameter cores were taken from the central part of the specimens. Figure 4-6 shows the coring of the columns. In total 40 core samples with 35 mm diameter, eight core samples with 93 mm diameter and three cylindrical samples were prepared for compressive testing. Figure 4-7 shows some 35 mm core samples taken from cover of corroded columns. As shown in Figure 4-7, macro cracks were observed on the core samples taken from cover of corroded columns. It is evident all visible cracks on 35 mm samples are vertical cracks.

It was observed that taking 93 mm core samples from the highly corroded column with appropriate length was not possible. The reason was that reinforcement corrosion and forming corrosion-by-product caused propagating horizontal cracks into central part of the column. Figure 4-8 shows 93 mm diameter core samples taken from the high corroded column with horizontal cracks produced as a result of corrosion product.

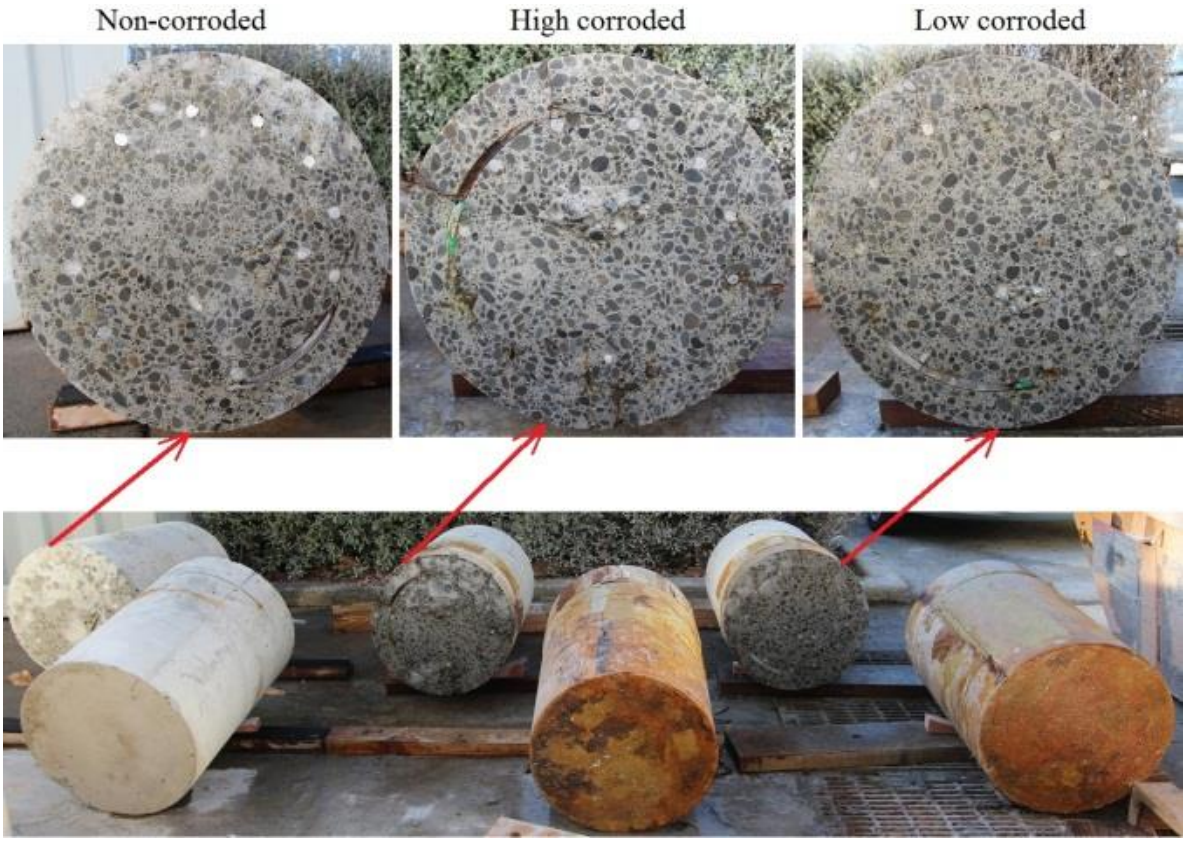

Figure 4-5 Cut columns and their cross sections for varying degrees of corrosion

Figure 4-6 Details of taking cores from column cover (OUT) and core column (IN)

Figure 4-7 Concrete core samples with 35 mm diameter taken from corroded RC columns

Figure 4-8 Horizontal cracks in the 93 mm diameter core samples taken from the high corroded column

4.1.2.4 PREPARATION, INSTRUMENTATION AND COMPRESSION TESTING SETUP

The concrete core samples needed to be prepared for compression tests. Figure 4-9 shows main steps performed to prepare a core sample for testing. First, the ends of the core samples were cut to achieve a flat end sample with height equal to twice the diameter. Second, the concrete surface was properly prepared to fill the voids and seal the surface with a suitable pre-coating material. Finally, to ensure flat ends condition, a few millimetres thick dental-stone plaster was used to cap the ends of samples, after which the strain gauges were installed on prepared surface.

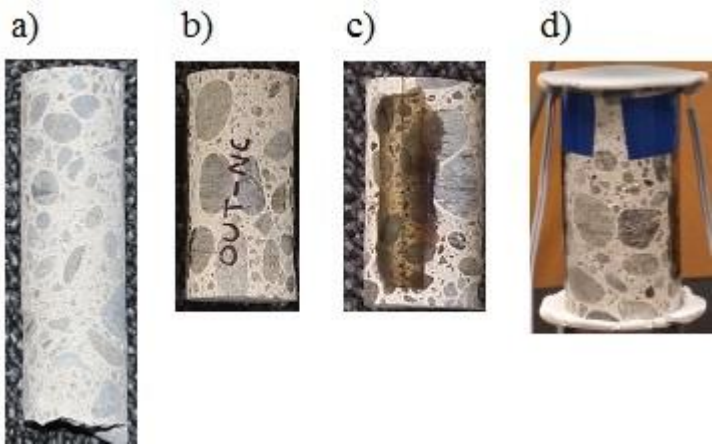

Figure 4-9 Concrete core samples with 35 mm diameter prepared for compression tests: a) core samples, b) cut end, c) coating with suitable material d) installing axial strain gauge

Figure 4-10 shows all samples after filling the voids and sealing the surface with a suitable pre-coating material to be prepared for installing strain gauges.

Figure 4-10 Photo of 35mm diameter core samples prepared for installing axial strain gauges

The samples were loaded under axial compression, and the axial compressive load was directly measured by the machine's load cell. The tests were conducted using displacement control at a rate of 0.00833 mm per second (0.5 mm per minute) and scan rate (reading per second) of 10. Therefore, the overall displacement of sample and corresponding compressive load were recorded within 0.000833 mm throughout the entire displacement range. The axial strain over the central 30 mm length of each sample was recorded by two 30 mm length PFL-30-11-3L electric resistance strain gauges at 180º intervals around the circumference.

Figure 4-11 shows the photos of the test setups. Figure 4-11a and Figure 4-11b show test setup of

35 mm and 93 mm concrete core samples respectively. An INSTRON 100 KN Universal Testing Machine was used with maximum capacity of 100 KN to test the 35 mm samples. The machine had maximum actuator stroke of 1500 mm, and the minimum and maximum velocities of 0.00167 to 1.67 mm/s (0.1 to 100 mm/min) respectively. The INSTRON is an electro-mechanical device using a precisely controlled variable speed drive. The samples were then placed in the INSTRON machine and centrally located on the rigid base platen. The samples were tested at a stroke rate of 0.00833 mm/s, equal to an average rate of strain of 0.00012/s. A similar electro-mechanical machine with maximum 400 KN load was used to test 93 mm and 100 mm diameter samples with an average rate of strain of 0.00012/s.

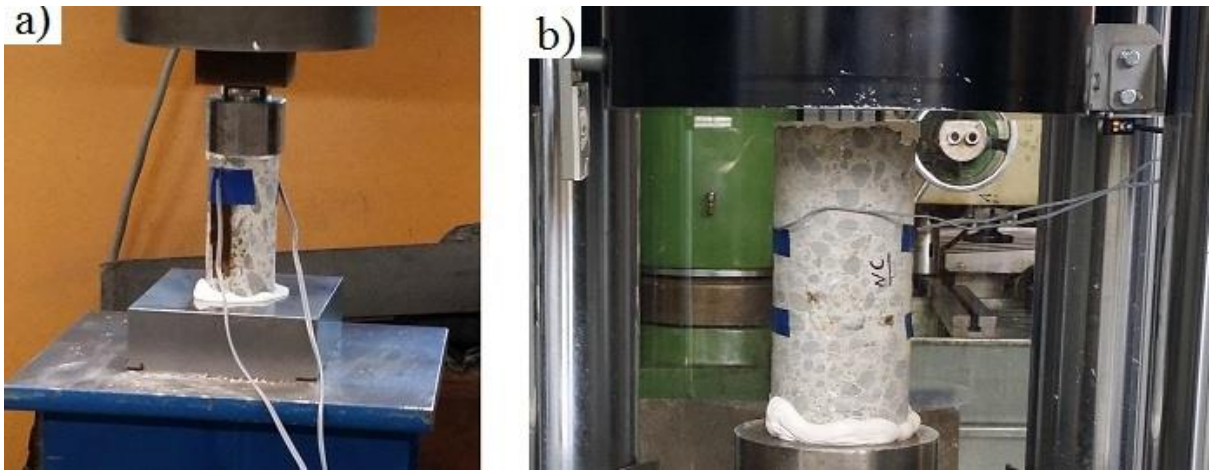

Figure 4-11 Photos of compressive testing a) 35mm diameter samples; b) 93mm and 100mm diameter samples

4.1.3 RESULTS AND DISCUSSIONS

The stress-strain relationships of 35 mm diameter concrete core samples taken from concrete cover of the RC columns are shown in Figure 4-12. The compression load, measured by the machine load cell, was used to calculate the compressive stress. The average of axial strains recorded by the two installed strain gauge for each sample was used to estimate strain of the samples. It is evident that samples taken from the cover of RC column with the high degrees of corrosion showed a significant reduction in strength and ultimate strain compared to the non-corroded columns. As shown in Figure 4-7, the reason is that corrosion product from the steel reinforcement propagated vertical cracks into concrete cover.

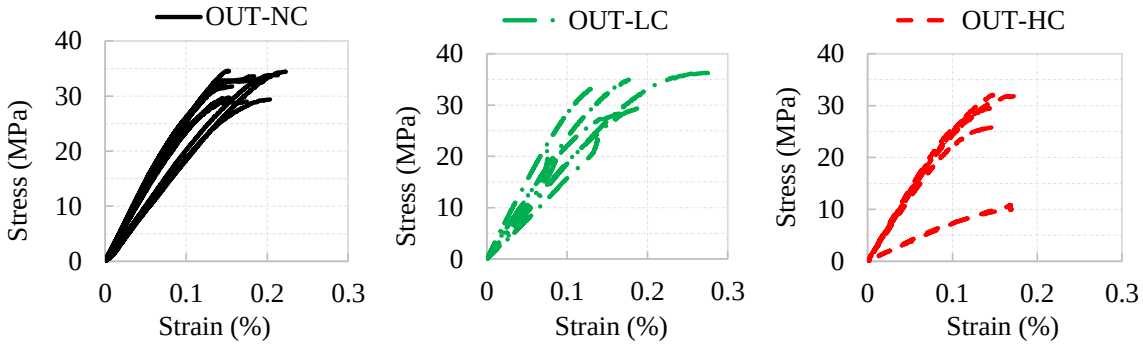

Figure 4-12 Stress- strain of 35mm samples taken from column cover (OUT) with varying degrees of corrosion: Non-corroded (NC); Low corroded (LC); High corroded (HC)

The average of the strength and the ultimate strain of all samples with varying degrees of corrosion tested in this research are summarized in Table 4-1. The results clearly showed that corrosion of steel reinforcement did not affect axial strength and the ultimate strain of central concrete of the RC columns (column core). As mentioned earlier, the reason is that corrosion product from the steel reinforcement propagated horizontal cracks into the central part of the RC columns and the horizontal cracks did not decrease either the axial compressive strength or the ultimate strain of the central parts of RC columns.

Comparing the results for 35 mm diameter samples taken from cover concrete (OUT-NC) and central part of the non-corroded column (IN-NC) revealed that it seems environmental effects such as shrinkage of concrete cover might be responsible for 13% reduction in axial compressive strength of concrete cover of the noncorroded column.

The axial strength and the ultimate strain of 35 mm diameter samples taken from central part of the columns are 23% and 20% respectively less than those for 93 mm diameter samples due to the size effects.

It was also observed that compressive strength of 93 mm diameter samples is 15% less than that experimentally obtained for the 100 mm diameter samples. It seems this reduction is due to damages caused by taking core operation, poorer compaction and less importantly by the size effects.

Evaluating the results obtained for 35 mm diameter samples taken from concrete cover showed corrosion of reinforcement caused reduction in the compression strength and the ultimate strain of concrete cover of the columns. More details regarding corrosion-induced reduction in the axial compression strength and the ultimate strain of concrete cover is discussed in the next section.

Table 4-1 Average experimental results of stress and axial strain of all samples

Sample name	$D = 35mm$				$D = 93mm$		$D = 100mm$		Transverse Reinforcement Corrosion (%)
	Column cover		Column core		Column core		Cast cylinders		
	Stress MPa	Strain (%)	Stress MPa	Strain (%)	Stress MPa	Strain (%)	Stress MPa	Strain (%)	
OUT-NC	32.10	18.4	–	–	–	–	–	–	0.0
OUT-LC	28.60	16	–	–	–	–	–	–	12
OUT-HC	24.10	15.5	–	–	–	–	–	–	33
IN-NC	–	–	36.00	17	48.00	19.5	–	–	0.0
IN-LC	–	–	38.40	18	48.20	24	–	–	12
IN-HC	–	–	37.00	17.4	–	–	–	–	33
Constructed	–	–	–	–	–	–	56.90	23	0.0

4.1.4 DETERIORATION MODEL FOR CONCRETE MATERIALS SUBJECTED TO CORROSION

The experimentally measured axial strength and ultimate strain of non-corroded and corroded columns was employed to develop a deterioration model for the reduction in the strength and the ultimate strain in corrosion damaged concrete

The normalized deterioration for the strength and the ultimate strain of concrete samples taken from concrete cover of non-corroded and corroded RC columns obtained from regression of experimental results are presented in Figure 4-13.

As shown in Figure 4-13, the results show that due to scatter of data, the regression of experimental results cannot be used to develop deterioration model. Therefore, statistical analysis will be discussed to develop deterioration models.

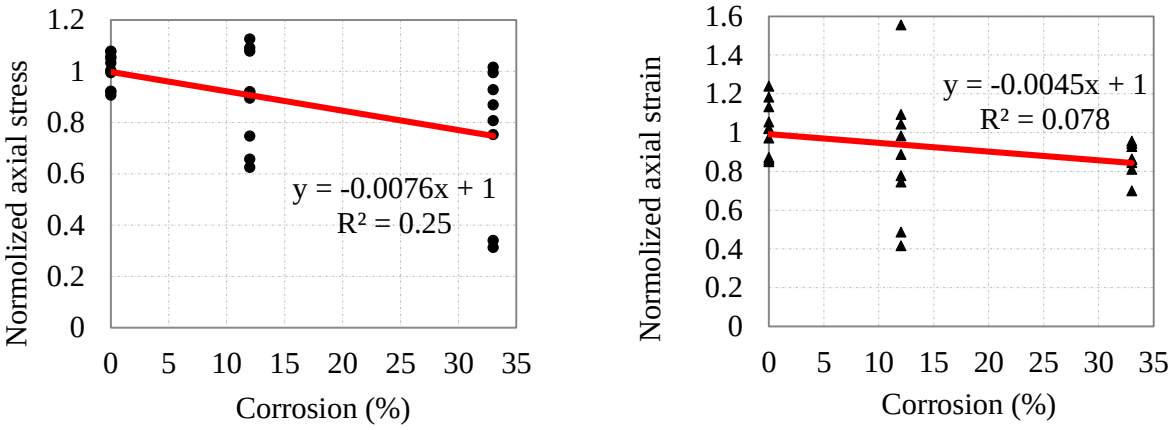

Figure 4-13 Normalized reduction in the axial compression strength and the ultimate strain of cover concrete due to corrosion of steel reinforcement

4.1.4.1 DETERIORATION MODEL FOR CORRODED CONCRETE BASED ON STATISTICAL NORMAL DISTRIBUTION

As shown in Figure 4-13, the variations of experimentally obtained compression strength and strain of concrete is very high for corrosion damaged concrete. Therefore, statistical normal distribution was used to analyse the experimental data. Figure 4-14 and Figure 4-15 show the results of probability mass function and cumulative probability function of compression strength and strain respectively for non-corroded, low corroded and high corroded concrete core samples taken from cover of the RC columns. The values corresponding to 5%, average and 95% stress and strain are shown in Figure 4-14 and Figure 4-15 using vertical lines. Table 4-2 also summarized 5%, average and corresponding standard deviation values of varying degrees of corrosion.

Due to high variation in experimentally obtained compression strength and strain, the values corresponding to 5 % were used to model the effects of corrosion on the compressive mechanical properties of concrete. Using Equation 4-4, the normalized deterioration for the compression strength and the ultimate strain of the concrete core samples due to corrosion based on 5% values are shown in Figure 4-16.

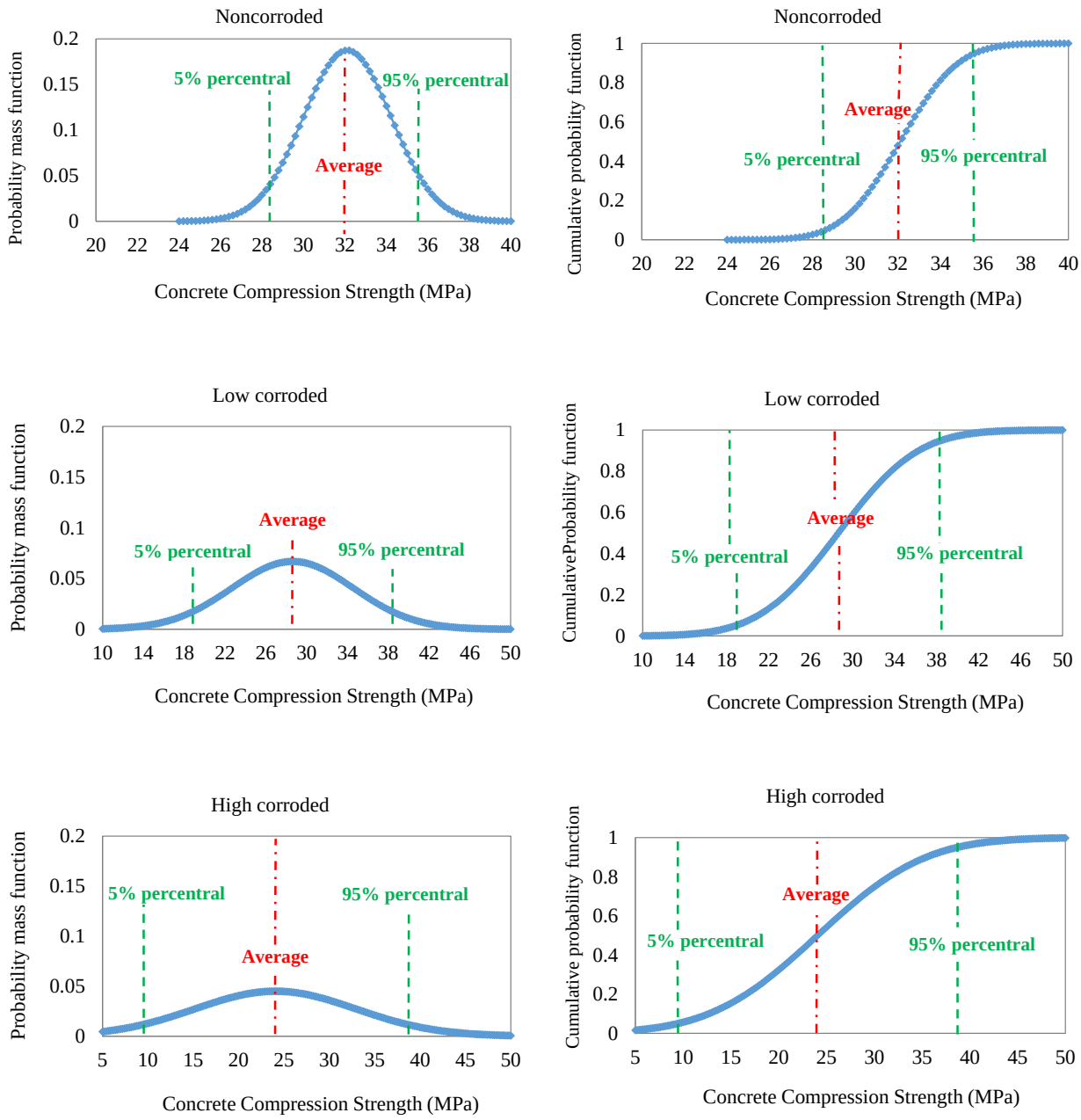

Figure 4-14 Probability mass function and cumulative probability function of compression strength

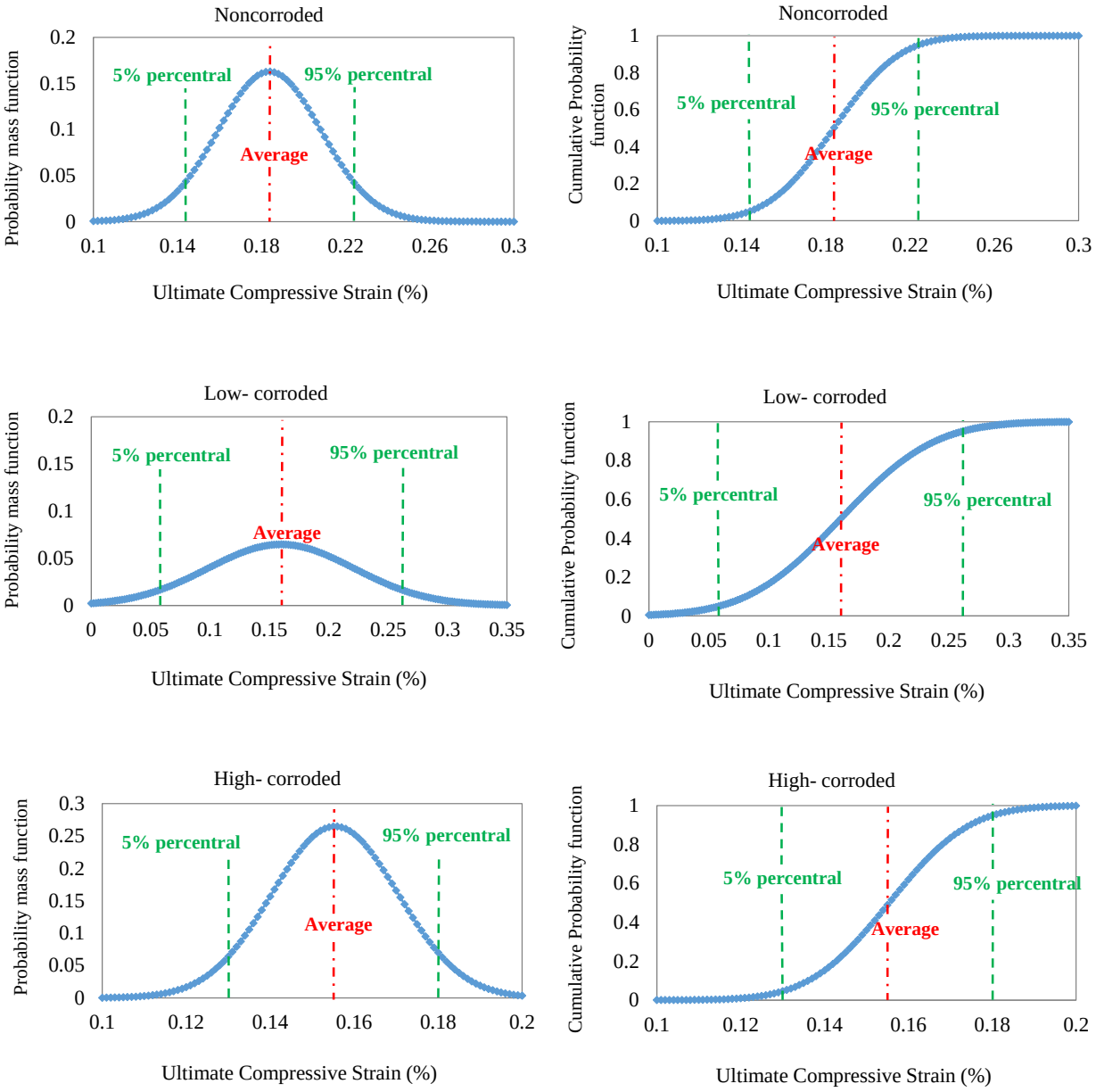

Figure 4-15 Probability mass function and cumulative probability function of compression strain

Table 4-2 Compression strength and ultimate strain corresponding to 5% and average values based on statistical normal distribution and their related standard deviations

Sample name	Mechanical properties of corroded concrete					
	Stress (MPa)			Strain (%)		
	5% precentral	Average	Standard deviation	5% precentral	Average	Standard deviation
OUT-NC	28.6	32	2.1	0.144	0.184	0.025
OUT-LC	18.8	28.6	6	0.058	0.16	0.062
OUT-HC	9.5	24	8.9	0.13	0.155	0.015

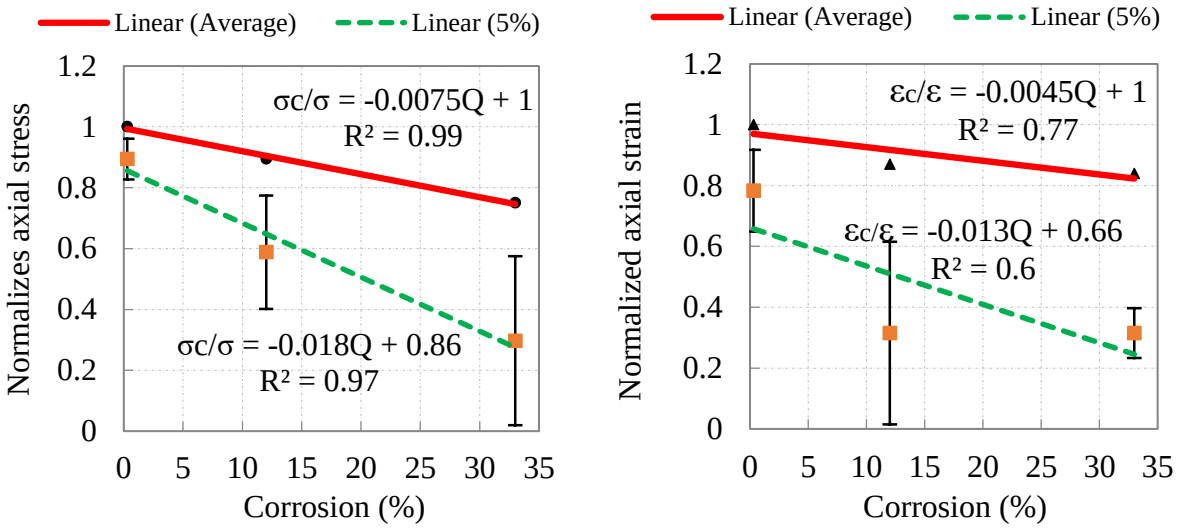

Figure 4-16 Normalized reduction in the axial compression strength and the ultimate strain of cover concrete due to corrosion of steel reinforcement based on average and 5 % values obtained from statistical normal distribution

Assuming a linear trend, as shown in Figure 4-16, the ratio of mechanical properties of corrosion induced cracked to non-cracked concrete can be generally expressed as:

$$\frac{P_c}{P} = 1 - \gamma[Q_{corr}^{T}(\%)] \qquad 4\text{-}4$$

Where: P_c and P are the mechanical properties of corrosion induced cracked and non-cracked concrete respectively, γ is the reduction factor that was regressed from the test result and $Q_{corr}^{T}(\%)$ is corrosion percentage of transverse reinforcement in terms of mass loss.

4.1.5 THE EFFECTS OF CORROSION-INDUCED CRACKED COVER ON THE STRUCTURAL PERFORMANCE OF RC COLUMNS

As the corrosion of reinforcement directly affects concrete cover cracking, the study of the effects of cracked concrete cover on structural performance RC columns is important. To meet this aim, cross- sectional analysis was performed using CUMBIA program (Montejo and Kowalsky, 2007). The effects of cracked cover on structural behaviour can be quantified by developing moment-curvature diagrams using the mechanical properties of sound and cracked cover. The mechanical properties of sound (noncorroded) cover were experimentally obtained in section 4-1-3, and those for cracked cover were predicted using deterioration models presented in Figure 4-16 based on reinforcing bar corrosion. It should be noted that the presented deterioration models were developed as a function of corrosion of transverse bars. Table 4-3 shows the cross-section details of the studied RC column, mechanical properties of concrete cover and average corrosion percentage of longitudinal and transversal steel reinforcement.

Table 4-3 Details of input data of scenarios A and B for moment-curvature analysis

Cross section configuration	Concrete cover	Mechanical properties of cover			Reinforcement corrosion (Average mass loss %)	
		f'_{co} (MPa)	ε_{co}	E_c (GPa)	Longitudinal	Transversal
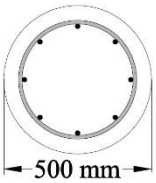	**Sound**	**32**	**0.0018**	**27.39**	**0**	**0**
	Cracked	**15**	**0.0011**	**19.36**	**12**	**30**

Figure 4-17 shows moment- curvature and bilinear moment-curvature of the RC column with Sound and Cracked concrete cover. The key parameters of bilinear moment-curvature results of the RC column with different concrete cover mechanical properties are compared in Table 4-4. The results show the effects of cracked cover on yield curvature can be neglected, but it decreases both yield moment and ultimate curvature.

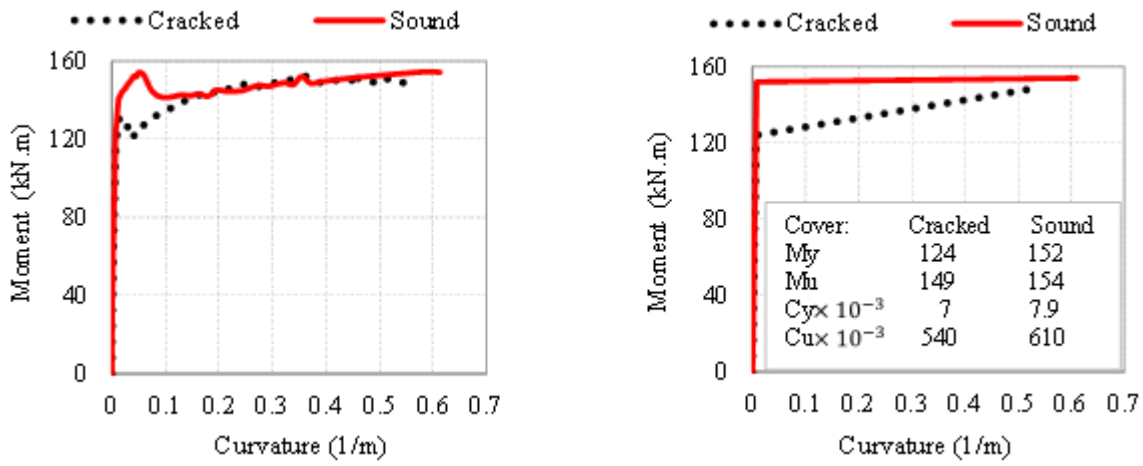

Figure 4-17 Moment-Curvature analysis of a RC column: Scenario1: Cracked cover; Scenrio2: Sound cover

Table 4-4 Results of key parameters of Moment-curvature of RC column for sound and cracked cover based on bilinear Moment-curvature

Cover condition	Yield Curvature (1/m)	Yield Moment (KN.m)	Ultimate Curvature (1/m)
Sound cover	0.0077	152	0.61
Cracked cover	0.0075	124	0.50

4.1.6 LIMITATIONS AND UNCERTAINTY

There are uncertainties in estimation of compression strength and strain of concrete samples through experimental tests. Taking core and testing concrete samples with different sizes increase these uncertainties. The ratio of standard deviation to average value of axial compression strength of 6.5% and 29% were calculated for noncorroded and corroded concrete samples respectively. Moreover, the ratio of standard deviation to average value of axial compressive ultimate strain of 13% and 29% for noncorroded and corroded concrete samples respectively show corrosion increases uncertainty.

4.1.7 CONCLUSIONS

The results from the investigation on the impact of reinforcing corrosion on the mechanical properties of the concrete can be summarized as follows:

- Corrosion of steel reinforcement causes propagation of horizontal and vertical cracks in column cover, and the propagation of only horizontal cracks in column core.
- Corrosion of steel reinforcement resulted in a deterioration of the axial stress and strain of column's concrete cover, but did affect the core of the column.
- The relationship between the degree of transverse reinforcement corrosion and axial compressive strength and strain of column cover samples were quantified to present a deterioration model that can be used in numerical simulation of corroded RC columns. To meet this aim, two methods, regression of experimental data and statistical normal distribution, were used.
- The results shows that cracks from reinforcement corrosion products cause more reduction in axial compressive strength than in axial ultimate strain, but the relationship between axial strain and degrees of corrosion exhibited higher order of non-linearity than that between ultimate compressive strength and degrees of corrosion.
- The experimental results show 14% reduction in compressive strength of concrete of column cover if compared to core column samples for non-corroded column. This reduction might be due to poorer curing or compaction of column cover with respect to column core.

4.2 INFLUENCE OF CORROSION ON THE EFFECTIVE MECHANICAL PROPERTIES OF STEEL REINFORCEMENT

4.2.1 INTRODUCTION

Reinforcement corrosion is one of the primary causes of deterioration in reinforced concrete (RC) structures. Chloride-induced corrosion (the topic of this thesis) is an electrochemical process whit anodic and cathodic half-cell reactions (Montemor et al., 2003). In the absence of chlorides, the reactions produce a stable film that passivates the steel reinforcement. In presence of chlorides the passive film is destroyed and reinforcement corrosion can start once the chloride content at steel surface reached a certain threshold value. Irregular mass loss of steel reinforcement is often a result of corrosion which can lead to a decrease in the effective mechanical properties of steel reinforcement. To quantify the effects of corrosion on the effective mechanical properties of steel reinforcement, reduction factors have been proposed by a number of researchers. A number of experimental studies have been carried out to propose corrosion-induced reduction factors. As presented in Chapter 2, the studies can be classified into three groups in terms of testing type and samples. The first group, the most common tests, used tensile tests on corroded bare reinforcing bars (Allam et al., 1994, Andrade et al., 1991, Maslehuddin et al., 1990a, Saifullah, 1994, Lee et al., 1996b, Almusallam, 2001, Du et al., 2005, Apostolopoulos and Papadopoulos, 2007, Oyado et al., 2011, Hawileh et al., 2011, Andisheh et al., 2016a). The second group performed tensile tests on corroded reinforcing bars embedded in concrete, but concrete was removed before testing (Zhang et al., 1995, Du, 2001, Du et al., 2005, Cairns et al., 2005b, Lee and Cho, 2009, Zhang et al., 2012b). The third group carried out bending tests on corrode RC members (Oyado et al., 2011, Castel et al., 2000).

Despite the multitude of studies undertaken, many aspects of chloride induced reduction factors in the mechanical properties of steel reinforcement are still incompletely understood. And no general agreement on the values of reduction factors have been achieved. As previously discussed, results reported in the literature scatter over a large range. Chapter 2 presented the maximum and minimum values of reduction factors in the effective mechanical properties of steel reinforcement obtained experimentally from 18 published articles. The recently developed reduction factors were used to update the survey presented in Chapter 2 (Andisheh et al., 2016a, Meda et al., 2014). Finally, to illustrate variations in the values reported by past studies, the maximum and minimum values of reduction in yield and ultimate stress, modulus of elasticity

and elongation are shown in Figure 4-18. The maximum to minimum ratios of reduction in yield and ultimate stress, modulus of elasticity and elongation are 2.8, 2.5, 1.53 and 3.68 respectively. As can be seen, there is a wide variation in the results of reduction factors published in the literature, indicating need for further studies.

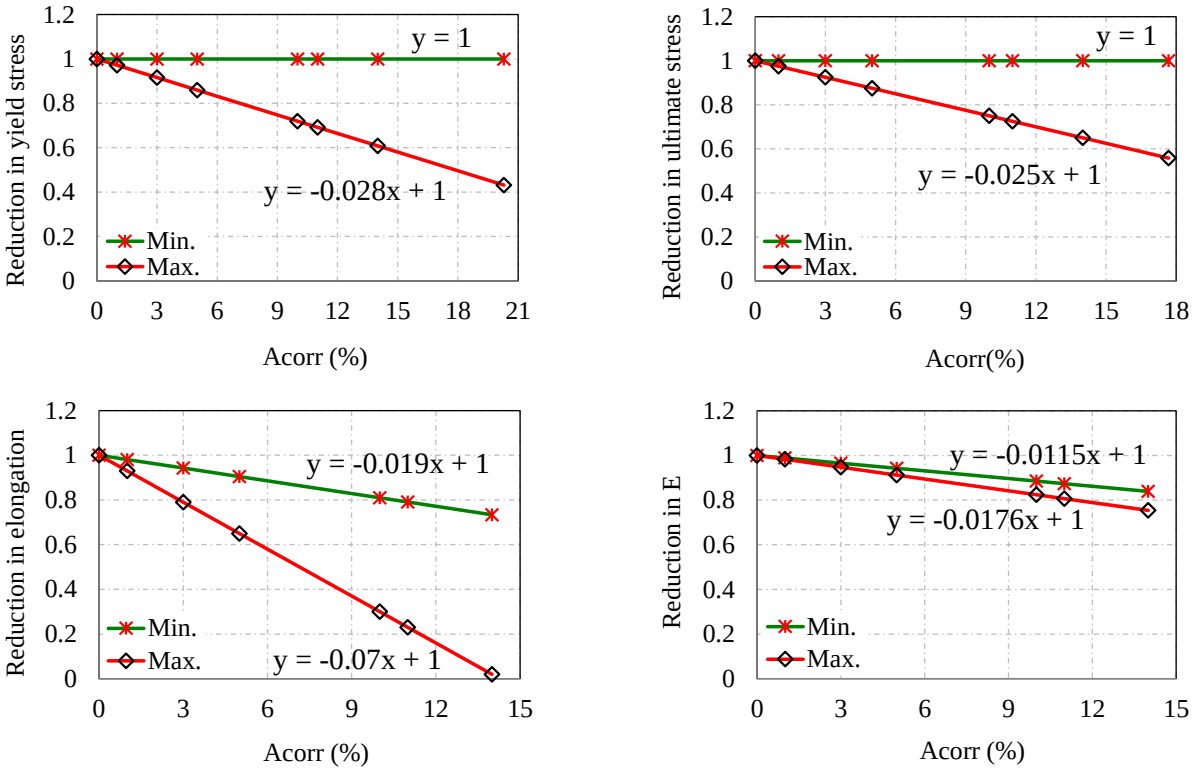

Figure 4-18 Maximum and minimum reduction factors for elongation, modulus of elasticity, yield stress and ultimate stress

Corrosion test set-ups of bare bars are simple, fast and much more cost effective if compared with corrosion test set-ups of full-scale RC members such as RC columns and piers. Therefore, the majority of the suggested reduction factors developed were based on experimental results carried out on bare bars exposed to accelerated corrosion. The main question is whether the suggested reduction factors for bare bars can precisely model the effects of corrosion on the effective mechanical properties of steel reinforcement in RC structures. An experimental study showed that the reduction factors for corroded bare steel reinforcement and those corroded while embedded in concrete are similar (Du et al., 2005). However, a recent experimental study showed that the reduction factors for corroded steel bars while embedded in concrete are significantly greater than those for bare bars (Meda et al., 2014). The conflicting results and

opposing conclusions published by previous studies indicate a need for further studies. In this regard, critical questions arise, such as the reason(s) for these conflicting results. Which reduction factors are more accurate to model corrosion-induced deterioration in RC structures? This chapter will provide answer to these questions based on reviewing past studies and the results observed from experimental inspection of corroded steel reinforcement carried out in this research. The experimental results were used to develop a refined analytical model for corrosion-induced deterioration in real RC structures.

The analytical model was developed, based on the results of inspection of corroded steel reinforcement while embedded in concrete, and was validated against experimental results published by a recent study (Meda et al., 2014). Unlike corroded bare reinforcement, an unequal mass loss was observed on the two sides of corroded reinforcement while embedded in concrete. More mass loss accrued on the side nearer the concrete cover compared with the back side, causing centroid relocation leading to a bending moment when the corroded steel reinforcement is subjected to axial force. The corroded steel reinforcement with unequal mass loss reached the yield point with less axial force than a similar corroded sample with equal mass loss. Therefore, it can be concluded that the bending moment induced by unequal mass loss increases corrosion-induced reduction factors. It is obvious that using the reduction factors of corroded bare steel reinforcement for corroded RC columns and piers is not safe.

To meet the objectives of this chapter, a novel methodology is used to develop advanced corrosion-induced reduction factors for steel reinforcement of corroded RC columns and piers, based on unequal mass loss. The advantages of the presented methodology are as follows:

1. It provides advanced and accurate reduction factors to estimate the effective mechanical properties of steel reinforcement of corroded RC structures.
2. It is much more time- and cost-effective than experimental methods for full-scale RC members.
3. The advanced reduction factors can be estimated for a wide range of corrosion percentage, geometrical and mass loss details.
4. It can be used to update the existing reduction factors for corroded bare steel reinforcement published in past studies.

The presented methodology illustrated in Figure 4-19 has three main steps. Step 1 is the

development of corrosion-induced reduction factors for corroded bare steel reinforcement.

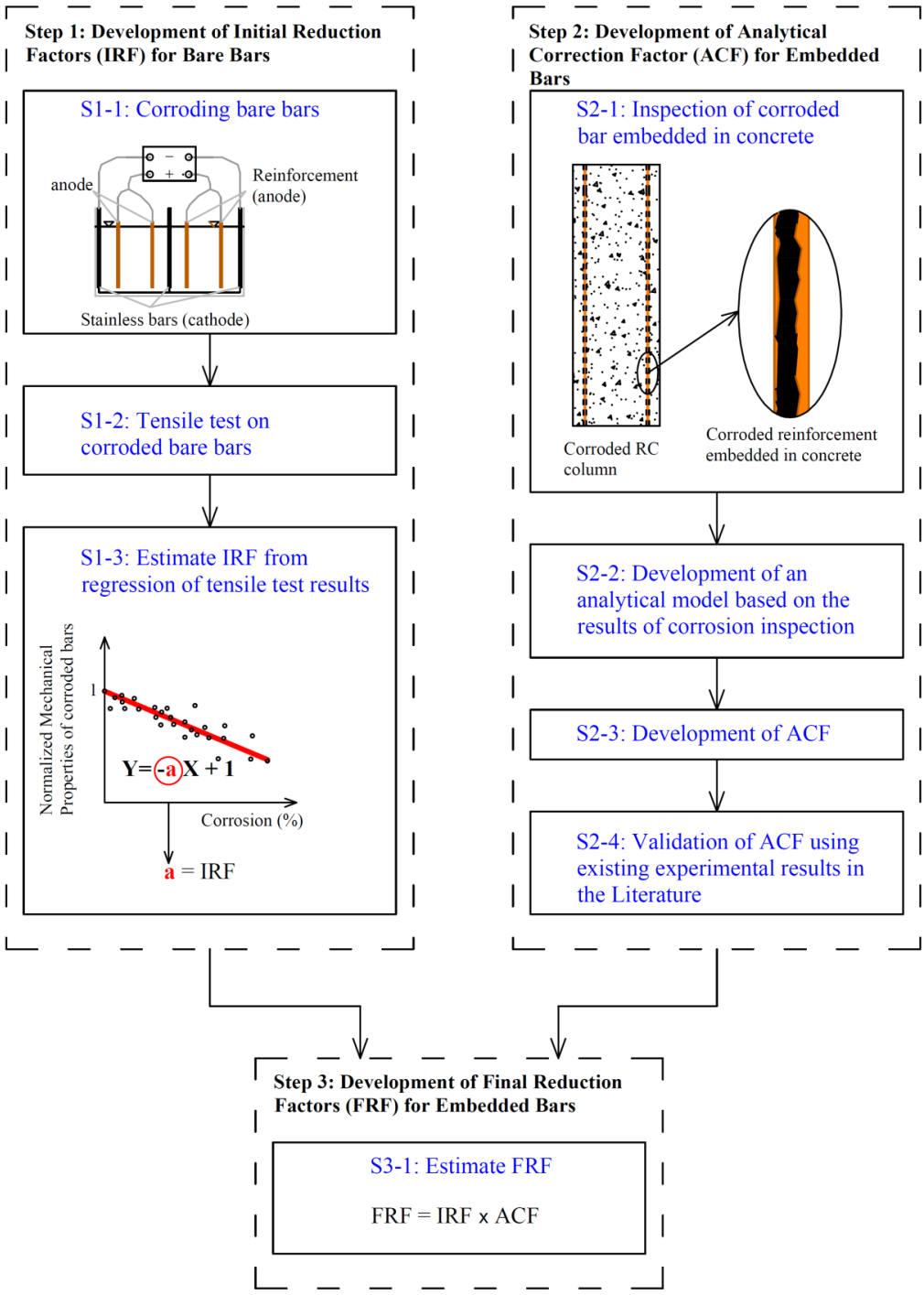

Figure 4-19 The proposed methodology to develop reduction factors for corroded steel reinforcement of RC structures

Step 1 (S1) includes three sections. After corroding bare steel reinforcement, tensile tests are

carried out on the corroded and noncorroded steel reinforcement. The recorded stress and strain of samples during tensile tests are used to estimate the effective mechanical properties of tested samples. The reduction factors for bare steel reinforcement (named *initial reduction factors* [IRF]) are estimated based on regression of the experimental results of tensile tests. Step 2 is the development of analytical correction factors (ACFs) based on the results of inspection of corroded steel reinforcement while embedded in concrete. The analytical model was used to suggest correction factors for various geometrical and mass-loss details. The analytical correction factors, the maximum tensile stress of a corroded sample subjected to tensile force assuming unequal mass loss to that of equal mass loss ratio, were validated using existing experimental results published by Meda et al (Meda et al., 2014).

Step 3 is the development of reduction factors for corroded steel reinforcement of RC structures (named *final reduction factors* [FRF]). The final reduction factors equal the initial reduction factors multiplied by the appropriate analytical correction factors. As mentioned before, the final reduction factors are greater than the initial reduction factors due to unequal mass loss occurring in corroded steel reinforcement of full-scale RC members. Therefore, the results of this research confirm that modelling deterioration in RC structures using reduction factors obtained for bare bars is not safe. It means that the residual structural capacity of corroded RC structures is lower than that estimated by developed deterioration models based on corroded bare steel reinforcement. The importance of advanced and more accurate reduction factors for retrofit, optimal design based on life cycle analysis, and asset management of RC infrastructure is obvious.

4.2.2 EXPERIMENTAL PROGRAM TO DEVELOP REDUCTION FACTORS FOR THE EFFECTIVE MECHANICAL PROPERTIES OF CORRODED BARE STEEL REINFORCEMENT (STEP 1)

As discussed in Chapter 3, the corrosion that causes 1 % loss of cross section usually leads to more than 1 % reduction in the effective mechanical properties of reinforcing steel.

The experimentally measured stress and strain values of the bare bar samples during tensile tests were used for modelling the corrosion-induced reduction in the effective mechanical properties of steel reinforcement. The investigated mechanical properties include yield and ultimate stress, modulus of elasticity, and elongation. The experimental program of Step 1 includes (a) corrosion testing setup for bare steel bars, (b) monotonic tensile tests on noncorroded and corroded

samples, and (c) analysis the results to estimate the reduction factors.

4.2.2.1 CORROSION TESTING SETUP

In order to corrode the bare steel reinforcement within a reasonable time period, an accelerated corrosion method, called the impressed current method, was used in this study. An accelerated corrosion rate of 800 $\mu A/cm^2$ was achieved by applying a constant electrical current to the steel reinforcement using a power supply. The steel reinforcement, acting as the anode, was submerged in a 3.5% NaCl solution and directly connected to the positive terminal. Some stainless steel plates, submerged in the NaCl solution, acting as the cathode, were directly connected to the negative terminal. The current flowed from the steel reinforcing to the stainless steel plates through the 3.5% NaCl solution, acting as electrolyte. Figure 4-20 shows details of the corrosion test set-up of the steel reinforcement. The central 300 mm length of the total 600 mm length of each sample was corroded. The corrosion tests were conducted within two predetermined times to obtain two different degrees of corrosion corresponding to low and high degrees of corrosion. The target mass-loss percentages were up to 10% and 30% for low and high degrees of corrosion, respectively.

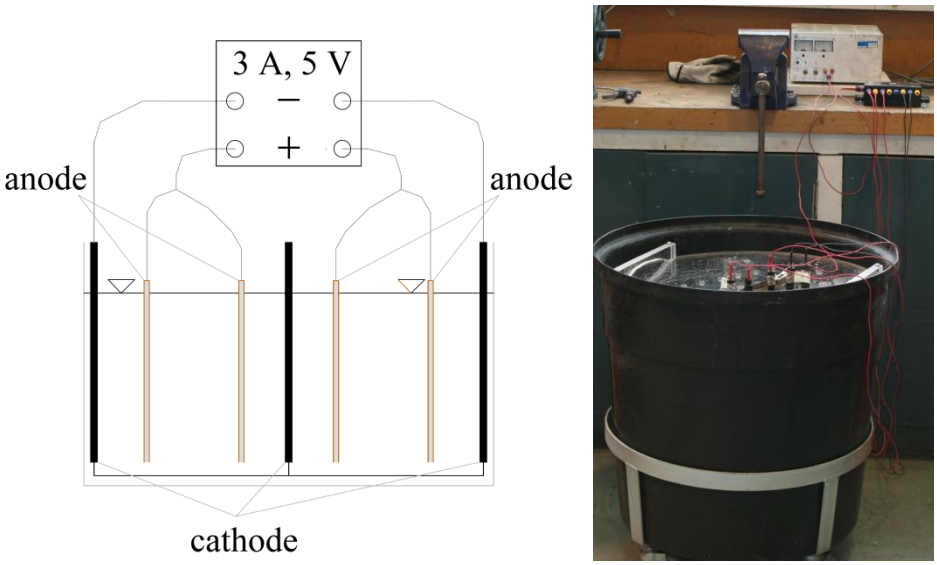

Figure 4-20 Details of corrosion test set up of steel reinforcement

4.2.2.2 TENSILE TESTING SETUP AND THE RESULTS

Eighteen corroded and 9 noncorroded bare steel samples, each 600 mm in length with 300 mm gauge length, were tested under static tensile tests. The tensile tests were run with a loading rate

of 1 mm of deformation per minute in the elastic region and 2 mm per minute in the plastic region. All tests were continued until rupture of the samples. The results of tensile tests in terms of stress–strain graphs of all samples with varying degrees of corrosion are shown in Figure 4-21. Strain at the middle of each sample was measured during tensile testing.

The results clearly show that corrosion decreased the effective mechanical properties of the steel reinforcement.

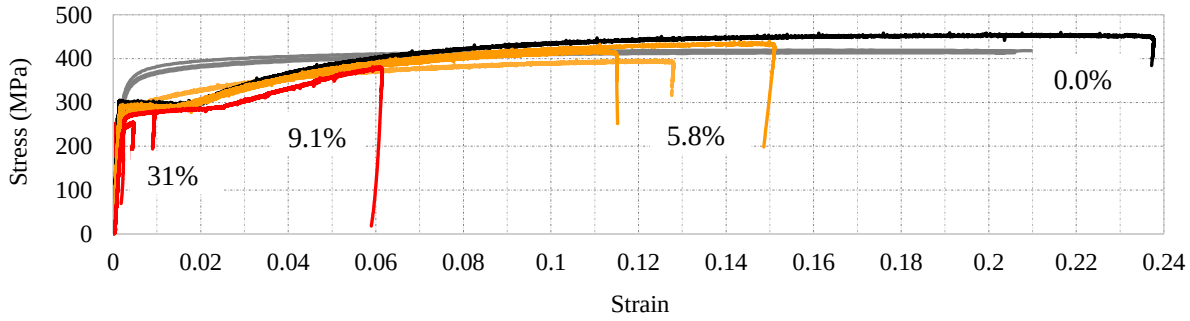

Figure 4-21 Stress–strain graphs of reinforcing bars with varying degrees of corrosion

4.2.2.3 REDUCTION FACTORS FOR THE EFFECTIVE MECHANICAL PROPERTIES OF CORRODED BARE STEEL REINFORCEMENT

The measured responses for corroded and noncorroded steel reinforcement were used for modelling the chloride corrosion-induced reduction in the effective mechanical properties of steel. The investigated mechanical properties include yield and ultimate stress, elongation (ultimate strain), and modulus of elasticity. As discussed in Chapter 3, past studies have modelled the reduction in the mechanical properties of steel reinforcement using linear regression. However, the study carried out by the author confirms that linear regression is not appropriate for chloride-induced corrosion. An observation from the results of this research is that the increment reduction in the effective mechanical properties of steel reinforcement tends to be greater for lower amounts of corrosion than for higher amounts of corrosion, certainly implying a nonlinear trend. To simplify the estimate of reduction factors for the effective mechanical properties of bare steel reinforcement, the nonlinear trends have been replaced by piecewise linear trends consisting of two segments. The segment boundaries have been selected considering the corrosion levels and the intersection of the two sequential segment lines. This simplification provides the possibility to compare the results of this research with results in the literature.

The normalised deterioration for the mechanical properties of corroded steel bars, are presented in Figure 4-22. In this figure, the symbols of mechanical properties with and without the subscript “c” correspond to the mechanical properties of corroded and noncorroded steel bars respectively.

Assuming a linear trend, the relationship between the mechanical properties of corroded and noncorroded bare steel reinforcement can be generally expressed as:

$$P_c = [1 - \gamma(Q_{corr})] \times P \qquad 4\text{-}5$$

where, P_c and P are the mechanical properties of corroded and noncorroded bare steel reinforcement respectively; γ is the corresponding reduction factor that was obtained from regression of the test results; and $\mathrm{Q_{corr}}$ is the corrosion percentage.

The reduction factors, estimated for the mechanical properties of bare bars (IRF) assuming a bilinear regression model, are shown in Table 4-5. The upper boundaries of the two segments for the bilinear regression model were taken to be 10% and 30% reduction in cross-sectional area.

The mechanical properties of corroded bare steel reinforcement can be easily estimated using Equation 4-5 and the information presented in Table 4-5 as a function of the mechanical properties of the noncorroded steel reinforcement. The estimation of the appropriate reduction factors are proposed should be carried out based on selecting whether the amount of corrosion is considered low or high.

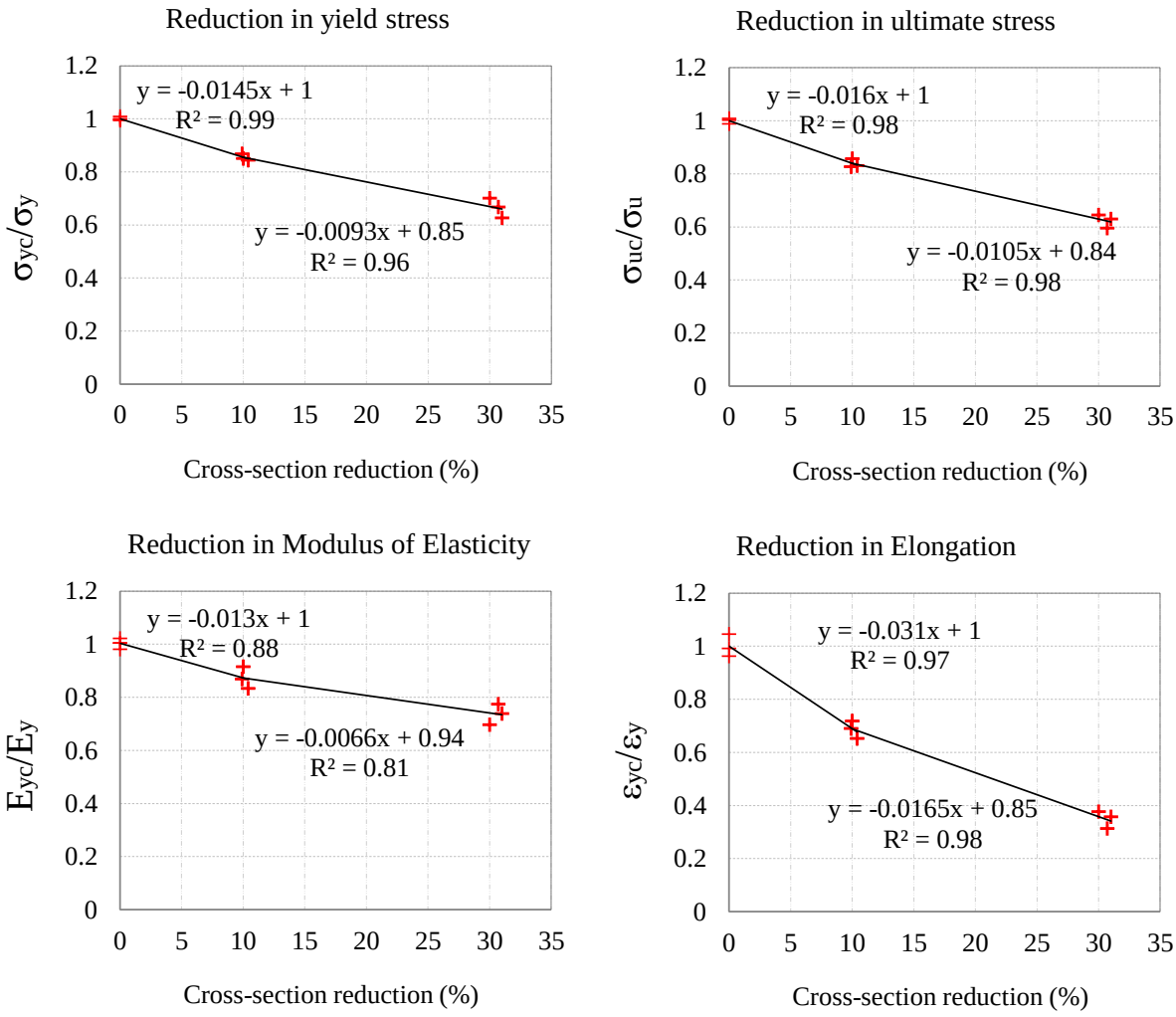

Figure 4-22 Normalised reduction in the effective mechanical properties of bare steel reinforcement

Table 4-5 Initial reduction factors (IRF) based on experimental results of bare bars

The degree of corrosion in terms of mass loss percentage (Q_{corr})	Reduction factors (γ) in:			
	Yield stress (σ_y): γ_{σ_y}	Ultimate stress (σ_u): γ_{σ_u}	Modulus of Elasticity (E): γ_E	Elongation (ε_u): γ_{ε_u}
$0 < Q_{corr} \leq 10$	0.0145	0.016	0.013	0.031
$10 < Q_{corr} \leq 30$	0.0093	0.0105	0.0066	0.0165
Correlation coefficient, R^2	0.98	0.96	0.81	0.98

4.2.3 COMPARING REDUCTION FACTORS FOR CORRODED BARE AND CORRODED BARS WHILE EMBEDDED IN CONCRETE PUBLISHED BY PAST STUDIES

As discussed in Section 4.2.1, there are conflicting results and opposing conclusions regarding chloride-induced reduction factors for corroded bare steel reinforcement and those corroded while embedded in concrete. Du et al. compared the reduction factors of corroded bare steel bars and those corroded while embedded in a thin concrete slab submerged in NaCl solution with the same concrete cover at the top and bottom (Du et al., 2005). They concluded that the reduction factors for bare steel bars and those corroded while embedded in concrete are similar (Du et al., 2005). Meda et al. estimated the reduction factors for bare steel bars and those corroded while embedded in square RC columns with 300×300 mm cross section, 1500 mm height, and unknown concrete cover (Meda et al., 2014). In the corrosion test set-up of this current study, thickness of concrete cover either side of the steel reinforcement is not equal, so it is similar to real RC members subjected to corrosion. The results showed that the reduction factors for corroded reinforcement while embedded in the RC columns are significantly greater than those for corroded bare steel reinforcement (Meda et al., 2014). Reduction factors in the effective mechanical properties of steel reinforcement, based on the experimental results obtained by the above studies for bare bars and bars embedded in concrete, are compared in Table 4-6 (Meda et al., 2014, Du et al., 2005). Here, $A_{corr}\%$ is corrosion percentage of steel reinforcement; α_y; α_u; ε_u are reduction factors in yield stress, ultimate stress and ultimate strain respectively.

Table 4-6 Corrosion-induced reduction factors in the effective mechanical properties of bare bar and bars embedded in concrete (Du et al. 2005; Meda et al. 2014)

References	**Sample(Diameter (mm)); test; number of samples**	**Corrosion Method and condition**	$A_{corr}\%$	α_y	α_u	ε_u
Meda et al. (2014)	Bare bars (16); T; 3	Acc. 50 mA/cm^2; 3% Na-Cl;	21.57	0.02	0.02	0.023
	Embedded bars (16); T; 8	Acc. 3% Na-Cl	20.29	0.028	0.025	0.035
Du et al. (2005)	Bare and embedded bars	Acc. 3.5% Na-Cl	≤ 25	0.018	0.019	---

It can be concluded that the main reason for the opposite conclusions reported by the studies above is because of the different corrosion test set-ups. Therefore, corrosion inspection is needed

in further studies on corroded bare steel reinforcement and corroded bars while embedded in large-scale RC columns. The experimental corrosion inspection of corroded bare bars and corroded bars embedded in large-scale RC columns will be discussed in the next section.

4.2.4 EXPERIMENTAL PROGRAM TO EVALUATE CORRODED STEEL REINFORCEMENT (STEP 2)

The objective of the evaluation is to compare the corroded bare bars with corroded steel reinforcement retrieved from the corroded RC columns and piers. The corroded bars while embedded in concrete were retrieved from 14 corroded RC columns. The details of the corrosion test set-up of RC columns are presented in Section 4-1. An accelerated electrochemical method – the impressed current – was used to corrode both bare steel bars and steel reinforcement of RC columns within a reasonable time frame. The main steps to experimentally evaluate corroded steel reinforcement are (a) estimating the average corrosion of corroded bars after removing corrosion by-product, (b) visual inspection of corroded bare bars and bars embedded in concrete, (c) measuring the maximum pit depth, and (d) 3D scanning of the corroded steel reinforcement embedded in concrete.

4.2.4.1 ESTIMATING CORROSION AND OBSERVATIONS

In order to evaluate the corrosion percentage of corroded steel bars, corrosion by-products were removed using a wire brush. After cleaning the corroded steel reinforcement, a mass-loss approach was used to estimate the average corrosion of steel reinforcement as follows:

$$\text{Corrosion (Mass loss)}\ \% = \frac{W_0 - W_2}{W_0} \times 100 \qquad 4\text{-}6$$

W_0: Weight of the sample before corrosion (N)

W_2: Weight of the sample after corrosion (N)

The results of estimating corrosion percentage of the samples are presented in the second column of Table 4-7.

4.2.4.2 VISUAL INSPECTION OF CORRODED STEEL REINFORCEMENT

Visual inspection of the steel reinforcement retrieved from the corroded RC columns and piers revealed that more mass loss occurred on the side of the steel reinforcement closer to the

concrete cover (cover side) compared to that of the back side (core side). It was also observed that for the majority of the surveyed samples with corrosion up to 8 %, virtually all mass losses were observed on the cover side. In the present investigation, using an impressed current to drive the corrosion process, the cover side (outer surface) of the stirrups and the longitudinal bars (anodes) were closest to the external stainless steel cathodes resulting in a shorter ionic pathway. In the case of a real structure the Cl^- ions would penetrate the outer cover first causing de-passivation on the cover side of the steel prior to the interior. The results of visual inspection also show that, unlike the steel reinforcement retrieved from corroded RC columns, mass losses were almost uniformly distributed on either side of the bare bars. Therefore, further investigation using 3D scanning was only applied for steel bars embedded in concrete. Figure 4-23 compares the corrosion configurations of the two opposite sides for both bare bars and bars embedded in concrete since there was little difference in observed pattern of corrosion for the bare bars.

Figure 4-23 Upper: real corroded steel reinforcement in concrete, (a) back side, (b) cover side; Lower: Corroded bare bar, (c) back side (d) front side

4.2.4.3 THREE DIMENSIONAL (3D) SCANNING OF CORRODED BARS AND THE RESULTS

To quantify the difference in mass loss between the cover side and the interior side of the steel reinforcement retrieved from corroded RC columns and piers, a three-dimensional (3D) scanning approach was used.

The corroded bars were first marked with various colours of liquid chalk. These marks and corrosion features allowed later alignment of the scans. With the bars resting on feature-rich supports they were scanned using an Artec Spider handheld device, Figure 4-24. Due to the

shape and size, multiple scans were taken and aligned together using the Artec Studio software. The surface model generated was then imported into Geomagics Design X software to convert the stereolithographic file to one that SolidWorks computer aided design (CAD) software which could be manipulated. By overlaying a virtual, noncorroded bar over the virtual corroded bar and performing a Boolean subtraction for the outer (cover) half and inner (core) half the remaining volume for each was determined by the CAD software.

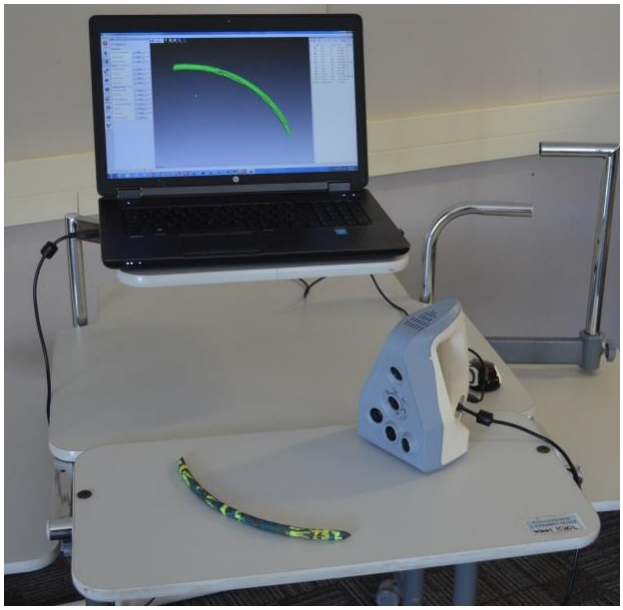

Figure 4-24 Photo of 3D scanning machine and sample scanning

Table 4-7 summarizes the results of 3D scanning of corroded steel reinforcement. Columns 2 and 3 show the total mass lost using weighing, and the 3D scanning approach, respectively. The errors of differences between values shown in columns 2 and 3 are presented in column 4. The error values show that 3D scanning results are in very good agreement with the results obtained based on the weighing approach. Columns 5 and 6 compare mass loss on the cover side and on the core side respectively. The results show that the average 15% mass loss consisted of 10.9% mass loss occurring on the cover side and only 4.1% mass loss occurring on the core side.

Figure 4-25 illustrates the details of corroded steel reinforcement in a corroded RC column or bridge pier based on the results of the 3D scanning.

Table 4-7 Experimental results of 3D scanning of corroded reinforcement

Sample	Total lost (%) Measuring mass	Total lost (%) 3D scanning	Error (%)	Outer lost (%)	Inner lost (%)	$\frac{Outer\ lost}{Inner\ lost}$
1	7.3	7.28	-0.3	4.64	2.64	1.76
2	20.2	20.29	+0.4	16.61	3.68	4.51
3	23.5	23.35	-0.6	14.18	9.17	1.55
4	24.5	24.47	-0.1	15.80	8.67	1.82
5	14.1	14.16	+1.1	13.33	0.83	16.1
6	22.0	22.04	+0.2	14.38	7.66	1.88
7	21.0	20.67	-1.6	14.11	6.56	2.15
8	11.5	11.66	+1.4	10.81	0.85	12.72
9	17.0	17.12	+1.7	9.79	7.33	1.34
10	14.7	14.69	0.0	11.04	3.65	3.00
11	13.1	13.09	0.0	9.53	3.56	2.67
12	12.7	12.79	+0.7	7.54	5.25	1.44
13	7.9	7.87	-0.4	6.88	1.00	6.88
14	7.1	7.12	+0.3	5.86	1.26	4.65
15	15.0	15.04	+0.2	13.38	1.67	8.00
16	8.5	8.50	0.0	6.81	1.70	4.00
Average	**15.0**	**15.00**	**0.0**	**10.90**	**4.10**	–

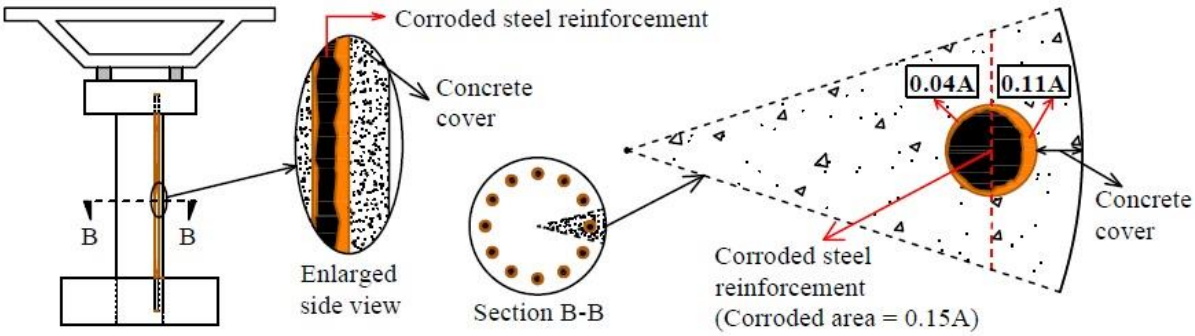

Figure 4-25 Details of corroded steel reinforcement in a bridge pier

The results of visual inspection and 3D scanning clearly show the differences in the proportioning of mass loss around the cross section of reinforcing bars that have been corroded while embedded in concrete compared to the uncovered bare bars. The unequal mass loss and pit damage found in corroded embedded bars is a likely explanation for the reported discrepancies

in reduction factors for the two types of bars. Greater mass losses, deeper pits and the distribution of more pits on the cover side of steel reinforcement in RC columns lead to relocation of the neutral axis and consequently influence the effective mechanical properties of steel reinforcement under axial loads.

To study the effects of pitting corrosion on the residual capacity of corroded RC structures, other researchers have estimated pitting factors and used it to calculate pit depth and associated loss of cross sectional area. Pitting factor is the ratio of maximum pit depth to average corrosion penetration. Chapter 3 presented pitting factors research published in eight past studies. The pitting factors were developed based on equal corrosion penetration either side of the steel reinforcement. Considering the experimental observations in this research, pitting factors for the cover side of steel reinforcement are smaller than those reported by past studies, due to greater corrosion penetration. It is noted that for corroded samples with unequal mass loss pitting factor for the side with greater mass loss is smaller than that for the other side.

4.2.5 ANALYTICAL MODELLING OF BEHAVIOUR OF CORRODED STEEL UNDER AXIAL LOADS

To study tensile behaviour of corroded steel reinforcement while embedded in concrete, an analytical model was developed. Figure 4-26 illustrates the details of the analytical model. The model shows a bridge pier with corroded longitudinal steel reinforcement. It is evident when the bridge pier is subjected to lateral loads such as an earthquake that the corroded longitudinal steel reinforcement is subjected to axial loads.

The simulated model of the corroded bar and its geometrical parameters are shown in Figure 4-26, where α is the length of noncorroded parts, and β is the length of the corroded part of the steel reinforcement. Using the results of 3D scanning, aa, is the neutral axis relocation due to unequal mass loss on the either side of the steel reinforcement.

The analytical model was developed based on the following assumptions:

- Corrosion-induced irregularities on the cover side and the core side offset (cancel) each other, so the corrosion was modelled as uniform mass loss.
- The maximum pit damage, a hemispherical cavity, was modelled at the middle of the corroded steel reinforcement on the cover side. Depth of the modelled pit at the middle

was equated by differential pit depths of either side of the bar. It was assumed that the other pit damages on the cover side and the core side offset each other.

- The parts of longitudinal steel reinforcement of the pier/column, which are located in the cap beam at the top and the foundation at the bottom of the bridge pier, were not corroded due to thick concrete cover. Since the bridge column is located at the centre of the cap beam and foundation, the concrete cover of the longitudinal reinforcement of the pier located at the cap beam and foundation is much greater than for the rest of column.
- The bond between corroded steel reinforcement and concrete over the corroded length was neglected. It should be noted that once the corrosion of steel reaches a critical level, cover spalling and debonding occurs between steel and concrete. Therefore, a part of severely corroded steel reinforcement of a corroded RC column or bridge pier is likely to be similar to the structural model shown in Figure 4-26

In accordance with above assumptions, compared to noncorroded bar, the simulated corroded bar is a circular bar with smaller diameter but having a hemispherical cavity at the middle on the cover side and a relocated centre of cross section due to unequal mass loss and pit damage.

The structural model of the corroded longitudinal steel reinforcement subjected to tensile force and its response in terms of a bending moment diagram are shown in Figure 4-26. It is evident that the bending moment is because of the eccentric tensile force caused by different mass loss on either side of the steel reinforcement and by the pit damage. For the structural model of corroded steel reinforcement shown in Figure 4-26, the maximum bending moment, M_{max}, for varying pit depths and α/β ratio values were calculated.

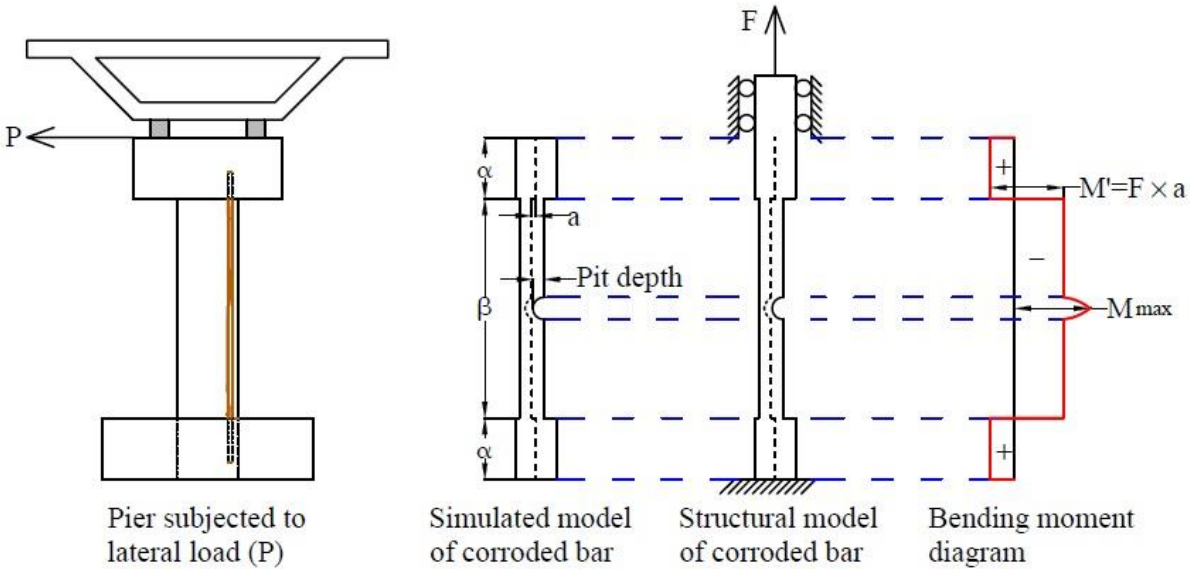

Figure 4-26 Details of analytical model of corroded longitudinal steel reinforcement and its bending moment diagram

When the corroded steel reinforcement embedded in concrete is subjected to axial load, the unequal mass loss and pit damage on the either side of the corroded steel reinforcement cause a bending moment. The bending moment decreases the residual effective yield stress, ultimate stress and ultimate strain of the corroded steel reinforcement. To quantify the effects of the aforementioned phenomena on the effective mechanical properties of corroded steel reinforcement, a correction factor is defined as the ratio of the maximum elastic stress value of unequal mass loss to that of equal mass loss either side of corroded steel reinforcement:

$$\sigma_y^{Equal} = \frac{F_{max}}{A_0 - A_{Corr}} \quad 4\text{-}7$$

where σ_y^{Equal} (MPa) is the maximum elastic stress of corroded steel reinforcement at pit location assuming equal mass loss either side of steel reinforcement; A_0 (m^2) is the cross sectional area of noncorroded reinforcing steel; F_{max} (kN) is the maximum elastic force; A_{corr} (m^2) is the cross-sectional area of corroded reinforcing steel in the pit location.

$$\sigma_y^{Unequal} = \frac{F_{max}}{A_0 - A_{corr}} + k.\frac{F_{max} \times |a + a'| \times (h_{cf})}{I_c} \quad 4\text{-}8$$

$$k = f\left(a, pit\ depth, {}^{\alpha}/_{\beta}\right) \quad 4\text{-}9$$

where $\sigma_y^{\text{unequal}}$ (MPa) is the maximum elastic stress of corroded steel reinforcement in pit location considering greater mass loss on the cover side compared with core side of steel

reinforcement; k is a function of corrosion-induced relocation, pit depth. and α/β which is obtained from analysis of structural model of corroded bars; a is the neutral axis relocation due to unequal corrosion either side; a' (m) is the pit-induced relocation; I_c (m^4) is the second moment of area of the corroded cross section about the neutral axis (NA) in the pit location; h_{cf} (m) is the distance between the neutral axis, and the farthest point on the cover face side.

$$I_c = k' I_0 \qquad 4\text{-}10$$

where I_0 (m^4) is the second moment of area of the noncorroded cross section about the neutral axis (NA); $k' < 1$ depending on corrosion percentage and pit depth; and D_0 (m) is the noncorroded diameter of steel reinforcement (mm).

$$I_c = k' \times 0.25 \times \pi \left(\frac{D_0}{2}\right)^4 = k' \times (0.25)^2 \times A_0 \times \left(\frac{D_0}{2}\right)^2 \qquad 4\text{-}11$$

$$Correction\ Factor\ (C.F.) = \frac{\sigma_y^{Unequal}}{\sigma_y^{Equal}} = 1 + k.\frac{|a+a'|\times(h_{cf})}{k'(0.25)^2 D_0^2 \times (A_0 - A_{corr})} \qquad 4\text{-}12$$

The correction factor is composed of two different factors: the factor due to the unequal mass loss, and the factor due to the pit damage. These factors are shown in Table 4-8 for total average 15% corrosion, $D_0 = 16$ mm, and for various pit depths and α/β ratios. The final correction factors shown in Table 4-9 for each α/β ratio are found by multiplying the factor due to unequal mass loss by the corresponding factor due to pit damage.

Therefore, multiplying the IRF obtained for corroded bare bars (presented in Table 4-5) by an appropriate final analytical correction factor (AFC) presented in Table 4-9 resulted in the final reduction factor (FRF) for corroded bars embedded in concrete. In other words, the ratios of the reduction factors obtained for corroded steel reinforcement in a RC column to those for corroded bare bars are equal to related correction factors.

Table 4-8 Pit induced and unequal mass loss induced correction factors for average 15% corrosion, various α/β ratio, and various pit depth

	α/β				
	0.125	**0.5**	**1**	**2**	**8**
C.F. due to pit depth 0.8 mm	1.02	1.02	1.01	1.02	1.02
C.F. due to pit depth 2.4 mm	1.17	1.18	1.17	1.18	1.18
C.F. due to pit depth 3.2 mm	1.33	1.34	1.32	1.34	1.34
C.F. due to unequal corrosion	1.02	1.07	1.11	1.12	1.13

Table 4-9 The analytical correction factors for 15% corrosion obtained by multiplying pit induced and unequal mass loss induced correction factors

Pitting factor (R): $R = \frac{\text{Pit depth}}{\text{Average penetration}}$	Pit depth (mm)	α/β				
		0.125	**0.5**	**1**	**2**	**8**
2	**0.8**	1.04	1.09	1.12	1.14	1.15
5	**2.4**	1.2	1.26	1.29	1.32	1.33
7	**3.2**	1.36	1.43	1.46	1.5	1.51

The results show that the correction factors directly related to the α/β ratio and pitting factor. Therefore raising the α/β ratio and pitting factor increases the correction factors.

To study the effects of corrosion percentage on the correction factors, the analytical correction factors (ACF), assuming a pitting factor of 5 (R=5) for α/β ratios of 0.5 and 1, are compared in Figure 4-27 and Table 4-10.

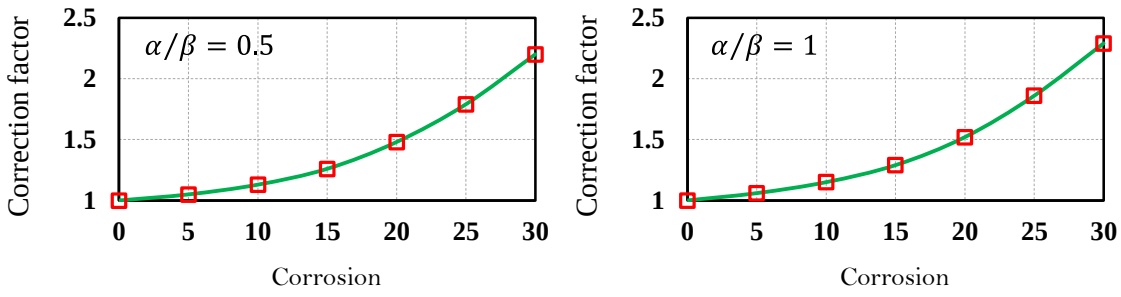

Figure 4-27 Comparing the analytical correction factors assuming pit factor of 5 and α/β ratios of 0.5 and 1

Table 4-10 The final correction factors for pit factor of 5 and α/β ratios of 0.5 and 1

Max. Pit depth	0.8	1.5	2.4	3.2	4	4.8
Corrosion %	5	10	15	20	25	30
Correction Factors $\alpha/\beta = 0.5$	1.04	1.13	1.26	1.48	1.79	2.21
Correction Factors $\alpha/\beta = 1$	1.06	1.15	1.29	1.52	1.86	2.29

The results in Figure 4-27 and Table 4-10 clearly show that the correction factors increase with increasing corrosion percentage. The reason is that increasing corrosion percentage causes greater centroid relocation which leads to higher correction factors.

4.2.5.1 EXPERIMENTAL VALIDATION OF THE ANALYTICAL MODEL

In order to validate the analytically proposed correction factors, the experimental results presented in Table 4-6 were used (Meda et al., 2014). For the results presented by Meda et al in Table 4-6, the ratios of reduction factors for corroded bars while embedded in concrete to those for bare bars are 1.4, 1.25 and 1.52 for yield stress, ultimate stress and ultimate strain, respectively. The samples tested by that study had α/β ratio equal to 1, and approximately 20% corrosion (Meda et al., 2014). Therefore, in accordance with Table 4-10, the analytically proposed ratio of reduction factors for bars embedded in concrete to those for bare bars is 1.52. The differences between the analytically obtained values and the experimental findings obtained by (Meda et al., 2014) are +8.6%, +21.6% and 0% for yield stress, ultimate stress and ultimate strain, respectively. The results of the comparison confirm the efficiency and validity of the proposed analytical model.

4.2.6 FINAL REDUCTION FACTORS FOR CORRODED EMBEDDED BARS (STEP 3)

As mentioned in previous section, the final reduction factors were developed by multiplying the IRF by appropriate ACF, and presented in Table 4-11. The results of this study clearly showed that using the deterioration models based on the results of corroded bare bars for real corroded RC columns is not safe, because the reduction factors for corroded bare bars are significantly lower than those for corroded steel reinforcement in a real RC column.

Table 4-11 Suggested final reduction factors (FRF) based on experimental results from bare bars and correction factors

The degree of corrosion in terms of mass loss percentage (Q_{corr})	Reduction factors (γ) in:					
	Yield stress (σ_y): γ_{σ_y}		Ultimate stress (σ_u): γ_{σ_u}		Elongation (ε_u): γ_{ε_u}	
	IRF	FRF	IRF	FRF	IRF	FRF
$0 < Q_{corr} \leq 10$	0.0145	**0.0151**	0.016	**0.0166**	0.031	**0.032**
$10 < Q_{corr} \leq 20$	0.011	**0.0139**	0.0125	**0.0158**	0.021	**0.0265**
$20 < Q_{corr} \leq 30$	0.0075	**0.0134**	0.0085	**0.0152**	0.012	**0.0215**

The FRF presented in Table 4-11 can be used for corroded reinforcement while embedded in RC structures. As previously mentioned, the majority of existing reduction factors developed were based on the results of corroded bare steel reinforcement. The ACF presented in this research (Table 4-9 and Table 4-10) also can be used for upgrading the reduction factors for bare steel

bars published by past studies.

4.2.7 LIMITATIONS AND UNCERTAINTY

ACF values were calculated as ratio of the maximum elastic stress of unequal to that of equal mass loss. The correction factors were applied to estimate the final reduction factors of the effective yield stress, ultimate strength and ultimate strain. In this chapter the analytical model was developed based on simplified morphology of corroded reinforcement. In environmental corrosion, the corroded surface is much more complicated. While the simplified model can capture the key effects of corrosion morphology on tensile behaviour of corroded reinforcement, the differences (if compared with environmental corroded reinforcement while embedded in concrete) may causes error in final results. As mentioned in section 4.2.5.1, In accordance with the results, the average, minimum and maximum error of 10.1%, 0.0% and 21.6% respectively were calculated for the developed analytical model compared to experimental results.

4.2.8 CONCLUSIONS

In this chapter, a novel methodology is presented to estimate advanced corrosion-induced reduction factors for steel reinforcement of corroded RC structures based on unequal mass loss. The final reduction factors developed for corroded RC reinforcement while embedded in concrete were based on initial reduction factors for corroded bare reinforcement multiplying by analytical correction factors. The main results can be summarised as follows:

- The configuration of corroded bare bars was compared with that of corroded steel reinforcement of RC columns, and two critical differences were observed:
    1. While almost identical mass loss was distributed on the either side of corroded bare bars, for corroded steel reinforcement of RC columns, more mass loss was observed on the side that was close to column cover (cover side)
    2. The maximum pit depth and more pit damage (cavities) were observed on the cover side of the steel reinforcement of RC columns.
- The aforementioned differences result in greater reduction of the effective mechanical properties of steel reinforcement of RC columns than that of bare bars.

- Past studies that found similar reduction factors for bare reinforcement and that of corroded bars whilst embedded in concrete used a corrosion test set-up where the thickness of concrete cover on either side of the steel reinforcement was identical. It is obvious that unequal mass loss cannot occur in this corrosion test set-up, so it cannot model corrosion of RC columns and beams.
- It was observed that corrosion was usually distributed only on the cover side surface of corroded steel reinforcement of RC columns, with a corrosion percentage less than or equal to 8%.
- The results of 3D scanning of corroded steel reinforcement retrieved from RC columns with 15% average mass loss, showed that 10.9% mass loss occurred on the cover side versus 4.1% on the core side.
- In accordance to experimental observations and the results of 3D scanning of corroded steel bars, pitting factors must be smaller than those reported by past studies due to greater corrosion penetration on the cover side of corroded steel reinforcement.
- The majority of the existing reduction factors in the effective mechanical properties of steel reinforcement have been developed based on the experimental results of corroded bare bars. An experimental program to develop reduction factors for bare steel reinforcement is much simpler and more time- and cost-effective than that for large-scale RC members. However, using these reduction factors in numerical simulations of corroded RC structures is not safe because they are significantly lower than the reduction that happens in real corroded RC columns.
- An analytical model was developed to quantify the effects of the unequal mass loss and pit cavities on corrosion-induced reduction in the mechanical properties of steel reinforcement. The analytical correction factors were used to modify the initial reduction factors obtained from the results of bare bars.

- The suggested analytical correction factors were in good agreement with existing experimental results in the literature.
- The final reduction factors suggested for real corroded RC structures were built on the initial reduction factors multiplied by the appropriate analytical correction factors.

- Increasing centroid relocation and the noncorroded to corroded length of steel bars increase the final correction factors.

5 THE EFFECTS OF CORROSION ON STRESS–STRAIN BEHAVIOUR OF CONFINED CONCRETE

5.1 INTRODUCTION

Prevention of structural collapse is the basic seismic design approach of reinforced concrete (RC) structures in severe earthquakes. To meet this requirement, sufficient ductility is needed to ensure that capacity is greater than demand in the plastic hinge region, Mander et al. (1988b). To provide the required ductility capacity, compressive concrete is confined by using adequate transverse reinforcement, to decrease the potential buckling of longitudinal reinforcement and shear failure Mander (1983).

The effects of confinement on strength and ductility of compressive concrete has been comprehensively studied and well documented (Mander et al., 1988b, Mander et al., 1988a). When curvature of RC columns increases in large seismic events, sufficient volumetric ratio of confinement is crucial to ensure the required flexural strength (Mander et al., 1988b). It is obvious that predicting the stress–strain curve of confined concrete of RC columns is essential for the seismic design of RC structures based on a ductility design approach. The configuration of the stress–strain curve of confined concrete is shown in terms of four key features: the maximum compressive stress (f'_{cc}), the strain at maximum compressive stress (ε_{cc}), the modulus of elasticity of concrete (E_c), and the ultimate compressive strain of concrete (ε_{cu}) (Mander et al., 1988b).

The stress–strain behaviour of confined concrete of noncorroded RC columns has been comprehensively addressed (Scott et al., 1982, Mander, 1983, Mander et al., 1988b). In accordance with past studies, there is no experimental study on the effects of corrosion on the stress–strain behaviour of confined concrete (Ou and Nguyen, 2014, Ou et al., 2013b).

Corrosion leads to deterioration of structural performance, and thereby a reduction in the service life of structures, and increased maintenance costs (Akiyama and Frangopol, 2014). While one of the main effects of reinforcement corrosion is a reduction in the ductility capacity of corroded RC columns, little attention has been devoted to the effects of corrosion on the stress–strain response of corroded RC columns. Moreover, few analytical models have been suggested to

predict the stress–strain curve of corroded RC columns. For example, Ou et al. (2013b) modified the ultimate strain of confined concrete suggested by Mander et al (Mander, 1983). The modified ultimate strain model was achieved using corrosion-induced reduction models of the mechanical properties of steel reinforcement. However, the model needs to be improved for high degrees of corrosion (higher than 20% mass loss). The fact that the existing model has not been validated using experimental tests shows a critical need for a reliable stress–strain model of corroded confined concrete.

As a part of the present study, experimental tests were carried out to create a data base to improve understanding stress strain response of confined concrete subjected to reinforcement corrosion. The test units were designed to near full scale RC columns using realistic steel reinforcement detailing.

This chapter presents an analytical model for the stress–strain behaviour of corroded confined concrete. The analytical model developed was based on a modification of Mander's model using corrosion-induced deterioration models for steel reinforcement and concrete materials. The model presented is compared with the results of an experimental programme of 12 full-scale RC columns with varying degrees of corrosion. The experimental programme consisted of 10 circular RC and 2 plain columns subjected to a monotonic compressive concentric load with a deformation rate of 0.1 mm per minute. The RC columns had identical size, the same longitudinal steel reinforcement and spiral confinement type with different spiral pitches.

5.2 MANDER'S MODEL FOR STRESS–STRAIN OF CONFINED CONCRETE

Mander, (1983) proposed a model to predict the stress–strain behaviour of confined concrete, based on an equation suggested by Popovics (Popovics, 1973). Based on Popovics' equation, the maximum compression strength of confined concrete for a slow strain rate and monotonic compressive loading is expressed as follows (Popovics, 1973):

$$f'_{cc} = f'_c \frac{n-1+(\varepsilon_c/\varepsilon_{cc})^n}{n(\varepsilon_c/\varepsilon_{cc})} \quad 5\text{-}1$$

$$n = \frac{E_c}{E_c - E_{sec}} \quad 5\text{-}2$$

$$E_{sec} = \frac{f'_{cc}}{\varepsilon_{cc}} \quad 5\text{-}3$$

where f'_{cc} is the compression strength of confined concrete, ε_{cc} is strain at f'_{cc}, ε_c is longitudinal compressive strain of concrete, f'_c is the longitudinal compressive strength of concrete, E_c is the tangent modulus of elasticity of concrete.

The ultimate strain of confined concrete is defined as strain at the first transverse bar fracture. The Mander's model is a unified model that can be applied to both circular and rectangular transverse reinforcement. More details can be found in (Mander, 1983).

5.3 EXPERIMENTAL PROGRAM

The experimental programme included 12 circular reinforced concrete columns, with testing performed at the Main Structural Laboratory at the University of Canterbury. Seven columns were corroded using accelerated corrosion methods. The five noncorroded columns included two plain columns and three reinforced concrete columns.

5.3.1 TEST CONCEPT

The 12 RC circular columns were tested under quasi-static monotonic compressive loading. The compressive tests were run at a rate of 0.1 mm of deformation per minute. All tests were continued until rupture of the transverse confining steel bars. The load and deformation of the columns and strain of the confining steel bars at the middle of column were recorded to obtain stress–strain curves for the confined concrete. Figure 5-1 shows a photo of the test set-up. A DARTEC 10 MN Universal Testing Machine was used with maximum 10 MN load, maximum actuator stroke of 300 mm, and minimum and maximum velocities of 0.02 and 16 mm/s respectively. To ensure the flat-ends condition, a few millimetres of dental-stone plaster was used to level the ends of the columns.

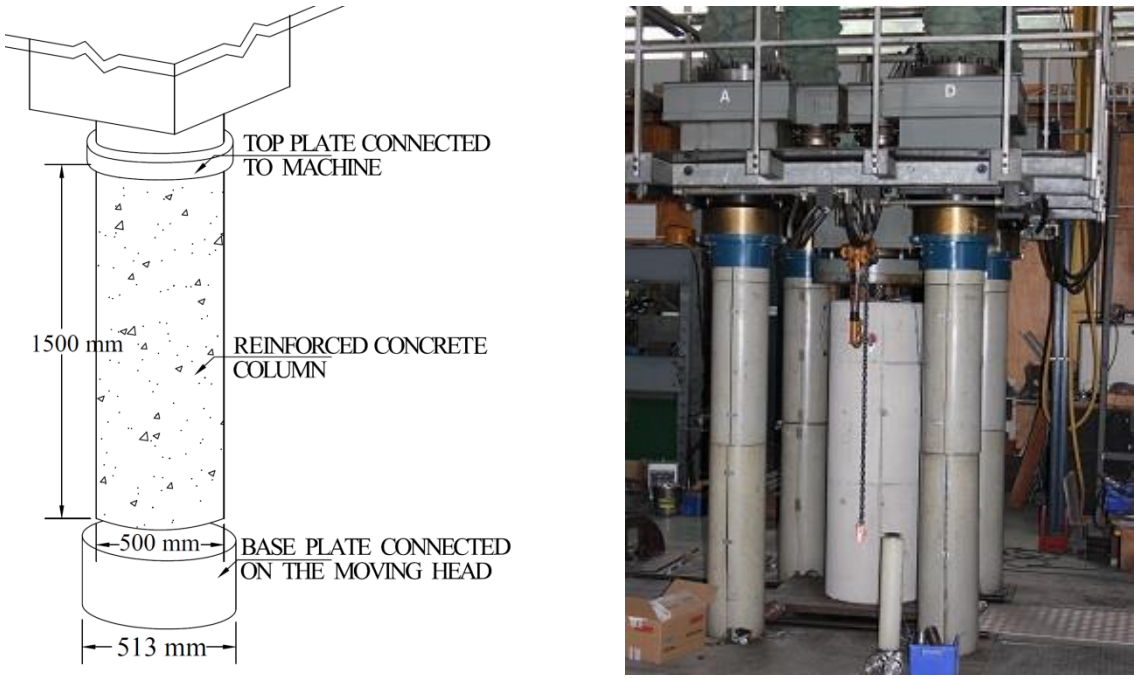

Figure 5-1 Photo of monotonic compressive test set up

5.3.2 DETAILS OF COLUMNS

The details of columns are given in Figure 5-2. The 12 columns consisted of two unreinforced and ten reinforced columns. The unreinforced columns were tested to obtain the stress–strain curve of unconfined concrete. The RC columns had identical arrangements of longitudinal reinforcement and various arrangements of transverse reinforcement. Twelve 16-mm diameter deformed steel bars were used as longitudinal reinforcement, and spiral form 12-mm diameter round steel bars with different spiral pitches were used as transverse reinforcement. In terms of the configuration of transverse reinforcement, the RC columns were grouped into three forms: comparatively low volumetric ratios (LCON), medium volumetric ratios (MCON), and high volumetric ratios (HCON) of confining steel. The volumetric ratios (ρ_s) for LCON, MCON and HCON confining steel are 0.01, 0.015 and 0.025 respectively. A photo of the different reinforcement configurations is given in Figure 5-3.

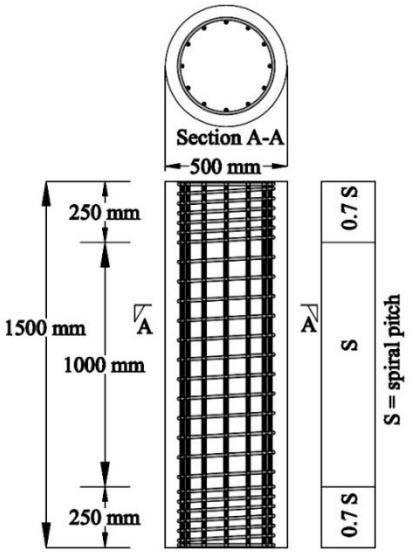

Column Type	Spiral pitch S (mm)	Longitudinal reinforcement		Confining reinforcement
		Number	Diameter D (mm)	Diameter D (mm)
Low confined	103	12	16	12
Medium confined	69	12	16	12
High confined	41	12	16	12

	Concrete		Steel
f'_c (MPa)	Aggregate (mm)	Slump (mm)	Grade
30	19	100	300

Figure 5-2 Details of the columns and materials

Figure 5-3 Details of different reinforcement configurations

According to NZS3101 the volumetric ratio of ductile column and piers should be greater than the following two values:

$$\rho_s = \frac{(1-\rho_t m)}{2.4} \times \frac{A_g}{A_c} \times \frac{f'_c}{f_{yt}} \frac{N^*}{\Phi f'_c A_g} \quad 5\text{-}4$$

$$\rho_s = \frac{A_{st}}{155 d''} \frac{f_y}{f_{yt}} \frac{1}{d_b} \quad 5\text{-}5$$

Where for the columns shown in Figure 5-2 the parameters are as follows:

$\rho_t = \frac{A_{st}}{A_g} = 0.0129$

$m = \frac{f_y}{0.85 f'_c} = 11.76$

$f_y = f_{yt} = 300$ MPa is yield stress of reinforcement, $A_g = o.196\ \mathrm{m}^2$ is total sectional area, $A_c = 118\ \mathrm{m}^2$ is sectional area of confined concrete, $f'_c = 30$ MPa is compression strength of

concrete, N^* is design axial load, $A_{st} = 2414\ \text{mm}^2$ is total area of longitudinal reinforcement, $d^{"} = 388\ \text{mm}$ is the diameter of spiral, and $d_b = 12\ \text{mm}$ is diameter of transverse reinforcement.

The volumetric ratio versus axial load ratio for the columns is illustrated in Figure 5-4.

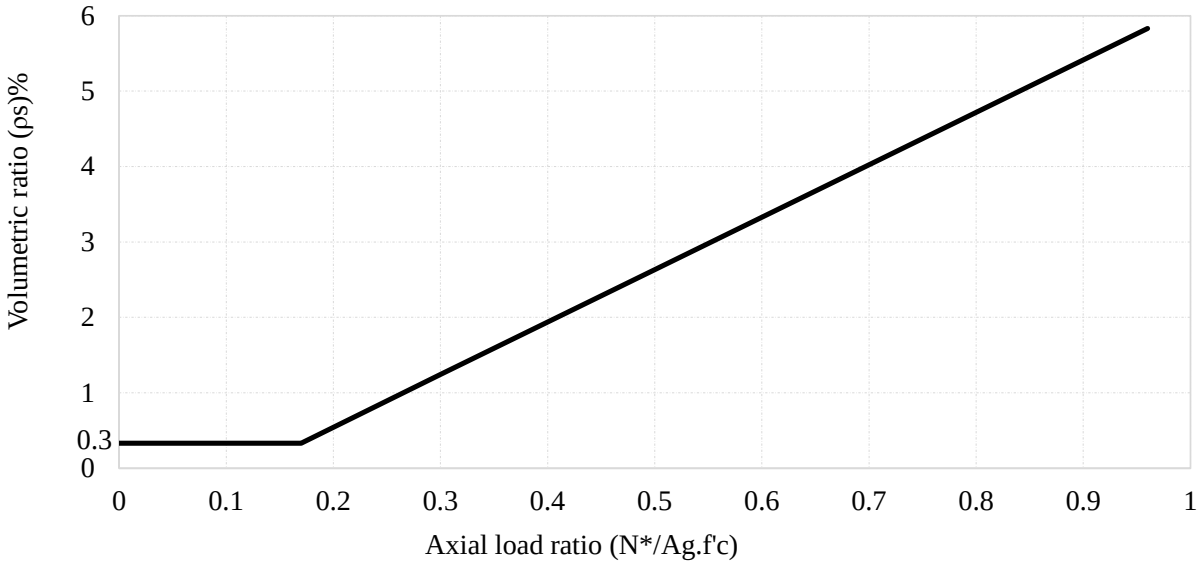

Figure 5-4 The volumetric ratio versus various axial load ratio for the columns

In terms of corrosion, LCON was categorised into four groups: noncorroded; comparatively low corroded, high corroded and pitting corroded. The pit damages were mechanically produced. MCON and HCON were categorised into three groups: noncorroded, comparatively low corroded, and high corroded.

5.3.3 CONSTRUCTION AND INSTRUMENTATION

Reinforcing caging was prefabricated with a construction tolerance of 2 mm. Prefabricated modular plastic moulds of 500 mm diameter, and 300 mm and 600 mm height allowed for varying range of total height. Six cylindrical moulds were vertically erected on a horizontal plywood sheet. 50 mm concrete spacer blocks were used to attach the reinforcing cages to the moulds in order to cast the RC column with 50 mm concrete cover. Ready-mix concrete was poured in three layers, and each layer was mechanically vibrated prior to pouring the next layer. The fabricated columns were cured at 20ºC and their top surfaces were covered by wet hessian and polythene to hold moisture. After seven days of curing, the columns were kept in the laboratory until testing or corroding. Figure 5-5 shows the poured concrete to cast the RC

columns. The 12 columns were constructed in two 6-column sets, all identical in size. Each set included five RC columns and one plain (without reinforcing caging) column to obtain the stress–strain curve of unconfined concrete while avoiding size effects.

Figure 5-5 Construction of RC columns before and after pouring

The displacement over the central 450 mm gauge length of each column was recorded by eight linear potentiometers at 45º intervals around the circumference. The potentiometers were connected to either 10 mm diameter bars horizontally embedded in the concrete, or to coupler nuts welded to longitudinal reinforcing bars. To avoid measurement errors caused by crushed cover, Clearance holes were provided in the cover concrete. In order to compare displacements recorded by the potentiometers connected to coupler nuts and those connected to transverse rods, the slip of longitudinal reinforcement was monitored. Transverse strains on the spiral reinforcement were recorded at nine locations spaced equidistantly over the central 450 mm gauge length, using 5 mm FLA-5-11 electric resistance strain gauges. The details of the instrumentations are shown in Figure 5-6 . The columns were loaded in axial compression, which was directly measured by the machine load cell. A displacement control approach was used to conduct the tests, which were run with a displacement rate of 0.1 mm/s and scan rate of 10. Therefore, the overall displacement of each column and the corresponding compressive load were recorded every 0.01 mm throughout the entire displacement range. Figure 5-7 compares the strains measured by the DARTEC machine (M), the potentiometers connected to horizontal bars (PHB) and potentiometers connected to longitudinal reinforcing bars (PLB). Figure 5-7 shows that the corresponding strain of maximum axial load measured by the machine is in good

agreement with those measured by the potentiometers. The maximum difference in the strain at maximum load is 15 %.

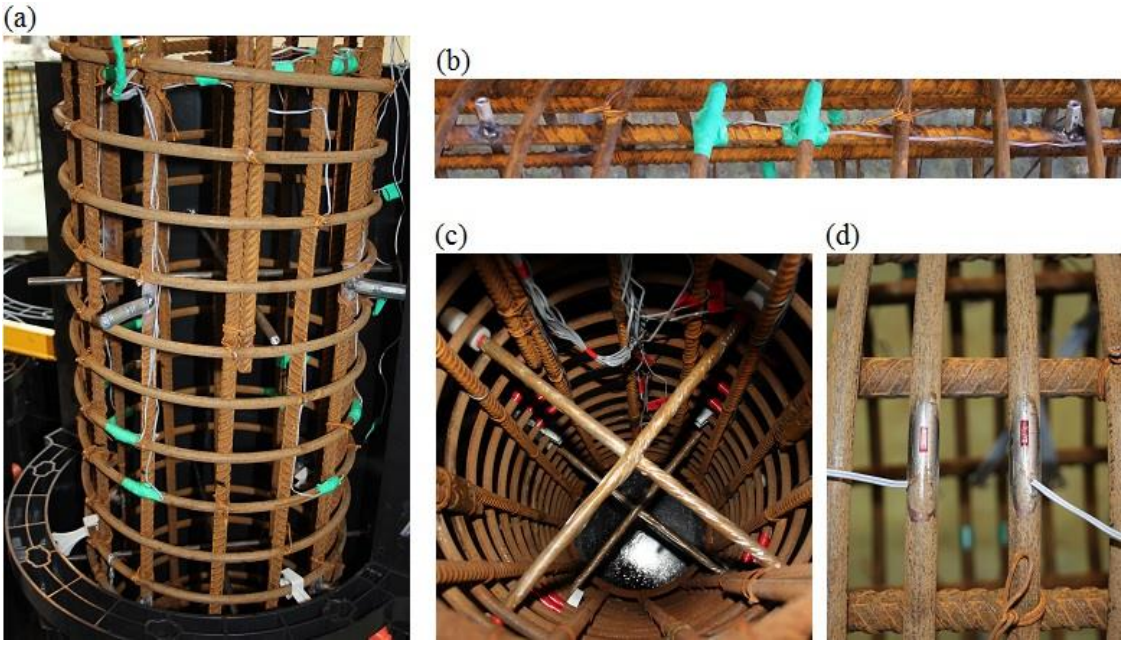

Figure 5-6 (a) Reinforcement and instrumentation details of circular columns; (b) Coupling nuts welded to longitudinal steel reinforcement; (c) steel rods passing through concrete core; (d) Strain gauges installed on transverse steel reinforcement

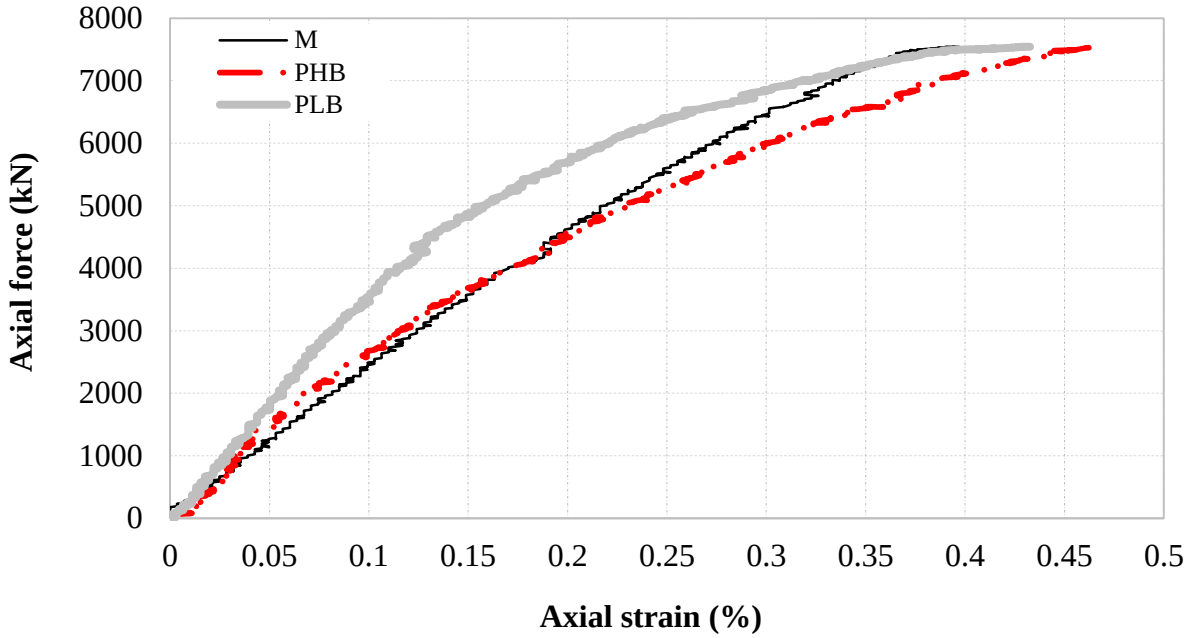

Figure 5-7 Comparing strain measured by the machine (M), potentiometers connected to horizontal transverse bars (PHB) and potentiometers connected to longitudinal reinforcing bars (PLB)

5.3.4 CORROSION TESTING SET-UP

The simulated corrosion method was performed to simulate pitting corrosion on a column. Pit damages were artificially induced by machining hemispherical cavities in the transverse reinforcement. The three pits, having identical pit depths of 4 mm, were located on the same face of the reinforcing cage along a straight line. Figure 5-8 shows the details of simulated pitting corrosion. The pits were simulated on caging with comparatively low volumetric ratios (LC) of confining steel.

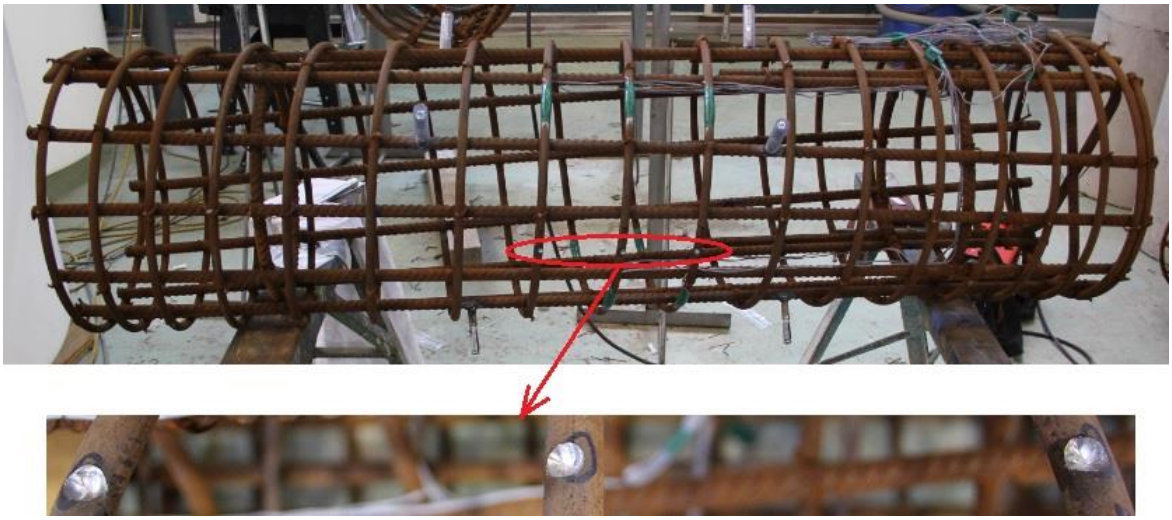

Figure 5-8 details of simulated pit damages

As already mentioned, six RC columns with various volumetric ratios of confining steel were corroded. In order to corrode the RC columns within a reasonable time period, an accelerated corrosion method, called the impressed current method, was used in this study. An accelerated corrosion rate of 600 to 900 $\mu A/cm^2$ was achieved by applying a constant electrical current to the steel reinforcement using a power supply. The RC columns were submerged in a 3.5% NaCl solution. The steel reinforcement of the RC columns, acting as the anode, were directly connected to the positive terminal. Stainless steel plates, acting as the cathode, were submerged in the NaCl solution and directly connected to the negative terminal. The current flowed from the steel reinforcing to the stainless steel plates through the 3.5% NaCl solution, acting as the electrolyte. Figure 5-9 shows details of the corrosion test set-up for columns. The lower 600 mm length of the columns and all the connections were covered by a rubber-type material to safeguard against corrosion. Therefore, only the central 450 mm of each column was corroded. The RC columns have less transverse reinforcement at the middle than the end of columns to ensure failure will occur at the middle of RC column. Providing rubber around the base of the

columns protect this part of the columns from corrosion-induced deterioration. Figure 5-10 shows a constructed column, another column prepared for corrosion, and a corroded column. The corrosion tests were conducted within two predetermined times to obtain two different degrees of corrosion. Faraday's law of corrosion provides a relationship between corrosion current density, mass loss and time. According to Faraday's law for steel reinforcement, a uniform corrosion current density, $i_{corr} = 1\,\mu A/cm^2$, will result in 11.6 $\mu m/yr$ loss of cross section (Alonso et al., 1998c). Faraday's law was used to theoretically predict degrees of corrosion according to the corrosion exposure time. To meet this aim, the current for each column was monitored and the daily average was recorded. The corrosion percentage of transverse and longitudinal reinforcement for each column was measured using the mass loss approach: a wire brush was used to remove rust on the surface of corroded bars. Then the weight of the cleaned corroded bars was compared to that of noncorroded bars to calculate the corrosion percentage. Table 5-1 compares the experimental corrosion test results with the theoretical prediction results.

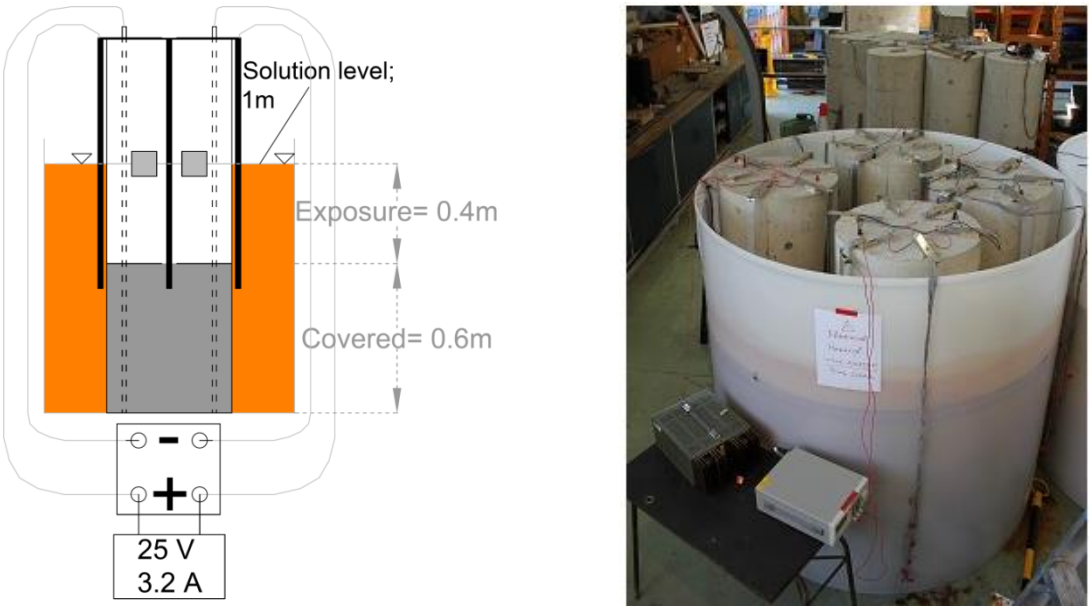

Figure 5-9 Details and photo of corrosion test set-up of RC columns

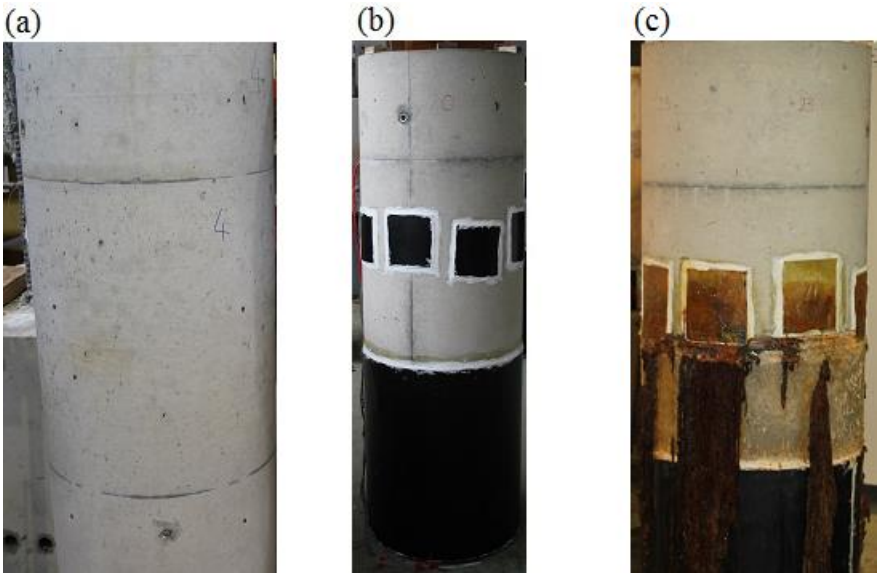

Figure 5-10 (a) a RC column; (b) a prepared column for corroding; (c) corroded RC column

Table 5-1 The experimental corrosion test results and the theoretical prediction results

Cross section configuration	Name	Corrosion rate $\mu A/cm^2$	Average corrosion experimentally measured (%)	Average corrosion theoretically calculated (%)	Exposure time (days)
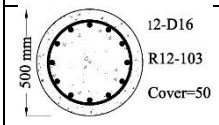	NC-LCON	0	0	0	0
	LC-LCON	620	7.1	6.5	10
	HC-LCON	620	18.6	19.3	31
	Pit-LCON	–	4 mm pit depth	–	–
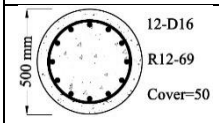	NC-MCON	0	0	0	0
	LC-MCON	625	9.8	6.5	10
	HC-MCON	900	31.6	26.5	30
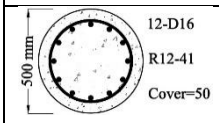	NC-HCON	0	0	0	0
	LC-HCON	580	11.3	6.3	10
	HC-HCON	500	19.3	16	30

5.3.5 MATERIAL PROPERTIES

To calculate the stress–strain curve of confined concrete core, it was necessary to subtract the stress-carrying contributions for both unconfined cover concrete and the longitudinal steel reinforcement from the overall column response.

As discussed in the previous chapter, the compression strengths of concrete materials with

varying degrees of corrosion were studied and the experimental results found. The columns were tested with very low deformation rate. Mander (1983) stated that the steel characteristics obtained from tensile tests at low deformation rate can be used for the compression characteristics of reinforcing steel. The experimental results of tensile tests considering inelastic buckling behaviour of longitudinal reinforcement were used for estimating the compression characteristics of steel reinforcement (Mander, 1983).

5.3.6 COMPRESSION TESTING SET-UP

The ends of the columns were capped with dental-stone plaster to avoid problems caused by the rigid cross-head of the DARTEC machine and to make the ends precisely flat. The columns were then placed in the DARTEC machine and centrally located on the rigid base platen. Eight linear potentiometers were installed in the specially designed assemblies. The potentiometers and strain gauges installed on the transverse reinforcement were wired to the appropriate recording instruments. The columns were tested at a stroke rate of 0.1 mm/s, equal to an average rate of strain of 67.5 /μs. One of the columns before and after the compression test is shown in Figure 5-11.

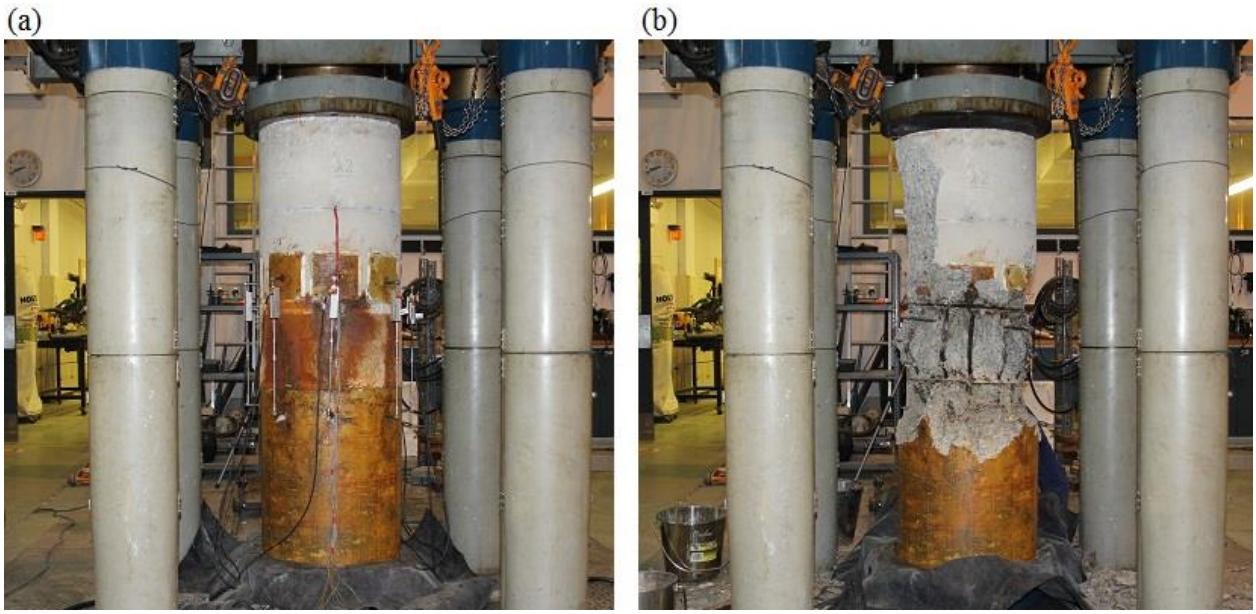

Figure 5-11: Monotonic compression testing (a) before testing; (b) after testing

5.4 OBSERVATIONS

The visual data observed during the column testing programme are shown in Figure 5-12.

Figure 5-12a-d compares failure types of a plain column and noncorroded (NC) columns with low, medium and high confining reinforcement. A number of vertical microcracks were observed on the surface of the plain column once loading started. Following the peak load, a large inclined crack formed, which led to a brittle type of failure, shown in Figure 5-12a.

Vertical cracks were observed on the surface of confined concrete columns once loading started. The spiral reinforcement significantly improved the strength and ductility of the confined concrete core when the cover concrete completely spalled.

One of the main functions of confining reinforcement was to prevent bucking of longitudinal reinforcement. Therefore, following the loss of cover concrete, a large strain demand was produced in confining reinforcement due to longitudinal reinforcement restraint provided by confinement, and Poisson expansion and transverse stretch of concrete. The strain demand led to fracture of the spirals, buckling of longitudinal bars and loss of confining stress, and resulted in a sudden drop in axial compressive load. Therefore, when more spirals fractured a progressive drop in load-carrying capacity occurred. In general, two types of failure were observed, depending on the amount of confining reinforcement. The first type occurred in low confined columns, in the form of a diagonal failure plane due to disparate spalling of cover, which led to the development of shear stresses. Figure 5-12b shows the diagonal failure plane of a low confined column. The vertical length of the diagonal failure plane was almost 1000 mm and it is evident that the buckling of longitudinal bars occurred along the diagonal failure plane.

Photos of failure over time for all columns are shown in Appendix B.

The second type of failure is seen in the columns with sufficiently high confining reinforcement. As shown in Figure 5-12c, the vertical cracks of cover occurred in a rather symmetrical fashion along the overall length of the column. This type of failure had two main characteristics: first, the location of failure was random; therefore, the failure did not occur in the central part of the columns; second, the shape of failure was transverse expansion over a length, and the buckling of longitudinal bars took place at relatively similar heights. Figure 5-12d clearly shows the characteristics of this type of failure – called “random failure” by Mander (1983).

Figure 5-12e-h compares the failure types for pitting corroded column (pit-LCON) and low corroded (LC) columns comprising low (LC-LCON), medium (LC-MCON) and high (LC-HCON) confining reinforcement. Figure 5-12e and Figure 5-12f evidently show the diagonal failure plane of pit-LCON and LC-LCON. The failure plane of pit-LCON is evident in Figure 5-12e. Figure 5-12f shows buckling of longitudinal bars, which occurred along the

inclined line of the failure plane. The random failure type for LC-MCON and LC-HCON columns are shown in Figure 5-12g and Figure 5-12h respectively.

Figure 5-12i-k compares failure types of high corroded (HC) columns with low (HC-LCON), medium (HC-MCON) and high (HC-HCON) confining reinforcement. Figure 5-12i shows the diagonal failure plane of HC-LCON. Figure 5-12j and Figure 5-12k show the random failure type. Comparison of the failure in noncorroded and low corroded columns with the ones for high corroded columns shows that higher degrees of corrosion reduce the length of spalled cover of columns. This is because corrosion-induced cracks decrease the compressive strength of cover at the corroded portion (500 mm at the middle of the column), which results in spalling of cover at that section.

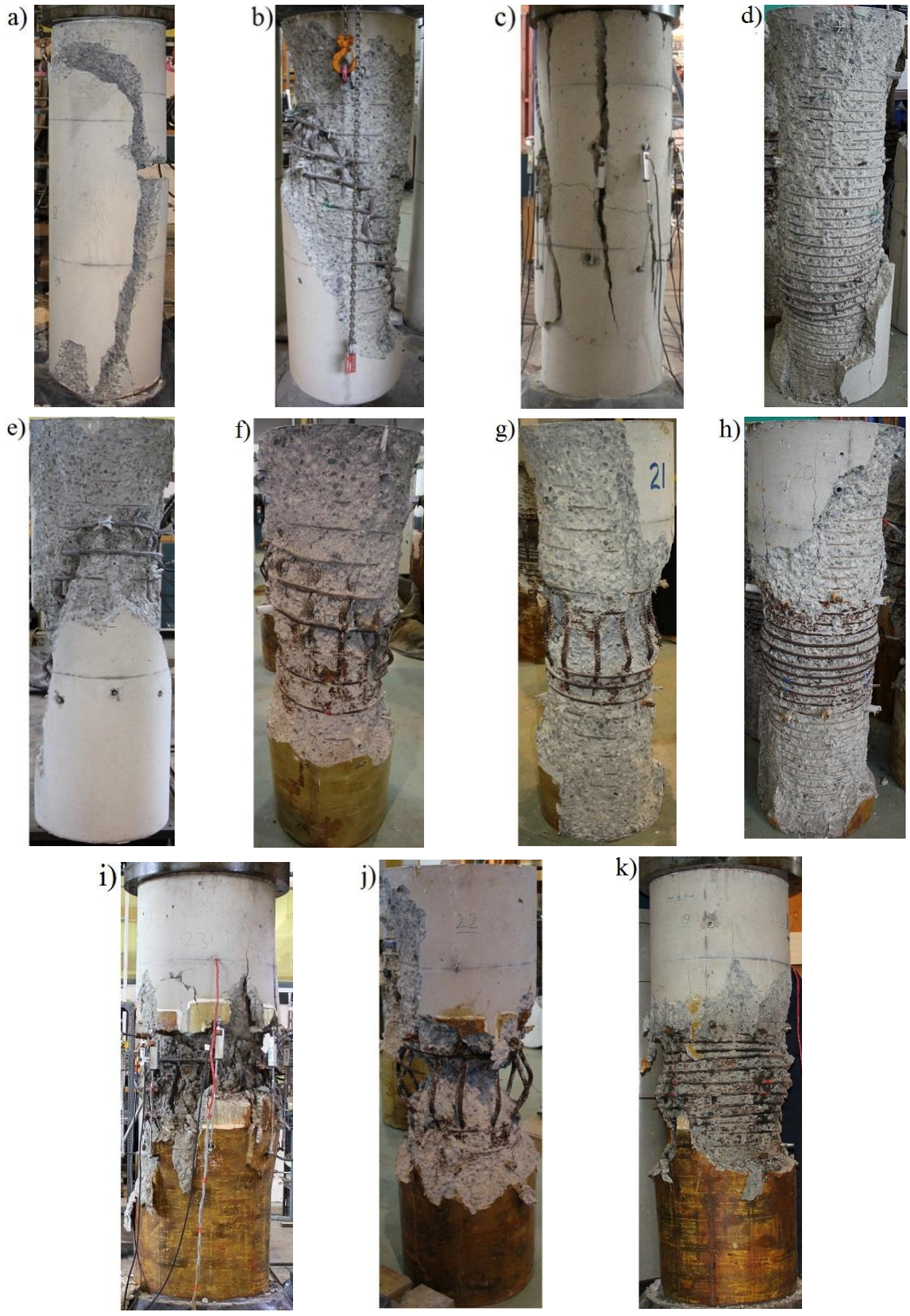

Figure 5-12 Failure of columns (a) plain column (cylinder); (b) low confined (NC-LCON); (c) medium (NC-MCON) confined; (d) high confined (LC-HCON); e: pit simulated (pit-LCON); f: low confined (LC-LCON); g: medium confined (LC-MCON); h: high confined (LC-HCON); i: low confined (HC-LCON); j: medium confined (HC-MCON); k: high confined (HC-HCON)

More details regarding the behaviour of the columns under monotonic compressive load based on the analysed recorded data are illustrated in Figure 5-13 . In the left-hand graph, overall response of a noncorroded column was compared with the response of a plain column (also unconfined); this graph shows the measured force–displacement graph of confined concrete and strain of spirals. The overall force–displacement graph of the column showed two clear peaks. The first peak occurred when axial stress reached the compression strength of unconfined concrete. Comparing the axial displacement of the column at the first peak with that of the plain column confirms that the drop following the first peak took place due to cover spalling. The second peak took place once axial stress reached the compression strength of confined concrete. The ultimate compression strain of confined concrete was defined as the compressive axial strain at which failure of the first spiral took place. The strain of spirals recorded by the strain gauges shows that axial stretch of spirals occurs once the cover has spalled, and yielding took place when the axial stress of the confined concrete reached the compression strength.

Right-hand graph compares the stress–strain curves for unconfined column and noncorroded (NC) columns with low (NC-LCON), medium (NC-MCON) and high (NC-HCON) confining reinforcement. It is evident that the corrosion significantly decreases both compressive strength and ultimate strain of confined concrete.

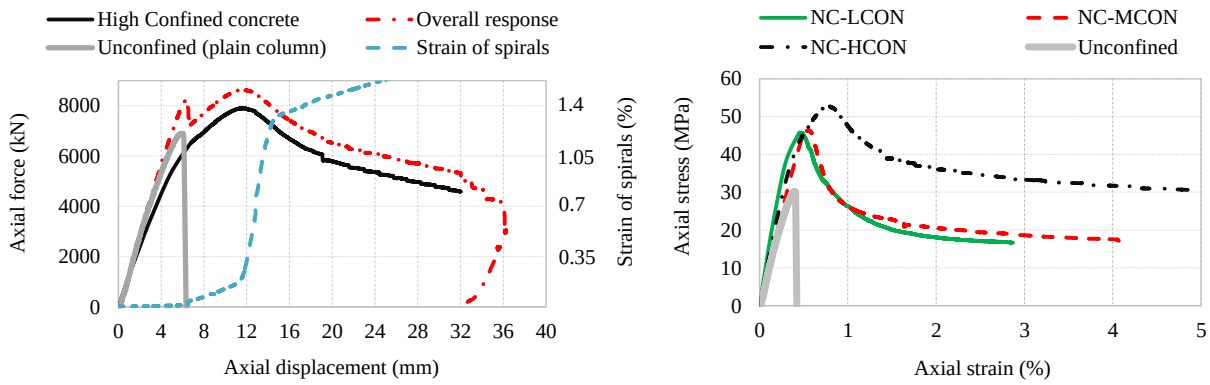

Figure 5-13 (Left) Axial force-displacement of high confined column (Right) Stress- strain of unconfined vs. noncorroded RC columns with different confinement

5.5 STRESS-STRAIN RELATIONSHIP OF CONFINED CONCRETE IN CORRODED RC COLUMNS

The main objective of the experimental programme was to study the effects of the reinforcement corrosion on the stress–strain characteristics of confined concrete of RC columns under

concentric axial compression.

To obtain the confined core stress, the longitudinal steel force contribution and the cover concrete force contribution were subtracted from the overall force responses of the columns. The results of tensile tests of steel reinforcement were used to obtain the compression capacity of the steel reinforcement. The force contribution of the unconfined cover concrete was computed by multiplying the concrete stress of plain concrete tests by the total cover area of the RC column. To calculate the confined concrete core stress, the load carried by the concrete core was divided by the confined core area (based on centre line of the spiral diameter).

In most specimens, it was observed that the transverse bars embedded in the concrete, and the coupler nuts to support the potentiometers bent after the maximum compression strength was reached. Therefore, determining axial strain using potentiometers was rarely possible, and instead, the machine stroke records were used to obtain the axial strain. The same problem was observed in previous studies (Scott, 1980, Mander, 1983), whose authors used the machine stroke records to determine the axial strain. As shown in Figure 5-7, the axial strains recorded by the machine stroke within the compressive strength of confined concrete are in good agreement with those recorded by potentiometers. The maximum difference between the measured strain at the compressive strength of confined concrete using the three different devices was only 15%. In order to obtain the strain up to the strain at compression strength of the confined concrete, the axial displacement recorded by the machine stroke was divided by the overall length of the column (1500 mm). However, for the strain beyond the compression strength, different lengths were used. For the low confined columns with diagonal failure plane, the vertical length of the diagonal failure plane (1000 mm) was used, but for columns with the random failure type, the used length was equal to 33% of the column length (500 mm). The reasons for selecting the lengths above were the following observations by the author and the other researchers. In the low confined columns, it was observed that the failure occurred along the diagonal failure plane. For columns with random failure, a recent study conducted at the University of Canterbury confirmed that the average length of random failure was 500 mm (Malek eta al 2018). Mander (1983) used a 450 mm failure length for the columns with the random failure type.

The stress–strain curves of low, medium and high confined columns with varying degrees of corrosion are shown in Figure 5-14 to Figure 5-16 respectively. Figure 5-14 shows the effects of pit damage in the confining reinforcement and the effects of corrosion of steel reinforcement on the stress–strain relationship of the low confined columns. The results clearly show that corrosion decreases compression strength and ultimate strain of confined concrete, and the pit

damages slightly decreased the compression strength but, more importantly, decreased the ultimate strain of confined concrete.

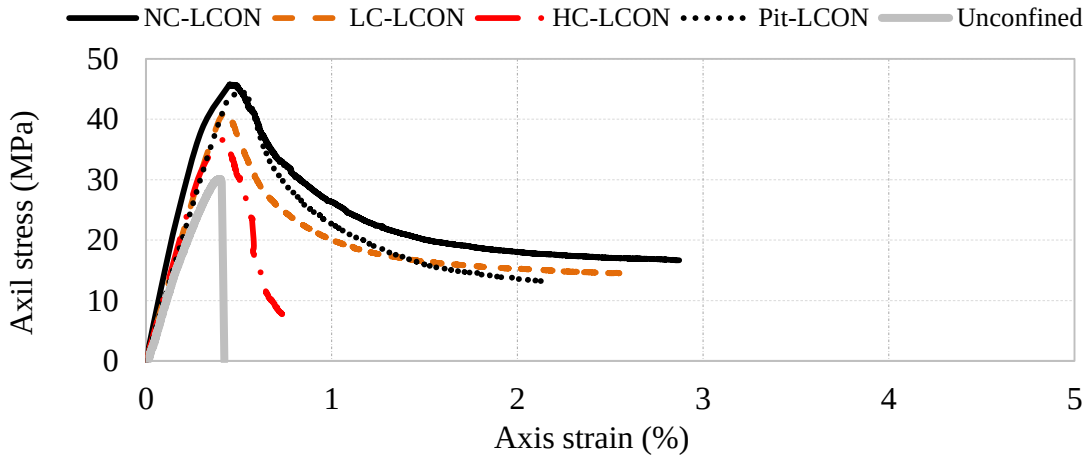

Figure 5-14: Stress–strain relationship of low confined concrete with varying degrees of corrosion

Figure 5-15 compares the experimentally obtained stress–strain curves of medium confined concrete with varying degrees of corrosion. It is evident that corrosion deceases compression strength, the strain at compression strength and the ultimate strain of medium confined columns.

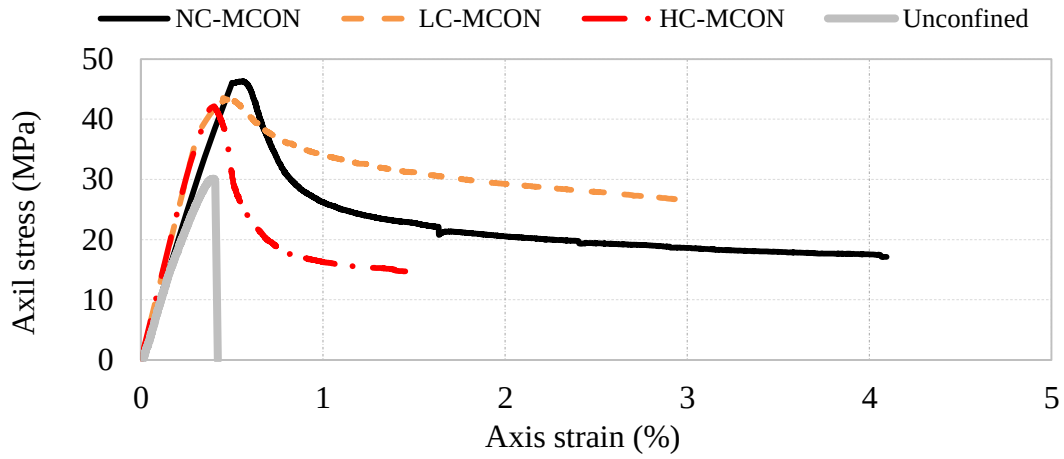

Figure 5-15 Stress–strain relationship of medium confined concrete with varying degrees of corrosion

Figure 5-16 compares the experimental results of stress–strain curves for high confined columns with varying degrees of corrosion. The results show that while a low degree of corrosion only decreases the ultimate strain of confined concrete, a higher degree of corrosion significantly decreases both strength and strain of confined concrete.

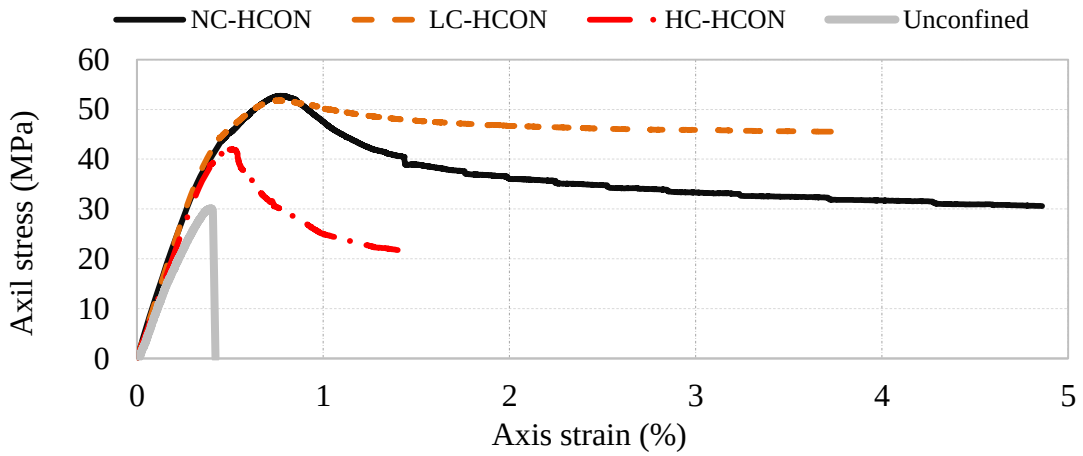

Figure 5-16 Stress–strain relationship of high confined concrete with varying degrees of corrosion

Table 5-2 summarizes the experimentally obtained values for the key features of the stress–strain curves (f'^{c}_{cc}, ε^{c}_{cc} and ε^{c}_{cu}) of the confined concrete and plain (unconfined) concrete for all specimens.

There are a number of uncertainty sources that could affect the experimental results. The uncertainties in mechanical properties of concrete materials and chloride-induced corrosion of steel reinforcement (uncertainties for low amount of corrosion is higher because the amount of reduction is relatively low and variation in the results of reduction factors is higher if compared with higher degrees of corrosion) are among the main parameters affect the results. Please note that the experimental results clearly show that corrosion deteriorates the effective strength, and ultimate strain of confined concrete. On the other hand, the experimental results (LC-MCON and LC-HCON) show reduction in all key control parameters of the stress–strain curve of the confined concrete compared to non-corroded columns.

Table 5-2 Experimental results for columns with various degrees of corrosion and confining reinforcement configuration

Cross section configuration	Name	Corrosion (%)		Plain concrete			Confined concrete		
		Longitudinal reinforcement	Transverse reinforcement	f'_c (MPa)	f'_{co} (MPa)	ε_{co} (%)	f'_{cc} (MPa)	ε_{cc} (%)	ε_{cu} (%)
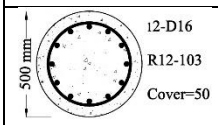	NC-LCON	0	0	30	30	0.15	45.8	0.45	2.87
	LC-LCON	4	11	29	29	0.16	41.2	0.42	2.59
	HC-LCON	12	27	29	30	0.16	36.7	0.44	0.74
	Pit-LCON	0	Pit	31	30	0.18	44.5	0.53	2.1
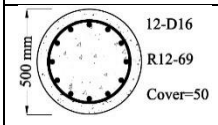	NC-MCON	0	0	30	30	0.18	46.3	0.56	4.1
	LC-MCON	4	15	28	30	0.16	43.5	0.45	2.9
	HC-MCON	18	40	30	31	0.16	42.2	0.4	1.5
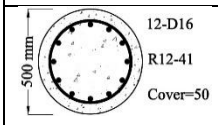	NC-HCON	0	0	30	30	0.17	52.7	0.77	4.9
	LC-HCON	4	15	30	31	0.17	51.8	0.75	3.79
	HC-HCON	10	24	31	30	0.16	42	0.51	1.46
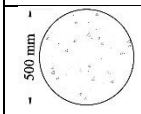	Cylinder 1	–	–	30	30	0.19	–	–	–
	Cylinder 2	–	–	31	30	0.18	–	–	–

The compressive strength, strain at compressive strength, and ultimate strain of confined to unconfined concrete ratio are summarised in Table 5-3. The ratios of mechanical properties of confined to unconfined concrete were compared with volumetric ratio and the effective mechanical properties of confining reinforcement. The results clearly show that for noncorroded columns, increasing the volumetric ratio of confining reinforcement enhances the key feature of the stress–strain curve of confined concrete. However, for corroded RC columns, the key features of confined concrete are more strongly dependent on the effective mechanical properties than the volumetric ratio of confining reinforcement. For example, the results for HC-HCON and NC-MCON evidently show that while the volumetric ratio of the confining reinforcement of HC-HCON is much greater than that of NC-MCON, the confined to unconfined mechanical characteristics ratios for NC-MCON are greater than those for HC-HCON. This is because the effective mechanical properties of confining reinforcement for NC-MCON are greater than those for HC-HCON.

Table 5-3: Experimental results for columns with various degrees of corrosion and the effective mechanical properties of confining reinforcement

Cross section configuration	Column name	Corrosion of confining reinforcement (%)	ρ_s	Effective mechanical properties of confining reinforcement		Confined concrete to unconfined concrete properties ratio		
				f_{yh}^{c} (MPa)	ε_{su}^{c} (%)	$\frac{f'_{cc}}{f'_{co}}$	$\frac{\varepsilon_{cc}}{\varepsilon_{co}}$	$\frac{\varepsilon_{cu}}{\varepsilon_{co}}$
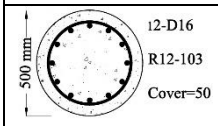	NC-LCON	0	0.0113	300	22	1.53	3	19.1
	LC-LCON	11	0.01	246	14.2	1.42	2.63	16.2
	HC-LCON	27	0.00825	166	2.87	1.22	2.75	4.6
	Pit-LCON	Pit	0.0112	248	14.52	1.48	2.94	11.7
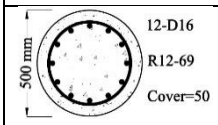	NC-MCON	0	0.0169	300	22	1.54	3.11	22.8
	LC-MCON	15	0.0144	226	11.37	1.45	2.81	18.1
	HC-MCON	40	0.0095	102	4.4	1.36	2.5	9.4
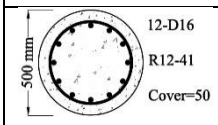	NC-HCON	0	0.0284	300	22	1.76	4.5	28.8
	LC-HCON	15	0.0241	226	11.37	1.67	4.4	23.7
	HC-HCON	24	0.0216	181	5	1.4	3.2	9.1

5.6 ANALYTICAL MODEL

The analytical formulas presented in this chapter were developed based on Mander's model and corrosion-induced deterioration models (presented in chapter 4) for concrete materials and steel reinforcement (Mander, 1983, Mander et al., 1988b). The objective of the analytical formulation is to calculate four key control parameters to predict the form of the stress–strain curve of the confined concrete of corroded RC circular columns.

In the previous chapter, it was shown that corrosion of reinforcement does not affect the axial strength, strain and concrete modulus of elasticity of the core confined concrete of RC columns. Therefore, the concrete modulus of elasticity of noncorroded RC columns can be used for corroded RC columns.

5.6.1 THE CONFINEMENT EFFECTIVENESS COEFFICIENT (k_e)

The confinement effectiveness coefficient for circular columns confined by spirals is as follows (Mander et al., 1988b):

$$k_e = \frac{1-\frac{s'}{2d_s}}{1-\rho_{cc}} \qquad 5\text{-}6$$

where s' is clear vertical spacing between spirals, d_s is diameter of spiral between bar centres and ρ_{cc} the ratio of longitudinal reinforcement area to sectional area of core, as follows (Mander et al., 1988b):

$$\rho_{cc} = \frac{A_{sl}}{A_c} \qquad 5\text{-}7$$

where A_c is the sectional area of core surrounded by the centre lines of spirals and A_{sl} is the sectional area of longitudinal reinforcement.

Figure 5-17 illustrates some of the parameters above for RC circular columns confined by spirals.

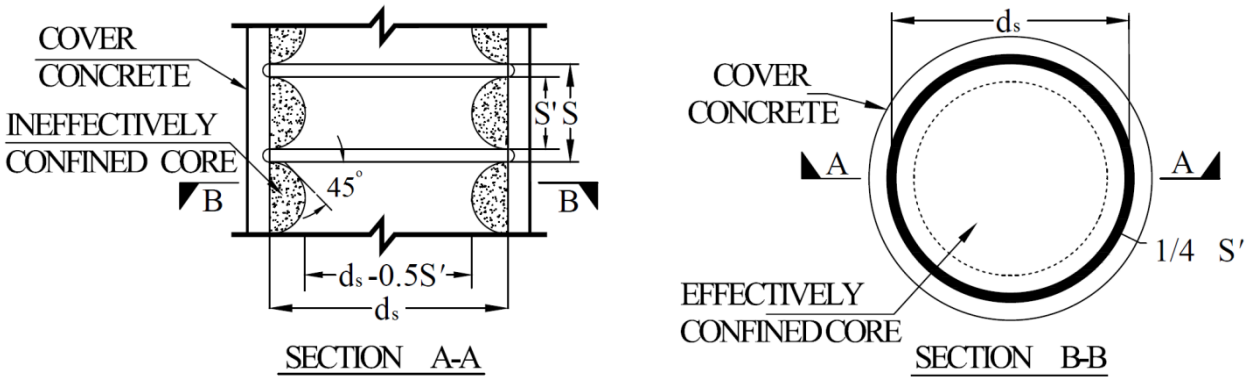

Figure 5-17: Sectional parameters of circular columns confined by spirals

Assuming s'= 100 mm, d_s= 388 mm, ρ_{cc}= 0.02 for a noncorroded RC column, k_e is equal to 0.889. Also, with 20% corrosion of transverse bars and 8% corrosion of longitudinal bars the above parameters become as follows:

s'= 101.2 mm, d_s= 387.7 mm, ρ_{cc}= 0.019 and k_e= 0.886

It is evident that a degree of corrosion equivalent to 20 % loss of sectional area of transverse reinforcement caused less than 0.3% change in the confinement effective coefficient; therefore, the effects of corrosion on confinement effectiveness coefficient (k_e) and its related parameters due to corrosion can be neglected.

5.6.2 THE EFFECTIVE LATERAL CONFINING STRESS

The effects of corrosion on the effective lateral confining stress on the concrete are dependent on

the effective yield stress of the corroded transverse reinforcement; therefore, the modified form of the effective confined stress on the concrete for corroded RC columns $f_l'^c$ is as follows:

$$f_l'^c = k_e \times \frac{2f_{yh}^c A_{sp}}{d_s s} \quad 5\text{-}8$$

where A_{sp} is the sectional area of transverse reinforcement, f_{yh}^c, the effective yield stress of the corroded transverse reinforcement, which may be expressed as follows:

$$f_{yh}^c = f_{yh}[1 - (\gamma_{fy} Q_{corr})] \quad 5\text{-}9$$

where f_{yh} is the yield stress of noncorroded transverse reinforcement, γ_{fy} is the reduction factor of the yield stress of transverse reinforcement. γ_{fy} can be estimated using reduction factors for yield stress presented in Table 3-6 or Table 3-7 for pitting-corroded RC columns and using FRF for yield stress presented in Table 4-11 for other corroded RC columns. Q_{corr} is the corrosion percentage of transverse reinforcement in term of average mass loss of the bar over the corroded area.

5.6.3 THE COMPRESSIVE STRENGTH OF CONFINED CONCRETE

The compressive strength of confined concrete has been proposed by Mander et al (1988b) as follows:

$$f_{cc}' = f_{co}' \left(2.254 \sqrt{1 + \frac{7.94 f_l'}{f_{co}'}} - \frac{2f_l'}{f_{co}'} - 1.254 \right) \quad 5\text{-}10$$

In this research, the Mander's model was modified to predict the compressive strength of confined concrete subjected to reinforcement corrosion. The compressive strength of confined concrete for corroded RC columns, $f_{cc}'^c$, is as follows:

$$f_{cc}'^c = f_{co}' \left(2.254 \sqrt{1 + \frac{7.94 f_l'^c}{f_{co}'}} - \frac{2f_l'^c}{f_{co}'} - 1.254 \right) \quad 5\text{-}11$$

where f_{co}' is the compressive strength of unconfined concrete.

5.6.4 THE STRAIN AT COMPRESSIVE STRENGTH OF CONFINED CONCRETE

The Mander's model suggested for non-corroded confined concrete was modified in this research. The modified form of strain at compressive strength of confined concrete for corroded columns, ε_{cc}^c, is

$$\varepsilon_{cc}^{c} = 0.002\left[1 + 5\left(\frac{f_{cc}^{\prime c}}{f_{co}^{\prime}} - 1\right)\right] \quad 5\text{-}12$$

5.6.5 THE ULTIMATE STRAIN OF CONFINED CONCRETE

Mander (1983) defined the ultimate strain of confined concrete as the strain at which first fracture of the transverse reinforcement occurs. To be easily used for practical applications, Priestley et al. (1996) modified the representation of the ultimate strain of confined concrete. The proposed ultimate strain of confined concrete for corroded RC columns, ε_{cu}^{c}, based on the modified form is as follows:

$$\varepsilon_{cu}^{c} = 0.004 + \frac{1.4\rho_s f_{yh}\varepsilon_{su}^{c}}{f_{cc}^{\prime c}} \quad 5\text{-}13$$

where ρ_s is the ratio of volume of transverse reinforcement to the volume of confined concrete core, f_{yh} is the yield stress of transverse reinforcement, ε_{su}^{c} is the ultimate strain of corroded transverse reinforcement:

$$\varepsilon_{su}^{c} = \varepsilon_{su}[1 - (\gamma_\varepsilon Q_{corr})] \quad 5\text{-}14$$

where, ε_{su} and γ_ε are the ultimate strain of noncorroded transverse reinforcement and its reduction factor, respectively. γ_ε can be estimated using reduction factors for ultimate strain presented in Table 3-6 or Table 3-7 for pitting-corroded RC columns and using FRF for ultimate strain (elongation) presented in Table 4-11.

It is important to note that volumetric ratio and the yield stress of noncorroded transverse reinforcement are used in Equation 5-12, because the effects of corrosion on the ultimate strain of confined concrete are only dependent on the effective ultimate strain of corroded transverse reinforcement.

5.7 EXPERIMENTAL RESULTS VS. ANALYTICAL MODEL

To validate the analytical formulations presented in the section 5.6, the analytically calculated stress–strain curves were compared with those experimentally obtained. The results of the comparison were shown in Figure 5-18. The results clearly show that the predicted values have good agreement with the test results. The experimentally measured versus the analytically predicted results for the column specimens are summarised in Table 5-4. The errors show the difference between the experimental and the predicted values was calculated as follows:

$$Error\ (\%) = \frac{Analytically\ redicted\ value - experimentally\ measured\ value}{Experimentally\ measured\ value}$$

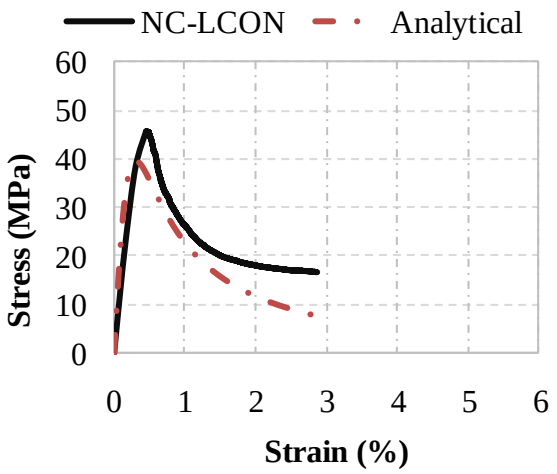

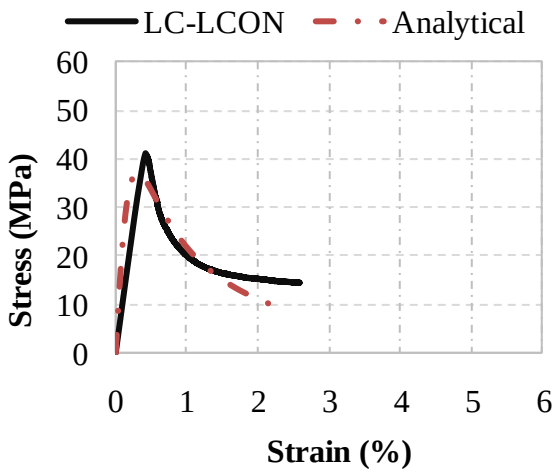

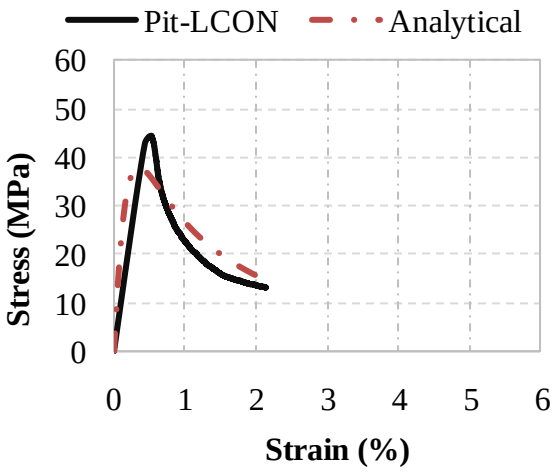

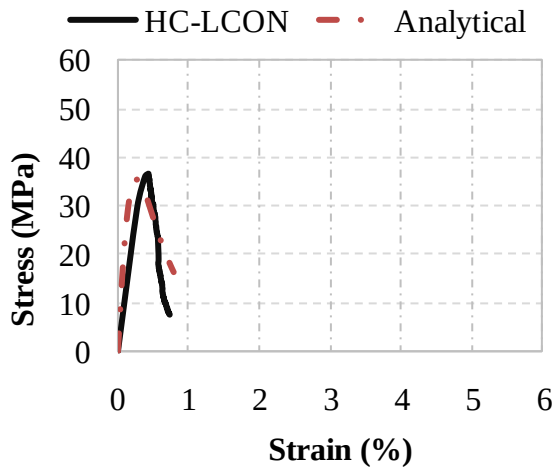

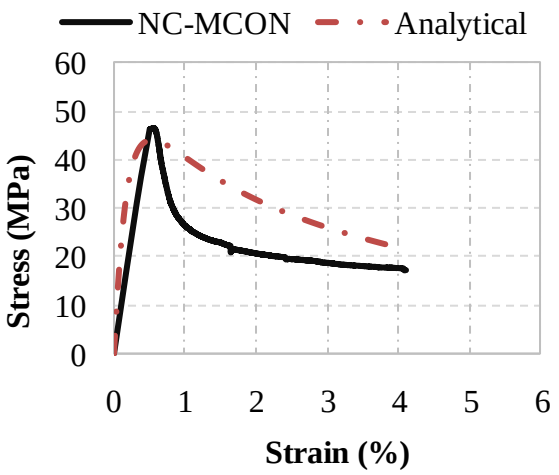

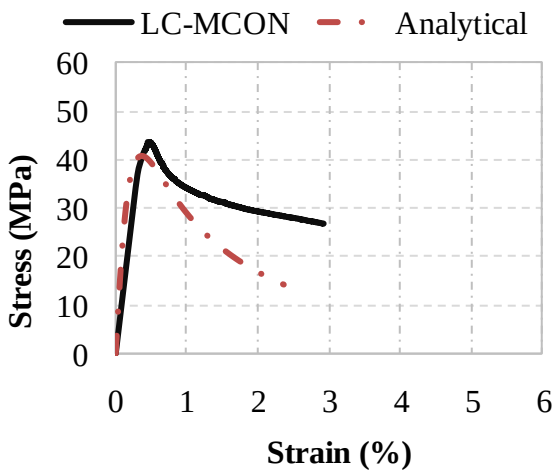

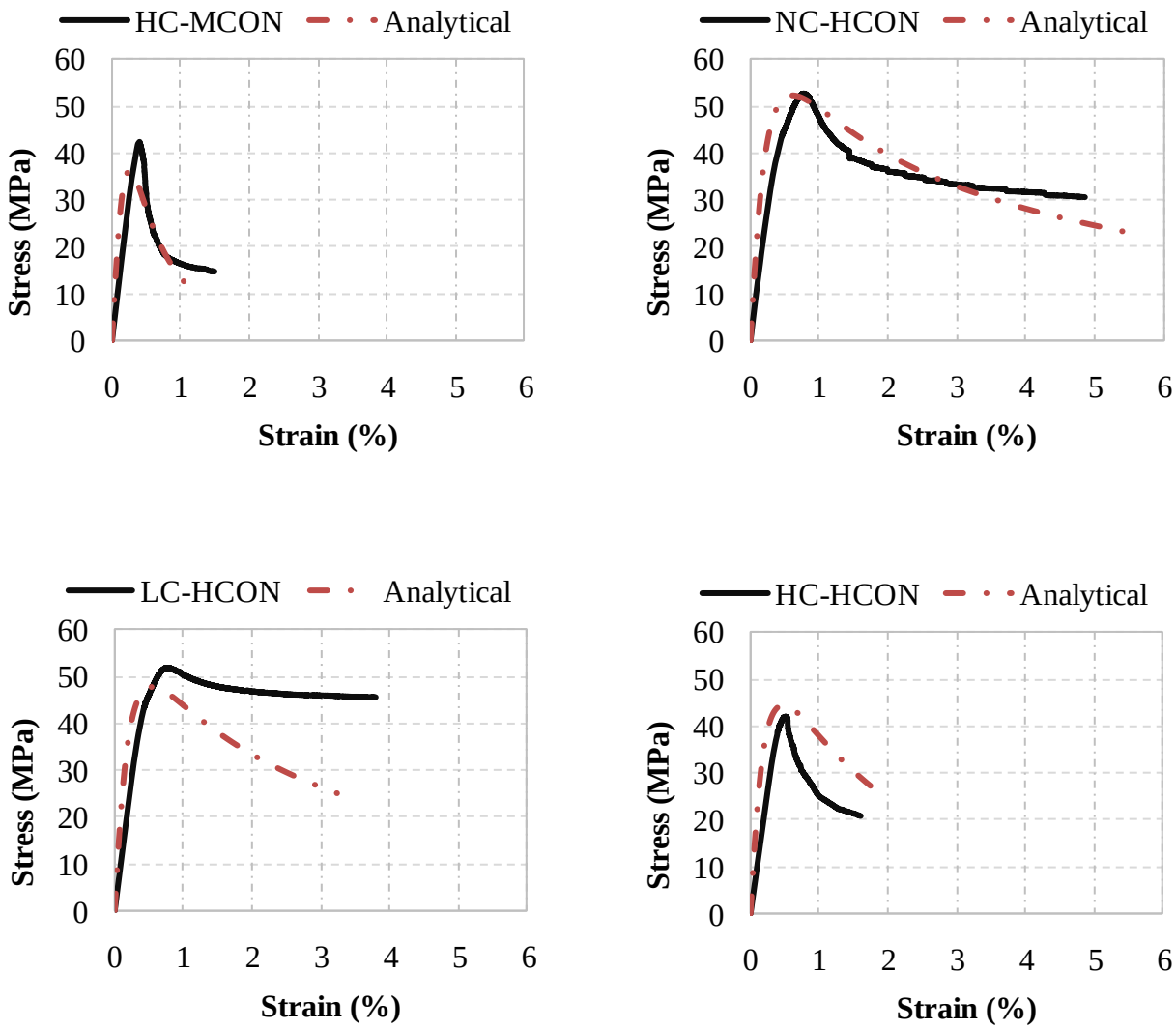

Figure 5-18: The stress–strain curves of confined concrete, analytically calculated versus experimentally obtained

Table 5-4: Experimental results versus analytical model

Column name	Corrosion (%)		Confined strength: f'_{cc}			Confined strain: ε_{cc}(%)			Ultimate strain: ε_{cu}(%)		
	L	T	Experimental (MPa)	Theory (MPa)	Error (%)	Experimental	Theory	Error (%)	Experimental	Theory	Error (%)
NC-LCON	0	0	45.8	45	-2	0.45	0.49	+9	2.87	2.7	-6
LC-LCON	4	11	41.2	37	-10	0.42	0.47	+12	2.59	2.22	-14
HC-LCON	12	27	36.7	35	-5	0.44	0.37	-16	0.74	0.79	+7
Pit-LCON	0	21	44.5	44	-1	0.53	0.42	-20	2.1	1.81	-14
NC-MCON	0	0	46.3	49	+6	0.56	0.6	+7	4.1	3.6	-12
LC-MCON	4	15	43.5	40	-8	0.45	0.53	+18	2.9	2.41	-17
HC-MCON	18	40	42.2	36	-15	0.4	0.36	-10	1.5	1.29	-14
NC-HCON	0	0	52.7	61	+16	0.77	0.8	+4	4.9	4.7	-4
LC-HCON	4	15	51.8	48	-7	0.75	0.75	0.0	3.79	3.23	-15
HC-HCON	10	24	42	47	+12	0.51	0.62	+21	1.46	1.67	+14

The maximum error 21% confirms the developed analytical formulations are able to predict the stress–strain response of corroded RC columns.

5.8 LIMITATION AND UNCERTAINTY

Pit damage was artificially induced by machining hemispherical cavities. This means cracked concrete due to corrosion by product was ignored. Moreover, for each corrosion level and confinement arrangement only one large scale test was performed. Considering uncertainties in corrosion and concrete materials, increasing number of tests may improve post-pick part of stress strain graphs of confined concrete. The errors of predicted values compared to experimental measurements were calculated and shown in Table 5-4. To quantify uncertainties in the developed analytical model, the absolute average, minimum and maximum errors for f'_{cc}, ε_{cc} and ε_{cu} have been calculated. In accordance with the results, the absolute average, minimum and maximum error of 1.4%, 1% and 16% respectively for f'_{cc}, 2.5%, 0.0% and 21% respectively for ε_{cc} and 7.5%, 4% and 17% for ε_{cu} were calculated.

5.9 CONCLUSIONS

Experimental tests were conducted on RC columns with circular cross section. The loading was a monotonic concentric compressive load at a strain rate of 67.5 /μs. The various arrangements of transverse reinforcement and degrees of corrosion were investigated. The experimental results were compared with suggested analytical formulations to predict stress–strain behaviour of

corroded RC circular columns. In summary:

- The analytical formulations which were developed in this study were able to predict the stress–strain curve of the corroded RC columns. The analytical models show good agreement with experimental results.
- The Mander's model to predict the stress–strain curve of noncorroded RC columns has good agreement with the experimental results at strain rate of 67.5 /μs.
- Corrosion that deteriorates the strength, the strain at strength and the ultimate strain of confined concrete caused significant change in the shape of the stress–strain curves of RC columns.
- The maximum reduction values of 20%, 30%, and 76% were observed for the strength, the strain at strength and the ultimate strain of confined concrete due to reinforcement corrosion.
- A high degree of corrosion of transverse reinforcement significantly increased the slope of the falling branch of the stress–strain curve.
- The stress–strain response of the corroded RC columns is directly related to corrosion of transverse reinforcement.

6 QUASI-STATIC CYCLIC RESPONSE OF A BRIDGE PIER SUBJECTED TO CORROSION

6.1 INTRODUCTION

Each average mass loss percentage of steel reinforcement due to corrosion is intended to represent a level of corrosion associated with a certain time, depending on key parameters affecting the corrosion process. Therefore, studying the residual capacity of corroded reinforced concrete structures with different amounts of mass loss can be considered as investigations into time-dependent structural performance subjected to corrosion. Ma et al. (2012) stated that while low levels of corrosion slightly affect the response of RC structures, higher degrees of corrosion cause significant deterioration, making the study of structures subjected to different amount of corrosion important. New Zealand is an earthquake-prone country, and it has its major population centres close to coastlines where steel is susceptible to chloride corrosion caused by the marine environment. Consequently, corrosion can seriously damage the seismic capacity of structures, ultimately endangering the seismic safety of structures. It is very important to regularly assess and monitor reinforced concrete structures subjected to earthquakes and corrosion, using reliable models to predict the seismic response of corroded structures.

As mentioned in Chapter 2, there is a critical need for both large-scale experimental testing and numerical simulations on corroded reinforced concrete structures. In this regard, there are some experimental studies on corroded reinforced concrete members (Ma et al., 2012, Ou et al., 2012, Meda et al., 2014). There is no doubt that all the studies above are very useful, but are only a very limited number of large-scale experimental studies on seismic performance of RC bridge piers, indicating need to further studies. Therefore, the quasi-static cyclic experimental tests were designed to study seismic response of RC bridge piers subjected to reinforcement corrosion. The effects of reinforcement corrosion on drift ductility of studied bridge pier was investigated

In this chapter, the cyclic response of precast emulative cast-in-place bridge piers with varying degrees of corrosion was experimentally studied. Three large bridge piers with three foundations were prefabricated in accordance with Advanced Bridge Construction (ABC) technology.

Two piers out of the three were corroded using an accelerated corrosion method. A 500-mm length measured from the top of the foundation of each of the two piers was corroded at two

different levels of corrosion. The quasi-static cyclic tests were carried out on all corroded and noncorroded bridge piers. A series of three cycles at increasing level of drift, followed by a half single cycle was applied through a horizontal hydraulic actuator. In total, three large-scale quasi-static cyclic tests were carried out. The cyclic responses of the noncorroded pier were compared with those of corroded piers. The results show that corrosion causes a reduction in the seismic capacity of the corroded piers in terms of their energy dissipation capability and drift ductility. Finally, a parametric study was carried out to investigate the effects of various parameters on the moment–curvature response of corroded bridge piers. To numerically predict the moment–curvature or force–displacement responses of corroded bridge piers, the deterioration models developed in Chapter 4 and 5 were used in the pushover analysis.

6.2 TEST UNIT

6.2.1 DIMENSIONS AND REINFORCEMENT

Three piers whose dimensions and reinforcement details are shown in Table 6-1 and Figure 6-1 were constructed for this test programme. All piers were designed according to NZS3101 (NZS, 2006).

Test unit NC is noncorroded, CL1 is corroded at level 1 (relatively low corrosion), and CL2 is corroded at level 2 (relatively high corrosion).

Table 6-1 Details of dimension and reinforcement of the test units.

Test Unit	NC	CL1	CL2
Height (mm)	3100	3100	3100
Cross-sectional diameter (mm)	500	500	500
Longitudinal reinforcement	$8 \times \phi 16$	$8 \times \phi 16$	$8 \times \phi 16$
Longitudinal reinforcement ratio	0.84%	0.84%	0.84%
Transversal reinforcement	$\phi 10$ @ $75mm$	$\phi 10$ @ $75mm$	$\phi 10$ @ $75mm$

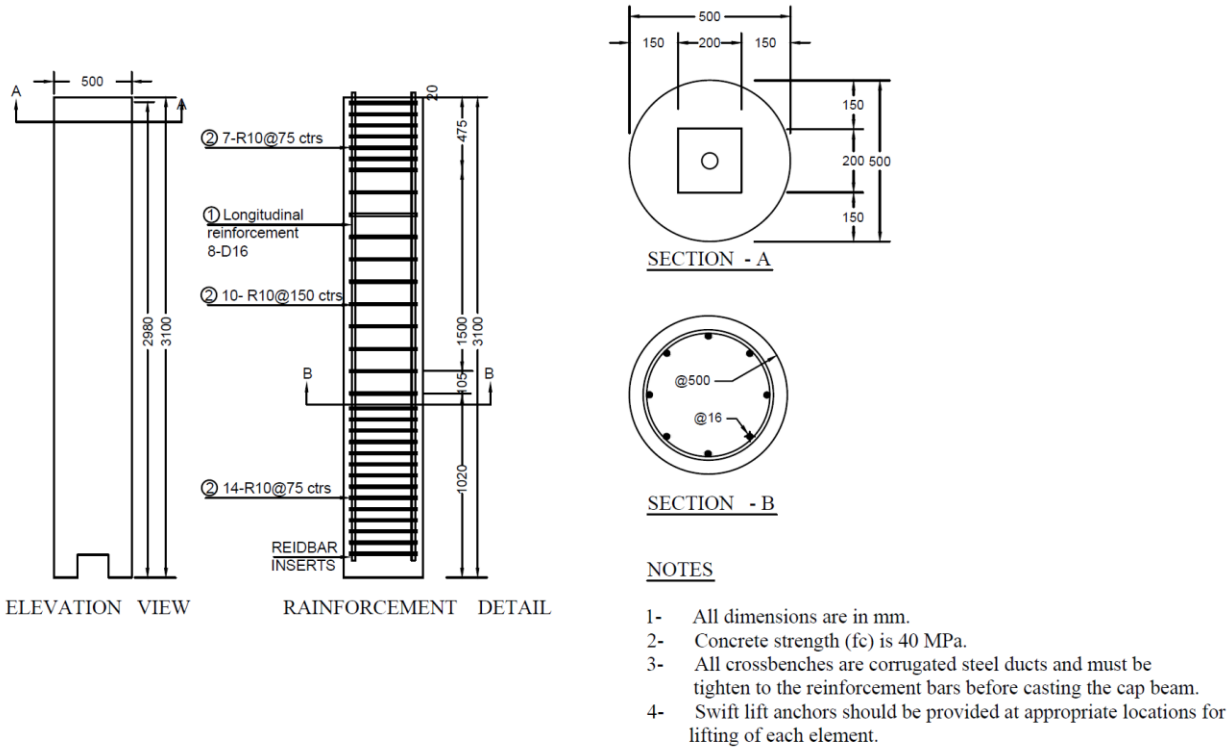

Figure 6-1 ECIP bridge pier geometry and reinforcement arrangement

6.2.2 CONSTRUCTION

Cast-in-place (CIP) substructure is the most common system used to bridge piers. As mentioned in Chapter 1, CIP has proven to be efficient at achieving life safety and structural collapse prevention, but low construction speed and poor quality fabrication are the main issues of CIP. Advanced Bridge Construction (ABC) uses precast concrete technology aiming at solving the above problems. To achieve the same life safety and structural collapse prevention, the prefabricated pier and foundation needs a connection to emulate the behaviour of cast-in-place connections (ECIP) through the formation of plastic hinges in the piers (White 2014). Although there are different types of ECIP connections, member socket connection was used for all specimens in this research (White 2014). The member socket connection of the bridge piers is a type of ECIP connection where the prefabricated column is embedded in the prefabricated foundation. A grout material is used to secure the connection. The prefabricated foundation and pier was assembled at the laboratory and formed a test unit. Figure 6-2 shows details of ECIP bridge pier and Member Socket connection, and Figure 6-3 shows photos of the main elements of ECIP piers.

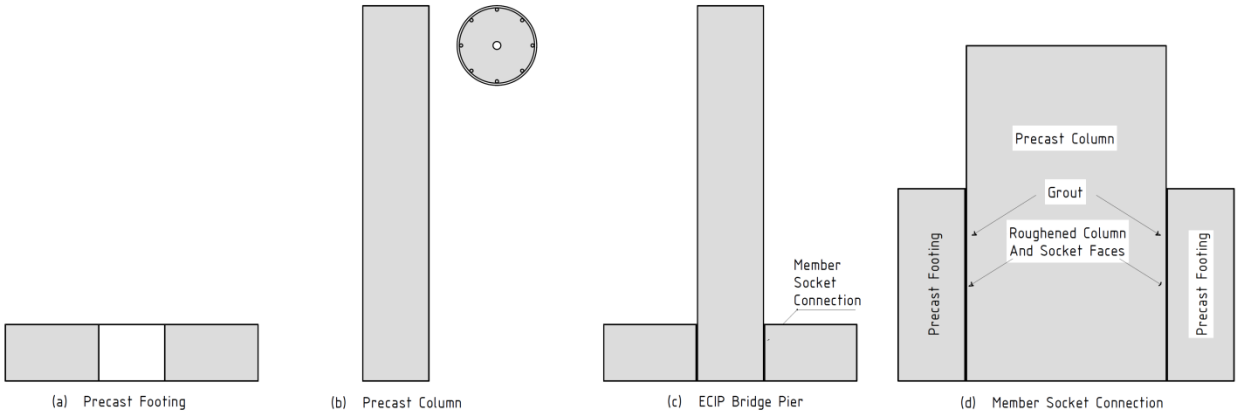

Figure 6-2 details of ECIP and member Socket Connection

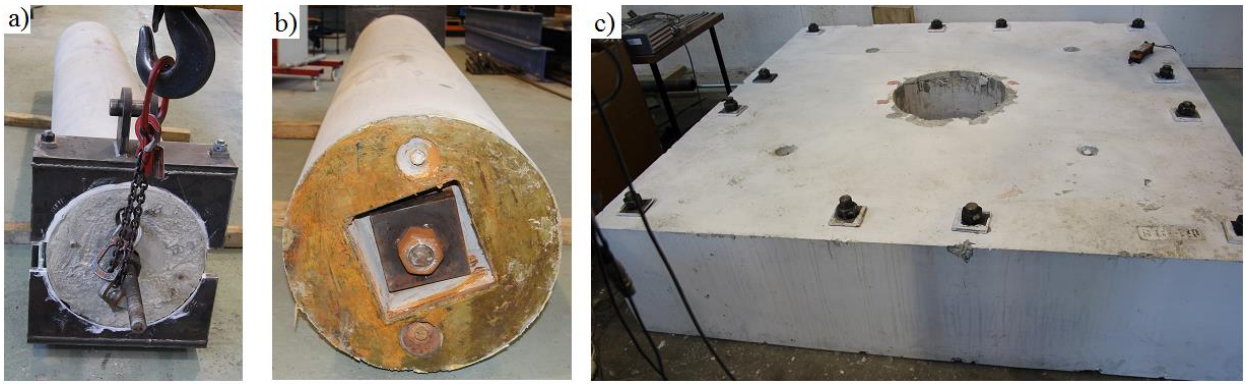

Figure 6-3 Prefabricated key components of ECIP, a) Post-tensioned pier with lateral load transfer element; b) details of post-tensioning anchorage at the bottom of the pier; c) foundation.

6.2.3 MATERIALS

6.2.3.1 CONCRETE

The same concrete was used to prefabricate all test units (pier and foundations) with a designed compression strength of 40 MPa. Table 6-2 lists the details of the concrete material used in this research.

Table 6-2 Details of concrete material.

Aggregate size (mm)	19 mm
Water-to-cement ratio	0.6
Slump (mm)	75 to 120 mm
Type of samples	Cylindrical
Dimensions of samples	Height: 200 mm; Diameter: 100 mm
Compression strength of samples at 28 days	35 to 42 MPa

6.2.3.2 STEEL REINFORCEMENT

The reinforcing bars for all specimens and their components, were specified as Grade 300 according to AS/NZS 4671.

6.2.3.3 HIGH COMPRESSIVE STRENGTH GROUT MATERIAL

The specified minimum compressive strength for the grout material, was 38 MPa at 28 days. Sika Grout 212 was used for filling the pier-foundation connection.

Grout samples were taken during assembly of each test unit. The cylinder samples of 50 mm in diameter and 100 mm in height were tested on the testing day for each test unit. In general, the sampling and testing procedure were in accordance with ASTM C1019-05 “Standard Test Method for Sampling and Testing Grout” (ASTM). Table 6-3 summarises the average compressive strength for the grout samples on the testing day of each specimen.

Table 6-3 Average compression strength of grout material.

Test Unit	NC	CL1	CL2
Average compression strength (MPa)	45	60	65

6.2.3.4 UNBONDED POST-TENSIONED MACALLOY BAR

A Hot Rolled Macalloy 1030 Post-Tensioning System Bar with 40 mm nominal diameter was used to simulate the gravity loads on the half-scale test units. Table 6-4 summarises the mechanical properties for the 1030 Macalloy bar.

Table 6-4 Summary of the mechanical properties for the 1030 Macalloy bar.

Minimum Elongation (%)	Modulus of Elasticity (GPA)	Nominal 0.1% Proof Stress (Yielding) (MPa)	Nominal Ultimate Tensile Strength (MPa)
6	170	835	1030

6.3 TEST SET-UP AND PROCEDURES

6.3.1 CORROSION TEST SET-UP

To corrode RC columns within a reasonable time, the impressed current method as an

accelerated corrosion method was used in this study. Figure 6-4 shows a prefabricated column and the process of preparing the column for the corrosion test set-up. The objective was to corrode the piers in such a way as to simulate real, corroded RC bridge piers. To meet this aim, the piers were placed in 3.5% NaCl solution and an electric current was applied, so that the region of the piers where a plastic hinge is expected to be formed in seismic events was subjected to corrosion. Therefore, as shown in Figure 6-3, the bottom and the 500 mm length of the piers above it that will be located in the hole at the middle of the foundation was protected from corrosion by covering these using a 5-mm thick, rubber material. The base part of the pier is a part of emulative cast in place socket connection. Providing rubber around the base of the columns protect this part of the columns from corrosion-induced deterioration. The corrosion density, the ratio of electrical current to corroded area, was 1000 $\mu A/cm^2$ for all corrosion test set-ups.

Figure 6-5 shows a photo and details of the accelerated corrosion test set-up prepared for the ECIP bridge pier. Penetrating salt water into the bridge piers extended the length of corrosion to about 800 mm. The two bridge piers were corroded with relatively low (less than 10% average mass loss in reinforcement) and high (more than 20% average mass loss in reinforcement) degrees of corrosion.

Figure 6-4 Details of preparing a RC column for corrosion test set-up.

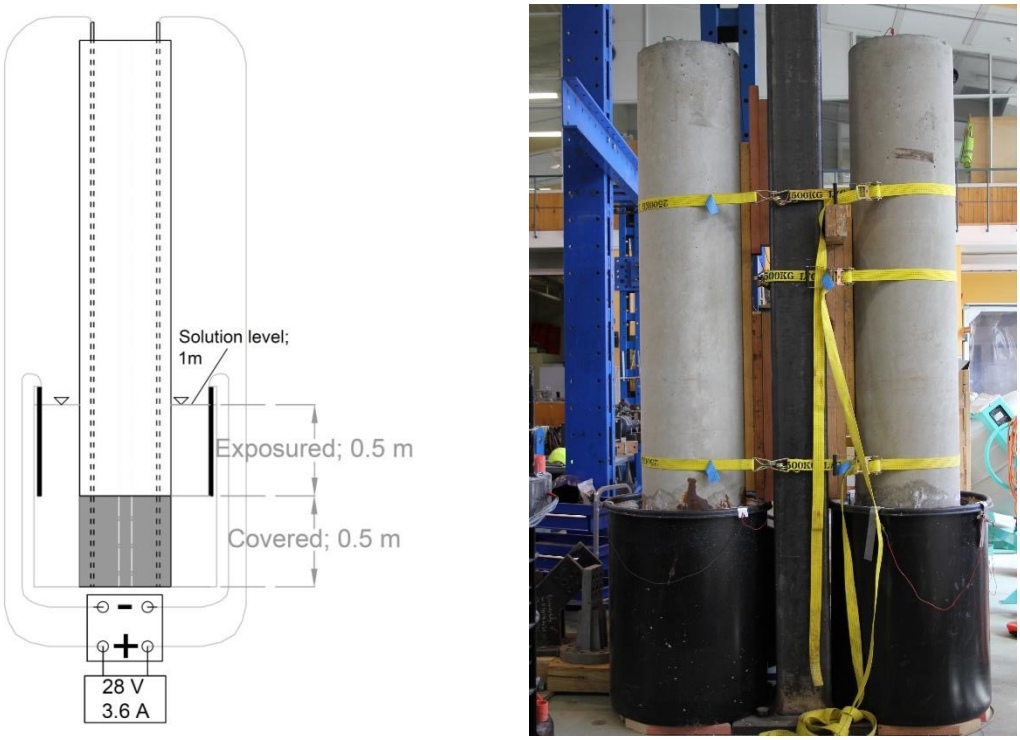

Figure 6-5 Details of accelerated corrosion process of the ECIP bridge pier

Figure 6-6 shows the corroded region of the columns. In this study the region located at the top of foundation with length of 500 mm, the region where the plastic hinge is expected to be formed, was corroded. The main reason is that the seismic response of the bridge pier is dependent on the response of the connections where the plastic hinge is expected to be formed when subjected to severe earthquakes (Ou et al., 2013b).

6.3.1.1 MEASURING OF THE CORROSION

Corrosion of reinforcing steels were calculated based on average mass loss over the corroded length. Therefore, the corrosion percentage of the longitudinal or transversal steel reinforcement can be calculated using the following equation:

$$Q\% = \frac{W_0 - W_t}{W_0} \times 100 \qquad 6\text{-}1$$

where W_0 is the original weight of the reinforcement; W_t is the weight of the corroded reinforcement; and $Q\%$ is corrosion percentage. The average corrosion of the transverse steel reinforcement was measured at 13% and 28% for CL1 and CL2 respectively. Table 6-5 shows details of the corrosion test results of transverse and longitudinal steel reinforcement for CL1

and CL2.

Figure 6-6 The corroded region of the columns.

Figure 6-7 shows the relationship between the corrosion of transverse and longitudinal steel reinforcement. While past studies highlighted that transverse reinforcement is more severely corroded than longitudinal steel reinforcement, no experimental study was found in the literature to address the relationship between the average corrosion of longitudinal and transverse reinforcement (Ou et al., 2013b, Ma et al., 2012). The results show that the average corrosion of the transverse bars is 2.5 times greater than the average corrosion of the longitudinal reinforcement. These results can be used in numerical simulations to better predict the seismic performance of corroded RC columns and piers. In this regard, further investigation into the effects of important parameters such as degrees of corrosion, corrosion methods, concrete cover thicknesses and water-to-cement ratio is recommended for future work.

Table 6-5 Details of corrosion test set-up of the longitudinal steel reinforcement in ECIP bridge piers.

Column	Sample name	Corrosion level	Time of exposure (days)	Corrosion of transverse bars (%)	Corrosion of longitudinal bars (%)
Column CL1	S1	L1	23	11.5	3.1
	S2	L1	23	11.3	4.8
	S3	L1	23	15.5	7.9
	S4	L1	23	12.3	5.5
	S5	L1	23	14.2	6.2
Column CL2	S6	L2	49	35.5	16.2
	S7	L2	49	27.9	14.2
	S8	L2	49	24.0	4.5
	S9	L2	49	24.5	9.1
	S10	L2	49	24.9	10.3

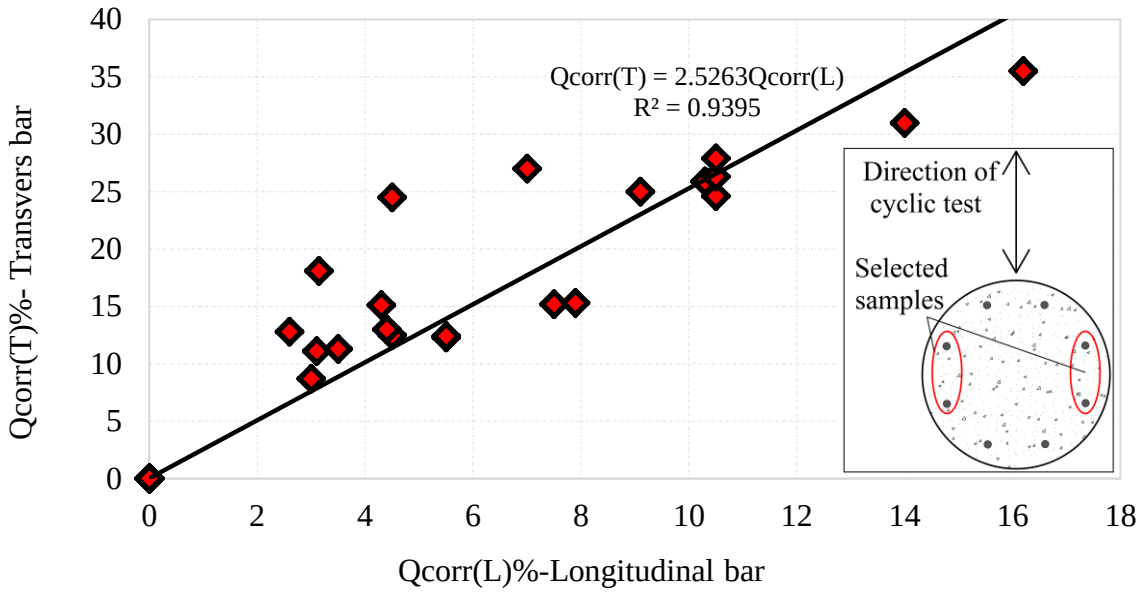

Figure 6-7 Relationship of corrosion of transverse and longitudinal reinforcement

The direction of the cyclic test and location of samples used to develop the relationship between the average corrosion of the longitudinal and transverse reinforcements are shown in Figure 6-7

It should be noted that the stirrups were corroded more than the longitudinal steel reinforcement, because they were closer to the concrete cover. However, the average corrosion of all the steel reinforcement, including longitudinal and transverse bars, was approximately 9.9% and 20.5% for CL1 and CL2 respectively.

6.3.1.2 CORROSION-INDUCED CRACKING

As mentioned in Chapter 2 steel reinforcement corrosion causes crack propagation in the column cover. In this study the shape, location, equivalent length and maximum width of corrosion-induced cracks were measured for both the corroded columns (CL1 and CL2), and the details are presented in Figure 6-8 and Figure 6-9 respectively. As shown in Figure 6-8, five individual cracks with maximum crack width of 1 mm and a maximum length of 580 mm were observed for the CL1 test unit. Figure 6-9 shows that ten cracks were observed for the CL2 test unit. The maximum crack width and length are 1.6 mm and 760 mm respectively. The results clearly show that more severe corrosion increases the number, length and maximum width of cracks,

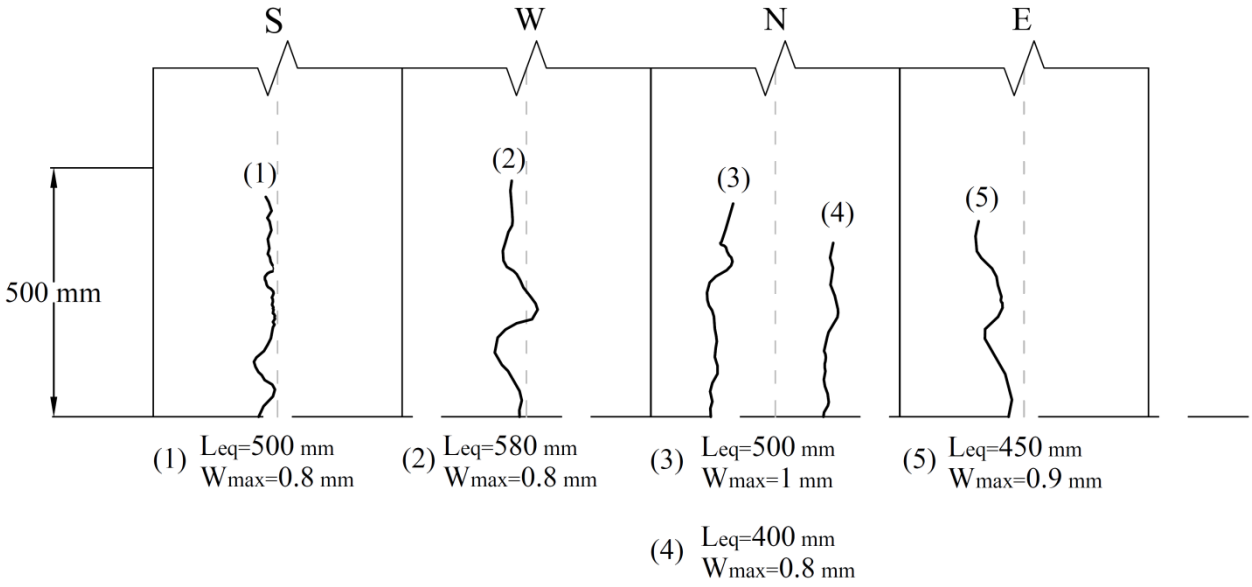

Figure 6-8 Details of corrosion-induced cracking for corroded L1 test unit on the four sides

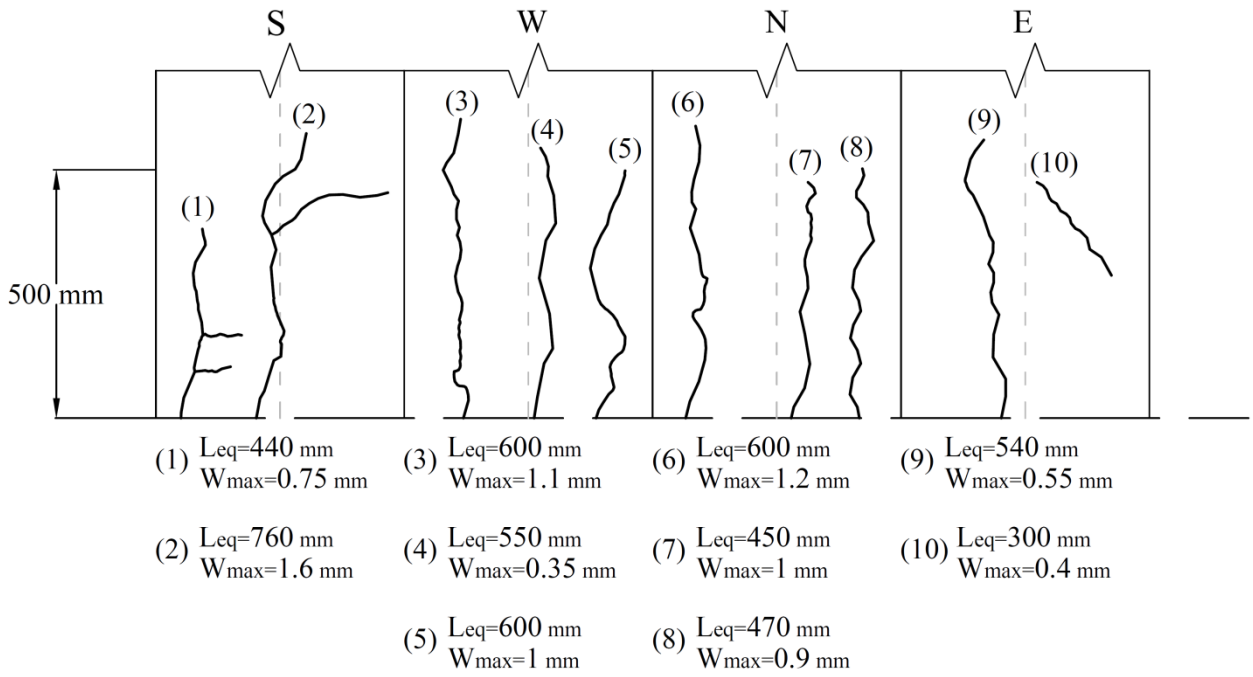

Figure 6-9 Details of corrosion-induced cracking for CL2 test unit on the four sides

6.3.2 QUASI-STATIC CYCLIC TEST SETUP

Figure 6-10 illustrates the quasi-static cyclic test set-up and instrumentation of the studied bridge piers. The load cell and tendon anchorage at the top of the column provided a 230kN vertical load, and the lateral hydraulic ram was used to push and pull the bridge piers. Before the test units were delivered to the laboratory, the 5 mm thick rubber material used to protect socket connection from corrosion was removed

After the test units were delivered to the laboratory, they were first measured, painted and prepared for instrumentation using linear variable differential transformers (LVDT) sensors, also called potentiometers (pots). After fixing the foundation to the strong floor, the precast piers were placed in the hole of the foundation. The diameters of the holes were 20 mm greater than the diameter of the piers. The pier was aligned perpendicular to the floor by means of three small timber wedges placed in the gap between the pier and the foundation. The gaps between the piers and foundations were filled with grouted material “Silka E212”. The pots were installed and a steel frame was used to support the actuator to apply cyclic loads.

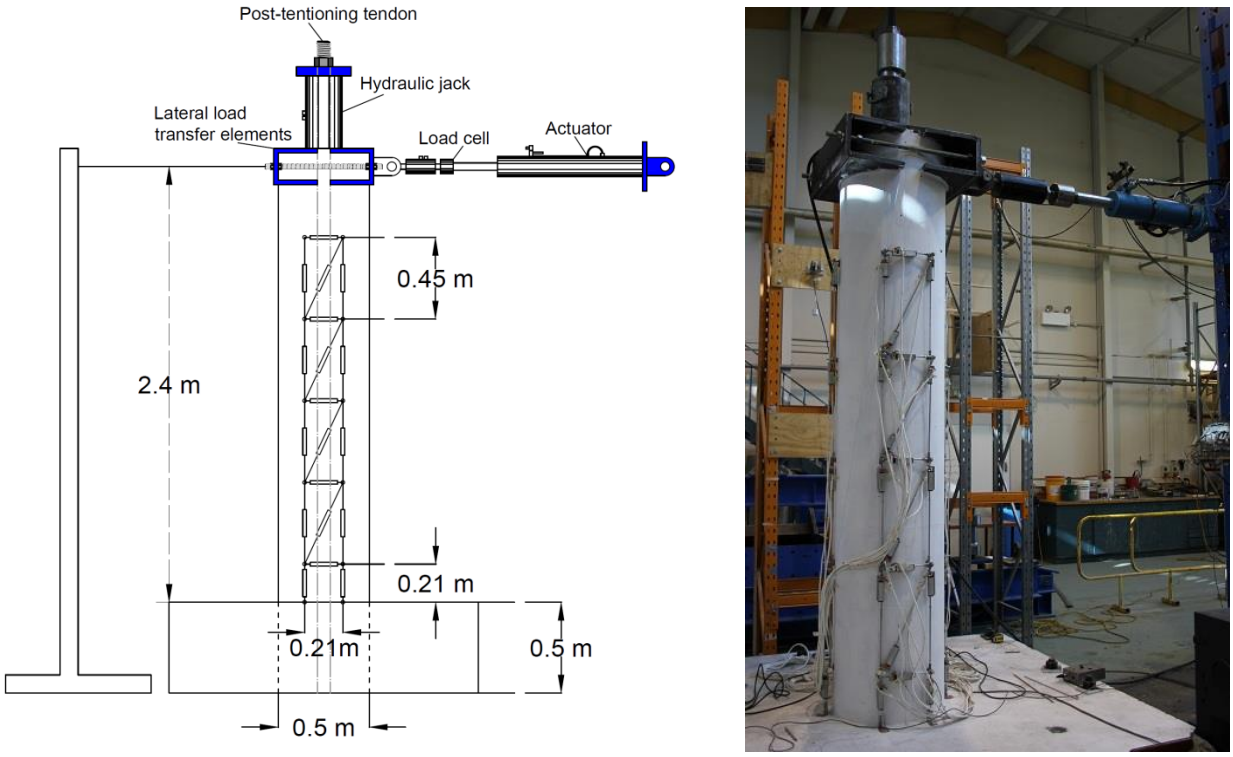

Figure 6-10: Test set-up for cyclic loading of ECIP bridge pier

6.3.2.1 MEASUREMENT

The LVDTs or pots, with which these measurements were made, were fastened to horizontal steel rods mounted on the piers. Figure 6-11 shows the details of installed pots. The displacement values recorded by the linear pots were used to measure the strain of the concrete materials and curvature of the piers. The vertical and cyclic loads were measured by load cells.

Three rotary pots were installed at the top of the pier to measure horizontal displacement of three points on the piers in the cyclic load direction. The three points were located on the back side of the actuator (North side of the pier), along a straight horizontal line, 2.4 m above the foundation level (see Figure 6-10). The difference between relative displacements recorded by the three pots can indicate torsional deformation. Lateral displacement of the piers was monitored using a rotary pot installed at the east side of the piers.

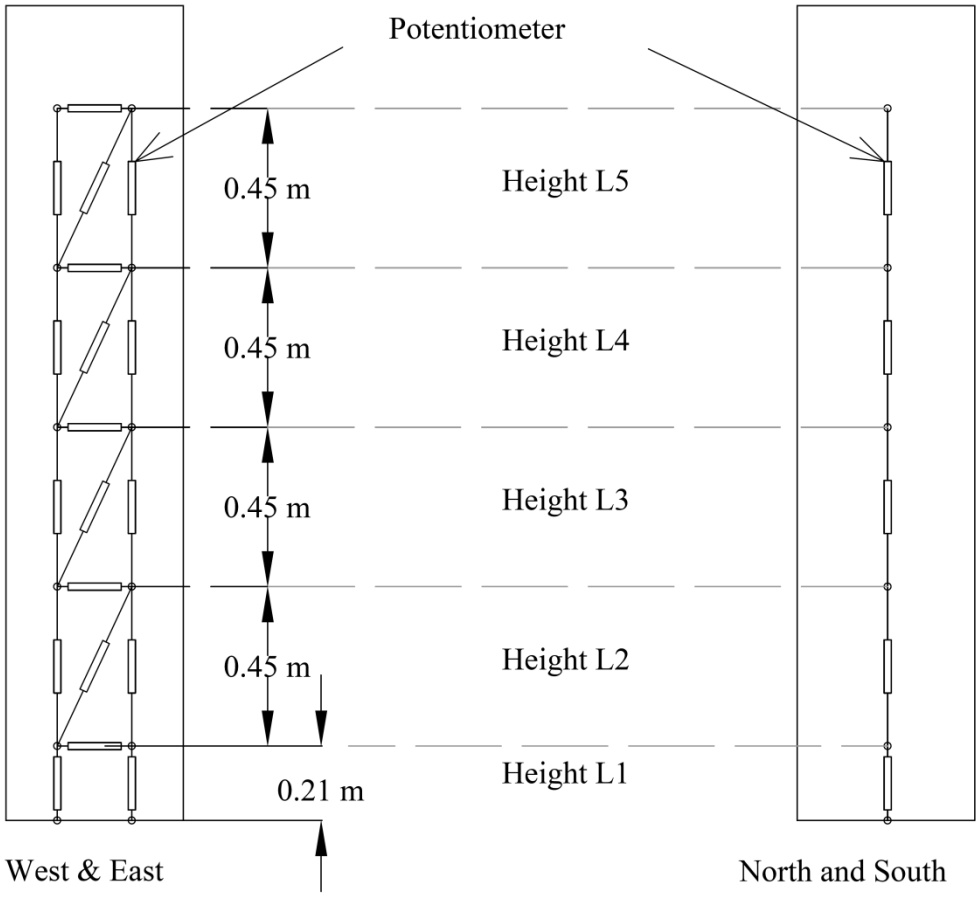

Figure 6-11 Details of LVDT installed on test units

6.3.2.2 TEST PROCEDURE

The tests were carried out using controlled drift method. A series of three cycles at increasing level of drift, followed by a half single cycle, was applied through a horizontal hydraulic actuator. This type of loading protocol was adopted from the ACI recommendations (ACI Innovation Task Group 1, 2001). Figure 6-12 shows details of load protocol used for the test units. The load protocols are similar with the exception of the maximum drift applied to each test. Maximum drifts of 6%, 5.5%, and 4.5% were applied to NC, CL1, and CL2 test units respectively.

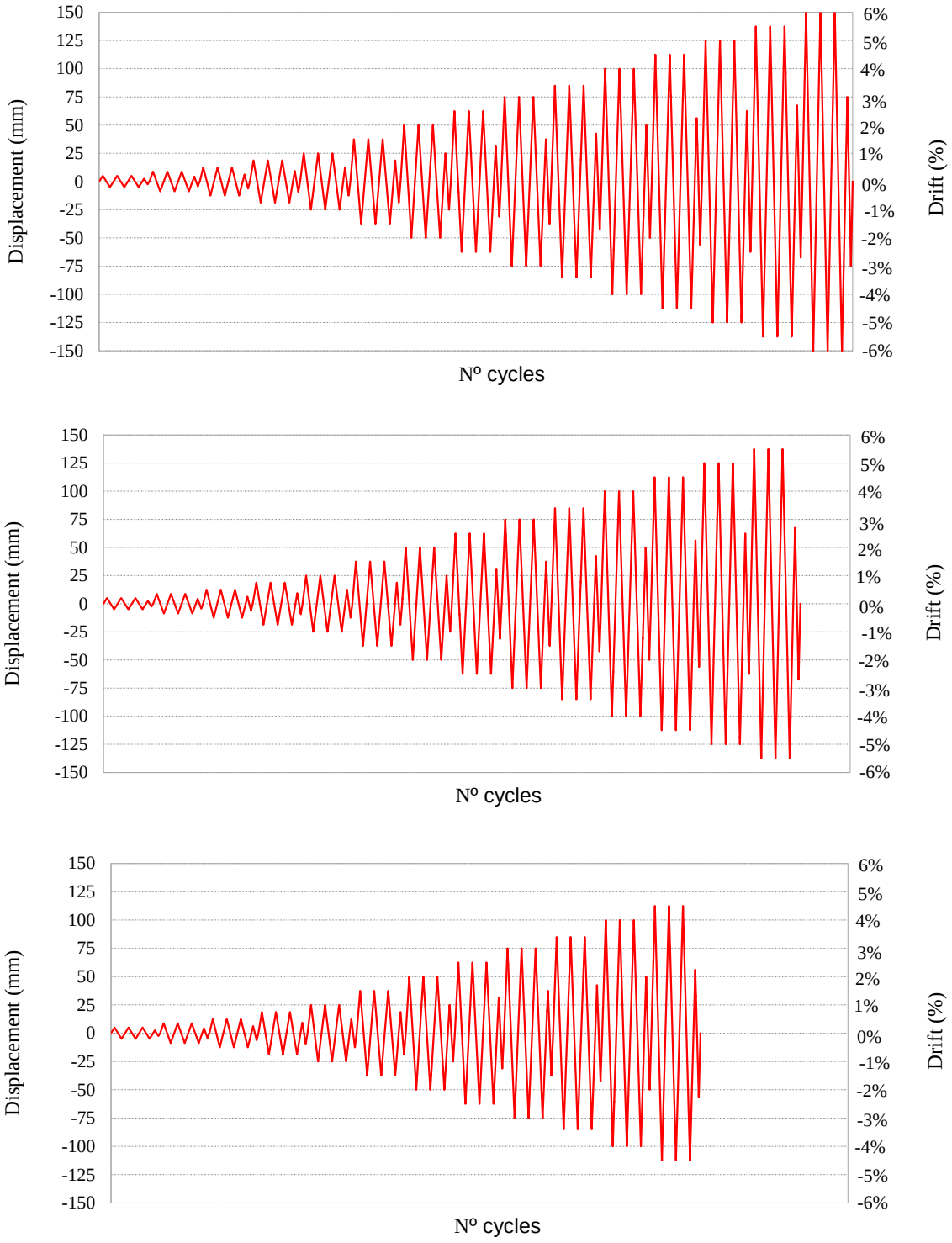

Figure 6-12 Details of load protocol for each test unit

6.4 RESULTS AND DISCUSSION

6.4.1 FORCE–DRIFT RESPONSE

The horizontal force measured by the actuator's internal load-cell is plotted against the top drift measured by the rotary pots. The positive and negative drifts represent pulling up and pushing down the piers respectively. Figure 6-13 shows the force–drift chart for test specimens. The test for the NC unit was terminated at 6% drift, due to the stroke limit. No longitudinal bar fracture was observed for the NC pier. At 6% drift, 20% reduction in horizontal force was observed with respect to the maximum horizontal load. The test for CL1 and CL2 was terminated when a number of longitudinal reinforcement bars ruptured at 5% and 4.5% respectively.

Since the same axial load of 230 kN was applied on all specimens, less stable hysteresis loops with smaller hysteresis loops for corroded piers indicates that corrosion decreases ability to dissipate energy. Although cyclic degradations in horizontal force and stiffness were observed for all test units, the results clearly show these reductions increase when degree of corrosion rises. The results also show that corrosion badly affects the ductility of the piers, indicating a negative impact on the seismic performance of corroded bridge piers.

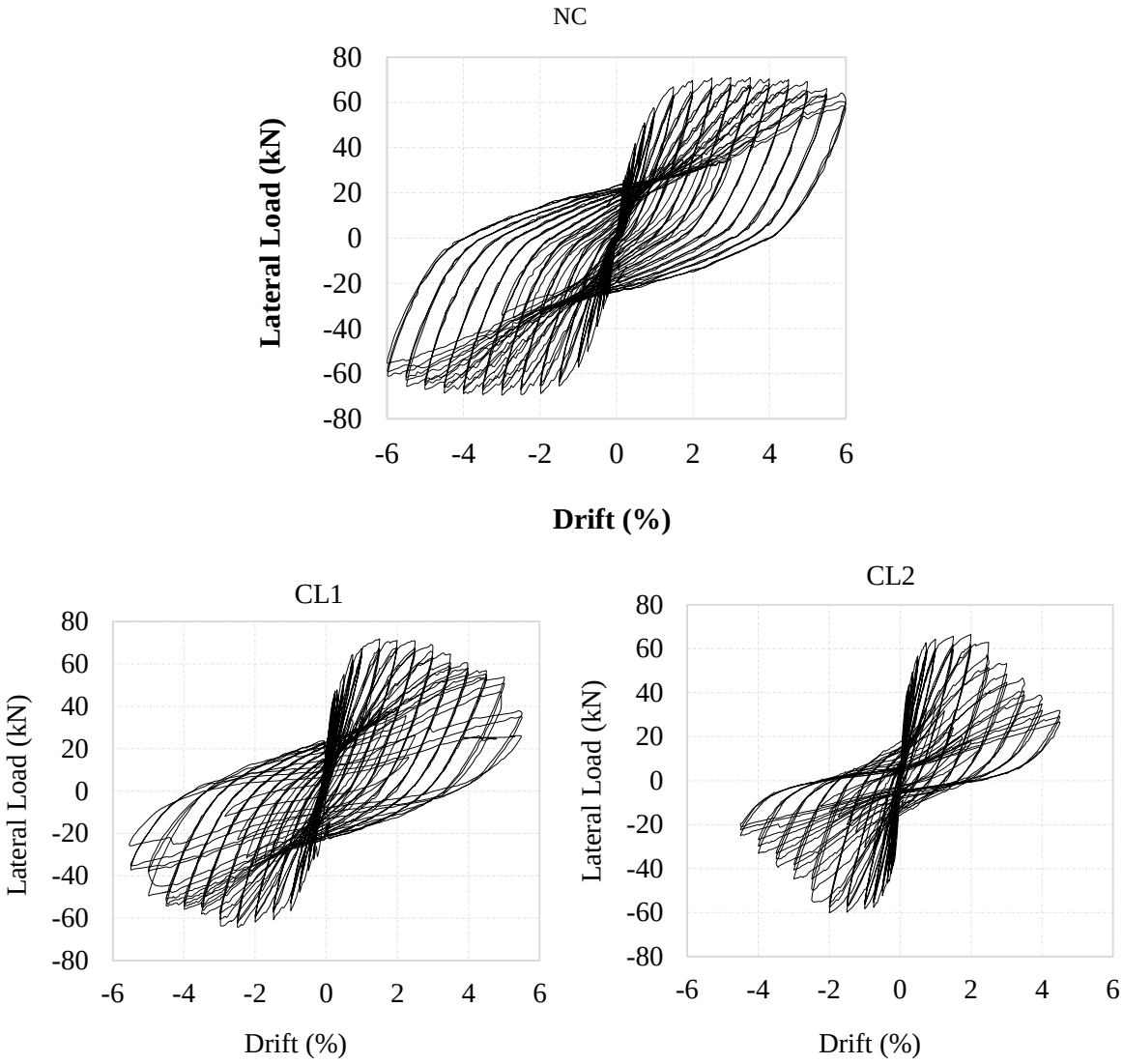

Figure 6-13 Force–drift response

6.4.2 FORCE–DRIFT ENVELOPE

Figure 6-14 shows the envelope graphs of the lateral force–drift of all specimens, obtained by the maximum absolute and the minimum values in the positive and negative directions respectively for each cycle of hysteresis loop shown in Figure 6-13. The results show degradation in the maximum lateral loads in cycles 2 and 3 compared with those in the first cycle for each drift. The cyclic degradation increases with increase of corrosion percentage. The results show that for CL1 pier, a minor reduction in load-carry capacity and significant degradation of the descending branch of the curve were observed. For the CL2 pier, significant degradation in both load-carry capacity and the descending branch of the graph was observed. It

seems that the stiffness is mainly dependent on the compression strength of the concrete materials. Table 6-3 compared the compression strength of concrete materials for all specimens. It is noted that the compression strength of CL1 and CL2 is more than 35% higher than that for the NC pier. Table 6-6 listed the important characteristics of the cyclic behaviour of the bridge piers based on the hysteresis response and envelope curves. In Table 6-6, F_y denotes yield load; Δ_y is the idealised yield drift value when the area underneath the idealised response curve equals that underneath the actual envelope response curve; Δ_u is ultimate drift, that is when the applied load declines more than 20% from the maximum value; F_{max} denotes maximum applied load; $\mu = \Delta_u/\Delta_y$, and denotes drift ductility; $\theta_p = \Delta_u - \Delta_y$ is plastic rotation.

Table 6-6 Cyclic test results

Specimen	F_y (kN)	Δ_y (Drift %)	F_{max} (kN)	Δ_u (Drift %)	μ	θ_p(Drift %)
NC	58	1	71	6	6	5
CL1	55	0.8	70	3.5	4.3	2.7
CL2	48	0.7	66	2.5	3.5	1.8

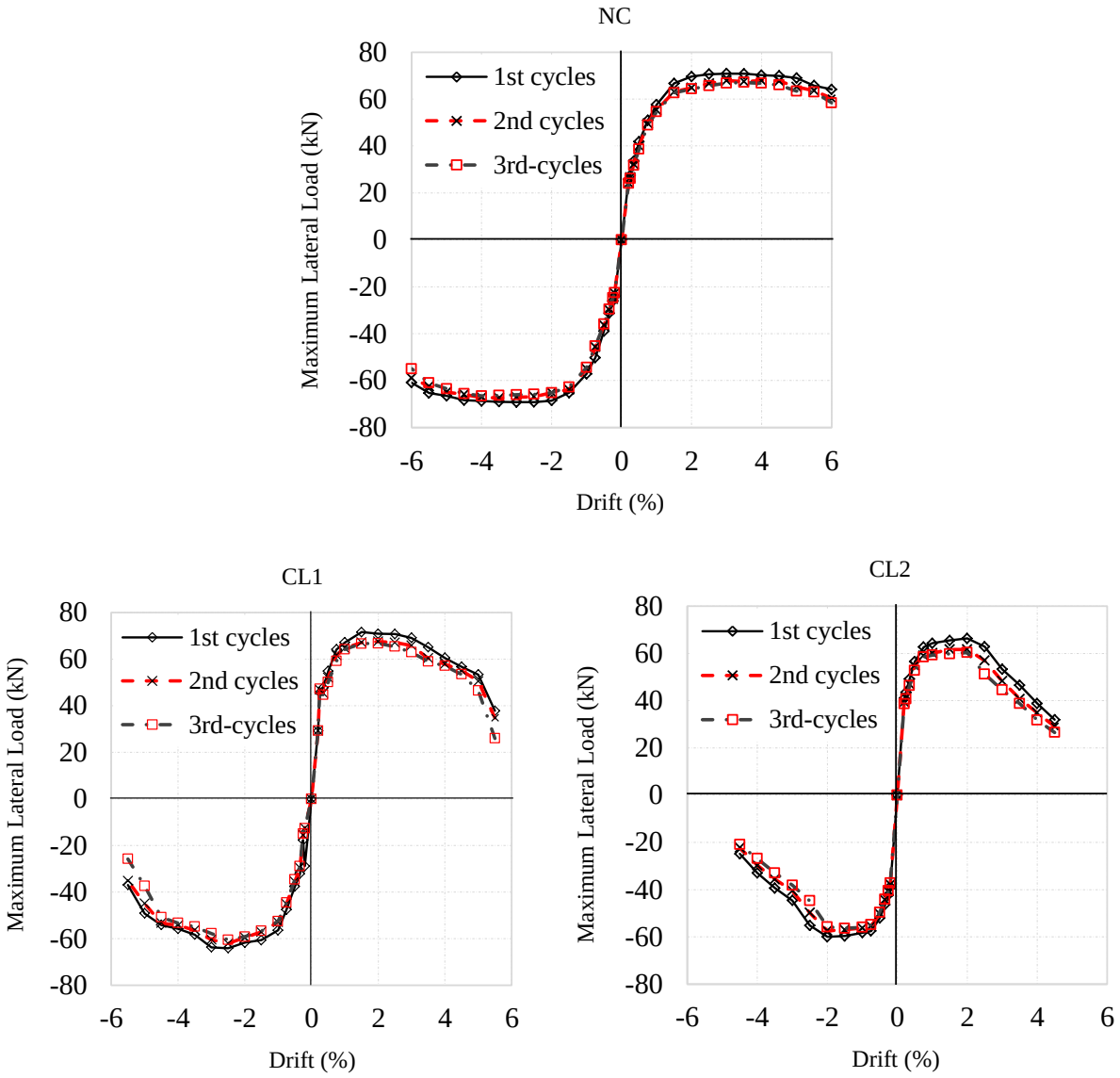

Figure 6-14 Force–drift envelope

6.4.3 STRAIN MEASURED FROM SOUTH AND NORTH FACE OF THE PIER IN NC TEST UNIT

Figure 6-15 compares strains along the south and north face of the piers, which are calculated using recorded displacements from the LVDT for different drifts for all specimens. The LVDTs were installed 20 mm away from the surface of piers to protect them from damage during testing. Assuming a plain section, the recorded strains were projected on the surface of the piers with linear interpolation. The positive and negative strains represent pulling up and pushing down the piers respectively. The results show that the tensile strains (strains during pulling-up

cycles) are greater than compressive strains (strains during pushing-down cycles). The reason is that during pulling up cycles, concrete cracks opened up. The results also show that the positive and negative strains for heights above 0.675 m are equal, confirming that concrete cracks were not opened. This probably indicates that bond deterioration resulted in strain penetration for heights below 0.675 m. The strains have an inverse relationship with height of the point at which strain was measured. The displacements on the surface of the piers are dependent on the bending moment, defined as the product of the lateral force and the distance from the lateral load to the measured point (location of LVDT). The lateral load at each time interval is the same for all points with different heights, whereas the distance decreases with height of the measured point.

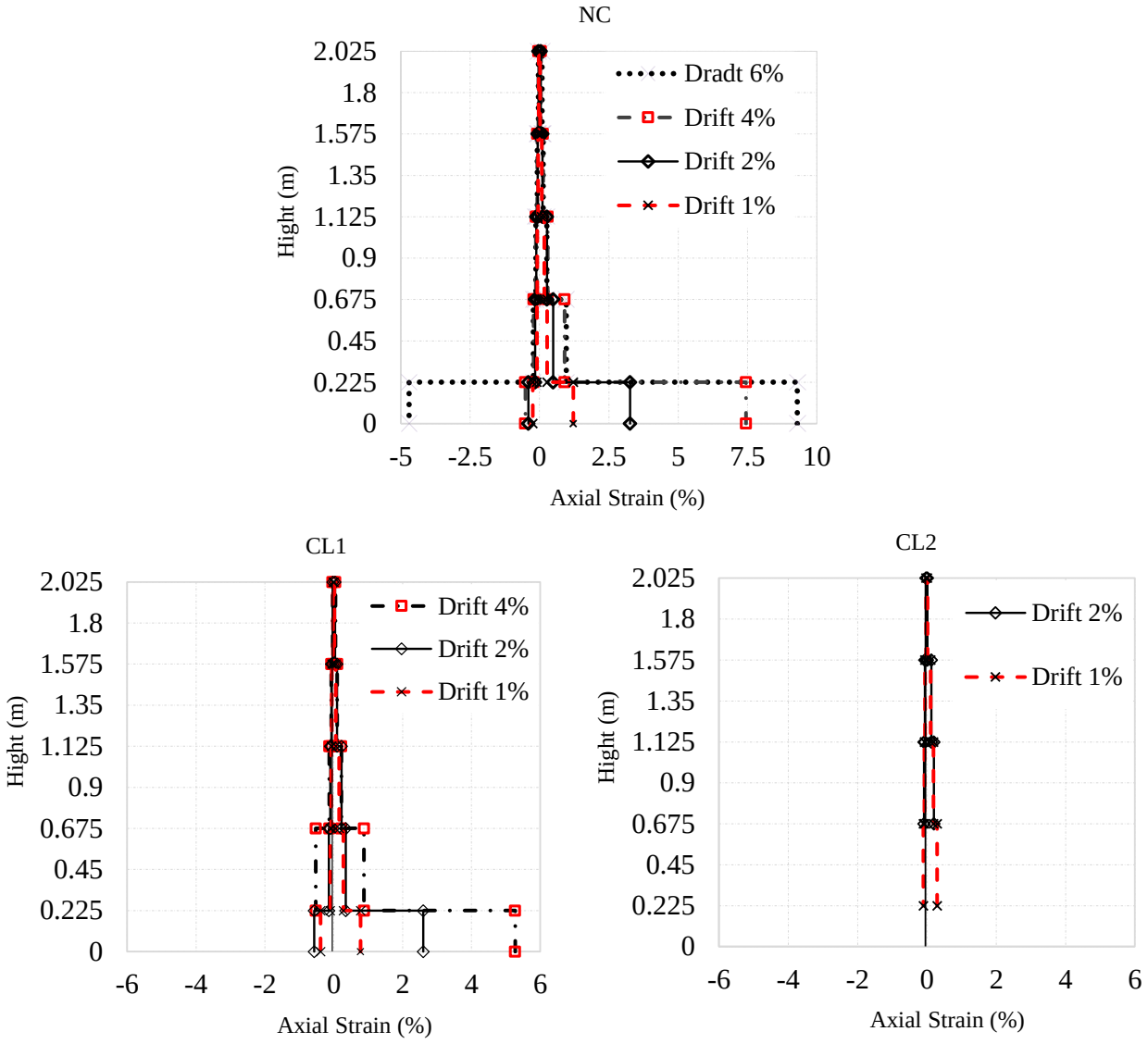

Figure 6-15 Strains along the south and north face of test unit NC calculated from deformations measured by means of the LVDTs

6.4.4 MEASURED MOMENT-CURVATURE OF NC TEST UNIT

The curvatures presented in Figure 6-16 to Figure 6-18 were calculated using the displacements measured by the LVDT chains along the side faces of the piers. The horizontal distance between the pots (LVDTs) was used to calculate the curvatures. In general, all curvatures are displayed until the devices had to be removed to protect them from damage. In this regard, the LVDTs located at height level 1 and 2 (see Figure 6-11) were removed at 6%, 4 % and 2% for NC, CL1, and CL2 piers respectively.

Figure 6-16 to Figure 6-18 show the moment-curvature relationship measured at the different levels of the NC, CL1, and CL2 piers respectively. For the same reason discussed in Section 6-4-3, the results show that the moment and curvature have an inverse relationship with the height of the point at which they were measured. The results show that the maximum moment at each level decreased with increasing degree of corrosion, indicating that corrosion decreases the load-carrying ability of the piers. Comparing the measured curvature at each level for all specimens reveals that there are differences in the moment-curvature trend. These differences might indicate different failure details for each pier, or cracked concrete cover of corroded piers. However, in this regard, more research studies would be useful to better understand the reasons for different trends in the moment-curvature graphs recorded for different piers.

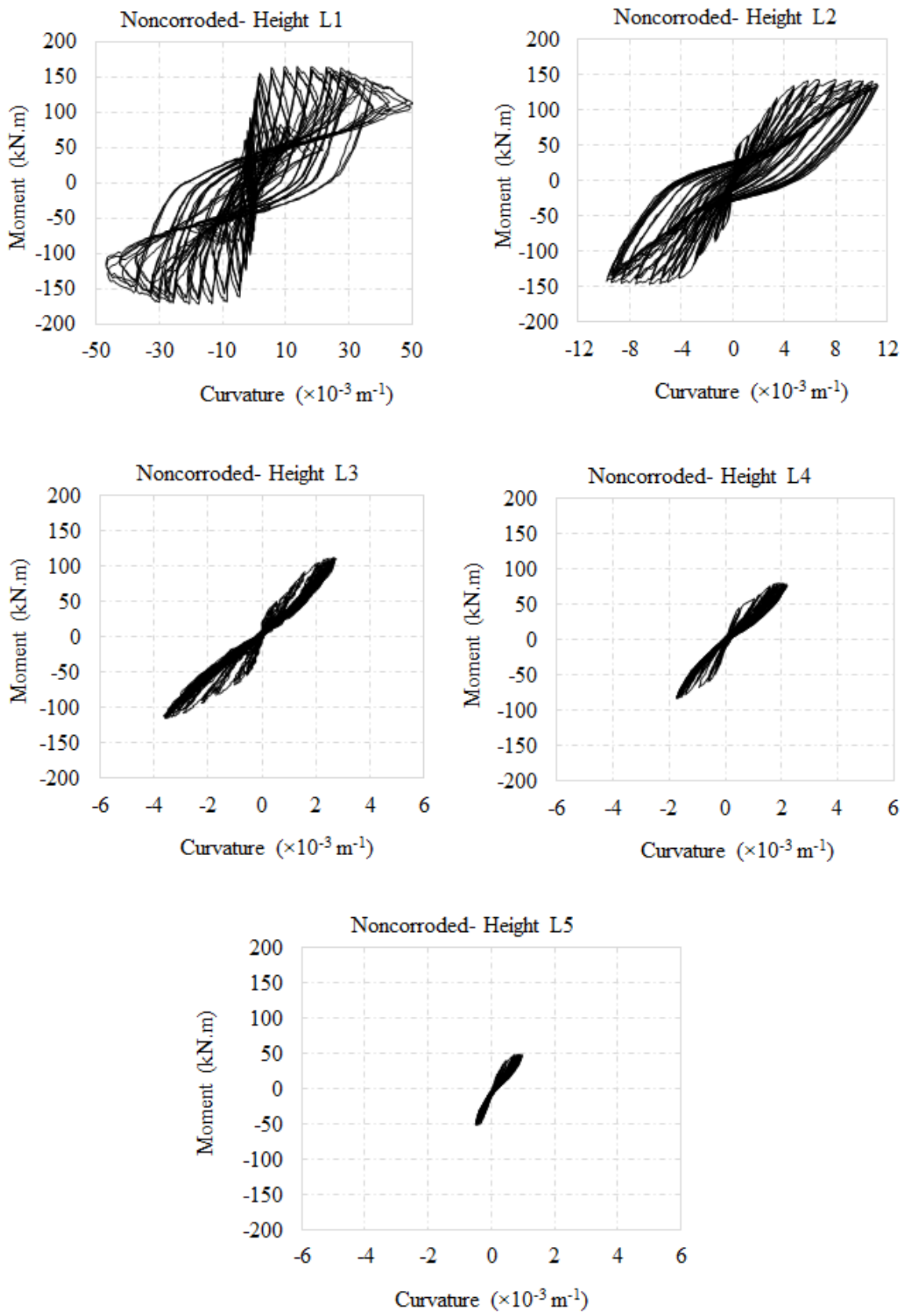

Figure 6-16 Measured moment-curvature at different levels of the NC bridge pier

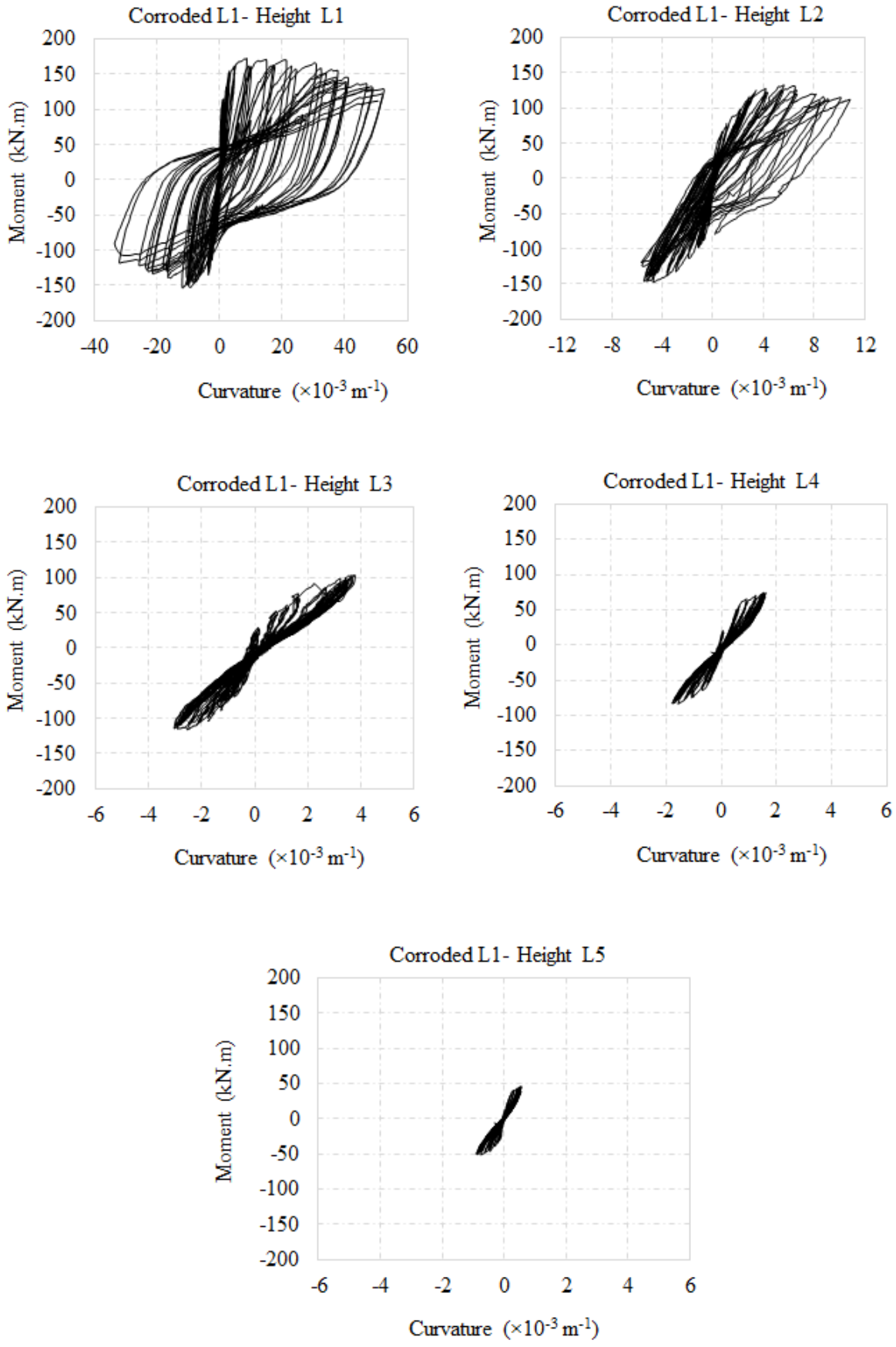

Figure 6-17 Measured moment-curvature at different levels of the Corroded-L1 (CL1) bridge pier

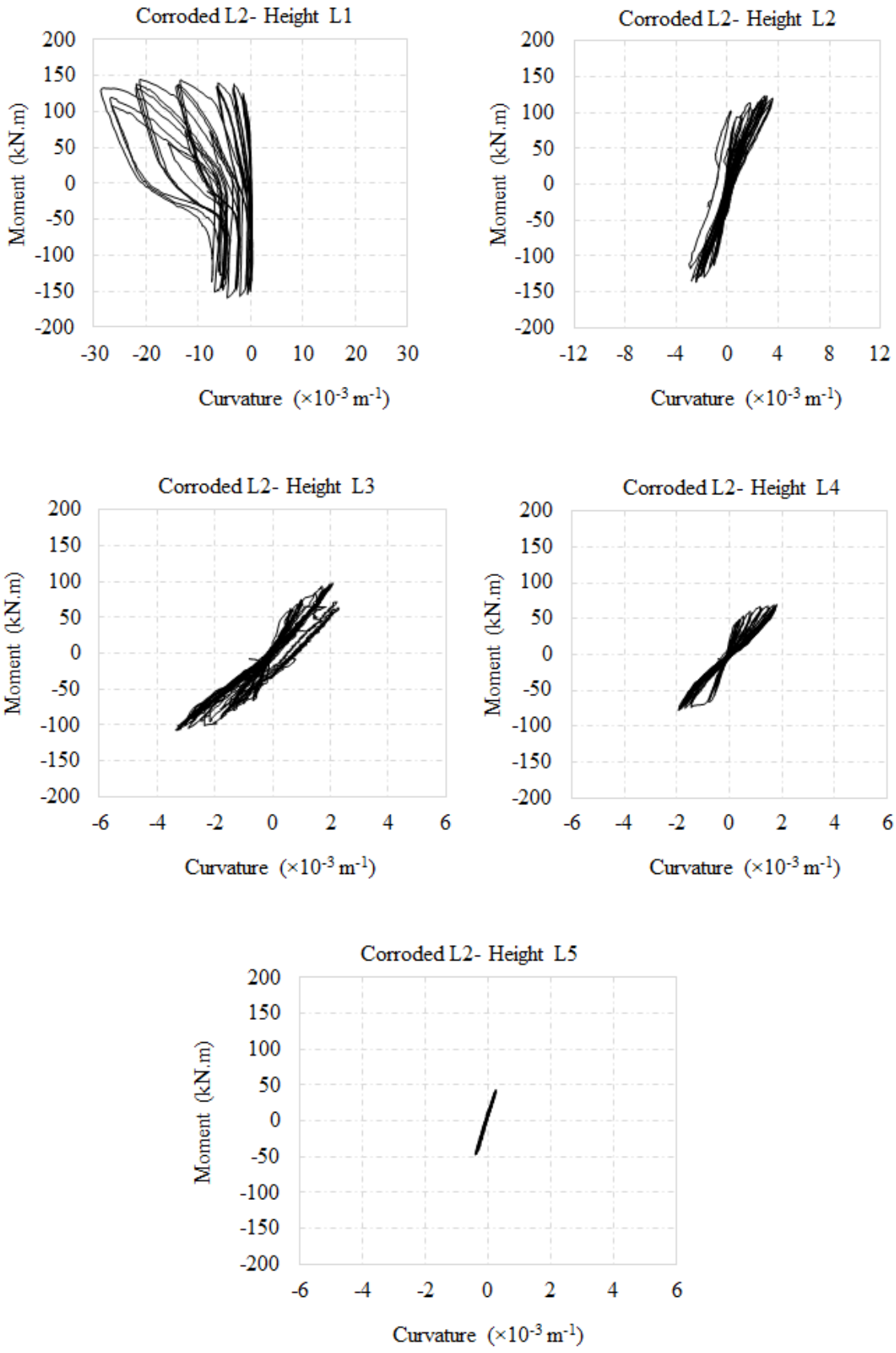

Figure 6-18 Measured moment-curvature at different levels of the Corroded-L2 (CL2) bridge pier

6.4.5 COMPARING FRONT VIEW AND MEASURED COVER SPALLING

Figure 6-19 compares the front view and length of measured cover spalling of bridge piers with different degrees of corrosion. The measured cover spalling lengths of 100 mm, 300 mm, and 500 mm for NC, CL1 and CL2 test units respectively indicate the increase of crushed cover length with the rising degree of corrosion. As already mentioned, the quasi-static tests were ended after completing cycles at 6.0%, 5.5%, and 4.5% drift for NC, CL1, and CL2 test units respectively. Reinforcement rupture was not observed for the NC test unit whereas, a number of ruptures of longitudinal reinforcement bars were observed for the CL1 and CL2 test units. The first longitudinal reinforcement failure occurred at 5% and 4% drifts for CL1 and CL2 respectively. Moreover, failure of transverse reinforcement was observed in the CL2 test unit that had the increased length of longitudinal bars unprotected against buckling.

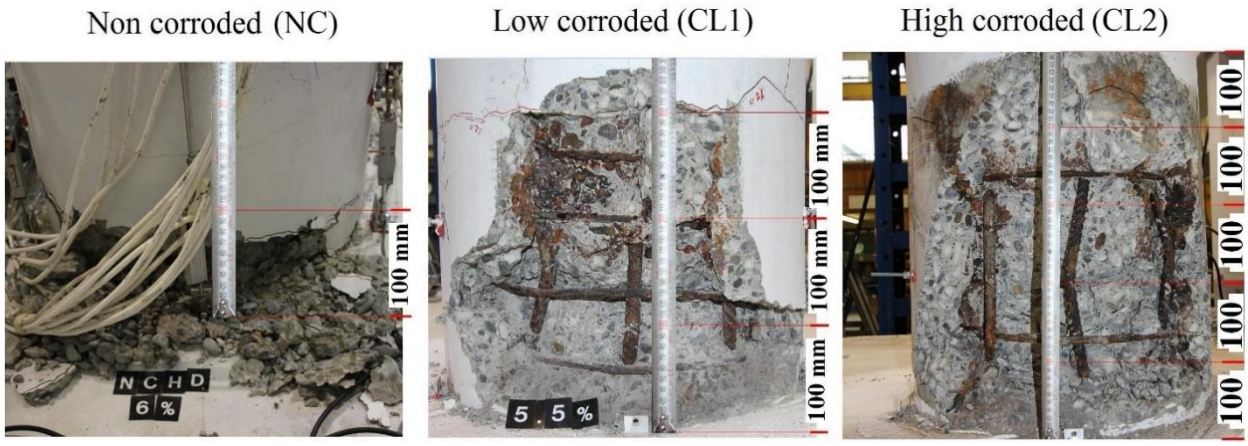

Figure 6-19 Comparing front view and measured cover spalling of bridge piers with different degrees of corrosion

6.4.6 COMPARING THE FORCE–DRIFT RESPONSE OF BRIDGE PIER WITH DIFFERENT DEGREES OF CORROSION

The lateral force–drift response of specimens has been discussed in Section 6-4-1. To better illustrate the effects of the corrosion-hysteresis response of the piers, the horizontal force and top drift for the bridge piers with different degrees of corrosion are compared in Figure 6-20. The results show that corrosion decreases the hysteresis response, leading to a reduction in structural capacity of the bridge piers. While a relatively low degree of corrosion (CL1) caused a reduction in lateral load-carrying capacity, higher degree of corrosion caused a significant reduction in

both stiffness and the lateral load-carrying ability. The results also show that corrosion causes a critical reduction in the maximum lateral load of corroded piers after 2% drift. Therefore estimation of residual ultimate lateral force is useful to predict the seismic capacity of corroded bridge piers. As shown in Table 6-4, the compression strength of concrete materials on the day of the quasi-static tests were 45, 60 and 65 MPa for NC, CL1 and CL2 respectively.

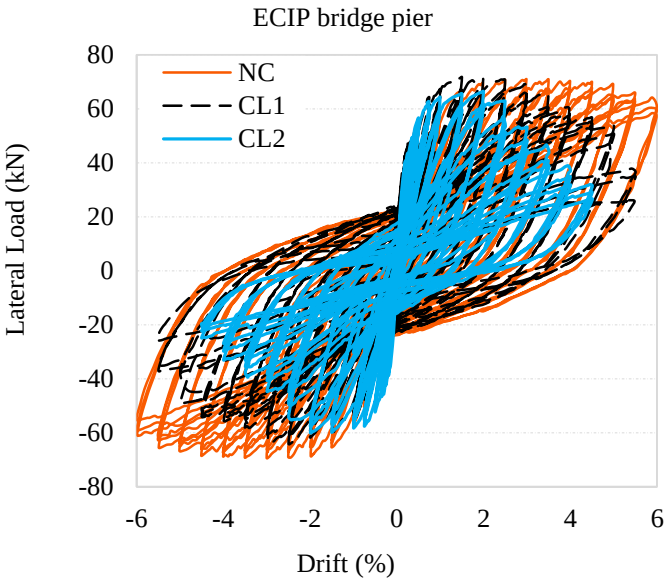

Figure 6-20 Comparing hysteresis response of specimens

6.4.6.1 DISSIPATED ENERGY

To quantify the effects of reinforcement corrosion on seismic response of ECIP bridge piers, energy dissipated by the piers were calculated for all tested piers. Figure 6-21compares energy dissipated by NC, CL1 and CL2 test units.

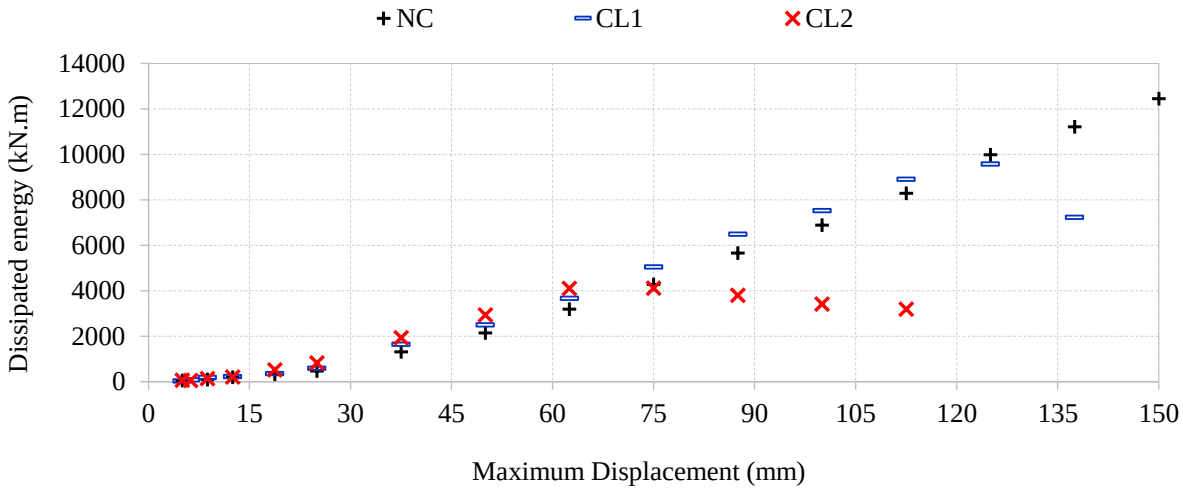

Figure 6-21: Energy dissipated by ECIP bridge piers for different degrees of corrosion

The results show that corrosion badly affects energy dissipation capability of the bridge piers.

6.4.7 ESTIMATION OF RESIDUAL LATERAL ULTIMATE FORCE

According to the accelerated corrosion results presented in Table 6-5, the average corrosion of longitudinal bars was approximately 5.5% and 10.9% for CL1 and CL2 respectively. The ultimate lateral force of piers with different levels of corrosion was estimated from the experimental tests and the results presented in Figure 6-22.

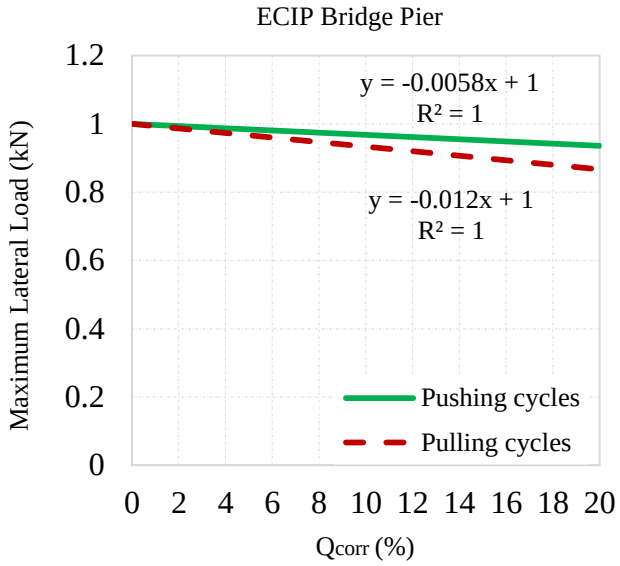

Figure 6-22: Estimation of residual lateral force of ECIP due to corrosion

The difference between reduction in ultimate lateral loading during pushing and pulling cycles can be related to irregularities caused by corrosion affecting the cyclic response of the corroded pier. However, in order to simplify the correlation, the average of pulling and pushing behaviour can be used for a general estimation of residual lateral ultimate force of a corroded pier. Therefore, the overall residual ultimate force can be estimated as follows:

$$\frac{F_{u-c}}{F_{u-NC}} = 1 - 0.00895Q_{corr} \qquad 6\text{-}2$$

Where, F_{u-c} is the ultimate lateral force of a corroded pier; F_{u-NC} is the ultimate lateral force of a noncorroded pier; and Q_{corr} is the corrosion percentage of the longitudinal reinforcement of columns.

Equation 6-2 shows that 10% corrosion (mass loss of longitudinal bars) causes 8.95% reduction in ultimate lateral force of the pier.

Ma et al. (2012) suggested Equation 6-3, based on a number of experimental tests:

$$\frac{F_{u-c}}{F_{u-NC}} = 1 - 0.00878Q_{corr} \quad 6\text{-}3$$

Equation 6-2 suggested by this study has very good agreement with Equation 6-3 suggested by Ma. et al. It should be noted that the columns tested by Ma et al. had a 1-m height above the foundation and the diameters of columns were 0.26 m. They could be 1:3 scale models of building columns. However, the piers tested in this study can be considered as full-scale building columns or half-scale bridge piers. It seems that uncertainties related to corrosion parameters and in the estimation of the residual capacity of corroded materials are the main reasons for the difference between the results of this study and that published by Ma et al.

6.5 SECTION ANALYSIS AND PARAMETRIC STUDIES

The cross-sectional analysis of the bridge piers was used to numerically predict the moment–curvature or force-displacement response, by assuming a linear distribution of concrete strain and neglecting the bond slips of reinforcement. Parametric studies were carried out to investigate the effects of important parameters on the moment-curvature response of the corroded bridge piers. In this study nine different cases were investigated. Figure 6-23 shows the details of all cases studied. Case I is a non-corroded column and the moment–curvature and results were used as a reference. Decreasing the effective mechanical properties of steel reinforcement due to corrosion is common knowledge in the literature, but there are huge variations in the reported corresponding reduction factors. Chapter 4 presented the maximum and minimum reduction factors for the effective mechanical properties of steel reinforcement reported by past studies. In this study, therefore the effective mechanical parameters of concrete and steel reinforcement were estimated based on the minimum, average, and the maximum reduction factors reported by past studies. For cases with corroded steel reinforcement, the effective mechanical properties of steel reinforcement were estimated based on 12% corrosion for longitudinal and 30% corrosion for transverse steel reinforcement.

6.5.1 VALIDATION OF NONLINEAR PUSHOVER ANALYSIS

To evaluate the efficiency of the numerical section analysis, the numerically estimated force–drift response of the specimens is compared to the experimentally recorded envelope curves. For corroded bridge piers, the effective mechanical properties of steel and concrete were calculated

based on deterioration models presented in Chapter 4 for corroded steel reinforcement embedded in concrete (Table 4-11) and cracked concrete cover (Table 4-2). Figure 6-24 compares the envelope graphs of the experimentally obtained lateral force–drift results with the numerically calculated force–drift response. The results show that pushover analysis cannot capture the descending branch of the envelope graphs. Ignoring bond slip, hysteresis behaviour of materials, and cyclic degradation in the cross-section analysis are probably among the main reasons for discrepancies between the descending branch of the envelope curves and the numerical force–drift response of the corroded piers. The results, however, show that the numerical force–drift behavior has a good agreement with the envelope curves: up to 6%, 4%, and 2.5% drift for NC, CL1, and CL2 pier respectively.

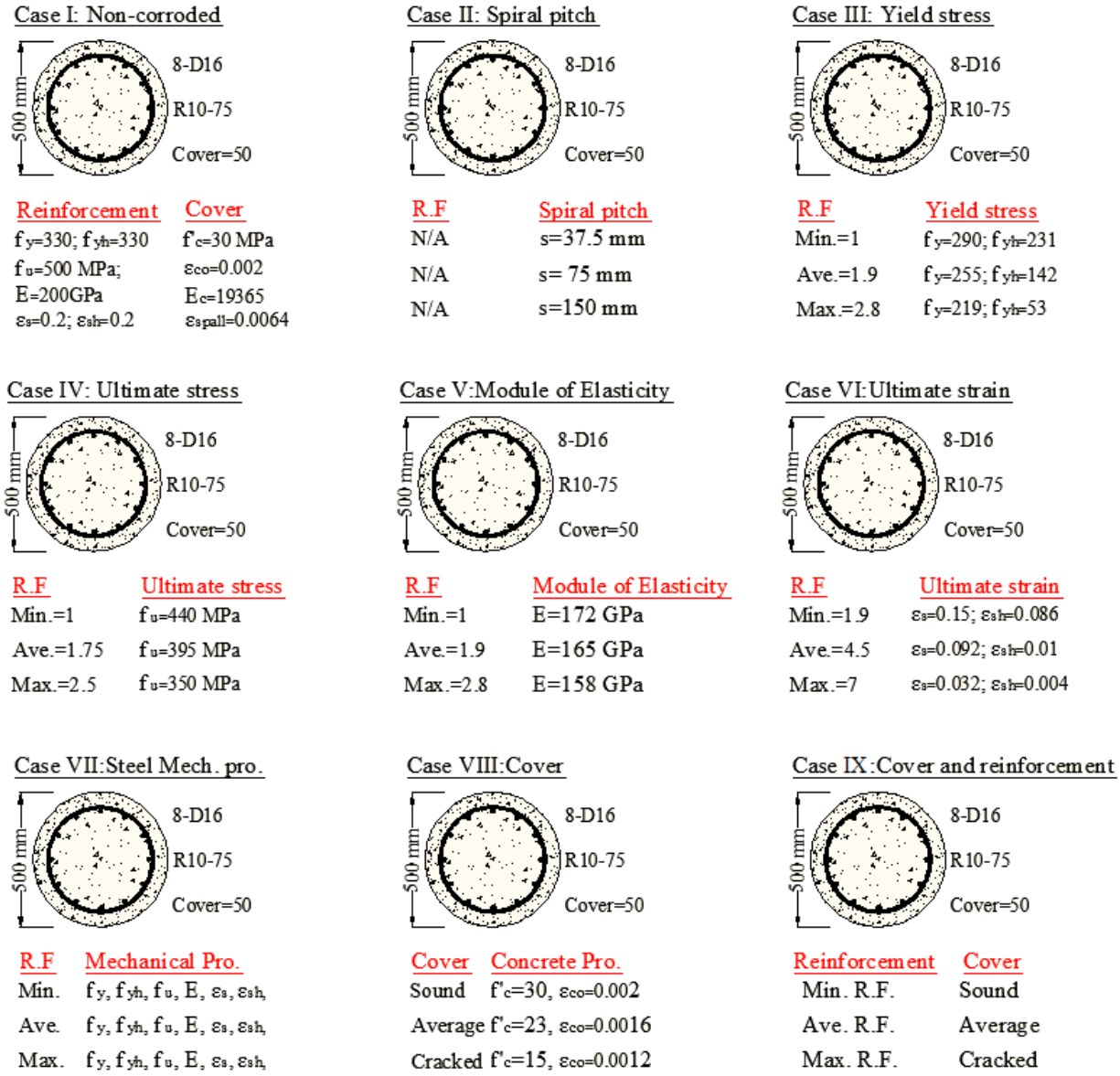

Figure 6-23 Details of case studies included in the section analysis

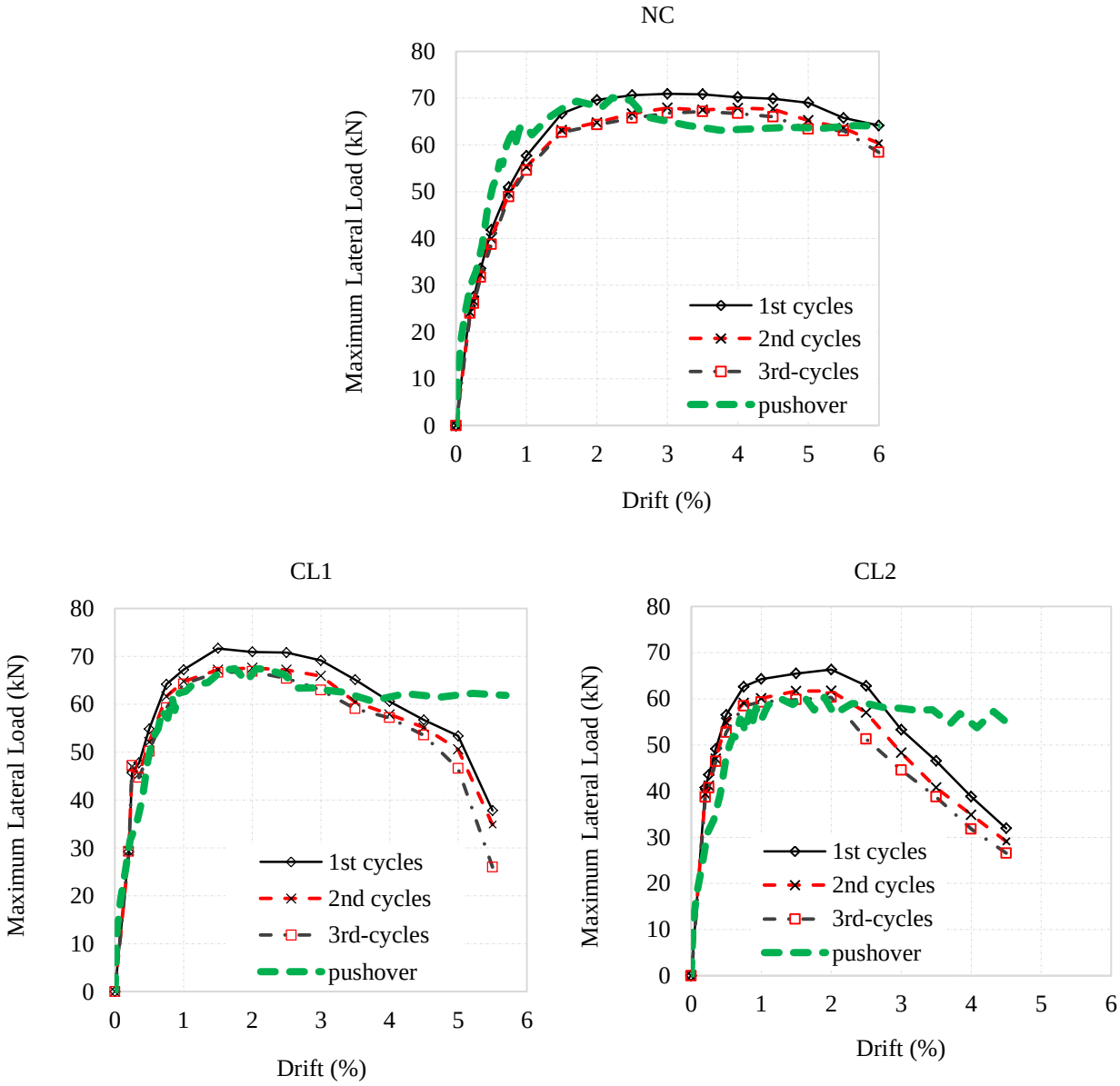

Figure 6-24 Comparing lateral load- drift envelope with pushover

Case I: Noncorroded

Case I is a noncorroded case, and the results are used as reference to compare with corroded cases. Figure 6-23 shows all the mechanical properties of steel reinforcement and concrete cover used in the section analysis. Figure 6-25 shows–moment curvature and bilinear moment–curvature of the noncorroded bridge pier.

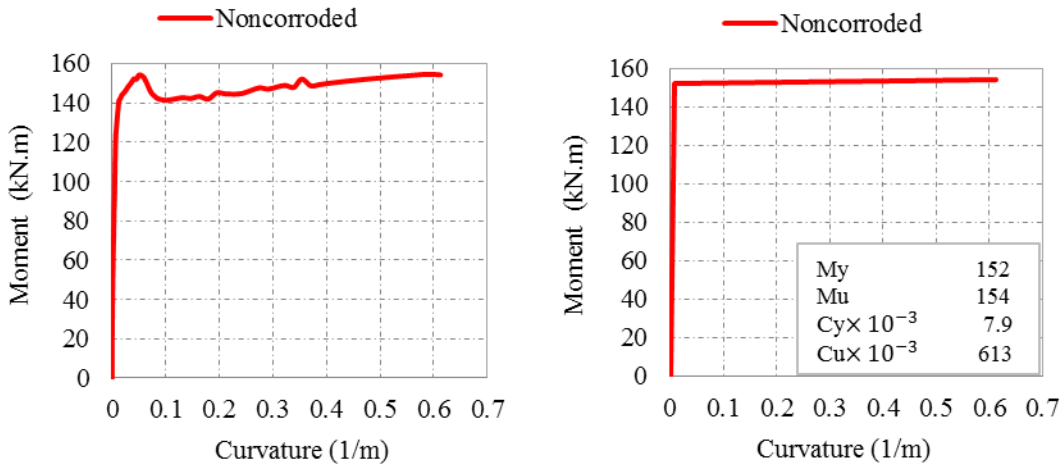

Figure 6-25 Moment–curvature and bilinear moment–curvature of the noncorroded bridge pier

Case II:

To investigate the effects of spiral pitch on structural performance of the RC bridge pier, Case II was studied. In this case, the studied RC bridge pier, using three spiral pitches of 37.5 mm, 75 mm, and 150 mm, was analysed. The mechanical properties of noncorroded steel reinforcement and sound concrete cover were used for this case. The moment–curvature results are shown in Figure 6-26. The results show that the spiral pitch significantly influences ultimate curvature, but it has no important effects on yield moment and yield curvature. The results also show that the spiral pitch influences the ultimate moment, but it doesn't affect the yield moment. Increase of spiral pitch decreases ductility of columns and piers. Transverse reinforcement significantly influences the ductility of columns and bridge piers. Therefore, it can be concluded that confinement is a very important factor affecting the moment–curvature response of RC bridge piers.

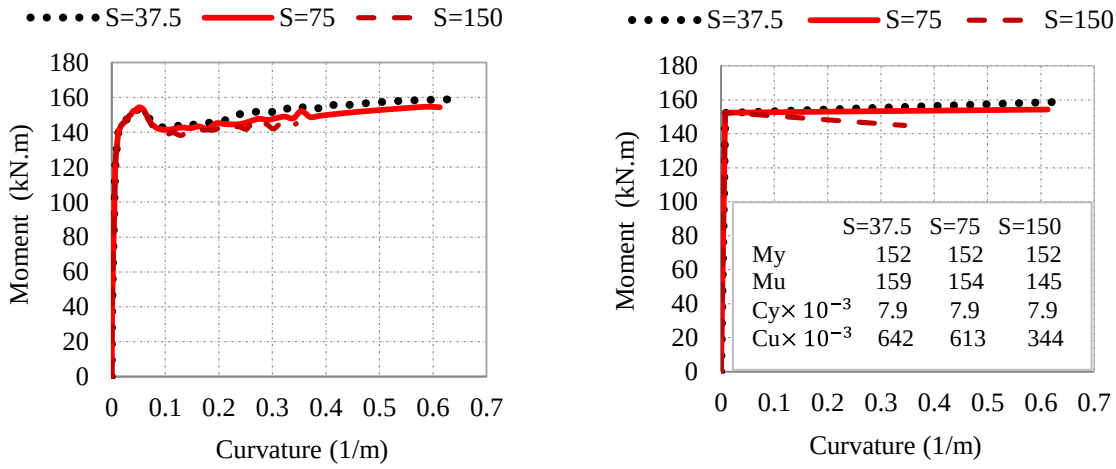

Figure 6-26 The effects of various values of distance between transverse reinforcement (spiral pitch) on moment–curvature and bilinear moment–curvature of the studied bridge pier

Case III: Yield stress

Case III investigated the effects of reduction in the effective yield stress of longitudinal and transversal steel reinforcement due to corrosion on structural performance of the RC bridge pier. To estimate the yield stress of longitudinal and transverse reinforcement, reduction factors (R.F) of 1.0, 1.9 and 2.8 were used for the minimum, average and the maximum reduction by assuming 12% longitudinal and 30% transverse reinforcement corrosion. The effective yield stress of longitudinal and transverse reinforcement used for this section analysis is shown in Figure 6-23, Case III. All yield stresses in Figure 6-23 measured in MPa. The moment–curvature and bilinear moment–curvature results are shown in Figure 6-27. The results show that the effective yield stress significantly influences the yield and ultimate moment and curvature. Reduction in the effective yield stress badly affect yield and ultimate strain of both longitudinal and confining reinforcement. The results confirm that effective yield stress is an important factor affecting the moment–curvature response of RC columns and bridge piers. Therefore, accurately predicting the effective yield stress of corroded reinforcement is very important.

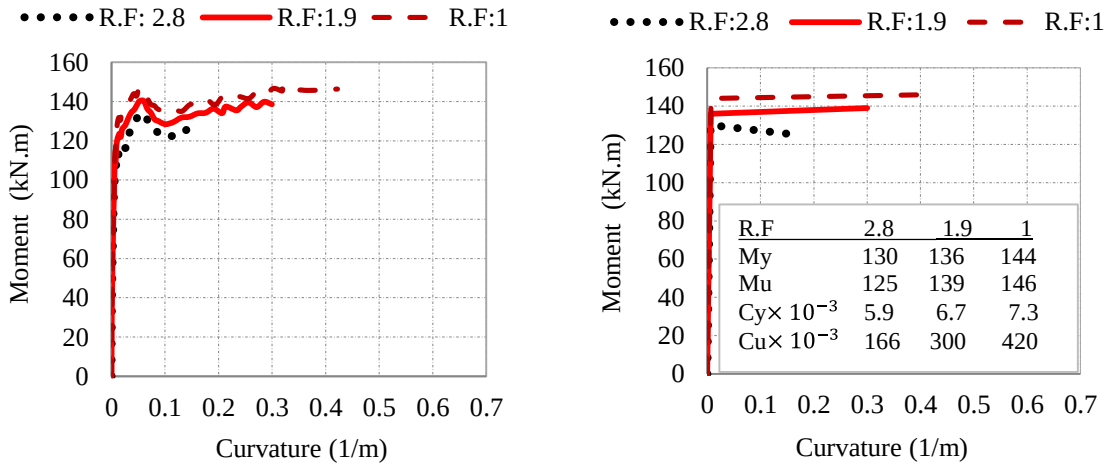

Figure 6-27 The effects of various values of effective yield stress on moment–curvature and bilinear moment–curvature of the studied bridge pier

Case IV: Ultimate stress

In Case IV, the effects of reduction in the effective ultimate stress of longitudinal steel reinforcement due to corrosion on structural performance of the RC bridge pier were investigated. To estimate the ultimate stress of longitudinal reinforcement, reduction factors (R.F) of 1.0, 1.8 and 2.5 were used for the minimum, average and the maximum reduction by assuming 12% longitudinal reinforcement corrosion. The effective ultimate stress of longitudinal and transverse reinforcement used in this section analysis was shown in Figure 6-23, Case IV. The moment–curvature and bilinear moment–curvature results for case IV are shown in

Figure 6-28. The results show that the effective ultimate stress significantly influences the ultimate moment, but it has no important effects on ultimate curvature. Reduction in the ultimate stress directly decreases strength of piers, but it has no effect on ductility. The results also show that various values of the ultimate stress have no important effects on yield moment and yield curvature.

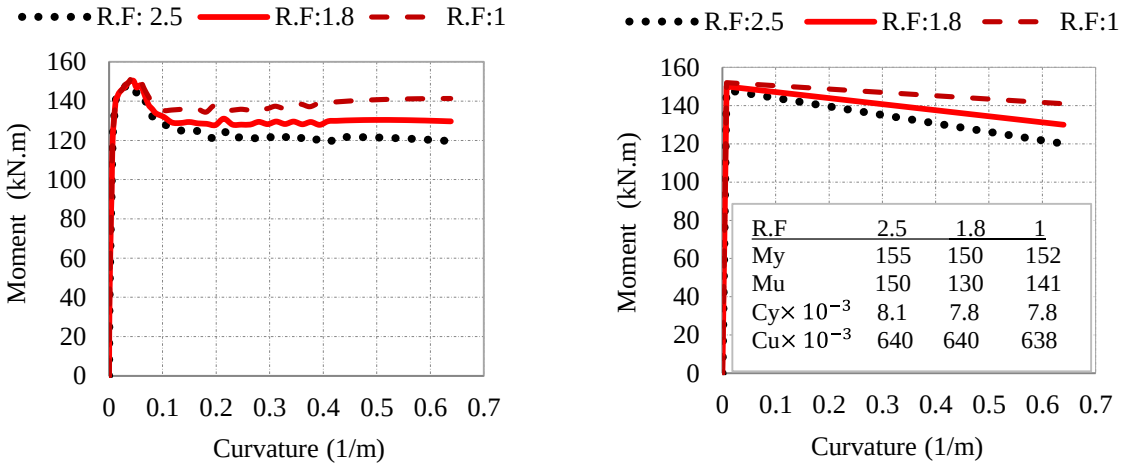

Figure 6-28 The effects of various values of effective ultimate stress on moment–curvature and bilinear moment–curvature of the studied bridge pier

Case V: Modulus of Elasticity

The case V was studied to investigate the effects of reduction in the effective modulus of elasticity of longitudinal steel reinforcement due to corrosion on structural performance of the RC bridge pier. To estimate the modulus of elasticity of longitudinal steel reinforcement, reduction factors (R.F) of 1.15, 1.45 and 1.76 were used for the minimum, average and the maximum reduction by assuming 12% reinforcement corrosion. The effective modulus of elasticity of longitudinal reinforcement used in the section analysis was shown in Figure 6-23, Case V. The moment–curvature and bilinear moment–curvature results for Case V are shown in Figure 6-29. The results clearly show that the various values of effective modulus of elasticity of steel reinforcement have no visible effects on moment and curvature response of RC bridge piers. Comparing the–moment-curvature graphs of the noncorroded bridge pier in Case I (Figure 6-25) with those for Case V show that reduction in the effective modulus of elasticity has no effect on the moment–curvature response of RC columns and bridge piers. Modulus of elasticity has no important impact on ductility or strength of bridge piers.

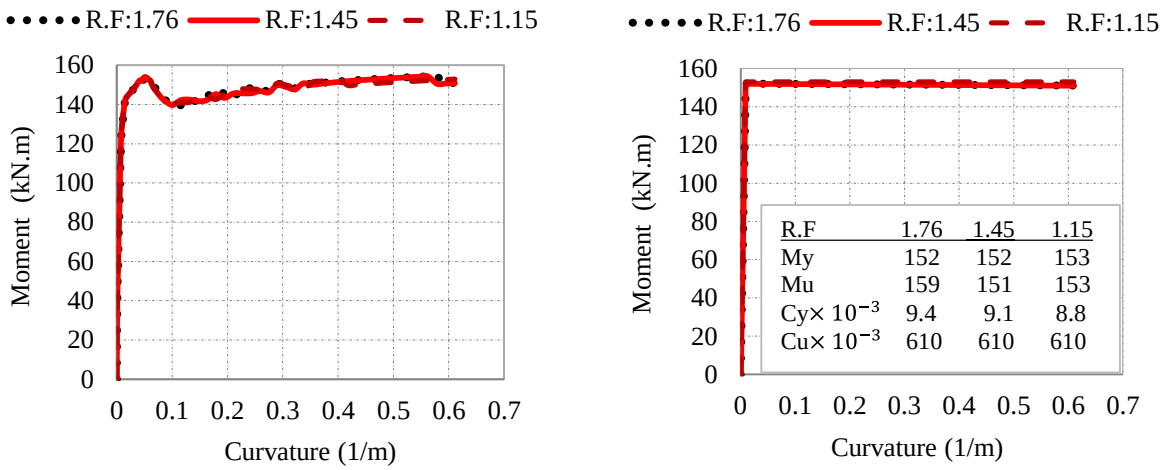

Figure 6-29 The effects of various values of effective modulus of elasticity on moment–curvature and bilinear moment–curvature of the studied bridge pier

Case VI: The ultimate strain

The case VI was undertaken to establish the effects of reduction in the effective ultimate strain (elongation) of longitudinal and transverse steel reinforcement due to corrosion on structural performance of the RC bridge pier. To estimate the effective elongation of longitudinal and transverse reinforcement, reduction factors (R.F) of 1.9, 4.5 and 7.0 were used for the minimum, average and the maximum reduction by assuming 12% longitudinal and 30% transverse reinforcement corrosion. The effective elongation of longitudinal and transverse reinforcement used in the section analysis is shown in Figure 6-23, Case VI. The moment–curvature and bi-linear moment–curvature results are shown in Figure 6-30. The results show that effective elongation significantly influences ultimate curvature, but its effects on the yield curvature can be neglected. Hence, various values of elongation have critical effects on curvature ductility. Reduction in the ultimate strain of steel reinforcement significantly decreases the ultimate curvature of bridge piers. The curvature ductility is the ratio of the ultimate curvature to the yield curvature. Therefore, accurately predicting effective elongation of corroded reinforcement is very important.

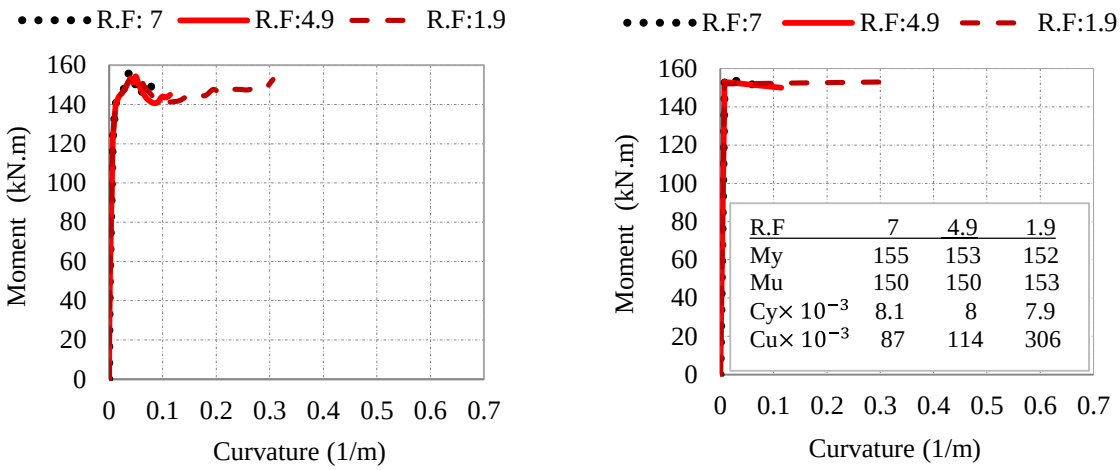

Figure 6-30 The effects of various values of effective ultimate strain on moment–curvature and bilinear moment–curvature of the studied bridge pier

Case VII: Mechanical properties of steel reinforcement

In case VII the effects of reduction in the effective mechanical properties of longitudinal and transverse steel reinforcement, including yield and ultimate stress, modulus of elasticity and ultimate strain due to corrosion on structural performance of the RC bridge pier were studied. In fact, the studies for Case VII were carried out by combining the Cases III, IV, V and VI; to estimate the effective mechanical properties of longitudinal and transverse reinforcement, the minimum, average and maximum reduction factors discussed in Cases III to VI were used in this study. For example, for the minimum reduction in the effective mechanical properties of steel reinforcement, the reduction factors of 1, 1, 1.15 and 1.9 were used for estimating effective yield stress, ultimate stress, modulus of elasticity and elongation respectively, by assuming 12% longitudinal and 30% transverse reinforcement corrosion. The moment–curvature and bilinear moment–curvature results for Case VII are shown in Figure 6-31. The results show that the effective mechanical properties of steel reinforcement significantly influence curvature ductility, yield, and ultimate moment and curvature. The results confirm that when a reduction in all the effective mechanical properties of steel reinforcement are estimated and used for section analysis, the reduction in the moment–curvature response of the bridge pier is much greater than that for a single effective mechanical property such as yield stress. The main reason is that moment-curvature response is significantly dependent the effective mechanical properties of transverse and longitudinal reinforcement. Estimating the reduction in all effective mechanical properties of steel reinforcement due to corrosion is more realistic, rather than considering a single mechanical property of steel reinforcement.

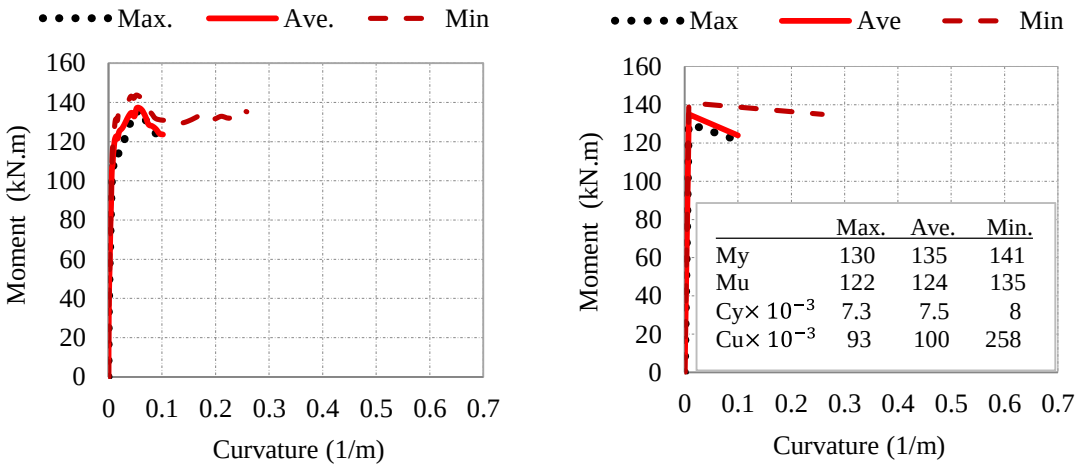

Figure 6-31 The effects of various values of the effective mechanical properties of steel reinforcement on moment–curvature and bilinear moment–curvature of the studied bridge pier

Case VIII: Concrete cover

To investigate the effects of reduction in the mechanical properties of unconfined concrete cover due to corrosion on structural performance of the RC bridge pier, Case VIII was undertaken. The mechanical properties studied included compression strength and maximum strain of unconfined concrete. The modulus of elasticity of unconfined concrete depends on compression strength, therefore it will be updated when the compression strength of concrete changes. The mechanical properties of sound cover were experimentally obtained in Chapter 4, and those for average and cracked cover were predicted using the deterioration models presented in Chapter 4. Figure 6-32 shows the moment–curvature and bilinear moment–curvature graphs for Case VIII. The details of the mechanical properties of the concrete cover and the average corrosion percentage of longitudinal and transverse steel reinforcement are presented in Table 4.4. The results show that the effects of corrosion-induced cracks in concrete cover significantly affect the yield moment and the ultimate curvature, but its effect on the ultimate moment can be neglected. Therefore, cracked concrete cover, caused by corrosion, critically affects the curvature ductility. It is obvious that neglecting the effects of cracked cover due to corrosion on the structural response of RC columns and bridge piers is not safe.

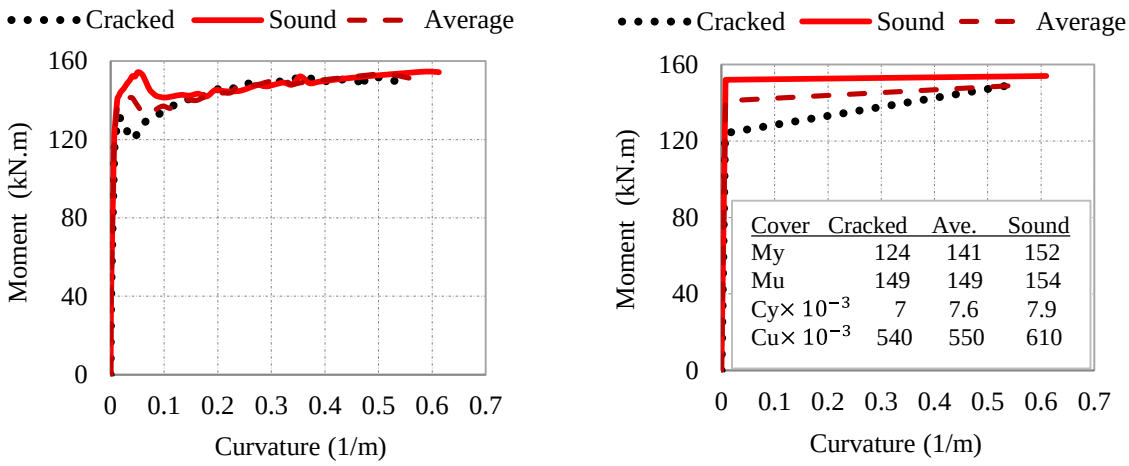

Figure 6-32 The effects of various values of the mechanical properties of concrete cover on moment–curvature and bilinear moment–curvature of the studied bridge pier

Case IX: Mechanical properties of reinforcement and concrete cover

The most realistic case when studying the effects of corrosion on the structural performance of the RC bridge pier is Case IX. This considers all the effects of corrosion on the effective mechanical properties of steel reinforcement and the mechanical properties of unconfined concrete. The procedure for selecting the reduction factors was similar to those used for previous cases. Hence, for example, the maximum reported reduction factors for the effective mechanical properties of steel reinforcement and the mechanical properties of cracked concrete cover were used to predict the maximum reduction in the moment–curvature graph of the bridge pier studied. The moment–curvature and bilinear moment–curvature for Case IX are shown in Figure 6-33. The results show that corrosion critically decreases all key parameters in the moment-curvature response of the bridge pier. The key parameters in the moment–curvature graphs are yield, and ultimate moment and curvature. Comparing the graphs presented in Figure 6-33 with those presented in Figure 6-32 (Case VIII) and Figure 6-31 (Case VII) confirms that the reduction in structural response for Case IX is greater than those obtained for Cases VII and VIII.

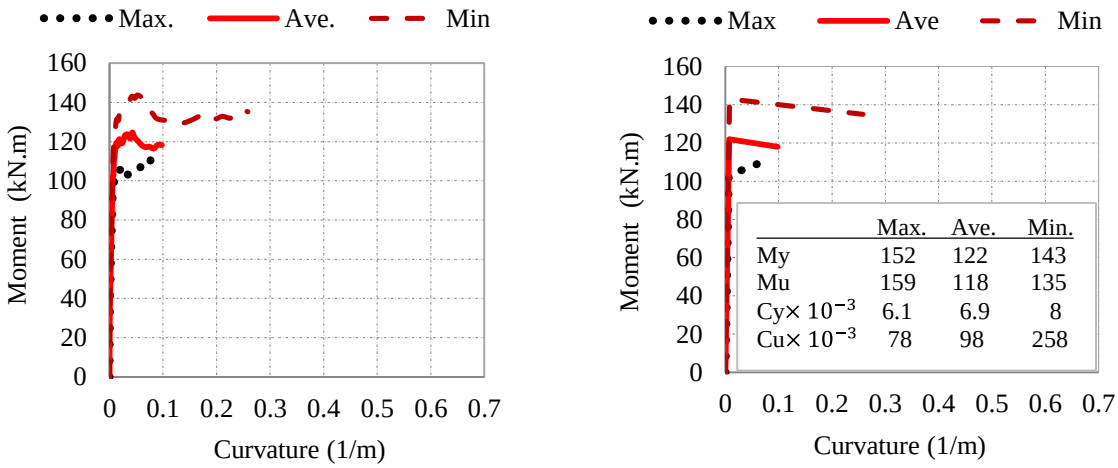

Figure 6-33 The effects of various values of the mechanical properties of concrete cover and the effective mechanical properties of steel reinforcement on moment–curvature and bilinear moment–curvature of the studied bridge pier

6.6 LIMITATIONS

For each corrosion level and confinement arrangement only one large scale test was performed. Considering uncertainties in corrosion and concrete materials, increasing number of tests may improve quasi-static cyclic behaviour of corroded RC concrete.

6.7 CONCLUSIONS

In this chapter, the quasi-static cyclic responses of three large (half scale) ECIP bridge piers, including a noncorroded and two corroded piers, were experimentally studied. Pushover analysis was also used to study the effects of important parameters on the moment–curvature response of corroded bridge piers. The main findings and conclusions can be summarised as follows:

- ❖ Corrosion monitoring
  - According to the experimental results of this research, the average corrosion of transverse reinforcement is 2.5 times greater than the average corrosion of longitudinal reinforcement. This need to be considered in numerical simulations of corroded RC structures.
  - Corrosion causes propagation of longitudinal cracks into the concrete cover. The number of visible individual cracks and maximum width of cracks increase with rising degrees of corrosion.

❖ Quasi-static cyclic test

- Force–drift, force–drift envelope, strain along the north and the south faces of the piers, moment–curvature, and length of cover spalling were measured for all test units. The results clearly show that corrosion causes reductions in all the parameters above.
- Up to 6% drift with no reinforcement fracture was observed for the NC test unit. The first reinforcement fracture was observed at 5% and 4% drift for the CL1 and CL2 test units respectively.
- While a relatively low degree of corrosion (CL1) causes a reduction in the maximum lateral load, a higher degree of corrosion (CL2) causes more reduction in both the maximum lateral load and stiffness. Unlike the NC test unit, a significant reduction in the maximum lateral load for drift after 2% was observed in the CL1 and CL2 test units.
- Cover spalling lengths of 100 mm, 300 mm, and 500 mm were measured for NC, CL1 and CL2 respectively. The results indicate that the length of cover spalling has a direct relationship with the degree of corrosion.
- While for all test units cyclic degradation was observed (the maximum lateral loads for second and third cycles were less than for the first cycle), more reduction was observed for corroded test units.
- Based on the experimental results in this study, a model was proposed to predict the ultimate lateral load of the piers with various degrees of corrosion. The model has good agreement with a model suggested by a past study.

❖ Parametric analysis

- Pushover analysis of the piers were carried out to study the effects of corrosion on key parameters affecting the moment–curvature response of the bridge piers,. The studied parameters included the effective mechanical properties of steel reinforcement (yield and ultimate stress, modulus of elasticity, and ultimate strain); confining reinforcement; unconfined compression strength and ultimate strain of cover concrete. The maximum, minimum and average corrosion-induced reduction factors published by past studies for each key parameter were used for the pushover analysis. The mechanical properties of noncorroded concrete and the values which were developed in this research (presented in Chapter 4) were used as the maximum and minimum amounts respectively for the mechanical properties of cover concrete.

- The results show that different effective values of modulus of elasticity of steel reinforcement has no effect on the moment–curvature response of the piers. The mechanical properties of cover concrete significantly affect the yield moment and ultimate curvature, indicating the importance of modeling the corrosion-induced reduction in mechanical properties of cover concrete in numerical simulations of RC structures subjected to the corrosion. The various values of effective yield stress and ultimate strain have quite significant effects on the moment–curvature response of the piers. The value of effective ultimate stress for reinforcement only affects the ultimate curvature of the piers. The spiral pitch of the confining reinforcement significantly affects the ultimate curvature.

7 CONCLUSIONS AND RECOMMENDATION FOR FURTHER RESEARCH

Among the different causes of degradation for reinforced concrete structures, such as alkali silica reaction, freezing-thawing or acid attack, it is widely accepted that reinforcement corrosion is by far the most common deterioration mechanism. Chloride-induced reinforcement corrosion in particular can cause highly localised (pitting) corrosion. Although seismic resistance of CIP and ECIP bridges is provided by design-in-ductility for the piers, reinforcement corrosion badly affects both the strength and ductility of reinforced concrete bridges. There are a large number of studies on chloride-induced reinforcement corrosion, often aimed at investigation of the corrosion mechanism and its prevention, or the effective mechanical properties of bare steel reinforcement rather than the effects of corrosion on reinforcement embedded in concrete or concrete materials. There is also very limited detail in relation to the effects of pitting corrosion on the behaviour and effective mechanical properties of steel reinforcement. These aspects have been addressed in this research project. In addition, the effects of corrosion on confining reinforcement, the stress–strain response of confined concrete subject to reinforcement corrosion, and the large-scale seismic performance of bridge piers have been experimentally investigated.

It should be noted that the general results of this research can be used for carbonation corrosion, but the details such as corrosion-induced reduction factors depends on morphology of corroded surface, so using reduction factors of this research for carbonation corrosion probably will decrease accuracy of corrosion-induced modelling. Pitting corrosion is mainly observed in chloride-induced corrosion, whereas carbonation corrosion causes general corrosion. Pitting corrosion increases corrosion-induced reduction factors.

7.1 SUMMARY OF THE RESEARCH GAPS FOUND IN THIS RESEARCH

The research gaps addressed in this research have been marked as "*".

i. The main identified research gaps in chloride-induced corrosion can be summarised as follows:

   - More accurate models to predict corrosion rate, initiation time and important factors

affecting these parameters

- Accurate value and main factors affecting critical content of chloride for RC structures
- The properties of corrosion by-product for real RC structures.
- Investigation of pitting factor for real RC structures.*

ii. The main highlighted research gaps in the corrosion-induced deterioration model are as follows:

- Robust deterioration model to predict bond between steel and concrete in corroded RC structures
- Robust deterioration model for corroded steel reinforcement considering cyclic behaviour of steel reinforcement in seismic events
- Corrosion-induced deterioration model for corroded steel reinforcement while embedded in concrete*
- Corrosion-induced deterioration model for concrete materials*
- Corrosion-induced stress–strain response of confined concrete.*

iii. The main research gaps discovered in the evaluation of the seismic performance of corroded reinforced concrete bridge piers can be summarised as follows:

- Robust numerical modelling of corroded bridge piers
- Experimental tests on efficiency of repair methods used for corroded bridge piers
- Large scale experimental tests on seismic behaviour of corroded bridge piers and bridge structures (half-scale and full-scale tests).*

7.2 KEY CONTRIBUTIONS AND MAIN FINDINGS

7.2.1 PITTING CORROSION

Chapter 3 illustrated how pitting corrosion affects tensile behaviour and the effective mechanical properties of steel reinforcement. An analytical model was developed to study the effects of pit cavities on cross-section parameters and the tensile behaviour of pitting-corroded steel bars. The model was validated using experimental results. An analytical time-dependent pit-depth model for localised corrosion based on time-dependent corrosion rates was developed, which can provide a link between the values of pit depth and the lifetime analysis of corroded RC

structures. Deterioration models in terms of reduction in the effective mechanical properties for steel reinforcement due to pitting corrosion were developed based on experimental tensile tests on corroded and noncorroded samples. The main contribution of Chapter 3 can be summarised as follows:

- Pitting corrosion not only alters the overall effective mechanical properties of steel reinforcement but also causes specific changes to the pit back compared to the pit face side.
- To model corrosion-induced degradation in the effective mechanical properties of steel reinforcement, nonlinear regression should be applied for pitting corrosion.
- The analytical modelling reveals that pit cavities had significant impact on the cross-section parameters affecting the tensile behaviour of pitting-corroded steel bars.
- Time-dependent pit depth can provide a link between the amount of pitting corrosion and the lifetime seismic or structural response of corroded RC structures.

7.2.2 EXPERIMENTAL EVALUATION OF CORRODED STEEL REINFORCEMENT

To compare the mass loss configuration of corroded bare steel bars and that of corroded bars while embedded in concrete, an experimental programme was planned (see Chapter 4). The experimental programme consists of two inspection approaches: (a) visual inspection, and (b) 3D scanning.

(a) Visual inspection

The visual inspection was carried out for a number of corroded bare bars and many corroded bars while embedded in concrete retrieved from 14 corroded RC columns. The main findings are as follows:

- Unequal mass loss configuration was observed either side of corroded steel reinforcement retrieved from RC columns.
- While almost identical mass loss was distributed on the circumference of corroded bare reinforcement, for corroded steel reinforcement of RC columns, more mass loss was observed on the side that was closer to the column cover (outer side).
- The maximum pit depth, and more pit cavities were observed on the outer side of the steel reinforcement retrieved from corroded RC columns.

- It was observed that corrosion was usually distributed only on the outer side of corroded steel reinforcement of RC columns, with a corrosion percentage less than or equal to 8%.

(b) 3D scanning

To quantify the difference in mass loss between the cover side and the interior side of the steel reinforcement retrieved from corroded RC columns and piers, the 3D scanning approach was used. The main finding can be summarised as follows:

- For corroded samples with 15% average mass loss, 10.9% mass loss occurred on the outer side versus 4.1% on the interior side.

Past studies defined the pitting factor as the ratio of maximum pit depth to average corrosion penetration. The existing pitting factors were developed based on an equal mass loss configuration, so might need to be modified based on the results observed in this research.

7.2.3 CORRODED STEEL REINFORCEMENT WHILE EMBEDDED IN CONCRETE

In Chapter 4 (Section 4-2), in relation to reduction factors for corroded bare bars and embedded bars, conflicting results and opposing conclusions published by past studies were highlighted. A methodology was shown to develop corrosion-induced deterioration in terms of reduction factors in the effective mechanical properties of steel reinforcement embedded in concrete. The initial reduction factors (IRFs) were experimentally obtained for corroded bare steel reinforcement. Based on visual inspection and the results obtained from the 3D scanning approach, an analytical model was developed to address the effects of unequal mass loss configuration on the tensile behaviour of corroded steel reinforcement of RC structures. The analytical model was used to compare the tensile behaviour of corroded bare bars and corroded bars while embedded in concrete and to develop the analytical correction factor (ACF). The ACF was validated by existing experimental results published by past studies. The final reduction factors (FRFs) were estimated by multiplying the appropriate IRF and ACF. The main conclusions are as follows:

- The reduction factors in the effective mechanical properties of steel reinforcement of RC columns are greater than those of bare bars.
- The differences in details of corrosion test set-ups were the main reason for the opposing results published by past studies.
- The majority of the existing reduction factors have been developed based on the experimental results of corroded bare bars. However, using these reduction factors in

numerical simulations of corroded RC structures is not safe, because they are significantly lower than the reduction that happens in real corroded RC columns.

- The ACFs can be used to modify the existing reduction factors obtained from the corroded bare bars.

7.2.4 CRACKED CONCRETE DUE TO REINFORCEMENT CORROSION

The effects of corrosion on the mechanical properties of concrete materials were illustrated in Chapter 4 (Section 4-1). Concrete core samples taken from the core and cover parts of noncorroded and corroded RC columns and samples poured at the time of fabrication of RC columns were prepared for a monotonic compression test. A regression of experimental data and a statistical normal distribution were used to develop reduction in the axial stress and ultimate stain of concrete materials due to reinforcement corrosion. The main findings are as follows:

- Reinforcement corrosion causes the propagation of horizontal and vertical cracks in column cover, and only horizontal cracks in the column core.
- Reinforcement corrosion only degraded the axial stress and ultimate strain of the column's concrete cover.
- The experimentally developed corrosion-induced deterioration model for concrete materials obviously affected the moment-curvature response of the corroded RC column. Hence, ignoring the deterioration model in numerical simulations leads to overestimation of the residual capacity of corroded RC column, which is not safe.

7.2.5 STRESS–STRAIN RELATIONSHIP OF CONFINED CONCRETE SUBJECTED TO REINFORCEMENT CORROSION

In Chapter 5, the effects of corrosion on the stress–strain response of confined concrete due to reinforcement corrosion were experimentally investigated. The analytical formulas were developed based on Mander's model and the deterioration models developed in this research to predict the stress–strain response of confined concrete affected by reinforcement corrosion. The developed deterioration models were presented in Chapters 3 and 4. The key contributions are as follows:

- The analytical model can predict the stress–strain response of confined concrete subjected to reinforcement corrosion.

- Corrosion of transverse reinforcement significantly degrades the strength, the strain at strength, and the ultimate strain of confined concrete.
- The degree of corrosion significantly affects the slope of the falling branch of the stress–strain curves.

7.2.6 RESPONSE OF CORRODED BRIDGE PIERS

In Chapter 6, the quasi-static cyclic response of noncorroded and corroded large-scale bridge piers were experimentally investigated. Longitudinal and transverse reinforcing bars retrieved from the corroded piers were visually inspected and their corrosion percentage was estimated based on a mass loss approach. The developed deterioration models and the model developed for the stress–strain response of confined concrete were used to numerically predict the moment-curvature and force-displacement responses of the bridge piers subjected to reinforcement corrosion. The main conclusions can be summarised as follows:

- The average corrosion of transverse reinforcement is about 2.5 times greater than the average corrosion of longitudinal reinforcement.
- Corrosion badly affects the cyclic response (including dissipated energy and curvature ductility) of ECIP bridge piers.
- Corrosion increases the length of cover spalling of ECIP bridge piers.
- Among the studied parameters, the ultimate stress and strain of concrete cover, the yield stress, and the effective ultimate strain of steel reinforcement significantly affect the moment-curvature response of corroded bridge piers. The effective ultimate stress of steel reinforcement and the spiral pitch of confining reinforcement only affect the ultimate curvature of corroded bridge piers.

7.3 RECOMMENDATIONS FOR FUTURE WORK

Chapter 3 presented the influence of pitting corrosion on the effective mechanical properties of bare corroded steel reinforcement. An analytical model was developed to predict the tensile behaviour of corroded bars, neglecting the effects of the bond between steel and concrete, or the deformation of corroded samples. Once the corrosion of steel reaches a critical point, de-bonding will occur. The response of a portion of severely corroded reinforcing steel in concrete subject to tensile forces is likely therefore to be similar to that of bare bars. However, the effects of the bond between steel and concrete on the tensile behaviour of steel reinforcement for lower

degrees of corrosion need to be studied. In this research, three pits with the same pit depth on each sample were artificially induced by machining hemispherical cavities. There is a need to investigate the effects of irregular pit shapes and the random distribution of pit cavities in corroded samples on the tensile behaviour and corrosion-induced reduction in the effective mechanical properties of steel reinforcement.

In Chapter 4 (Section 4-1) the effects of corrosion on the mechanical properties of concrete materials was experimentally investigated. During the experimental tests, only axial strains of samples were recorded. More experimental tests are recommended on samples with larger diameter and with recording of both axial and transverse strain. The effects of reinforcement corrosion on shear strength of concrete materials need to be investigated.

The effects of corrosion on corroded bare and embedded steel reinforcement were investigated in Chapter 4 (Section 4-2). The simplified analytical model to predict behaviour of corroded steel bar while embedded in concrete can be improved by considering more real corrosion configurations, the real distribution of pit damage, and the bond between steel and concrete for relatively low degrees of corrosion. In this regard, experimental tensile tests on steel reinforcement retrieved from corroded reinforced concrete columns is recommended for future studies.

Chapter 5 studied the effects of reinforcement corrosion on the stress–strain response of confined concrete of circular columns. The developed analytical model needs to be validated for rectangular columns and RC walls. More experimental tests to study the effects of pitting corrosion on the stress–strain response of confined concrete could be very useful.

Chapter 6 investigated the effects of corrosion on the cyclic response of reinforced concrete bridge piers. While the results can be used to validate the numerical simulation and are vital for better understanding the seismic response of corroded bridge piers, more large-scale experimental tests with different parameters – such as axial load ratio and pier type – will be very helpful for future research. Developments of advanced numerical simulations to predict the seismic response of corroded bridges need to be critically investigated.

Moreover, the following identified research gaps require future studies:

- Importnat corrosion parameters

  Important corrosion parameters such as corrosion initiation time, critical chloride content, potential of pitting corrosion, and parameters affecting pitting corrosion need to be studied. These parameters significantly affect service life and prediction of structural capacity. In this

regards, there are many uncertainties, and usually there is no general agreement in literature.

- Corrosion method

Some aspects of corrosion methods need to be studied. For example comparing the structural behaviour of accelerated and open air (environment) corroded RC members or physical and mechanical properties of corrosion by-product from different corrosion methods need to be investigated. The characteristics of accelerated corrosion methods need to be compared with that of open air corrosion.

- Seismic impact

Effects of corrosion on the cyclic behaviour of corroded steel bars while embedded in concrete are an important study area. High-speed experimental cycling testing or shake-table tests on corroded RC structures to investigate the impact of earthquake induced dynamic loading are critically need to be investigated

- Numerical modelling of corroded RC structures

There are few numerical simulations presented by past studies, but usually some important effects are not modelled or very simplified models were considered. The existing numerical simulations also need to be regularly updated using advanced recently developed deterioration models.

REFERENCES:

ABOUTAHA, R. S., JNAID, F., SOTOUD, S. & TAPAN, M. 2013. Seismic Evaluation and Retrofit of Deteriorated Concrete Bridge Components.

AKIYAMA, M. & FRANGOPOL, D. M. 2013. Long-term seismic performance of RC structures in an aggressive environment: emphasis on bridge piers. *Structure and Infrastructure Engineering*, 1-15.

AKIYAMA, M. & FRANGOPOL, D. M. 2014. Long-term seismic performance of RC structures in an aggressive environment: emphasis on bridge piers. *Structure and Infrastructure Engineering,* 10**,** 865-879.

AKIYAMA, M., FRANGOPOL, D. M. & MATSUZAKI, H. 2011. Life-cycle reliability of RC bridge piers under seismic and airborne chloride hazards. *Earthquake Engineering & Structural Dynamics,* 40**,** 1671-1687.

AL-SULAIMANI, G., KALEEMULLAH, M. & BASUNBUL, I. 1990. Influence of corrosion and cracking on bond behavior and strength of reinforced concrete members. *ACI Structural Journal,* 87.

ALIPOUR, A., SHAFEI, B. & SHINOZUKA, M. 2010. Performance evaluation of deteriorating highway bridges located in high seismic areas. *Journal of Bridge Engineering,* 16**,** 597-611.

ALLAM, I. M., MASLEHUDDIN, M., SARICIMEN, H. & AL-MANA, A. I. 1994. Influence of atmospheric corrosion on the mechanical properties of reinforcing steel. *Construction and Building Materials,* 8**,** 35-41.

ALMUSALLAM, A., AL GAHTANI, A., GAHTANI, A., MM, K. & AR, A. 1997. Evaluation of repair materials for functional improvement of slabs and beams with corroded reinforcement. *Proceedings of the ICE-Structures and Buildings,* 122**,** 27-34.

ALMUSALLAM, A. A. 2001. Effect of degree of corrosion on the properties of reinforcing steel bars. *Construction and Building Materials,* 15**,** 361-368.

ALMUSALLAM, A. A., AL-GAHTANI, A. S. & AZIZ, A. R. 1996. Effect of reinforcement corrosion on bond strength. *Construction and building materials,* 10**,** 123-129.

ALONSO, C., ANDRADE, C., CASTELLOTE, M. & CASTRO, P. 2000. Chloride threshold values to depassivate reinforcing bars embedded in a standardized OPC mortar. *Cement and Concrete research,* 30**,** 1047-1055.

ALONSO, C., ANDRADE, C. & GONZÁLEZ, J. 1988. Relation between resistivity and corrosion rate of reinforcements in carbonated mortar made with several cement types. *Cement and concrete research,* 18**,** 687-698.

ALONSO, C., ANDRADE, C., NÓVOA, X., IZQUIERDO, M. & PÉREZ, M. 1998a. Effect of protective oxide scales in the macrogalvanic behaviour of concrete reinforcements. *Corrosion science,* 40**,** 1379-1389.

ALONSO, C., ANDRADE, C., RODRIGUEZ, J. & DIEZ, J. 1998b. Factors controlling cracking of concrete affected by reinforcement corrosion. *Materials and Structures,* 31**,** 435-441.

ALONSO, C., ANDRADE, C., RODRIGUEZ, J. & DIEZ, J. M. 1998c. Factors controlling cracking of concrete affected by reinforcement corrosion. *Materials and structures,* 31**,** 435-441.

AMLEH, L. & MIRZA, S. 1999. Corrosion influence on bond between steel and concrete. *ACI Structural Journal,* 96.

ANDISHEH, K., SCOTT, A. & PALERMO, A. 2016a. Modeling the influence of pitting corrosion on the mechanical properties of steel reinforcement. *Materials and Corrosion,* 67**,** 1220-1234.

ANDISHEH, K., SCOTT, A. & PALERMO, A. 2016b. Seismic Behavior of Corroded RC Bridges: Review and Research Gaps. *International Journal of Corrosion,* 2016.

ANDRADE, C., ALONSO, C., GARCIA, D. & RODRIGUEZ, J. 1991. Remaining lifetime of reinforced concrete structures: Effect of corrosion on the mechanical properties of the steel.

ANDRADE, C., ALONSO, C. & MOLINA, F. 1993. Cover cracking as a function of bar corrosion: Part I-Experimental test. *Materials and structures,* 26**,** 453-464.

ANDRADE, C., MARIBONA, I., FELIU, S., GONZÁLEZ, J. & FELIU JR, S. 1992. The effect of macrocells between active and passive areas of steel reinforcements. *Corrosion science,* 33**,** 237-249.

ANDRADE, C., MUÑOZ, A. & TORRES-ACOSTA, A. Relation between crack width and corrosion degree in corroding elements exposed to the natural atmosphere.
ANGST, U., ELSENER, B., LARSEN, C. K. & VENNESLAND, Ø. 2009. Critical chloride content in reinforced concrete—a review. *Cement and Concrete Research,* 39**,** 1122-1138.
ANGST, U., ELSENER, B., LARSEN, C. K. & VENNESLAND, Ø. 2011a. Chloride induced reinforcement corrosion: Rate limiting step of early pitting corrosion. *Electrochimica Acta,* 56**,** 5877-5889.
ANGST, U., RØNNQUIST, A., ELSENER, B., LARSEN, C. K. & VENNESLAND, Ø. 2011b. Probabilistic considerations on the effect of specimen size on the critical chloride content in reinforced concrete. *Corrosion Science,* 53**,** 177-187.
ANN, K. Y. & SONG, H.-W. 2007. Chloride threshold level for corrosion of steel in concrete. *Corrosion Science,* 49**,** 4113-4133.
APOSTOLOPOULOS, C. & PAPADOPOULOS, M. 2007. Tensile and low cycle fatigue behavior of corroded reinforcing steel bars S400. *Construction and Building Materials,* 21**,** 855-864.
APOSTOLOPOULOS, C. A. & PASIALIS, V. 2010. Effects of Corrosion and Ribs on Low Cycle Fatigue Behavior of Reinforcing Steel Bars S400. *Journal of Materials Engineering and Performance,* 19**,** 385-394.
ASTM, C. 1019,"Standard Method of Sampling and Testing Grout". *Annual Book of ASTM Standards,* 4.
AUYEUNG, Y., BALAGURU, P. & CHUNG, L. 2000. Bond behavior of corroded reinforcement bars. *ACI Materials Journal,* 97.
BAIYASI, I. & HARICHANDRAN, R. Corrosion and wrap strains in concrete bridge columns repaired with FRP wraps. Proceedings (CD-ROM), 80th Annual Meeting of the Transportation Research Board, 2001.
BALABANIC, G., BICANIC, N. & DUREKOVIC, A. 1996. Mathematical modeling of electrochemical steel corrosion in concrete. *Journal of engineering mechanics,* 122**,** 1113-1122.
BALABANIĆ, G., BIĆANIĆ, N. & ĐUREKOVIĆ, A. 1996. The influence of w/c ratio, concrete cover thickness and degree of water saturation on the corrosion rate of reinforcing steel in concrete. *Cement and concrete Research,* 26**,** 761-769.
BASHEER, P., CHIDIACT, S. & LONG, A. 1996. Predictive models for deterioration of concrete structures. *Construction and Building Materials,* 10**,** 27-37.
BAYRAK, O. & SHEIKH, S. A. 2001. Plastic hinge analysis. *Journal of Structural Engineering,* 127**,** 1092-1100.
BAZANT, Z. P. 1979a. Physical model for steel corrosion in concrete sea structures--application. *Journal of the structural division,* 105.
BAZANT, Z. P. 1979b. Physical model for steel corrosion in concrete sea structures—theory. *Journal of the Structural Division,* 105**,** 1137-1153.
BERTO, L., SIMIONI, P. & SAETTA, A. 2008. Numerical modelling of bond behaviour in RC structures affected by reinforcement corrosion. *Engineering Structures,* 30**,** 1375-1385.
BERTOLINI, L., ELSENER, B., PEDEFERRI, P. & POLDER, R. 2004. Corrosion of steel in concrete: prevention diagnosis repair Wiley. VCH, Weinheim.
BERVER, E., FOWLER, D., JIRSA, J., WHEAT, H. & FORD, M. Corrosion in FRP-wrapped concrete members. Proc., Int. Conf. on Structural Faults and Repair, 2001. Engineering Technics London.
BHARGAVA, K., GHOSH, A., MORI, Y. & RAMANUJAM, S. 2005. Modeling of time to corrosion-induced cover cracking in reinforced concrete structures. *Cement and Concrete Research,* 35**,** 2203-2218.
BHARGAVA, K., GHOSH, A., MORI, Y. & RAMANUJAM, S. 2006. Analytical model for time to cover cracking in RC structures due to rebar corrosion. *Nuclear engineering and Design,* 236**,** 1123-1139.
BIONDINI, F., BONTEMPI, F., FRANGOPOL, D. M. & MALERBA, P. G. 2004. Cellular automata approach to durability analysis of concrete structures in aggressive environments. *Journal of Structural Engineering,* 130**,** 1724-1737.
BIONDINI, F., BONTEMPI, F., FRANGOPOL, D. M. & MALERBA, P. G. 2006. Probabilistic service life assessment and maintenance planning of concrete structures. *Journal of structural engineering,* 132**,** 810-825.

BIONDINI, F., CAMNASIO, E. & PALERMO, A. 2013. Lifetime seismic performance of concrete bridges exposed to corrosion. *Structure and Infrastructure Engineering***,** 1-21.
BIONDINI, F., CAMNASIO, E. & PALERMO, A. 2014. Lifetime seismic performance of concrete bridges exposed to corrosion. *Structure and Infrastructure Engineering,* 10**,** 880-900.
BIONDINI, F. & FRANGOPOL, D. M. 2008. Probabilistic limit analysis and lifetime prediction of concrete structures. *Structure and Infrastructure Engineering,* 4**,** 399-412.
BROOMFIELD, J. P. 2002. *Corrosion of steel in concrete: understanding, investigation and repair*, Taylor & Francis.
BURSTEIN, G., PISTORIUS, P. & MATTIN, S. 1993. The nucleation and growth of corrosion pits on stainless steel. *Corrosion Science,* 35**,** 57-62.
CABRERA, J. 1996. Deterioration of concrete due to reinforcement steel corrosion. *Cement and concrete composites,* 18**,** 47-59.
CAIRNS, J., PLIZZARI, G. A., DU, Y., LAW, D. W. & FRANZONI, C. 2005a. Mechanical properties of corrosion-damaged reinforcement. *ACI materials journal,* 102.
CAIRNS, J., PLIZZARI, G. A., YINGANG, D., LAW, D. W. & FRANZONI, C. 2005b. Mechanical properties of corrosion-damaged reinforcement. *ACI Materials Journal,* 102**,** 256-264.
CAPÉ, M. 1999. *Residual service-life assessment of existing R/C structures.* MSc thesis, Chalmers University of Technology, Gothenburg, Sweden, and Milan University of Technology, Milan, Italy.
CAPOZUCCA, R. 1995. Damage to reinforced concrete due to reinforcement corrosion. *Construction and Building Materials,* 9**,** 295-303.
CARÉ, S., NGUYEN, Q. T., L'HOSTIS, V. & BERTHAUD, Y. 2008. Mechanical properties of the rust layer induced by impressed current method in reinforced mortar. *Cement and Concrete Research,* 38**,** 1079-1091.
CASTEL, A., FRANÇOIS, R. & ARLIGUIE, G. 2000. Mechanical behaviour of corroded reinforced concrete beams—Part 1: experimental study of corroded beams. *Materials and Structures,* 33**,** 539-544.
CHOE, D.-E., GARDONI, P. & ROSOWSKY, D. 2010. Fragility increment functions for deteriorating reinforced concrete bridge columns. *Journal of engineering mechanics,* 136**,** 969-978.
CHOE, D.-E., GARDONI, P., ROSOWSKY, D. & HAUKAAS, T. 2008. Probabilistic capacity models and seismic fragility estimates for RC columns subject to corrosion. *Reliability Engineering & System Safety,* 93**,** 383-393.
CHOE, D.-E., GARDONI, P., ROSOWSKY, D. & HAUKAAS, T. 2009. Seismic fragility estimates for reinforced concrete bridges subject to corrosion. *Structural Safety,* 31**,** 275-283.
CHUNG, L., CHO, S.-H., JAY KIM, J.-H. & YI, S.-T. 2004. Correction factor suggestion for ACI development length provisions based on flexural testing of RC slabs with various levels of corroded reinforcing bars. *Engineering structures,* 26**,** 1013-1026.
CHUNG, L., JAY KIM, J.-H. & YI, S.-T. 2008. Bond strength prediction for reinforced concrete members with highly corroded reinforcing bars. *Cement and concrete composites,* 30**,** 603-611.
CORONELLI, D. & GAMBAROVA, P. 2004. Structural assessment of corroded reinforced concrete beams: modeling guidelines. *Journal of structural engineering,* 130**,** 1214-1224.
DAGHER, H. & KULENDRAN, S. 1992. Finite element modeling of corrosion damage in concrete structures. *ACI Structural Journal,* 89.
DE BRITO, J. & BRANCO, F. Whole life costing in road bridges applied to service life prediction. BRIDGE MANAGEMENT 3. INSPECTION, MAINTENANCE AND REPAIR. PAPERS PRESENTED AT THE THIRD INTERNATIONAL CONFERENCE ON BRIDGE MANAGEMENT, UNIVERSITY OF SURREY, GUILDFORD, UK, 14-17 APRIL 1996, 1996.
DEBAIKY, A. S., GREEN, M. F. & HOPE, B. B. 2002. Carbon fiber-reinforced polymer wraps for corrosion control and rehabilitation of reinforced concrete columns. *ACI Materials Journal,* 99.
DEMERS, M. & NEALE, K. 1999. Confinement of reinforced concrete columns with fibre-reinforced composite sheets-an experimental study. *Canadian Journal of Civil Engineering,* 26**,** 226-241.
DIETZ, M. S., DIHORU, L., ODDBJORNSSON, O., BOCIAN, M., KASHANI, M. M., NORMAN, J. A., CREWE, A. J., MACDONALD, J. H. & TAYLOR, C. A. 2012. Earthquake and Large Structures Testing at the Bristol Laboratory for Advanced Dynamics Engineering. *Role of Seismic Testing Facilities in Performance-Based Earthquake Engineering.* Springer.

DU, Y. 2001. *Effect of reinforcement corrosion on structural concrete ductility.* University of Birmingham.
DU, Y., CLARK, L. & CHAN, A. 2005. Residual capacity of corroded reinforcing bars. *Magazine of Concrete Research,* 57**,** 135-147.
EL MAADDAWY, T., CHAHROUR, A. & SOUDKI, K. 2006. Effect of fiber-reinforced polymer wraps on corrosion activity and concrete cracking in chloride-contaminated concrete cylinders. *Journal of Composites for Construction,* 10**,** 139-147.
EL MAADDAWY, T. & SOUDKI, K. 2007. A model for prediction of time from corrosion initiation to corrosion cracking. *Cement and concrete composites,* 29**,** 168-175.
EL MAADDAWY, T. A. & SOUDKI, K. A. 2003. Effectiveness of impressed current technique to simulate corrosion of steel reinforcement in concrete. *Journal of materials in civil engineering,* 15**,** 41-47.
ELSENER, B., ANDRADE, C., GULIKERS, J., POLDER, R. & RAUPACH, M. 2003. Hall-cell potential measurements—Potential mapping on reinforced concrete structures. *Materials and Structures,* 36**,** 461-471.
ENRIGHT, M. P. & FRANGOPOL, D. M. 1998. Service-life prediction of deteriorating concrete bridges. *Journal of Structural engineering,* 124**,** 309-317.
FANG, C., GYLLTOFT, K., LUNDGREN, K. & PLOS, M. 2006a. Effect of corrosion on bond in reinforced concrete under cyclic loading. *Cement and concrete research,* 36**,** 548-555.
FANG, C., LUNDGREN, K., CHEN, L. & ZHU, C. 2004. Corrosion influence on bond in reinforced concrete. *Cement and concrete research,* 34**,** 2159-2167.
FANG, C., LUNDGREN, K., PLOS, M. & GYLLTOFT, K. 2006b. Bond behaviour of corroded reinforcing steel bars in concrete. *Cement and Concrete research,* 36**,** 1931-1938.
FU, X. & CHUNG, D. 1997. Effect of corrosion on the bond between concrete and steel rebar. *Cement and Concrete Research,* 27**,** 1811-1815.
GADVE, S., MUKHERJEE, A. & MALHOTRA, S. 2009. Corrosion of steel reinforcements embedded in FRP wrapped concrete. *Construction and Building Materials,* 23**,** 153-161.
GARDONI, P., DER KIUREGHIAN, A. & MOSALAM, K. M. 2002. Probabilistic capacity models and fragility estimates for reinforced concrete columns based on experimental observations. *Journal of Engineering Mechanics,* 128**,** 1024-1038.
GARDONI, P. & ROSOWSKY, D. 2011. Seismic fragility increment functions for deteriorating reinforced concrete bridges. *Structure and Infrastructure Engineering,* 7**,** 869-879.
GERGELY, I., PANTELIDES, C. P., NUISMER, R. J. & REAVELEY, L. D. 1998. Bridge pier retrofit using fiber-reinforced plastic composites. *Journal of Composites for Construction,* 2**,** 165-174.
GHOSH, J. & PADGETT, J. E. 2010. Aging considerations in the development of time-dependent seismic fragility curves. *Journal of Structural Engineering,* 136**,** 1497-1511.
GLASS, G. & BUENFELD, N. 2000. The influence of chloride binding on the chloride induced corrosion risk in reinforced concrete. *Corrosion Science,* 42**,** 329-344.
GONZALEZ, J., ANDRADE, C., ALONSO, C. & FELIU, S. 1995. Comparison of rates of general corrosion and maximum pitting penetration on concrete embedded steel reinforcement. *Cement and Concrete Research,* 25**,** 257-264.
GREEN, M. F., BISBY, L. A., FAM, A. Z. & KODUR, V. K. 2006. FRP confined concrete columns: Behaviour under extreme conditions. *Cement and concrete composites,* 28**,** 928-937.
GULIKERS, J. 2005. Theoretical considerations on the supposed linear relationship between concrete resistivity and corrosion rate of steel reinforcement. *Materials and Corrosion,* 56**,** 393-403.
HANSEN, B. 2009. ASCE's Infrastructure Report Card Gives Nation a D, Estimate Cost at $2.2 Trillion. *ASCE News,* 34**,** 1-4.
HAWILEH, R. A., ABDALLA, J. A., AL TAMIMI, A., ABDELRAHMAN, K. & OUDAH, F. 2011. Behavior of Corroded Steel Reinforcing Bars Under Monotonic and Cyclic Loadings. *Mechanics of Advanced Materials and Structures,* 18**,** 218-224.
HSU, T. T. 1992. *Unified theory of reinforced concrete,* CRC press.
HUANG, R. & YANG, C. 1997. Condition assessment of reinforced concrete beams relative to reinforcement corrosion. *Cement and Concrete Composites,* 19**,** 131-137.

HUET, B., L'HOSTIS, V., SANTARINI, G., FERON, D. & IDRISSI, H. 2007. Steel corrosion in concrete: Determinist modeling of cathodic reaction as a function of water saturation degree. *Corrosion science,* 49**,** 1918-1932.

HUSSAIN, R. R. & ISHIDA, T. 2009. Critical carbonation depth for initiation of steel corrosion in fully carbonated concrete and development of electrochemical carbonation induced corrosion model. *Int. J. Electrochem. Sci,* 4**,** 1178-1195.

HUSSAIN, S. E. & AL-GAHTANI, A. S. 1996. Chloride threshold for corrosion of reinforcement in concrete. *ACI Materials Journal,* 93.

ISGOR, O. B. & RAZAQPUR, A. G. PREDICTING THE INITIATION AND PROPAGATION OF CORROSION IN REINFORCED CONCRETE STRUCTURES.

KATWAN, M., HODGKIESS, T. & ARTHUR, P. 1996. Electrochemical noise technique for the prediction of corrosion rate of steel in concrete. *Materials and Structures,* 29**,** 286-294.

KIVELL, A. R. L. 2012. Effects of Bond Deterioration Due to Corrosion on Seismic Performance of Reinforced Concrete Structures.

KRANC, S. & SAGÜÉS, A. A. 1997. Modeling the Time-Dependent Response to External Polarization of a Corrosion Macrocell on Steel in Concrete. *Journal of The Electrochemical Society,* 144**,** 2643-2652.

KUMAR, R. & GARDONI, P. 2011. Modeling Structural Degradation of RC Bridge Columns Subjected to Earthquakes and Their Fragility Estimates. *Journal of Structural Engineering,* 138**,** 42-51.

LAYCOCK, N. & NEWMAN, R. 1997. Localised dissolution kinetics, salt films and pitting potentials. *Corrosion science,* 39**,** 1771-1790.

LEE, C., BONACCI, J., THOMAS, M. D., MAALEJ, M., KHAJEHPOUR, S., HEARN, N., PANTAZOPOULOU, S. & SHEIKH, S. 2000. Accelerated corrosion and repair of reinforced concrete columns using carbon fibre reinforced polymer sheets. *Canadian Journal of Civil Engineering,* 27**,** 941-948.

LEE, H.-S. & CHO, Y.-S. 2009. Evaluation of the mechanical properties of steel reinforcement embedded in concrete specimen as a function of the degree of reinforcement corrosion. *International journal of fracture,* 157**,** 81-88.

LEE, H.-S., NOGUCHI, T. & TOMOSAWA, F. 2002. Evaluation of the bond properties between concrete and reinforcement as a function of the degree of reinforcement corrosion. *Cement and Concrete research,* 32**,** 1313-1318.

LEE, H., TOMOSAWA, F. & NOGUCHI, T. 1996a. Effects of rebar corrosion on the structural performance of singly reinforced beams. *Durability of building materials and components,* 7**,** 571-580.

LEE, H., TOMOSAWA, F. & NOGUCHI, T. 1996b. Effects of rebar corrosion on the structural performance of singly reinforced beams. *Durability of building materials and components,* 7**,** 571-580.

LESS, T. & ADELI, H. 2010. 'Computational earthquake engineering of bridges. *Scientia Iranica—Transaction A: Civil Engineering,* 17**,** 325-338.

LI, J., GONG, J. & WANG, L. 2009. Seismic behavior of corrosion-damaged reinforced concrete columns strengthened using combined carbon fiber-reinforced polymer and steel jacket. *Construction and Building Materials,* 23**,** 2653-2663.

LIANG, M.-T., LIN, L.-H. & LIANG, C.-H. 2002. Service life prediction of existing reinforced concrete bridges exposed to chloride environment. *Journal of Infrastructure systems,* 8**,** 76-85.

LIU, T. & WEYERS, R. 1998a. Modeling the dynamic corrosion process in chloride contaminated concrete structures. *Cement and Concrete Research,* 28**,** 365-379.

LIU, Y. 1996. *Modeling the time-to-corrosion cracking of the cover concrete in chloride contaminated reinforced concrete structures.* Virginia Polytechnic Institute and State University.

LIU, Y. & WEYERS, R. E. 1998b. Modeling the time-to-corrosion cracking in chloride contaminated reinforced concrete structures. *ACI Materials Journal,* 95.

LOPEZ, W. & GONZALEZ, J. 1993. Influence of the degree of pore saturation on the resistivity of concrete and the corrosion rate of steel reinforcement. *Cement and concrete research,* 23**,** 368-376.

LV, H., TENG, J. & ZOU, D. Seismic performance under environment corrosion for curved beam bridges with high piers. Multimedia Technology (ICMT), 2011 International Conference on, 2011. IEEE, 1693-1696.
MA, Y., CHE, Y. & GONG, J. 2012. Behavior of corrosion damaged circular reinforced concrete columns under cyclic loading. *Construction and Building Materials,* 29**,** 548-556.
MAADDAWY, T. E. 2008. Behavior of corrosion-damaged RC columns wrapped with FRP under combined flexural and axial loading. *Cement and Concrete Composites,* 30**,** 524-534.
MALEK A, ANDISHEH K., SCOTT A., STEFANO P., MCRAE G., PALERMO A. 2017, Permeability-Based Assessment of Residual Axial Capacity of Concrete Material in Damaged RC Columns. *ASCE Materials Journal*, Under Press.
MANDER, J., PRIESTLEY, M. & PARK, R. 1988a. Observed stress-strain behavior of confined concrete. *Journal of structural engineering,* 114**,** 1827-1849.
MANDER, J. B. 1983. Seismic design of bridge piers.
MANDER, J. B. & BASÖZ, N. Seismic fragility curve theory for highway bridges. Optimizing post-earthquake lifeline system reliability, 1999. ASCE, 31-40.
MANDER, J. B., PRIESTLEY, M. J. & PARK, R. 1988b. Theoretical stress-strain model for confined concrete. *Journal of structural engineering,* 114**,** 1804-1826.
MANGAT, P. & ELGARF, M. 1999a. Strength and serviceability of repaired reinforced concrete beams undergoing reinforcement corrosion. *Magazine of concrete research,* 51**,** 97-112.
MANGAT, P. S. & ELGARF, M. S. 1999b. Flexural strength of concrete beams with corroding reinforcement. *ACI Structural Journal,* 96.
MARCOTTE, T. D. 2001. Characterization of chloride-induced corrosion products that form in steel-reinforced cementitious materials.
MARTÍNEZ, I. & ANDRADE, C. 2009. Examples of reinforcement corrosion monitoring by embedded sensors in concrete structures. *Cement and Concrete Composites,* 31**,** 545-554.
MARUYA, T., HSU, K., TAKEDA, H. & TANGTERMSIRIKUL, S. 2003. Numerical modeling of steel corrosion in concrete structures due to chloride ion, oxygen and water movement. *Journal of Advanced Concrete Technology,* 1**,** 147-160.
MASLEHUDDIN, M., ALLAM, I. A., AL-SULAIMANI, G. J., AL-MANA, A. & ABDULJAUWAD, S. N. 1990a. Effect of rusting of reinforcing steel on its mechanical properties and bond with concrete. *Materials Journal,* 87**,** 496-502.
MASLEHUDDIN, M., ALLAM, I. A., AL-SULAIMANI, G. J., AL-MANA, A. & ABDULJAUWAD, S. N. 1990b. Effect of rusting of reinforcing steel on its mechanical properties and bond with concrete. *ACI Materials Journal,* 87.
MATSUKI, S., BILLINGTON, S. & BAKER, J. Impact of long-term material degradation on seismic performance of a reinforced concrete bridge. 8th US national conference on earthquake engineering. San Francisco, California, 2006.
MAU, S. & EL-MABSOUT, M. 1989. Inelastic buckling of reinforcing bars. *Journal of engineering mechanics,* 115**,** 1-17.
MEDA, A., MOSTOSI, S., RINALDI, Z. & RIVA, P. 2014. Experimental evaluation of the corrosion influence on the cyclic behaviour of RC columns. *Engineering Structures,* 76**,** 112-123.
MEHTA, P. 1994. Concrete Technology at the Crossroad Problem, and Opportunities. Conerete Technology. *Past, Present and Future. ACI SP144-1*.
MOEHLE, J. & DEIERLEIN, G. G. A framework methodology for performance-based earthquake engineering. Proceedings of the 13th World conference on earthquake engineering, 2004. 3812-3814.
MOEHLE, J., LYNN, A., ELWOOD, K. & SEZEN, H. Gravity load collapse of reinforced concrete frames during earthquakes. Proc., 1st US–Japan Workshop on Performance-Based Design Methodology for Reinforced Concrete Building Structures, 1999. Berkeley: Pacific Earthquake Engineering Research Center, Univ. of California, 175-189.
MONTEJO, L. A. & KOWALSKY, M. J. 2007. CUMBIA—Set of codes for the analysis of reinforced concrete members. *CFL Technical Rep. No. IS-07,* 1.
MONTEMOR, M., SIMOES, A. & FERREIRA, M. 2003. Chloride-induced corrosion on reinforcing steel: from the fundamentals to the monitoring techniques. *Cement and Concrete Composites,* 25**,** 491-502.

MONTI, G. & NUTI, C. 1992. Nonlinear cyclic behavior of reinforcing bars including buckling. *Journal of Structural Engineering,* 118**,** 3268-3284.
MORINAGA, S. 1996. Remaining life of reinforced concrete structures after corrosion cracking. *Durability of Building Materials and Components,* 71**,** 127-136.
MULLINS, G., SEN, R., TORRES-ACOSTA, A., GOULISH, A., SUH, K., PAI, N. & MEHRANI, A. 2001. Load capacity of corroded pile bents. *Final Report*.
NG, S. & MOSES, F. 1996. Prediction of bridge service life using time-dependent reliability analysis. *Bridge management,* 3**,** 26-32.
NZS, N. Z. S. 2006. 3101. *Concrete Structures Standard Part2-Commentary on The Design of Concrete Structures, New Zealand: Standards Association of New Zealand, Wellington*.
NZ TRANSPORT AGENCY (2013). *Bridge Manual Third Edition*.
OTIENO, M., BEUSHAUSEN, H. & ALEXANDER, M. 2011. Prediction of Corrosion Rate in RC Structures-A critical review. *Modelling of Corroding Concrete Structures.* Springer.
OTIENO, M., BEUSHAUSEN, H. & ALEXANDER, M. 2012. Prediction of corrosion rate in reinforced concrete structures–a critical review and preliminary results. *Materials and Corrosion,* 63**,** 777-790.
OU, Y.-C. & NGUYEN, N. D. 2014. Plastic hinge length of corroded reinforced concrete beams. *ACI Structural Journal,* 111**,** 1049.
OU, Y. C., FAN, H. D. & NGUYEN, N. D. 2013a. Long-term seismic performance of reinforced concrete bridges under steel reinforcement corrosion due to chloride attack. *Earthquake Engineering & Structural Dynamics*.
OU, Y. C., FAN, H. D. & NGUYEN, N. D. 2013b. Long-term seismic performance of reinforced concrete bridges under steel reinforcement corrosion due to chloride attack. *Earthquake Engineering & Structural Dynamics,* 42**,** 2113-2127.
OU, Y. C., TSAI, L. L. & CHEN, H. H. 2012. Cyclic performance of large-scale corroded reinforced concrete beams. *Earthquake Engineering & Structural Dynamics,* 41**,** 593-604.
OUGLOVA, A., BERTHAUD, Y., FOCT, F., FRANÇOIS, M., RAGUENEAU, F. & PETRE-LAZAR, I. 2008. The influence of corrosion on bond properties between concrete and reinforcement in concrete structures. *Materials and Structures,* 41**,** 969-980.
OYADO, M., KANAKUBO, T., SATO, T. & YAMAMOTO, Y. 2011. Bending performance of reinforced concrete member deteriorated by corrosion. *Structure and Infrastructure Engineering,* 7**,** 121-130.
PALERMO, A. & MASHAL, M. 2012. ACCELERATED BRIDGE CONSTRUCTION(ABC) AND SEISMIC DAMAGE RESISTANT TECHNOLOGY: A NEW ZEALAND CHALLENGE. *Bulletin of the New Zealand Society for Earthquake Engineering,* 45**,** 123-134.
PALERMO, A. & PAMPANIN, S. 2008. Enhanced seismic performance of hybrid bridge systems: Comparison with traditional monolithic solutions. *Journal of Earthquake Engineering,* 12**,** 1267-1295.
PALSSON, R. & MIRZA, M. S. 2002. Mechanical response of corroded steel reinforcement of abandoned concrete bridge. *ACI Structural Journal,* 99.
PANTAZOPOULOU, S., BONACCI, J., SHEIKH, S., THOMAS, M. & HEARN, N. 2001. Repair of corrosion-damaged columns with FRP wraps. *Journal of composites for construction,* 5**,** 3-11.
PANTAZOPOULOU, S. & PAPOULIA, K. 2001. Modeling cover-cracking due to reinforcement corrosion in RC structures. *Journal of Engineering Mechanics,* 127**,** 342-351.
PISTORIUS, P. & BURSTEIN, G. 1992. Metastable pitting corrosion of stainless steel and the transition to stability. *Philosophical Transactions of the Royal Society of London. Series A: Physical and Engineering Sciences,* 341**,** 531-559.
POLDER, R. B. 2009. Critical chloride content for reinforced concrete and its relationship to concrete resistivity. *Materials and corrosion,* 60**,** 623-630.
POPOVICS, S. 1973. A numerical approach to the complete stress-strain curve of concrete. *Cement and concrete research,* 3**,** 583-599.
PORTER, K. A. An overview of PEER's performance-based earthquake engineering methodology. Conference on Applications of Statistics and Probability in Civil Engineering (ICASP9), 2003. Civil Engineering Risk and Reliability Association (CERRA) San Francisco, CA, 6-9.

PRIESTLEY, M. N., SEIBLE, F. & CALVI, G. M. 1996. *Seismic design and retrofit of bridges*, John Wiley & Sons.
RAUPACH, M. 1996. Chloride-induced macrocell corrosion of steel in concrete—theoretical background and practical consequences. *Construction and building materials,* 10**,** 329-338.
RAUPACH, M. 2007. *Corrosion of reinforcement in concrete: mechanisms, monitoring, inhibitors and rehabilitation techniques*, Woodhead Pub Ltd.
RAUPACH, M. & GULIKERS, J. 1999. 36 A SIMPLIFIED METHOD TO ESTIMATE CORROSION RATES—A NEW APPROACH BASED ON INVESTIGATIONS OF MACROCELLS. *Durability of Building Materials and Components 8: Service life and durability of materials and components,* 1**,** 376.
RAUPACH, M., WEIZHONG, G. & WEI-LIANG, J. 2010. Korrosionsprodukte und deren Volumenfaktor bei der Korrosion von Stahl in Beton. *Beton-und Stahlbetonbau,* 105**,** 572-578.
RODRIGUEZ, J., ORTEGA, L. & CASAL, J. Load bearing capacity of concrete columns with corroded reinforcement. CORROSION OF REINFORCEMENT IN CONCRETE CONSTRUCTION. PROCEEDINGS OF FOURTH INTERNATIONAL SYMPOSIUM, CAMBRIDGE, 1-4 JULY 1996. SPECIAL PUBLICATION NO 183, 1996.
RODRIGUEZ, J., ORTEGA, L. & CASAL, J. 1997. Load carrying capacity of concrete structures with corroded reinforcement. *Construction and Building Materials,* 11**,** 239-248.
SAIFULLAH, M. 1994. *Effect of reinforced corrosion on bond strength in reinforced concrete.* The University of Birmingham.
SARRAF R. EL. MANDENO W., Xia J. (2013), "STAINLESS STEEL IN BRIDGES: A DISCUSSION", Steel inovation conference 2013, Christchurch, New Zealand, 21- 22 February 2013.
SCOTT, A. & ALEXANDER, M. 2007. The influence of binder type, cracking and cover on corrosion rates of steel in chloride-contaminated concrete. *Magazine of Concrete Research,* 59**,** 495-505.
SCOTT, B., PARK, R. & PRIESTLEY, M. Stress-strain behavior of concrete confined by overlapping hoops at low and high strain rates. Journal Proceedings, 1982. 13-27.
SCOTT, B. D. 1980. Stress: strain relationships for confined concrete: rectangular sections.
SEN, R. 2003. Advances in the application of FRP for repairing corrosion damage. *Progress in Structural Engineering and Materials,* 5**,** 99-113.
SHINOZUKA, M., FENG, M. Q., LEE, J. & NAGANUMA, T. 2000. Statistical analysis of fragility curves. *Journal of Engineering Mechanics,* 126**,** 1224-1231.
SIMON, J., BRACCI, J. M. & GARDONI, P. 2010. Seismic response and fragility of deteriorated reinforced concrete bridges. *Journal of Structural Engineering,* 136**,** 1273-1281.
SOUDKI, K. & SHERWOOD, T. 2003. Bond behavior of corroded steel reinforcement in concrete wrapped with carbon fiber reinforced polymer sheets. *Journal of materials in civil engineering,* 15**,** 358-370.
STANDARD, A. C876-91, Standard test method for half cell potentials of uncoated reinforced steel in concrete. *Annual Book of ASTM Standard,* 4.
STANISH, K., HOOTON, R. & PANTAZOPOULOU, S. 1999. Corrosion effects on bond strength in reinforced concrete. *ACI Structural Journal,* 96.
STEWART, M. G. 2004. Spatial variability of pitting corrosion and its influence on structural fragility and reliability of RC beams in flexure. *Structural Safety,* 26**,** 453-470.
STEWART, M. G. 2009. Mechanical behaviour of pitting corrosion of flexural and shear reinforcement and its effect on structural reliability of corroding RC beams. *Structural safety,* 31**,** 19-30.
STEWART, M. G. & AL-HARTHY, A. 2008. Pitting corrosion and structural reliability of corroding RC structures: Experimental data and probabilistic analysis. *Reliability Engineering & System Safety,* 93**,** 373-382.
TACHIBANA, Y., MAEDA, K.-I., KAJIKAWA, Y. & KAWAMURA, M. 1990. Mechanical behaviour of RC beams damaged by corrosion of reinforcement. *Elsevier Applied Science***,** 178-187.
TAKEWAKA, K., YAMAGUCHI, T. & MAEDA, S. 2003. Simulation model for deterioration of concrete structures due to chloride attack. *Journal of Advanced concrete technology,* 1**,** 139-146.
TAPAN, M. & ABOUTAHA, R. 2011. Effect of steel corrosion and loss of concrete cover on strength of deteriorated RC columns. *Construction and Building Materials,* 25**,** 2596-2603.

TENG, M.-H., SOTELINO, E. D. & CHEN, W.-F. 2003. Performance evaluation of reinforced concrete bridge columns wrapped with fiber reinforced polymers. *Journal of Composites for Construction,* 7**,** 83-92.
THOFT-CHRISTENSEN, P., JENSEN, F., MIDDLETON, C. & BLACKMORE, A. 1996. Assessment of the reliability of concrete slab bridges. Dept. of Building Technology and Structural Engineering.
TORRES-ACOSTA, A. A. & MART ı´ NEZ-MADRID, M. 2003. Residual life of corroding reinforced concrete structures in marine environment. *Journal of Materials in Civil Engineering,* 15**,** 344-353.
TORRES-ACOSTA, A. A., NAVARRO-GUTIERREZ, S. & TERÁN-GUILLÉN, J. 2007. Residual flexure capacity of corroded reinforced concrete beams. *Engineering structures,* 29**,** 1145-1152.
TOUTANJI, H. A. 1999. Durability characteristics of concrete columns confined with advanced composite materials. *Composite Structures,* 44**,** 155-161.
TUUTTI, K. 1982. Corrosion of steel in concrete.
VAL, D. V. & MELCHERS, R. E. 1997. Reliability of deteriorating RC slab bridges. *Journal of structural engineering,* 123**,** 1638-1644.
VAL, D. V., STEWART, M. G. & MELCHERS, R. E. 1998. Effect of reinforcement corrosion on reliability of highway bridges. *Engineering Structures,* 20**,** 1010-1019.
VAYSBURD, A. & EMMONS, P. 2000. How to make today's repairs durable for tomorrow—corrosion protection in concrete repair. *Construction and building materials,* 14**,** 189-197.
VECCHIO, F. J. & COLLINS, M. P. 1986. The modified compression-field theory for reinforced concrete elements subjected to shear. *ACI J.,* 83**,** 219-231.
VECCHIO, F. J. & COLLINS, M. P. 1993. Compression response of cracked reinforced concrete. *Journal of Structural Engineering,* 119**,** 3590-3610.
VIDAL, T., CASTEL, A. & FRANCOIS, R. 2004. Analyzing crack width to predict corrosion in reinforced concrete. *Cement and Concrete Research,* 34**,** 165-174.
VU, K., STEWART, M. G. & MULLARD, J. 2005. Corrosion-induced cracking: experimental data and predictive models. *ACI structural journal,* 102.
VU, K. A. T. & STEWART, M. G. 2000. Structural reliability of concrete bridges including improved chloride-induced corrosion models. *Structural safety,* 22**,** 313-333.
WARKUS, J. & RAUPACH, M. 2008. Numerical modelling of macrocells occurring during corrosion of steel in concrete. *Materials and corrosion,* 59**,** 122-130.
WARKUS, J. & RAUPACH, M. 2010. Modelling of reinforcement corrosion–geometrical effects on macrocell corrosion. *Materials and corrosion,* 61**,** 494-504.
WEYERS, R. E., PROWELL, B. D., SPRINKEL, M. M. & VORSTER, M. 1993. Concrete bridge protection, repair, and rehabilitation relative to reinforcement corrosion: A methods application manual. *Contract,* 100**,** 103.
WHITE S. (2014). "Controlled Damage Rocking Systems for Accelerated Bridge Construction." Master's thesis, University of Canterbury, New Zealand
WOOTTON, I. A., SPAINHOUR, L. K. & YAZDANI, N. 2003. Corrosion of steel reinforcement in carbon fiber-reinforced polymer wrapped concrete cylinders. *Journal of Composites for Construction,* 7**,** 339-347.
YALCYN, H. & ERGUN, M. 1996. The prediction of corrosion rates of reinforcing steels in concrete. *Cement and concrete research,* 26**,** 1593-1599.
ZEALAND, S. N. 2013. Are New Zealanders living closer to the coast.
ZHANG, P., LU, M. & LI, X. 1995. The mechanical behaviour of corroded bar. *Journal of Industrial Buildings,* 25**,** 41-44.
ZHANG, R., CASTEL, A. & FRANÇOIS, R. 2012a. Concrete cracking due to chloride-induced reinforcement corrosion–influence of steel–concrete interface defects due to the 'top-bar effect'. *European Journal of Environmental and Civil Engineering,* 16**,** 402-413.
ZHANG, W., SONG, X., GU, X. & LI, S. 2012b. Tensile and fatigue behavior of corroded rebars. *Construction and Building Materials,* 34**,** 409-417.
ZHAO, Y., REN, H., DAI, H. & JIN, W. 2011. Composition and expansion coefficient of rust based on X-ray diffraction and thermal analysis. *Corrosion Science,* 53**,** 1646-1658.

ZHONG, J., GARDONI, P. & ROSOWSKY, D. 2012. Seismic fragility estimates for corroding reinforced concrete bridges. *Structure and Infrastructure Engineering,* 8**,** 55-69.

APPEDIX A:

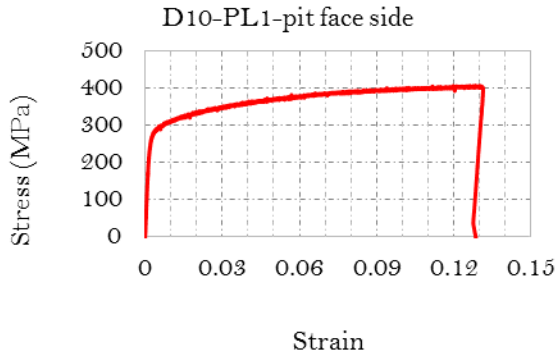
D10-PL1-pit face side
Stress (MPa)
500
400
300
200
100
0
0
0.03
0.06
0.09
0.12
0.15
Strain

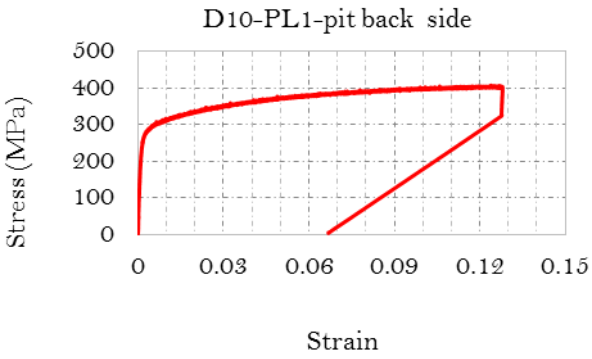
D10-PL1-pit back side
Stress (MPa)
500
400
300
200
100
0
0
0.03
0.06
0.09
0.12
0.15
Strain

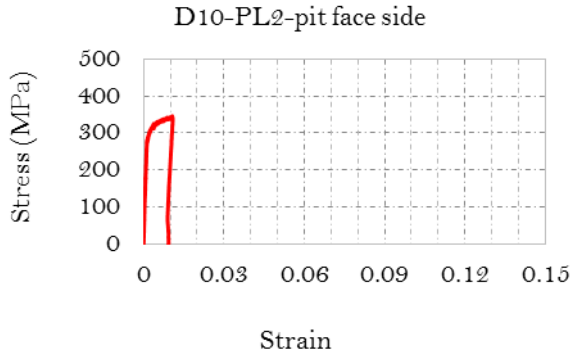
D10-PL2-pit face side
Stress (MPa)
500
400
300
200
100
0
0
0.03
0.06
0.09
0.12
0.15
Strain

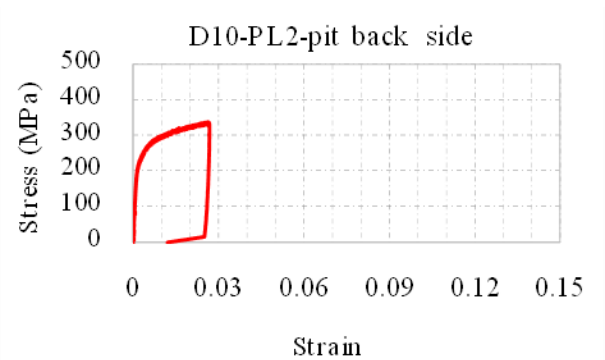
D10-PL2-pit back side
Stress (MPa)
500
400
300
200
100
0
0
0.03
0.06
0.09
0.12
0.15
Strain

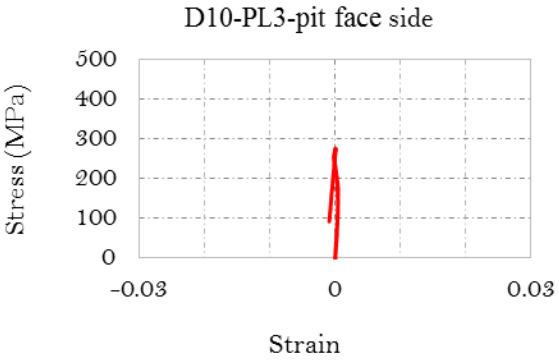
D10-PL3-pit face side
Stress (MPa)
500
400
300
200
100
0
-0.03
0
0.03
Strain

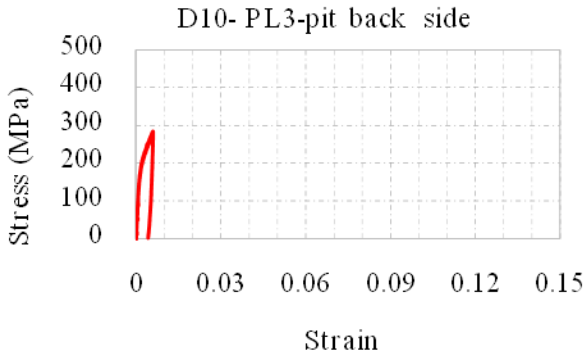
D10- PL3-pit back side
Stress (MPa)
500
400
300
200
100
0
0
0.03
0.06
0.09
0.12
0.15
Strain

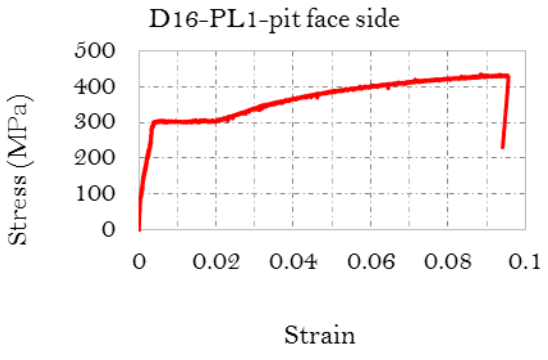
D16-PL1-pit face side
Stress (MPa)
500
400
300
200
100
0
0
0.02
0.04
0.06
0.08
0.1
Strain

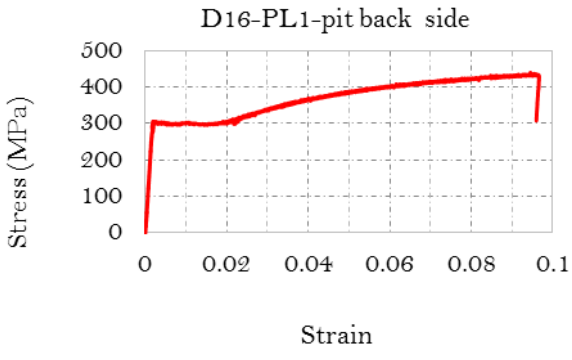
D16-PL1-pit back side
Stress (MPa)
500
400
300
200
100
0
0
0.02
0.04
0.06
0.08
0.1
Strain

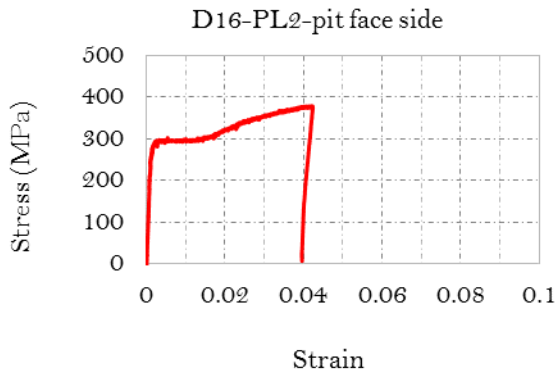
D16-PL2-pit face side
Stress (MPa)
500
400
300
200
100
0
0
0.02
0.04
0.06
0.08
0.1
Strain

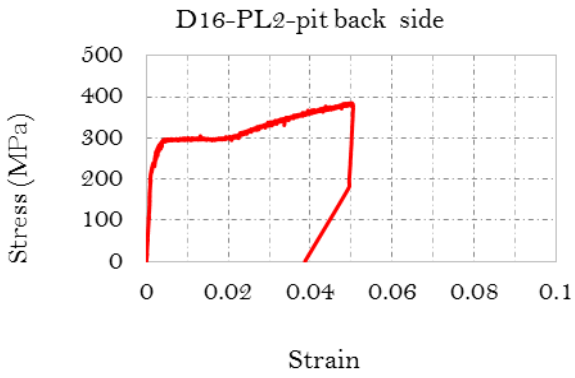
D16-PL2-pit back side
Stress (MPa)
500
400
300
200
100
0
0
0.02
0.04
0.06
0.08
0.1
Strain

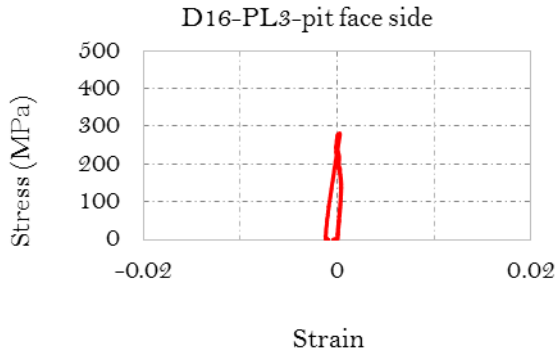
D16-PL3-pit face side
Stress (MPa)
500
400
300
200
100
0
-0.02
0
0.02
Strain

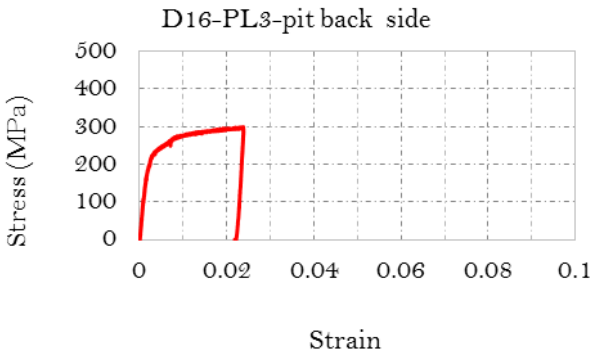
D16-PL3-pit back side
Stress (MPa)
500
400
300
200
100
0
0
0.02
0.04
0.06
0.08
0.1
Strain

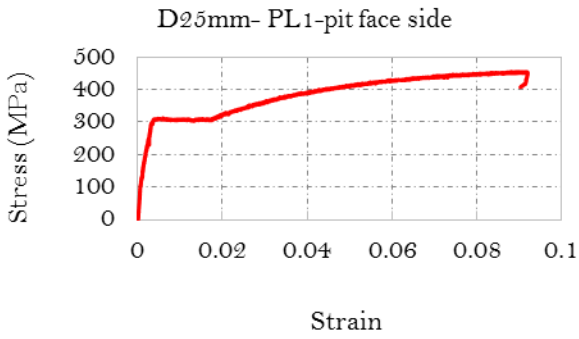
D25mm- PL1-pit face side
Stress (MPa)
500
400
300
200
100
0
0
0.02
0.04
0.06
0.08
0.1
Strain

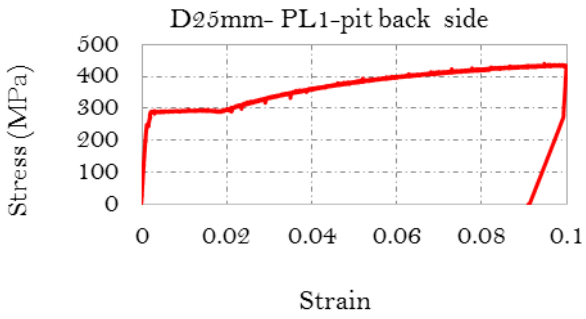
D25mm- PL1-pit back side
Stress (MPa)
500
400
300
200
100
0
0
0.02
0.04
0.06
0.08
0.1
Strain

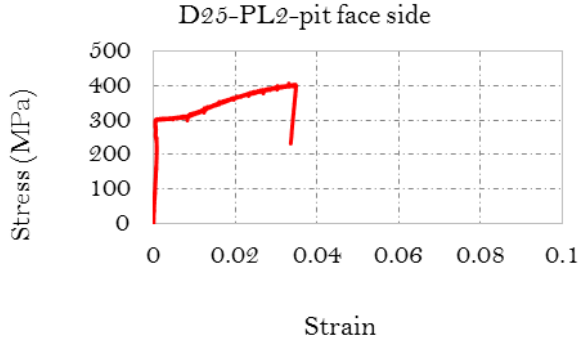
D25-PL2-pit face side
Stress (MPa)
500
400
300
200
100
0
0
0.02
0.04
0.06
0.08
0.1
Strain

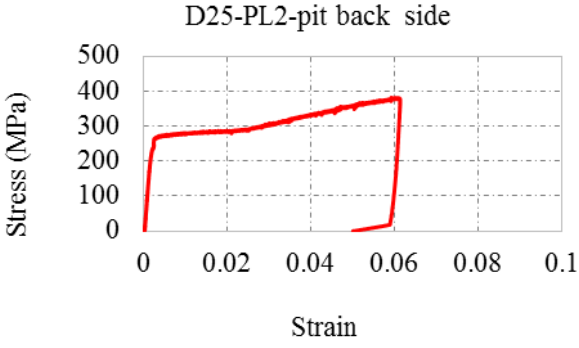
D25-PL2-pit back side
Stress (MPa)
500
400
300
200
100
0
0
0.02
0.04
0.06
0.08
0.1
Strain

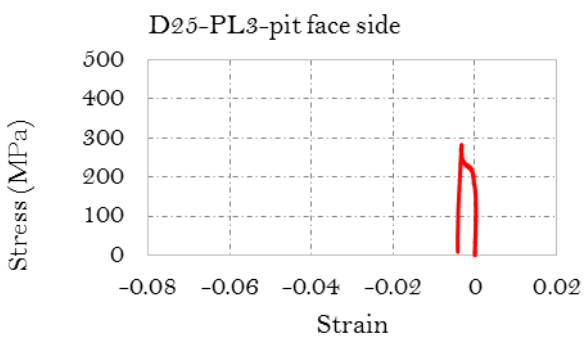
D25-PL3-pit face side
Stress (MPa)
500
400
300
200
100
0
-0.08
-0.06
-0.04
-0.02
0
0.02
Strain

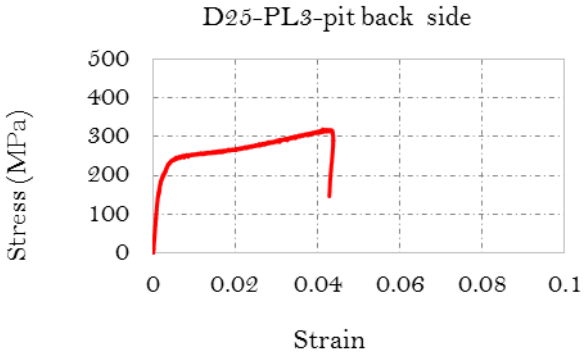
D25-PL3-pit back side
Stress (MPa)
500
400
300
200
100
0
0
0.02
0.04
0.06
0.08
0.1
Strain

APPENDIX B:

Noncorroded- Low confined:

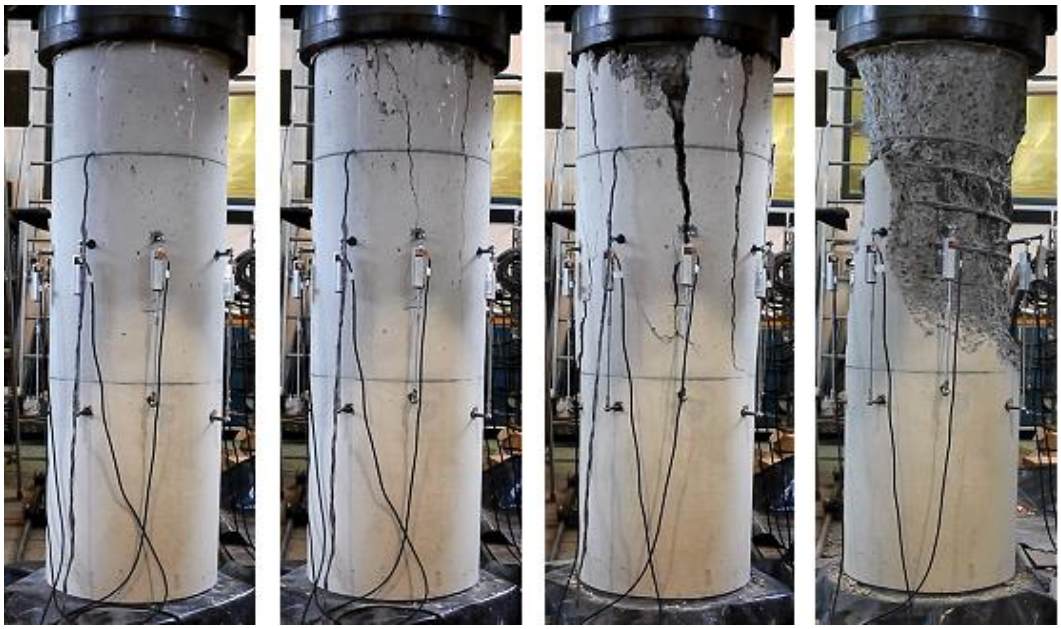

Initial Cracked cover Ineffective cover Stirrup failure

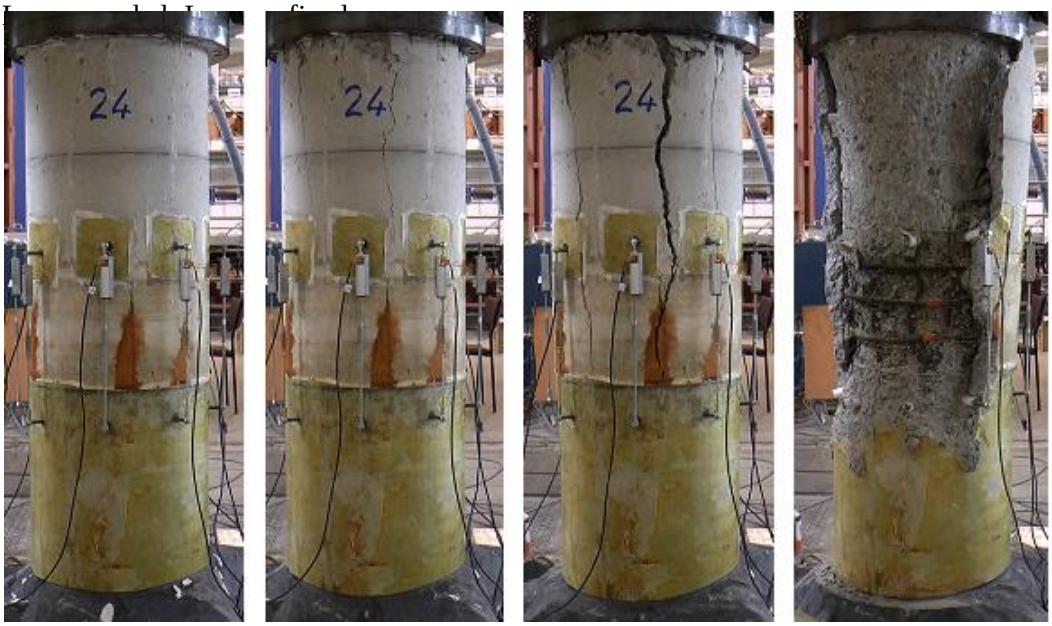

Initial Cracked cover Ineffective cover Stirrup failure

High corroded- Low confined:

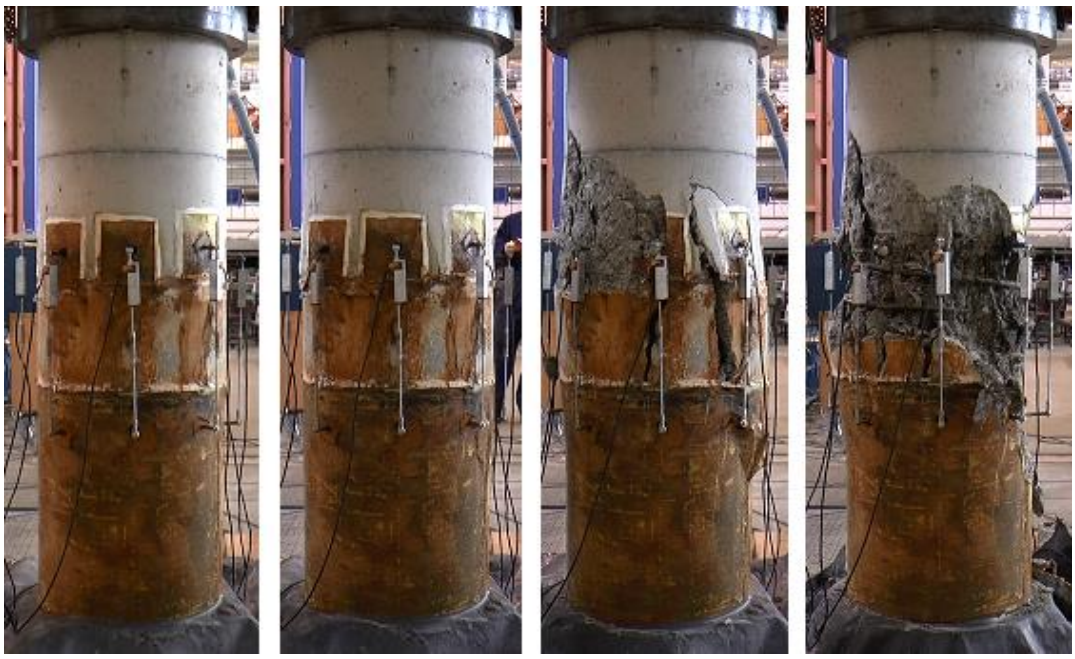

Initial Cracked cover Ineffective cover Stirrup failure

Pit corroded- Low Confined:

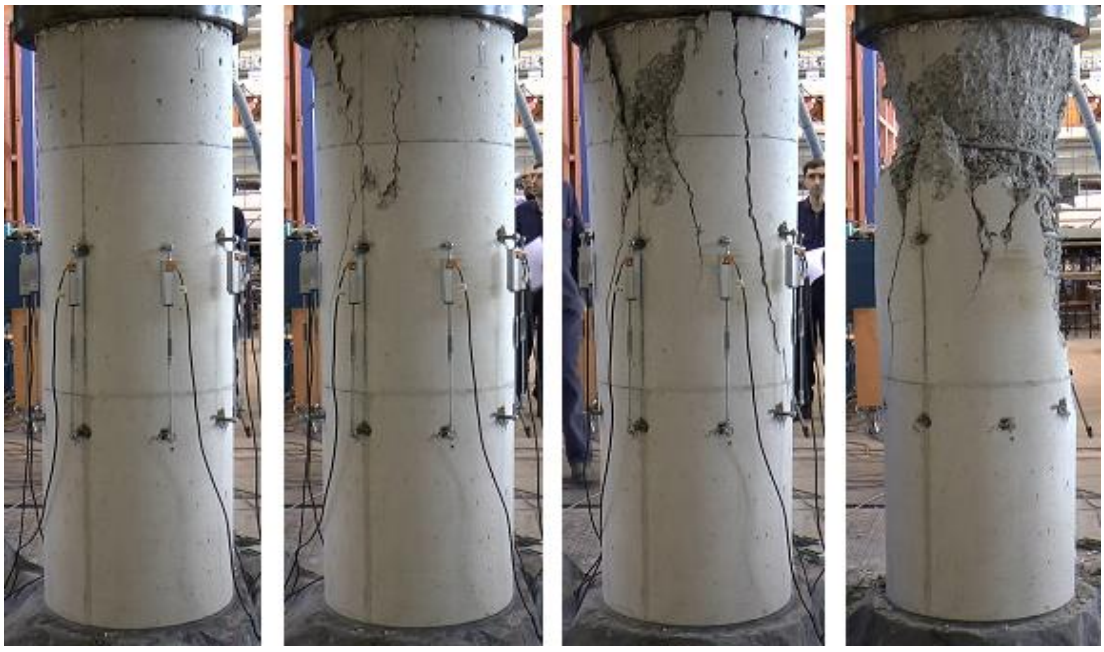

Initial Cracked cover Ineffective cover Stirrup failure

Noncorroded- Medium confined:

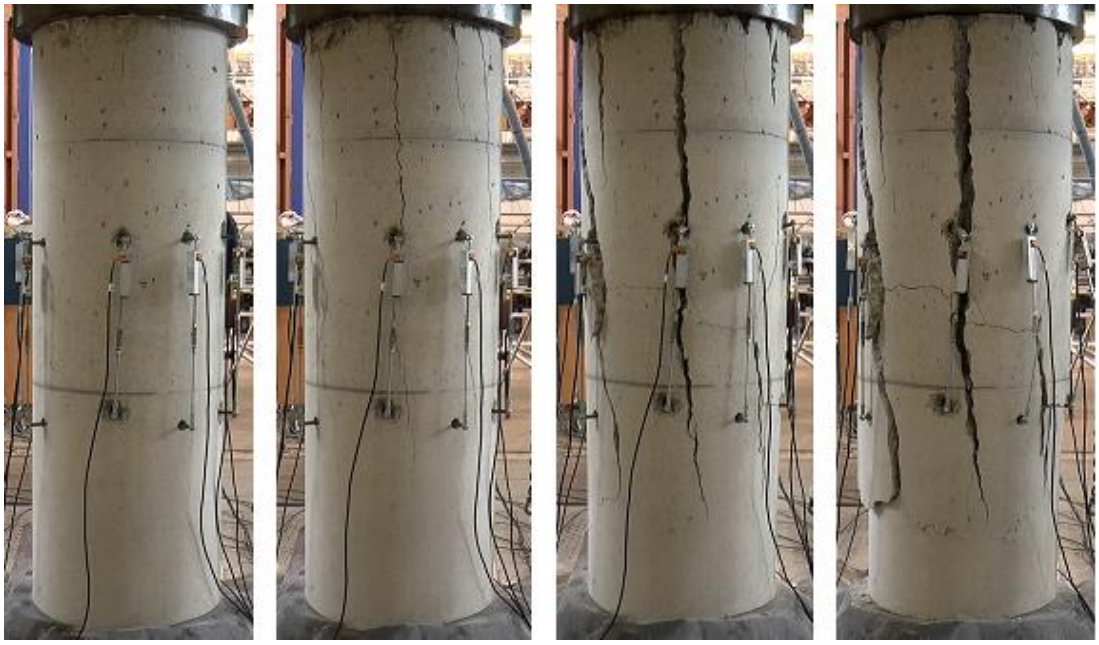

Initial Cracked cover Ineffective cover Stirrup failure

Low corroded- Medium confined:

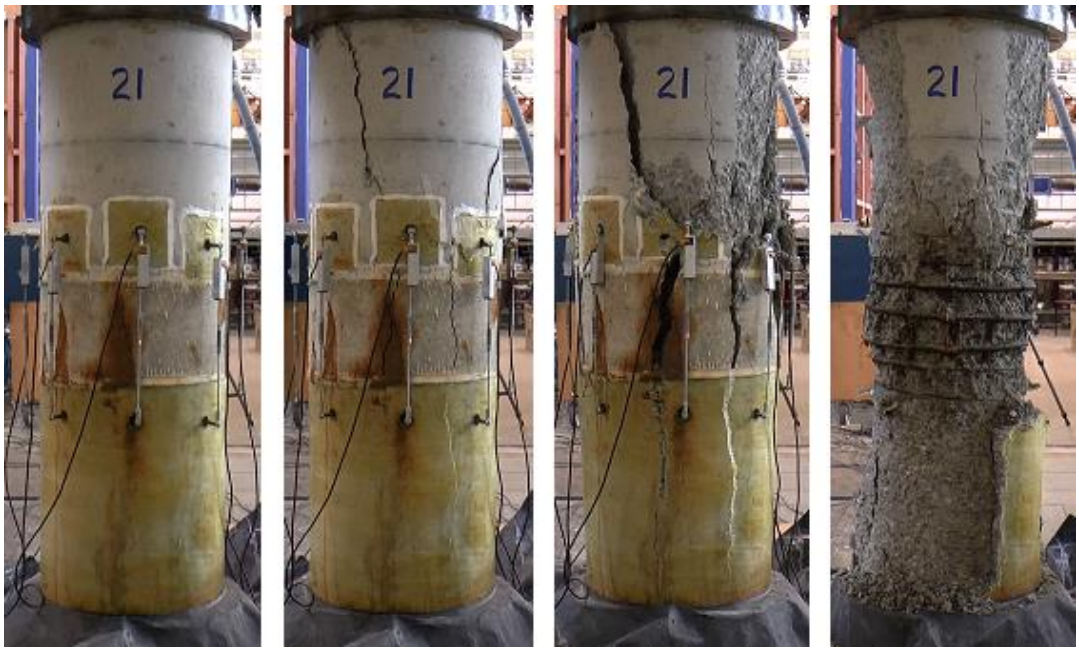

Initial Cracked cover Ineffective cover Stirrup failure

High corroded- Medium confined:

Initial Cracked cover Ineffective cover Stirrup failure

Noncorroded- High confined:

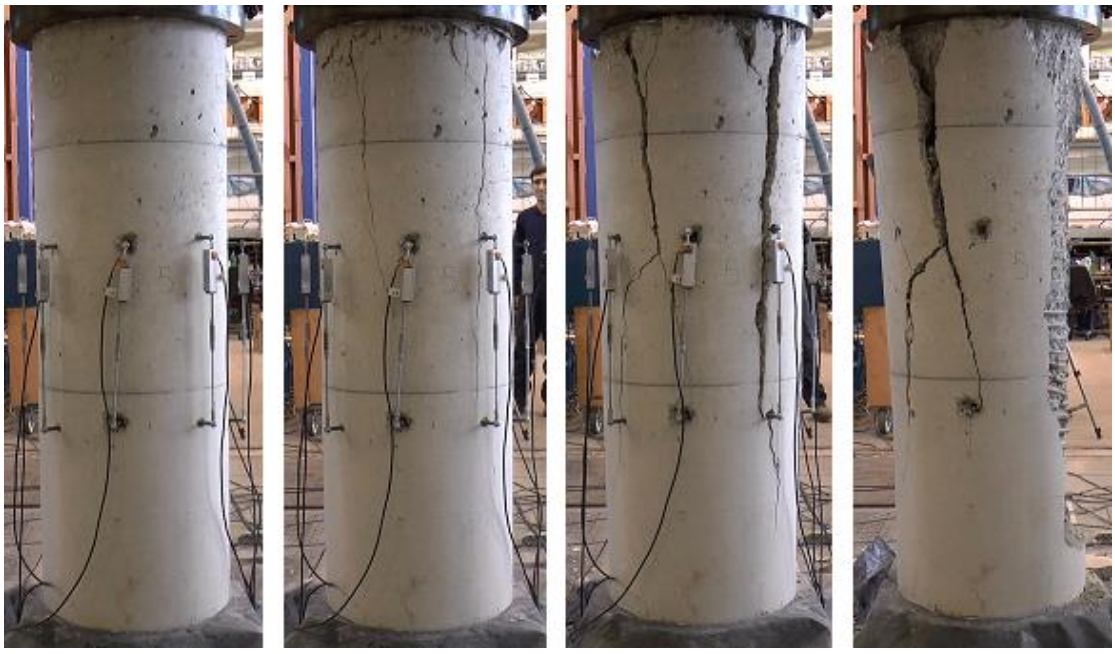

Initial Cracked cover Ineffective cover Stirrup failure

Low corroded- High confined:

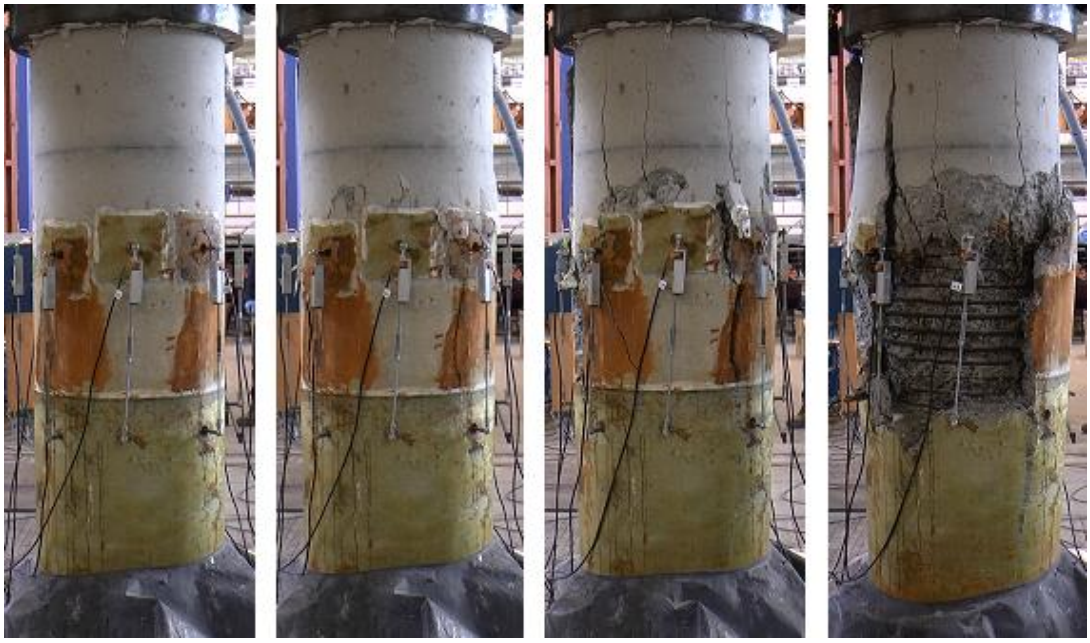

Initial Cracked cover Ineffective cover Stirrup failure

High corroded- High confined:

Initial Cracked cover Ineffective cover Stirrup failure

Cylinders 1 and 2:

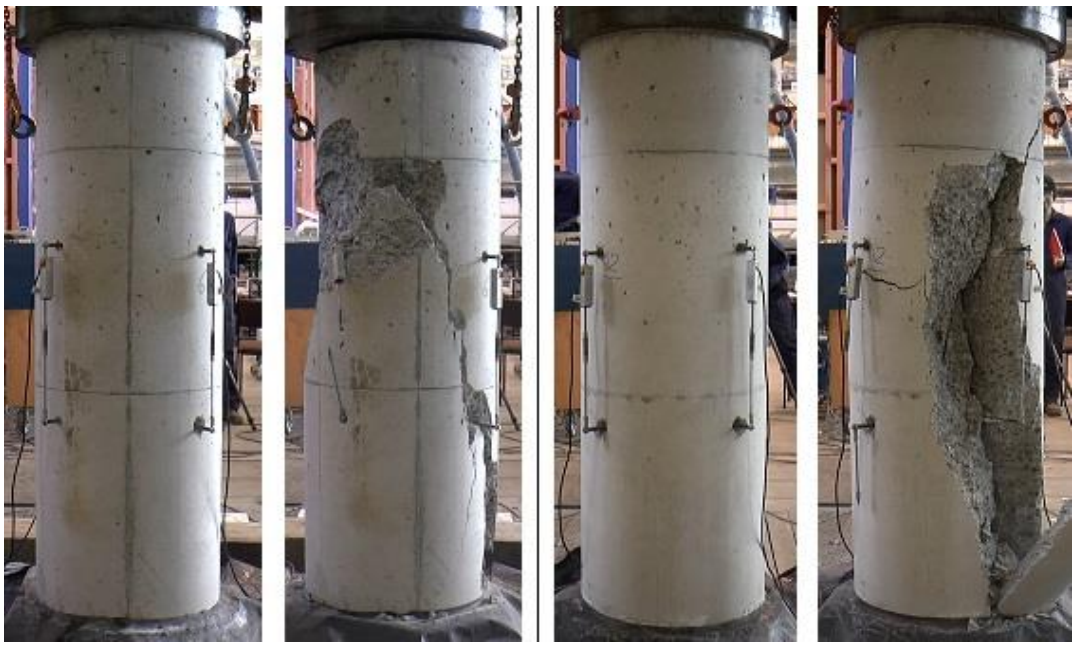

Initial Failure Initial Failure